Understanding the role of DUSP5 in the regulation of oncogenic KRAS and BRAF cell signalling

Bayley, Cassidy

Award date:
2021

Awarding institution:
University of Bath

Understanding the role of DUSP5 in the regulation of oncogenic KRAS and BRAF cell signalling

Cassidy Bayley

A thesis submitted for the degree of Doctor of Philosophy

Department of Biology and Biochemistry

March 2020

Acknowledgments

I would like to thank Paul Whitley for his kindness and endless patience. I cannot express how grateful I am for your encouraging and unconditional support. I would also like to thank Simon Cook, who was kind enough to take me under his wing in a difficult and unconventional situation. To Matt Sale, who paved the way to all things drug-resistance, thank you for your kindness. To Andrew Kidger, a master of DUSPs (and most other things), you will never know how much your help, kindness, patience and endurance has carried me. I am truly grateful. And last, to Jim Caunt, I feel like I might finally be able to keep up with you (kind of, maybe) in a conversation about cell signalling haha! Our loss is so profound. Thank you for everything you did for me. This work is dedicated to you.

Abbreviations

AKT – AKT8 virus oncogene cellular homolog

AP1 – Activator protein 1

APAF1 Apoptotic protease activating factor 1

APS – ammonium persulphate

APT – Adenosine triphosphate

Asp – Aspartic acid

BAD – BCL-2-associated death promoter

BAK – BCL-2 homologous antagonist/killer protein

BAX – BCL-2-associated X protein

BCA – Bicinchoninic acid

BCL2 – B–cell lymphoma 2

BCL-X_L – BCL2-like protein 1

BH3 – BCL2 homology domain

BID - BH3 interacting-domain death agonist

BIM – BCL2–like protein 11

BMF – BCL2 Modifying Factor

bp – Base pairs

BRAFi – BRAF inhibitors

BSA – Bovine serum albumin

cAMP – Cyclic adenosine monophosphate

CD – Common docking site

CDK – Cyclin–dependent kinase

c–Myc – Avian myelocytomatosis virus oncogene cellular homolog

CNK – Connector enhancer of kinase suppressor

COT – Spore coat protein

CREB – cAMP responsive element binding protein

CRC – colorectal cancer

DAPI – 4', 6'-diamino-2-phenylindole

Ddit3 – DNA Damage Inducible Transcript 3

DMEM – Dulbecco's modified Eagle's medium

DLK – Protein delta homolog 1

DTT – Diothiothreitol

DUSP – Dual specificity phosphatase

E2F – E2 factor

EDTA – Diaminoethanetetra-acetic acid disodium salt

EGF – Epidermal growth factor

ELK1 – ETS like-1 protein

ERK – Extracellular signal-regulated kinase

ETS – E26 transformation-specific transcription factor

FBS – Fetal bovine serum

FGF – Fibroblast growth factor

FOXO – Forkhead box O

GAB – GRB2-associated-binding protein

GAP – GTPase-activating protein

GEF – Guanine nucleotide exchange factor

GPCR – G-protein coupled receptor

GRB2 – Growth factor receptor-bound protein 2

GTP – Guanosine triphosphate

GDP – Guanosine diphosphate

H_2O – Hydrogen dioxide (water)

HRP – Horseradish peroxidase

HSP90 – Heat shock protein 90

IEC – Intestinal epithelial crypt

JNK – c-Jun amino-terminal kinase

kDa – Kilodaltons

KID – Kinase insert domain

KIM – Kinase interaction motif

KSR – kinase suppressor of RAS

LB – Luria broth

Lys – Lysine

mAb – Monoclonal antibody

MAPK – Mitogen-activated protein kinase

MAPKK – MAPK kinase

MAPKKK – MAPKK kinase

MCL1 – Myeloid cell leukemia 1

MEF – Mouse embryonic fibroblast

MEK – MAPK/ERK kinase

MEKi – MEK inhibitor

MEKK1 – MEK kinase 1

MKP – MAPK phosphatase

MOMP – Mitochondrial outer membrane permealisation

MORG1 – MAPK organiser 1

MP-1 – Monocyte chemoattractant protein-1

mRNA – Messenger ribonucleic acid

MSK – mitogen and stress activated protein kinase

NGF – Nerve growth factor

NGS – Normal goat serum

NLS – Nuclear localisation signal

NSCLC – Non-small cell lung carcinoma

OMM – Outer mitochondrial membrane

$p21^{CIP1}$ – cyclin-dependent kinase inhibitor 1/ CDK–interacting protein 1

PBS – Phosphate-buffered saline

PC12 – Pheochromocytoma of the rat adrenal medulla

PCNA – Proliferating cell nuclear antigen

PCR – Polymerase chain reaction

PDGF – Platelet-derived growth factor

PI3K – Phosphoinositide 3 kinase

PIP3 - Phosphatidylinositol (3,4,5)-trisphosphate

PKA- Protein kinase A

PKC – Protein kinase C

PP2A – Protein phosphatase A

PP2C – Protein phosphatase C

PUMA – p53 upregulated modulator of apoptosis

RAF – Rapidly accelerated fibrosarcoma

RAS – Rat sarcoma GTPase

RB – retinoblastoma protein

RNA – Ribonucleic acid

RSK – Ribosomal s6 kinase

RTK – Receptor tyrosine kinase

RT-PCR – Quantitative reverse transcription PCR

SDS – Sodium dodecylsulphate

SDS-PAGE – Sodium dodecylsulphate polyacrylamide gel electrophoresis

Ser – Serine

SFK – Src family kinase

SH2 – Src-homology 2

SH3 – Src homology 3

shRNA – Short hairpin RNA

siRNA – Short interfering RNA

SOC – Super optimal broth with catabolite repression

SOS – Son of sevenless guanine nucleotide exchange factor

TEMED – N,N,N',N-tetramethylethylenediamine

Thr – Threonine

Tob1 – Transducer of ERBB2

Tyr - Tyrosine

UTR – Untranslated region

WT – Wildtype

List of figures

List of tables

Abstract

The deregulation of kinase cascades drives the development and survival of many human tumours. Kinase-targeted therapeutics therefore offer great promise for 'personalised' medicine. However, the beneficial effects of kinase inhibition are often short-lived due to the evolution of drug resistance. Whilst we know that reprogramming of phosphorylation networks underpins drug resistance, the specific role of protein phosphatases in these processes remains largely unexplored. Using a mixture of conventional biochemical approaches and high content microscopy, we have evaluated spatial and temporal components of ERK activation in response to the administration or cessation of the MEK inhibitor AZD6244, in mutant BRAF- and KRAS-driven colorectal cancer (CRC) cell lines and their AZD6244-resistant derivatives. We have also determined the expression patterns of several MAPK phosphatases (MKPs) in these cell models and have correlated a robust induction of DUSP4, DUSP5 and DUSP6 with AZD6244 removal, ERK hyperactivation and nuclear accumulation of ERK in AZD6244-resistant CRC cells. The ablation of DUSP5 expression in these conditions led to enhanced ERK hyperactivation and reduced E-cadherin expression in AZD6244-resistant HCT116 cells which were previously shown to undergo an epithelial-to-mesenchymal transition in response to AZD6244 withdrawal. In AZD6244-resistant HT29 cells, where AZD6244 deprivation leads to cell death, DUSP5 loss had subtle, but inconclusive effects on *p*-ERK and downstream effectors. This work emphasizes the influential and highly context-dependent role that MKP regulation has in ERK-driven oncogenesis and drug-resistance and has contributed to our current understanding of signal reprogramming events that frequently occur in response to ERK pathway inhibition.

Table of Contents

Chapter 1. Introduction

1.1. Mitogen-activated protein kinase (MAPK) signalling

1.1.1. The structure and function of protein kinases in protein phosphorylation

Protein phosphorylation is a key mechanism of post-translational regulation often associated with cell signalling cascades. While the hydrolysis of ATP is highly energetically favourable, the reaction is extremely slow in the absence of catalysts, providing an opportunity for kinetic control of these modifications by specialised regulatory enzymes. In addition to this, protein phosphorylation is reversible and so the addition and subsequent removal of phosphate molecules can serve as a biological “switch” able to induce and reverse major changes in protein structure and function (Jin and Pawson, 2012).

The major biochemical implications of a phosphate moiety addition are a result of its negative charge, which can generate new interactions between nearby protein residues and/or disrupt existing ones. The negatively charged phosphate can attract positively charged protein residues, repulse negatively charged residues and form or disrupt hydrogen bonds, initiating the formation, stabilisation or disruption of local protein structure (Johnson and Lewis, 2001). If a phosphate molecule is added within or near to a protein’s active site, it may interact directly or indirectly with important catalytic residues, thereby inducing or preventing catalytic activity. Phosphorylation can also have longer range effects on tertiary or even quaternary protein structure, and act as a “mark” that initiates binding of other proteins or regulatory molecules (Johnson and Lewis, 2001). Through these mechanisms, phosphorylation can be functionally linked to protein activity and serves as a dynamic form of regulatory protein signalling.

Protein kinases are an extensive family of enzymes that are key effectors of protein phosphorylation in the cell. Not only are they able to catalyse the transfer of ATP to a substrate peptide, but they too are frequently activated by phosphorylation. These ubiquitous signalling proteins share a kinase sequence of approximately 290 amino acids, which contains the highly conserved catalytic site (Meharena et al., 2013). Protein kinases can be divided into two major sub-families, the Serine/Threonine (Ser/Thr) kinases and the Tyrosine (Tyr) kinases, based on the target amino-acids upon which the enzymes can act. The exquisite utility of protein kinases in regulating the structure and function of their substrates centres on their ability to catalyse protein phosphorylation. In both Ser/Thr and Tyr kinases this is enabled through the precise architecture of their catalytic domain, a folded and bilobed structure with binding sites for ATP and the substrate peptide group located within the groove of the “N” and “C” lobes (Figure 1.1) (Huse and Kuriyan, 2002; Johnson and Lewis, 2001; Meharena et al., 2013).

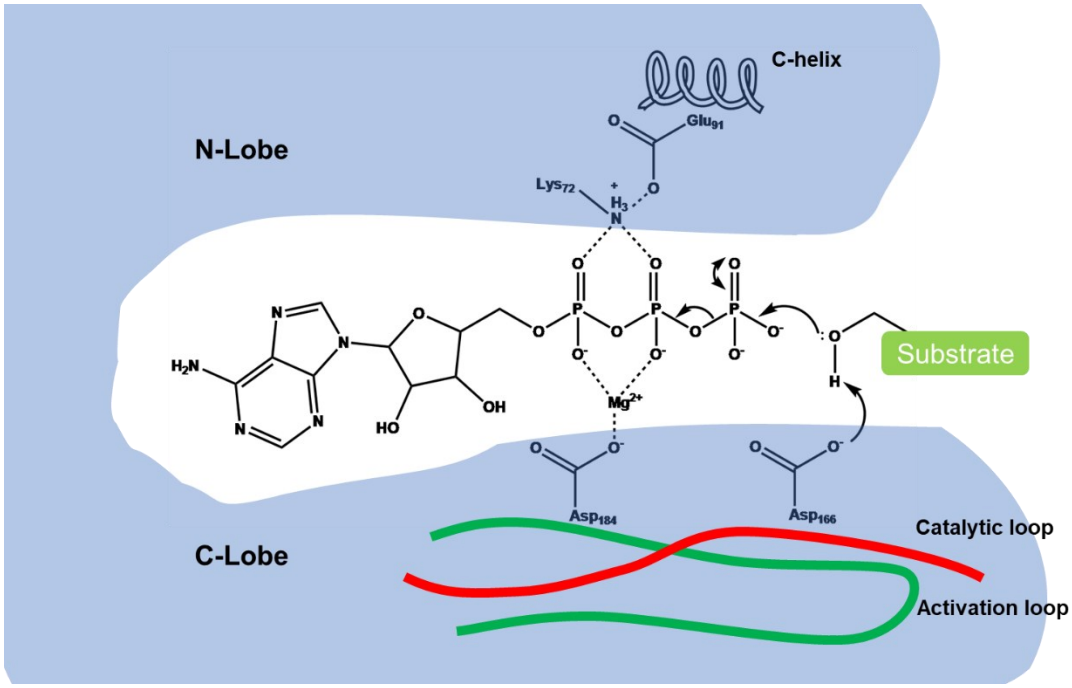

Figure 1.1. The prototypic protein kinase active site. Key catalytic residues Lys72, Asp184 and Asp166 (numbering based on the amino acid sequence of Protein Kinase C) are critical for ATP binding and phosphotransfer. The optimal configuration of the catalytic residues is co-ordinated by tertiary interactions with elements in the C-helix, catalytic loop and activation loop.

Within the catalytic domain, multiple conserved amino acid residues co-ordinate three critical catalytic mechanisms; ATP-binding, substrate-binding and phosphotransfer. In the N-lobe, a glycine rich “P loop” extends over the top of ATP, while a nearby lysine residue (Lys72 in Figure 1.1) interacts with the negatively-charged phosphate moieties of the ATP molecule. Together with aspartate (Asp184 in Figure 1.1) and asparagine (Asn171) residues in the C-lobe, these molecules bind and co-ordinate ATP in the active site (Huse and Kuriyan, 2002). Binding of the substrate peptide is largely coordinated by the C-helix in the N-lobe and the activation loop in the C-lobe. These “regulatory levers” facilitate or prevent substrate binding through their proximity to and interaction with residues adjacent to the catalytic residues (Johnson et al., 1996). In some protein kinases, the N- and C-lobes are in an inactive conformation prior to phosphorylation of conserved threonine and tyrosine residues in the activation loop and rely on phosphorylation to initiate the conformation changes required for substrate binding and catalysis (Huse and Kuriyan, 2002).

The activation of ERK2, a highly abundant, prototypic kinase, by phosphorylation has been structurally characterised and demonstrates common biochemical features of this mechanism. In unphosphorylated ERK2, the N- and C-lobes of the active site are rotated apart, and the active site residues are misaligned (Canagarajah et al., 1997). Phosphorylation of threonine (Thr-183) induces the proper orientation of the C-helix and promotes the closure of the N- and C-lobes through the formation of multiple ionic contacts and hydrogen bonds with various surface arginine residues (Canagarajah et al., 1997; Huse and Kuriyan, 2002). This allows the C-helix residue Glu91 to coordinate the catalytic residue Lys72 through a network of hydrogen bonds (Figure 1.1). The phosphorylation of tyrosine (Tyr-185) promotes it’s repositioning to the outer surface of the catalytic domain where it forms various bonds with nearby arginine residues. This results in refolding of the activation loop which contains a highly conserved Asp-Phe-Gly (DFG) motif comprised in part, of the catalytic Asp184 residue (Figure 1.1) (Canagarajah et al., 1997).

Once in the correct conformational arrangement, the kinase is able to bind both ATP and substrate. In the final catalytic step, a basic aspartate (Asp166) residue within the catalytic loop is able to remove the proton from the substrate peptide hydroxyl group, allowing nucleophilic attack of γ-phosphate and transfer of the phosphoryl group from ATP to the receiving substrate peptide (Figure 1.1) (Johnson et al., 1996). Through these intricately fine-tuned mechanisms of phosphorylation-induced activation, protein kinases can both receive and relay biochemical messages within the cell and thus serve as excellent signalling molecules. In many major cellular signalling pathways, these enzymes participate in protein kinase cascades where each kinase is primed to activate the next in a series of phosphorylation steps.

1.1.2. MAPK activation is initiated by cell membrane receptors and intracellular signalling complexes

The mitogen-activated protein kinase (MAPK) signalling proteins are a family of highly abundant, evolutionarily conserved signal transduction pathways responsible for relaying a plethora of cellular stimuli to effectors of fundamental cellular processes. These include but are not limited to proliferation, differentiation, cell growth, immune responses and apoptosis (Meloche & Pouysségur, 2007; von Kriegsheim *et al.*, 2009).

MAPKs are proline-directed serine/threonine kinases that are activated through the phosphorylation of conserved threonine and tyrosine residues. Their catalytic domains contain most major features common to the protein kinase family (described previously), with some additional MAPK-specific regions. The “P+1” specificity site in the C-lobe of the MAPK activation domain is essential for proline recognition and substrate specificity while a 50 amino acid MAPK insertion and an extended C-terminus facilitate conformational activation and protein-protein interactions (Canagarajah et al., 1997). The MAPK phosphorylation cascades share a common three-tiered architecture, comprised of a MAPK kinase kinase which phosphorylates a downstream MAPK kinase, which in turn, phosphorylates the MAPK itself (English *et al*., 1999). Activation of each cascade is initiated by extracellular signals and the membrane receptors that receive them.

Mammalian MAPKs are typically coupled to different receptor families that transfer signalling stimuli from the cellular environment to the intracellular signalling machinery. Specialised signalling receptors such as the cytokine receptors, the G protein-coupled receptors (GPCRs) and the RTKs have all been linked to MAPK cascade activation (Krishna and Narang, 2008). Receptor tyrosine kinases (RTKs) are an extensive and abundant family of signalling receptors with about 20 structural subfamilies each dedicated to a specific family of protein ligands. These include the growth factors EGF (epidermal growth factor), PDGF (platelet-derived growth factor) and FGF (fibroblast growth factor) (Lemmon and Schlessinger, 2010).

Like many transmembrane signalling receptors, RTKs typically constitute an extracellular ligand-binding domain, a transmembrane domain and an intracellular tyrosine kinase domain. In the absence of extracellular stimuli, most RTKs exist in an inactive monomeric form. Upon ligand-binding RTK monomers are able to dimerise in the lipid bilayer which facilitates trans-autophosphorylation of both kinase domains (Lemmon and Schlessinger, 2010). In addition to kinase domain activation, this phosphorylation can generate high-affinity docking sites for intracellular signalling proteins that bind the receptor and go on to propagate the initiating signal. Signalling molecules able to bind phosphotyrosines are structurally and functionally varied however, commonly share a highly conserved phosphotyrosine-binding domain called a Src homology region or SH2 domain (Lemmon and Schlessinger, 2010). Similar to SH2 domains, many intracellular signalling proteins contain SH3 domains which bind proline-rich motifs in other signalling proteins. Through these SH2 and SH3 domains intracellular signalling proteins are able to form large complexes at or near the site of RTK phosphorylation which cooperatively function to activate or inhibit downstream signalling. Adaptor proteins act specifically for this purpose and are composed almost entirely of SH2 and SH3 domains (Lemmon and Schlessinger, 2010).

The largest family of cell-surface receptors are the G-protein-coupled receptors (GPCRs) which form part of a highly dynamic and widely-used signal relay system. The binding of signalling ligands to an extracellular site in the GPCR causes a conformational change in protein structure which enables it to activate a GTP-binding protein (G protein) (Rosenbaum et al., 2009). In general, G-proteins that interact with GPCRs are heterotrimeric and are comprised of three protein subunits, α, β and γ. In

their inactive form the α subunit is bound by guanosine diphosphate (GDP). When bound to a GPCR, G-proteins become activated by the exchange of GDP for GTP (guanosine triphosphate). GTP-binding initiates the release of the G-protein as well as the disassociation of the α subunit from the $\beta\gamma$ pair. The monomeric GTP-bound α-subunit is a GTPase which, depending on its control by regulatory enzymes, is able to hydrolyse bound GDP to GTP. In this way it is able to function as an enzyme-coupled molecular switch which is active when bound by GTP and inactive when bound by GDP (Rosenbaum et al., 2009).

Other monomeric GTPases which are structurally similar to the α-subunit of heterotrimeric G proteins, known as the small GTPases, are not reliant on GPCRs for their activation. Members of the Ras superfamily of small GTPases can interact with other cell membrane receptors like RTKs. Three major, closely related Ras proteins have been identified in humans, H-, K- and N-RAS. Subtle differences in function have been delineated in these RAS isoforms, however, they are commonly referred to collectively as RAS. Inactive Ras GTPases are activated by guanine nucleotide exchange factors (GEFs), which stimulate the dissociation of GDP and subsequent loading of GTP. In contrast, GTPase-activating proteins (GAPs) catalyse the hydrolysis of GTP to GDP, deactivating GTPases (Mitin et al., 2005). RTKs are able to facilitate the activation of Ras GTPases bound to the cytoplasm by recruiting and binding Ras-GEFs, such as the *Son of Sevenless* protein, SOS (Figure 1.2). The association of RTKs to Ras-GEFs is mediated by the SH2 and SH3 domains of adapter proteins like growth factor receptor-bound protein 2 (GBR2) (Figure 1.2) (Mitin et al., 2005).

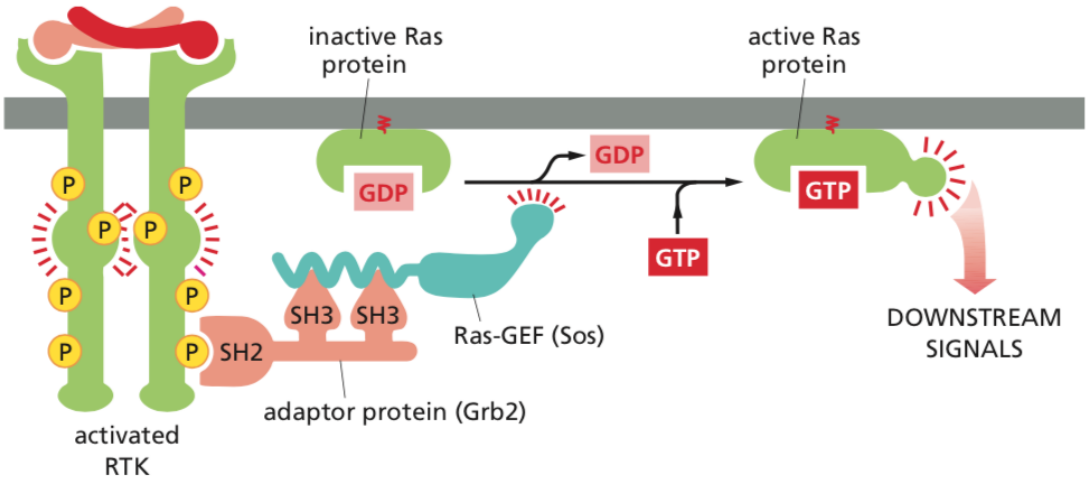

Figure 1.2. RAS activation by receptor tyrosine kinases. Adaptor protein GRB2 is able to bind phosphorylated tyrosine on an activated RTK via its SH2 domain. Recruitment and association with SOS is enabled through two SH3 domains. Once in proximity with membrane bound RAS, SOS activates RAS through the catalytic exchange of GDP for GTP. This figure was adapted from Alberts *et al*. (2011) with permission from Garland Science.

The autophosphorylation of RTKs and the subsequent activation of G proteins induced by extracellular ligand binding are important but short-lived events in signalling dynamics and can be quickly reversed by the action of phosphatases (enzymes that dephosphorylate their substrates) and GAPs. In order to propagate and enhance signals that occur at the cell membrane, cells utilise the dynamic and far-reaching signal relaying power of protein kinase cascades such as the MAPK signalling pathways.

1.1.3. Commonalities and specificities of conventional MAPK pathways

Three conventional MAPK pathways have been well characterized in mammals; the extracellular signal-regulated kinase (ERK) 1 and 2, the c-jun amino-terminal kinases (JNKs 1-3) and the p38 MAPK isoforms (English et al., 1999). While several other MAPKs have been discovered (ERK7/8, ERK3/4 and ERK5), they have not yet been as extensively studied. MAPK pathways are initiated by varied stimulants and direct multiple, different cell fate outcomes, however they share a common architecture. Ser/Thr MAPKKKs (MAPKK kinases) form the first tier of the cascade and are activated by phosphorylation or interactions with small GTPases such as Ras. MAPKKKs go on to phosphorylate dual-specificity MAPKKs (MAPK kinase), which in turn, phosphorylate conserved threonine and tyrosine residues in their MAPK targets (Krishna and Narang, 2008).

MAPKKs are highly substrate-specific and are only able to phosphorylate a few MAPK targets each. In contrast, a single MAPKKK can regulate several different MAPK cascades (Pearson et al., 2001). Interestingly, while MAPKKKs tend to be more diverse in type, they are not abundant, and are most commonly present in much lower numbers than their downstream MAPKK targets. This disparity in the relative concentrations of MAPKKK and MAPKK proteins may constitute a mechanism of signal amplification, where each successive kinase in the cascade is more abundant than its activator (Pearson et al., 2001).

The specific interactions that occur between MAPKKs and MAPKs as well as between MAPKs and their target substrates are regulated by biochemically distinct docking domains. These domains are generally separate from the protein catalytic sites and facilitate efficient, high-fidelity signalling (Bardwell, 2006; Tanoue et al., 2000). A docking domain that has been identified in a number of MAPK-targeted transcription factors is the D domain, comprised of a few positively charged residues encompassed by hydrophobic residues. D domains are recognised and bound by conserved common docking (CD) motifs found in the C terminals of many MAPKs. CD motifs are able to form electrostatic and hydrophobic interactions with D domains through their acidic and hydrophobic residues (Tanoue et al., 2000).

As previously mentioned, MAPKs are proline-directed Ser/Thr kinases that are able to phosphorylate a myriad of downstream effector proteins, including MAPK-activated protein kinases (MKs), transcription factors and various cytoplasmic proteins. While ERK 1/2 signalling typically responds to growth factors and hormones, the JNK and p38 MAPKs are predominantly implicated in cellular stress signalling (English *et al*., 1999; Chang and Karin, 2001).

In mammals, three genes encode JNK proteins, *JNK1*, *JNK2* and *JNK3*, with JNK1 and JNK2 being most prevalent (Barr and Bogoyevitch, 2001). JNK signalling has been implicated in response to a variety of cellular stresses including UV radiation, heat shock, DNA damage, growth factor withdrawal and exposure to inflammatory cytokines. Some studies have linked JNK activation to growth factors and serum, however this is relatively uncommon (Kyriakis and Avruch, 2001). MAPKKKs that have been identified as JNK signalling activators are diverse and many and include MAPKKK1-3 (or MAP3K1-3), DLK and TAK1 enzymes. These kinases relay signals to JNK targets by activating the MAPKKs MKK4 and MKK7 (Barr and Bogoyevitch, 2001). Once phosphorylated on the conserved T-P-Y motif in their activation loops, JNK are able to target a number of downstream effectors, including c-jun, c-myc, p53 and members of the BCL-2 protein family (Krishna and Narang, 2008). JNK-mediated phosphorylation of these proteins has frequently been associated with apoptosis (Barr and Bogoyevitch, 2001; Krishna and Narang, 2008) in response to cellular stress, strengthening the notion that JNKs are important mediators of stress signalling.

To date, p38 MAPK has four known isoforms, p38α, β,γ and δ MAPK, with p38α MAPK being the most extensively studied. Similar to the JNKs, p38 MAPKs are activated by numerous cellular stress signals and to a lesser extent, by insulin and growth factors (Kyriakis and Avruch, 2001). Many, if not all upstream stress signals of JNK have been shown to activate p38 MAPK and several MAPKKKs active in JNK signalling can also initiate the p38 MAPK cascade. Primarily, p38 MAPK is phosphorylated by MAPKKs MKK3 and MKK6 however JNK MAPKK proteins MKK4 and MKK7 have been shown to phosphorylate p38 MAPK isoforms. These various points of crossover between the JNK and p38 MAPK pathways suggest that crosstalk plays an important role in their regulatory function (Krishna and Narang, 2008). Like JNK, p38 MAPK has been shown to regulate several transcription factors and cytoplasmic proteins implicated in

apoptosis however p38 MAPK has been most extensively studied in immune function, where its role appears to be critical in inflammatory responses (Ashwell, 2006).

Both JNK and p38 MAPK signalling has been implicated in cancer, most likely a result of their prevalent roles in stress signalling. Numerous studies have demonstrated both tumour suppressive and oncogenic effects of the JNK and p38 MAPKs. The discovery that JNK and p38 MAPKK MKK4 is consistently inactivated through mutation or downregulated in several cancers (including pancreas, breast, colon and ovarian cancer) has suggested that activation of JNK and p38 MAPK through MKK4 can suppress tumourigenesis (Dhillon *et al.*, 2007). Additionally, p38 MAPK has been shown to function as a tumour suppressor through its activation of p53 (Dhillon *et al.*, 2007). Conversely, JNKs have been found to be upregulated in several cancer cell lines and several studies have demonstrated a critical role for JNK-mediated phosphorylation of c-jun in Ras-induced tumourigenesis, which may involve c-jun's ability to repress p53 (Kennedy and Davis, 2003). Studies with several chemotherapeutic agents have linked p38 MAPK activity with the induction of apoptosis, while others have shown that inhibition of p38 MAPK can lead to enhanced apoptosis in response to DNA-damaging agents (Olson and Hallahan, 2004; Dhillon *et al.*, 2007). Considered in combination, this research suggests that the relative tumour suppressive or promoting effects of the JNK and p38 MAP kinases are highly context-dependent and may depend on relative stress thresholds at various stages of tumourigenesis.

1.2. RAF/MEK/ERK signalling pathway

1.2.1. Sequential activation of ERK

The RAF/MEK/ERK pathway is activated by an array of extracellular signalling molecules such as, serums, growth factors and cytokines and their cognate signalling receptors, which include receptor tyrosine kinases (RTKs), G-protein-coupled receptors and cytokine receptors (Yoon and Seger, 2006). The highly conserved and widespread core cascade is frequently initiated by the small RAS GTPase and is comprised of the RAF family of MAPKKKs, the MAPKK enzymes MEK1 and MEK2 and finally, two canonical ERK proteins, ERK1 and ERK2.

ERK1 and ERK2 are 43 and 41 kDa proteins that are ubiquitously expressed in all tissues (Boulton et al., 1991). These isoforms share high protein sequence homology and various reports have suggested that they are functionally redundant (Pearson et al., 2001). Mouse knockout studies have demonstrated different phenotypic outcomes of ERK1 and ERK2 disruption (ERK2 ablation leads to early embryonic death but mice lacking ERK1 protein developing normally) however, further research has suggested that these results are likely due to differences in their relative expression levels, with the ERK2 isoform being expressed more abundantly (Buscà et al., 2016; Lefloch et al., 2008).

The activation of the ERK pathway through binding of growth factors like EGF and FGF to their respective RTKs, the EGF receptor (EGFR) and the FGF receptor (FGFR) has been thoroughly characterised and is typically referred to in describing the prototypic activation of RAF/MEK/ERK signalling (Figure 1.3). FGF-bound FGFRs induce the activation of RAS GTPases at the cytoplasmic face of the plasma membrane through the recruitment of adapter proteins (GRB2) and RAS-GEFs (SOS) (Figure 1.1). This prototypic activation of RTKs and the subsequent activation of RAS has been described in detail previously. GTP-bound RAS can then go on to facilitate the formation of RAF hetero- and homodimers which can phosphorylate and activate MEK1 and MEK2. MEK1 and MEK2 are dual specificity MAPK kinases that are solely responsible for the activation of ERK MAP kinases through the phosphorylation of their conserved threonine and tyrosine activation loop residues (Pearson *et al.* 2001; Yoon and Seger, 2006).

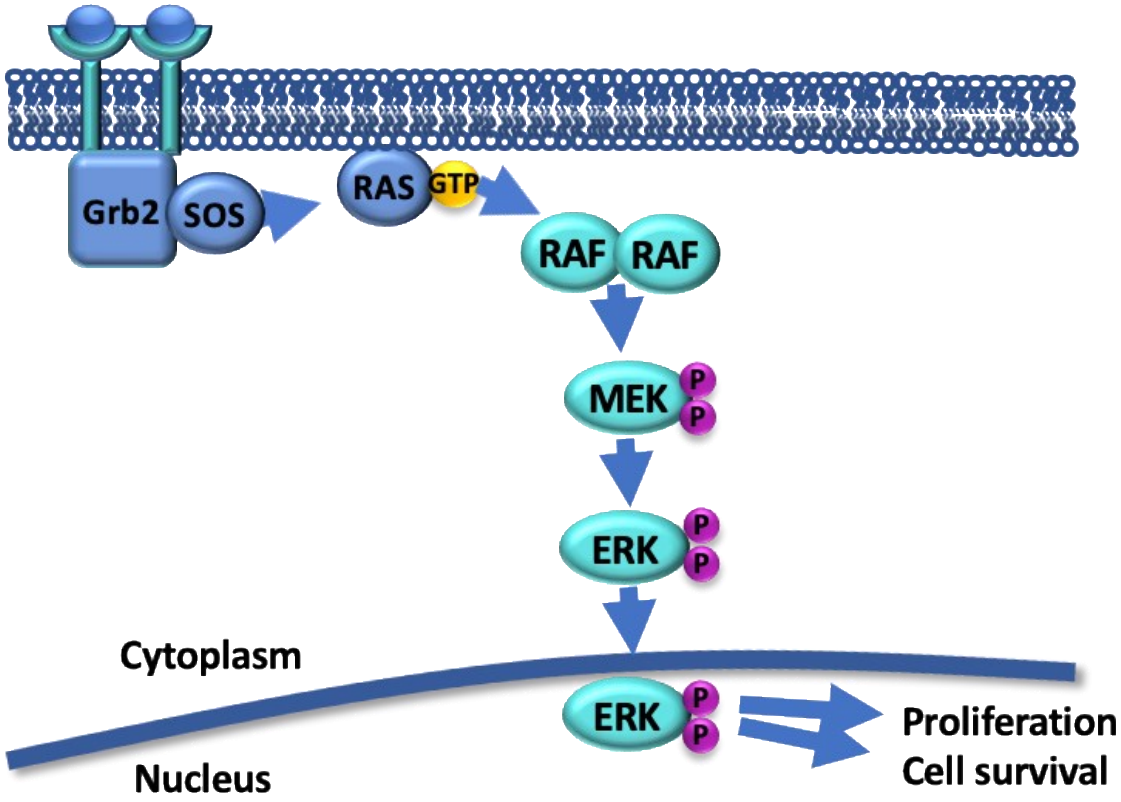

Figure 1.3. The prototypic RAF/MEK/ERK signalling cascade. A simplified linear representation of the RAS-regulated RAF–MEK–ERK signalling cascade. The ERK pathway is commonly induced by activated growth factor receptors such as EGFR or FGFR. ERK substrates include transcription factors of the ETS family that are responsible for mediating diverse cell fates.

In this simplistic summary, the RAS/RAF/MEK/ERK signalling procession seems fairly straightforward, however, in reality, each step is relatively complex and involves the delicately orchestrated function of numerous proteins. This is especially true at the level of RAF activation where activation and dimerization of A-, B- and CRAF isoforms is not singularly undertaken by RAS, but by the coordinated efforts of heat shock protein 90 (HSP90), 14-3-3, kinase suppressor of RAS (KSR) proteins and various kinases (Lavoie and Therrien, 2015).

In its inactive form, the RAF protein exists in a conformation that facilitates autoinhibition of its catalytic domain, through the repressive interaction of the N-terminal region (Lavoie and Therrien, 2015). This inhibitory state is enforced by phosphorylation of serine residues by protein kinase A (PKA) and AKT (Cook and McCormick, 1993; Zimmermann and Moelling, 1999) and the association of 14-3-3, a regulatory protein (Freed et al., 1994). Recruitment of RAF to the plasma membrane is a critical step in RAF activation, and is initiated by active RAS which interacts with the conserved Cys-rich domain (CRD) and RAS-binding domain of RAF. This interaction relieves RAF auto-inhibition, releases 14-3-3 and allows anchoring of RAF proteins to the inner cell membrane. Upon recruitment to the membrane RAF activation is implemented through SRC family kinase (SFKs) and casein kinase 2 (CK2) phosphorylation of RAF as well as dimerization of RAF monomers. Hetero- and homodimerization of RAF and association with the KSR scaffold protein induces RAF catalytic activity and enables the sequestration of RAF substrates MEK1 and MEK2 (Lavoie and Therrien, 2015).

RAF proteins are serine/threonine MAPKKKs that phosphorylate MEK1 and MEK2 on conserved serine residues in their activation loop. Similar to MAPKs, phosphorylation of MEK induces conformational changes in the catalytic domain that results in its activation. And like RAF, MEK1 and MEK2 are also able to form heterodimers which increase their catalytic activity (Zheng and Guan, 1994). The MEK isoforms are dual-specificity kinases which phosphorylate their ERK target on the conserved T-E-Y (Thr-Glu-Tyr) motif. An important regulatory feature of the MEK proteins is their ability to bind their ERK targets through their conserved D domain. The association of ERK and MEK is mediated by the ERK CD and MAPK insert or kinase insert domain (KID) and is important for ERK activation and localisation (Chuderland and Seger, 2005;

Fukuda et al., 1996; Roskoski, 2012). MEK1 and MEK2 are the only MAPKKs able to activate ERK1 and ERK2 and thus have been described as the “gatekeepers” of ERK activity. Conversely, activation of MEK1 and MEK2 can be performed by numerous MAPKKKs outside of the RAF family (Caunt *et al.*, 2015).

1.2.2. Regulation of ERK signalling

Active ERK has a manifold of downstream targets, many of which influence distinct cell fate decisions. It follows that in order to maintain fidelity of ERK signalling, tightly controlled spatio-temporal regulation is imperative. This includes regulation of the intensity, duration and location of ERK activation, factors that are critical determinants of the biological outcome of signalling (Ebisuya et al., 2005; Murphy and Blenis, 2006; Pouyssegur et al., 2002).

Multiple studies in rat PC12 cells (Gotoh *et al.*, 1990; Nguyen *et al.*, 1993; Marshall, 1995) and rodent fibroblasts (Balmanno and Cook, 1999; Dobrowolski et al., 1994; Murphy et al., 2002) have demonstrated that these cells can either differentiate, remain quiescent or enter the cell cycle in response to sustained or transient ERK activation. Work that investigated how the relative magnitude of active ERK can influence the growth and survival of murine fibroblasts, discovered that overexpression of upstream RAF led to ERK hyperactivation and stimulated the CDK inhibitor $p21^{CIP1}$. This led to the repression of cyclin-CDK activity and cell cycle arrest. In contrast, intermediate levels of active ERK facilitated cell cycle progression (Sewing et al., 1997; Woods et al., 1997a). Further studies in rodent cells have shown that the localisation of active ERK can influence its regulatory influence, and nuclear targeting of catalytic ERK is required for neurite outgrowth (Robinson et al., 1998) and cell cycle entry (Brunet et al., 1999; Hochholdinger et al., 1999).

In a normal cell, the ERK pathway is subject to numerous tiers of regulation that control ERK signalling duration, magnitude and subcellular compartmentalisation. These include scaffold proteins, crosstalk between other major signalling cascades and multiple feedback loops (Ebisuya et al., 2005; Mendoza et al., 2011; Morrison and Davis, 2003; Murphy and Blenis, 2006; Pouyssegur et al., 2002).

Scaffolding

The RAF/MEK/ERK signalling cascade is frequently summarised as a simplified, linear pathway, however multiple additional layers of protein coordination are required for the precise and timely activation of downstream ERK. Indeed, the complex activation of RAF demonstrates the role of various chaperone and scaffolding proteins which are crucial for increasing the efficiency of enzyme catalysis.

More than 50 scaffolding proteins have been implicated in the ERK cascade, some of which include KSR, connector enhancer of KSR (CNK) and IQGAP1, which enhance ERK activation by co-ordinating and increasing the efficiency of key interactions (Morrison & Davis, 2003). Scaffolding serves to bring signal components into close proximity with one another and increase their relative concentrations in a given cellular space. Scaffold proteins can also increase the stability of their cognate proteins or participate in their allosteric activation (Good et al., 2011). In addition to these functions, scaffolding can act to insulate pathway components from the influence of effectors of alternate pathways acting in parallel and in close proximity, thereby maintaining signal fidelity (Good et al., 2011).

KSR is perhaps the best-known scaffold protein involved in the upstream activation of ERK and in addition to its interaction with RAF, it is able to interact with MEK and ERK. In response to stimulation, KSR is translocated to the plasma membrane where it assembles RAF, MEK and ERK. This increases the efficiency of their consecutive activation, directly participates in the allosteric activation of RAF and controls the sub-cellular location of the kinase cascade (Nguyen et al., 2002). Interestingly, the positive regulation of ERK activation by KSR is concentration dependent, and in conditions where KSR is in excess of kinase substrates, serial phosphorylation is disrupted. This “combinatorial inhibition” can occur when scaffold proteins bind each substrate independently, and protein interaction is impaired (Ramos, 2008).

CNK is a large adapter protein that has been shown to bind RAF in mammalian cells and enhance RAS activation of CRAF (Lanigan 2003, Ziogras 2005, Jaffe 2004). Research in *Drosophila* has demonstrated that CNK may promote the activation of RAF by RAS by facilitating interactions of RAS, RAF and KSR (Douziech 2006, Laberge 2005, Claperon 2007), however it is not clear whether mammalian CNK can perform a similar function (Ramos, 2008). Another potential ERK cascade scaffold protein IQGAP1, is able to bind MEK and ERK as well as the BRAF isoform and has

been shown to participate in EGF-induced ERK activation (Roy 2005, Roy 2004, Ren 2007, Roy 2007). Other proteins implicated in scaffolding of ERK pathway components are β-Arrestin, MEK partner-1 (MP-1) and MAPK organiser 1 (MORG1), which appear to be involved in the activation of ERK at early and late endosomes, respectively. The existence and dynamic function of several ERK pathway scaffold proteins underscores the importance of efficient and highly-specific protein interactions upstream of ERK activation.

Crosstalk

While pathway insulation is required at some pivotal tiers of signal relay, the overall integration of multiple signalling pathways is critical for normal cell functioning. Numerous examples of this signalling crosstalk exist between the ERK signalling cascade, the JNK and p38 MAPK pathways (Junttila et al., 2008) and the PI3K/AKT pathway (Mendoza et al., 2011; Aksamitiene et al., 2012). Critical nodes of pathway integration occur through RAS, which can affect cell fate changes through both downstream ERK and AKT, and MEK, which in turn, can be phosphorylated by a number of kinases outside of the RAF repertoire (Caunt et al., 2015). Other MAPKKKs include MEKK1, MEKK3 and COT, which can activate not only downstream ERK through MEK phosphorylation, but p38 and JNK MAPKs through phosphorylation of their respective MAPKKs (Caunt *et al.*, 2015).

The PI3K/AKT pathway is another important signalling conduit in mammalian cells that responds to growth factor stimulation and cell stress. Similar to the ERK cascade, PI3K/AKT signalling can be initiated by RAS, which is able to bind and activate PI3K (phosphatidylinositol 3-kinase) a lipid kinase and mediator of AKT (protein kinase B) activation. PI3K signalling can either augment or reduce ERK signalling (and *vice versa*) through several integration nodes (Aksamitiene et al., 2012; Mendoza et al., 2011). GRB2-associated binder (GAB) is a docking/adapter protein active in the PI3K cascade that can recruit PI3K to growth factor receptors at the plasma membrane and assemble Ras-GAP, SHP2 (Src homology 2 domain- containing protein-tyrosine phosphatase) and PIP3 (phosphatidyl inositol 3.4.5 tri-phosphate) proteins critical for AKT activation. GAB is also able to bind the ERK signalling adaptor and Ras-GEF complex GRB2-SOS. Once in close proximity to the membrane SHP2 can dephosphorylate Ras-GAP binding sites on GAB and its associated RTKs, resulting in

a reduction in RAS inactivation. This can serve to promote ERK signalling activated by RAS (Mendoza et al., 2011).

Conversely, EGF-induced ERK activation can lead to phosphorylation of GAB by ERK, which disrupts its ability to recruit PI3K to the EGF receptor (Lehr et al., 2004). RAF constitutes another convergence point in the ERK and AKT pathways. AKT negatively regulates RAF by phosphorylating inhibitory sites in the Raf N-terminus (Zimmermann and Moelling, 1999). 14-3-3 dimers recognize this inhibitory mark and sequester RAF in the cytoplasm, away from RAS and MEK (Dumaz and Marais, 2003).

In addition to crosstalk upstream of ERK and AKT activation, ERK and AKT often target the same substrates and can act in concert to regulate proliferation and cell survival through interactions with cell fate effectors like FOXO, c-myc and BAD (Zimmermann and Moelling, 1999). The significance and ERK-mediated regulation of these proteins will be discussed in more detail later.

ERK compartmentalisation

While the detection of active and inactive ERK in both the nucleus and the cytoplasm in numerous reports suggests that ERK is able to shuttle between these subcellular locations, the mechanisms through which this is rendered possible is still a matter of debate. In quiescent cells, the subcellular location of ERK appears to be predominantly cytoplasmic (Caunt et al., 2008b; Murphy and Blenis, 2006). This has been attributed to the association of ERK with various cytoplasmic anchoring proteins including MEK (Fukuda et al., 1997) and Sef (Torii et al., 2004) and some cytoskeletal elements (Perlson et al., 2006; Reszka et al., 1997). In many instances, stimulus-induced phosphorylation of ERK by MEK releases ERK from its cytoplasmic anchors and pre-empts ERKs translocation to the nucleus.

More than one mechanism appears to facilitate the nuclear entry of phosphorylated and unphosphorylated ERK. Several studies have shown that ERK monomers can passively diffuse through the nuclear membrane, while ERK dimers have been shown to translocate to the nucleus through both carrier and energy-dependent and independent mechanisms (Adachi et al., 2000; Matsubayashi et al., 2001; Whitehurst et al., 2002). Independent studies by Matsubayashi *et al.* (2001) and Whitehurst *et al.* (2002) provided evidence of a nuclear pore complex-mediated mechanism whereby

ERK dimers interacted directly with nuclear pore proteins (nucleoporins or NUPs) in order to diffuse across the nuclear envelope. Further work by Ranganathan *et al*. (2006) showed that in addition to this proportion of ERK, a significant component of phosphorylated ERK entered the nucleus through active transport and required both the presence of carriers and energy. ERK does not contain a prototypic nuclear export signal (NES) or a nuclear localisation signal (NLS) and cannot bind carrier proteins such as importins or exportins directly. It has been posited therefore, that active translocation of ERK could be mediated by ERK binding partners such as MEK. In most cases, once inside the nucleus, ERK is rapidly dephosphorylated. Inactive ERK can remain tethered in the nucleus by nuclear anchors (for varying durations) or is exported from the nucleus once dephosphorylated. Again, nuclear export of ERK has been attributed to several mechanisms, one of which involves reassociation with MEK (Adachi et al., 2000; Fukuda et al., 1996) and the exportin CRM1 (Ranganathan et al., 2006). Additionally, similar to nuclear import of ERK, ERK can exit the nucleus through carrier and energy-independent interactions with the nuclear pore complex (Ranganathan et al., 2006).

Feedback loops

In addition to the activities of various upstream interactions, the ERK pathway is subject to critical regulation by homeostatic feedback controls (Figure 1.4). The activation of ERK signalling can be described as self-limiting as once ERK is activated it goes on to phosphorylate and inhibit many of its upstream inducers, including RAF, MEK and SOS (Ramos, 2008).

The phosphorylation of MEK by ERK can decrease subsequent ERK activation by preventing phosphorylation of MEK by PAK1 ($p21^{CIP1}$-activated kinase), a Ser/Thr kinase that enhances MEK activity (Eblen et al., 2004) or by disrupting a MEK1-MEK2 heterodimer that appears to stabilise MEK and ERK phosphorylation (Catalanotti et al., 2009). Similarly, phosphorylation of BRAF by ERK promotes the disassembly of BRAF and CRAF heterodimers which have highly increased catalytic activity compared to RAF homodimers or monomers (Rushworth et al., 2006). ERK phosphorylation of CRAF is able to inhibit its interaction with RAS, providing another mechanism through which ERK can downregulate RAF activity (Dougherty et al., 2005). Finally, phosphorylation of SOS, the RAS guanine exchange factor, inhibits its

interaction with GRB2 and prevents its recruitment to the plasma membrane. This leads to reduced RAS activation and downstream phosphorylation of ERK.

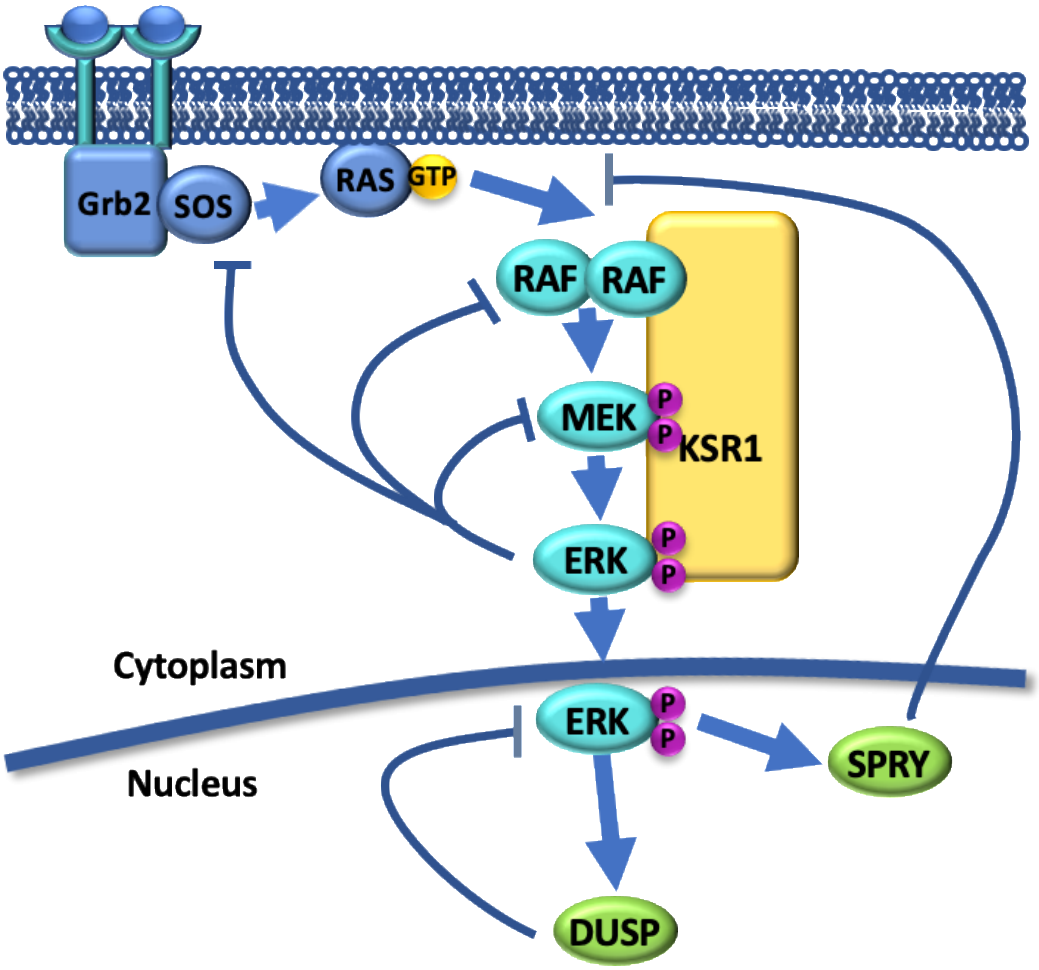

Figure 1.4. Regulation of ERK by negative feedback controls. Multiple negative feedback loops are responsible for fine-tuning ERK pathway output. ERK can phosphorylate and inhibit MEK1, RAF, KSR1, SOS and some RTKs to diminish further ERK activation. Induction of the negative regulator Sprouty (SPRY) acts to inhibit RAS activity while DUSP (MKP). expression leads to direct dephosphorylation of ERK.

Not only can active ERK exert direct control of its upstream activators, but it also induces the expression of various downstream regulators of ERK signalling. These include the Sprouty (SPRY) family members, whose transcription has been shown to be mediated by MEK activity (Lake et al., 2016; McKay and Morrison, 2007). Upon activation, Sprouty proteins are able to translocate to the cell membrane and sequester the GRB/SOS complex thus preventing RAS activation (Hanafusa et al., 2002). Sprouty proteins have also been implicated in preventing RAF phosphorylation through their interaction with the RAF catalytic domain (Sasaki et al., 2003).

Dephosphorylation and inactivation

The feedback mechanisms described above serve to attenuate signalling upstream of ERK, thereby reducing further ERK phosphorylation and activation. However, another more direct form of negative regulation is exerted quite simply through dephosphorylation and deactivation of ERK. As ERK requires phosphorylation of both threonine and tyrosine in its conserved T-E-Y motif, dephosphorylation of either residues by Ser/Thr phosphatases, protein tyrosine phosphatases or dual-specificity protein phosphatases (DUSPs), is sufficient to inactivate the kinase. Two well-known Ser/Thr phosphatases that have been shown to inactivate ERK are PP2A and PP2C (Alessi et al., 1995), while tyrosine phosphatases STEP and PTP-SL have both been shown to bind and dephosphorylate ERK in vitro (Pulido et al., 1998).

By far the most predominant and well-established enzymes capable of dephosphorylating MAP kinases such as ERK, are the extensive family of dual-specificity MAPK phosphatases (MKPs) that are solely dedicated to the regulation of their target MAP kinases. MKPs that are able to target ERK are commonly induced by ERK pathway signalling. This forms an auto-regulatory negative feedback loop that acts to restrain ERK responses in a manner that is temporally distinct from more immediate forms of ERK inactivation (Caunt and Keyse, 2013). Additionally, MKPs can act as nuclear or cytoplasmic tethers, thereby controlling the spatial distribution of ERK within the cell (Karlsson et al., 2006). Through these and other mechanisms, MKPs are able to co-ordinate the magnitude, duration and localisation of active ERK and constitute a unique and dynamic form of ERK regulation (Owens and Keyse, 2007).

1.3. Dual-specificity phosphatases/MAPK phosphatases (MKPs)

1.3.1. Structural and functional classification of MKPs

The prominent role of MKPs in dephosphorylating mammalian MAPKs has been strengthened with the identification and characterisation of ten catalytically active MKPs in mammalian cells (Camps et al., 2000; Theodosiou and Ashworth, 2002). These MKPs can be divided into three subfamilies based on sequence homology, subcellular localization and substrate specificity. DUSP1, DUSP2, DUSP4 and DUSP5 form the inducible nuclear MKPs, while DUSP6, DUSP7 and DUSP9 are ERK-specific, cytoplasmic MKPs. DUSP8, DUSP10 and DUSP16 are JNK/p38-specific phosphatases and are located both in the nucleus and cytoplasm (Figure 1.5) (Caunt and Keyse, 2013). The nuclear MKPs DUSP1, DUSP2 and DUSP4 and cytoplasmic MKP DUSP9 are able to target all three major MAPKs, ERK, p38 MAPK and JNK, however DUSP9 preferentially acts on ERK. DUSP7 is able to bind and dephosphorylate JNK, however also preferentially targets ERK (Kondoh and Nishida, 2007). Uniquely, DUSP5 shows exquisite specificity for ERK and has not been shown to act on any other MAPKs *in vitro* (Kucharska *et al.*, 2009). While DUSP6 can associate with JNK and p38 MAPK, it shows substantially higher catalytic activity towards ERK, and is considered ERK-specific (Arkell et al., 2008; Groom et al., 1996; Karlsson et al., 2004).

MKPs share a common protein structure; an N-terminal regulatory domain and a C-terminal catalytic domain, which contains the conserved phosphatase active site sequence. The N-terminal region contains the MKP “D domain” or kinase interaction motif (KIM), which interacts with the common docking (CD) site on the MAPK (Theodosiou and Ashworth, 2002). Also present in the N-terminus are subcellular localisation signals for those MKPs constrained to either the nucleus or the cytoplasm (Figure 1.5) (Owens and Keyse, 2007).

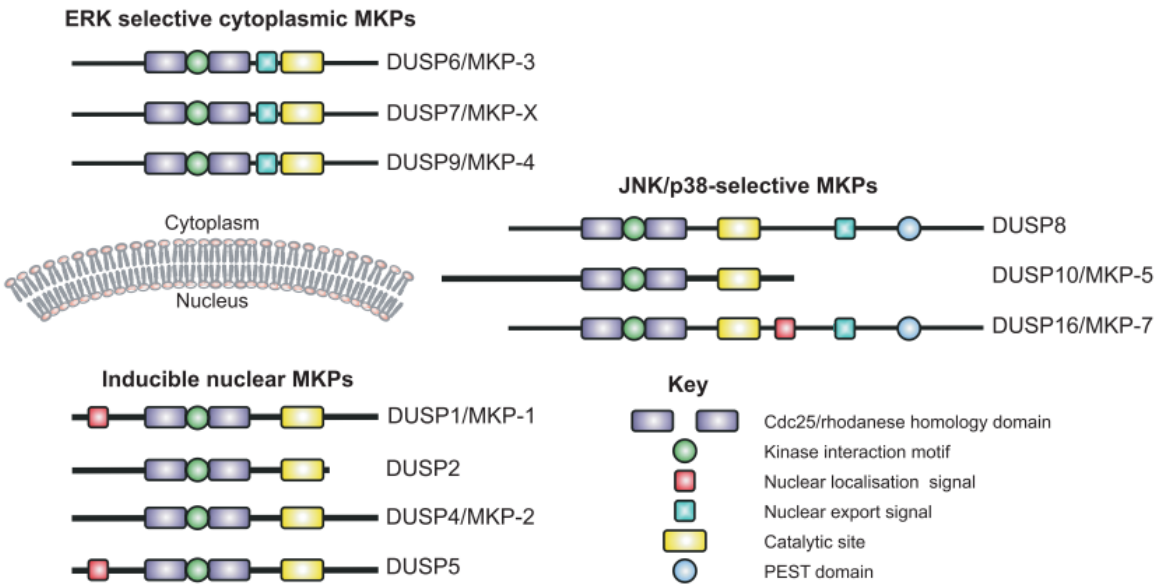

Figure 1.5. Classification, localization and domain structure of the MKPs. The three major groups of MKPs can be grouped according to their localisation, substrate specificity and sequence homology. This figure was adapted from Caunt and Keyse (2013) with permission from FEBS Journal.

All MKPs share a structurally and functionally similar catalytic domain, which contains the consensus cysteine-dependent tyrosine phosphatase active site sequence, I/VHCXAGXXR (Camps et al., 2000). The catalytic site is comprised of an active site loop which encompasses the catalytic cysteine and arginine residues and a general acid loop within which a highly conserved aspartate residue lies (Farooq and Zhou, 2004). The thiolate anion of the catalytic cysteine residue initiates dephosphorylation of either tyrosine or threonine on the substrate MAPK through a nucleophilic attack of the phosphorus atom and the formation of a MKP cysteinyl-phosphate intermediate (Figure 1.6). This is promoted by the conserved arginine residue which co-ordinates the phosphate molecule through electrostatic interactions and the general acid loop aspartate residue which donates a proton to the phosphate oxygen atom (Figure 1.6) (Farooq and Zhou, 2004). Thus, transient binding of phosphate to the MKP cysteine residue allows the release of the dephosphorylated MAPK. After catalysis, the conserved aspartate residue accepts a proton from a water molecule and forms a hydroxyl anion. This anion subsequently attacks the phosphorus atom in the cysteinyl-phosphate bond and facilitates the release of inorganic phosphate and the reformation of cysteines thiolate anion (Figure 1.6) (Farooq and Zhou, 2004).

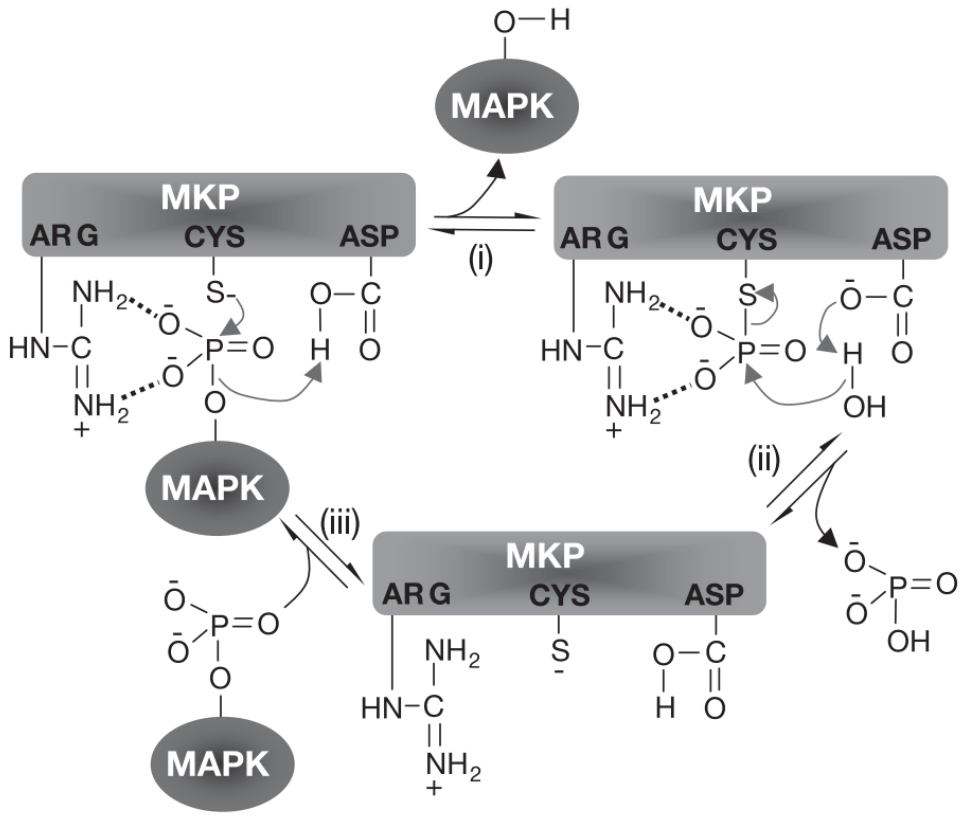

Figure 1.6. The catalytic dephosphorylation of a MAPK substrate by an MKP. Conserved arginine (Arg), cysteine (Cys) and aspartic acid (Asp) residues direct the formation of a transient phospho-MKP intermediate and the release of dephosphorylated MAPK. This figure was adapted from Farooq and Zhou (2004) with permission from Cellular Signalling, Elsevier.

While the C-terminal catalytic domain is conserved across all MKPs, both distinct and subtle variations in the modular N-terminal domains have been shown to direct differing MKP subcellular locations and substrate interactions (Owens and Keyse, 2007). The discovery of a canonical leucine-rich nuclear export signal (NES) in the N-terminal domain of DUSP6 and related MKPs DUSP7 and DUSP9, and experiments that showed that nuclear export mediated by the exportin-1 protein was required for the cytoplasmic retention of DUSP6, revealed a likely mechanism that controls the spatial distribution of these cytoplasmic MKPs (Caunt and Keyse, 2013; Karlsson et al., 2004). In contrast, the nuclear MKPs DUSP1 and DUSP5 both contain noncanonical nuclear localisations signals (NLS) in their N-terminal regions, and these sequences have been shown to be responsible for their nuclear targeting (Mandl et al., 2005; Wu et al., 2005). The N-terminal region is also home to the cdc25/rhodonese

homology domains. While these are highly conserved across MKPs, their regulatory function is yet to be formally demonstrated, however it is believed they may contribute to substrate binding (Theodosiou and Ashworth, 2002).

Imperative for MAPK binding is the MKP KIM domain. Similar to D domains in other MAPK target proteins, the KIM is comprised of a cluster of positively charged arginine residues, which have been proposed to interact with cognate negatively charged aspartic acid residues within the CD domain of the MAPK (Nichols et al., 2000; Tanoue et al., 2000). Further investigation of the MKP KIM domain revealed a second motif of positively charged amino acids flanked by hydrophobic residues, which has also been shown to interact with MAPK CD residues upon binding (Tanoue et al., 2002, 2001). Together these motifs comprise modular binding domains and variations in the number, relative position and type of residues within them have been posited to underpin the specificity of MAPK targeting (Owens and Keyse, 2007).

The detailed biochemical characterisation of ERK2 and DUSP6 binding led to the discovery that DUSP6 is catalytically activated upon its association with ERK2 (Camps *et al.*, 1998). This followed experiments that showed a 40-fold increase in DUSP6 catalytic activity in the presence of ERK2, which was independent of kinase activity (Camps *et al.*, 1998). Structural studies later showed that ERK2-DUSP6 binding caused a conformational change in the active site of DUSP6, such that the general acid loop containing the catalytic aspartate residue was flipped towards the catalytic arginine and cysteine residues, where it had previously faced the other way (Zhou and Zhang, 1999). Catalytic activation upon MAPK binding was also found to occur in DUSP1, DUSP4 and DUSP2 and has been proposed to enhance substrate selectivity, however, it does not occur in all MKPs (Owens and Keyse, 2007). As monomers, DUSP5 and DUSP10 have optimally orientated general acid loop arginine residues in their catalytic domains, and their catalytic activity is not increased through substrate binding (Jeong et al., 2006; Tanoue et al., 1999). These studies demonstrate the biological significance of structural and functional variations within the MKP family. The existence of this heterogeneity and its impact on distinct spatial and substrate targeting suggests non-redundant functions for individual MKPs.

Indeed, several MKPs have been implicated in diverse physiological processes and show wide tissue distribution (Camps et al., 2000). The nuclear MKPs DUSP1,

DUSP2, DUSP4 and DUSP5 are typically induced by growth factors or stress signalling and have been shown to play key roles in innate and adaptive immunity as well as metabolic homeostasis, cardiovascular development and neuronal differentiation (Seternes et al., 2019). DUSP6, the most extensively studied cytoplasmic MKP, has also been implicated immunity and inflammatory responses (Bertin et al., 2015; Hsu et al., 2018) as well as metabolic homeostasis (Feng et al., 2014; Wu et al., 2010) and embryo development (Eblaghie et al., 2003; Li et al., 2007). The physiological functions of the remaining MKPs are not as well established however DUSP9 has been shown to play a role in metabolic function (Fukuda et al., 2012; Ye et al., 2019), while the JNK and p38 MAPK-specific MKPs DUSP8, DUSP10 and DUSP16 appear to participate in immune function (Muda et al., 1996; Zhang et al., 2015, 2004).

1.3.2. Regulation of DUSP/MKPs

In general, MKPs are induced by MAPK signalling and outside of this, their basal levels remain low (Caunt and Keyse, 2013). While most MKPs appear to be regulated transcriptionally, the mechanisms of this control have only been characterised in the context of specific signalling responses. Multiple studies have shown the transcriptional upregulation of several MKPs to be regulated by ERK signalling and well-established downstream transcription factors such as ETS-1 and ETS-2, Elk1, c-jun and CREB (Buffet et al., 2015; Huang and Tan, 2012; Nunes-Xavier et al., 2010; Zhang et al., 2010). In addition to this, the expression of several MKP genes have been shown to be regulated by epigenetic modifications (Tebbutt et al., 2018; Waha et al., 2010).

Once expressed, the protein levels of MKPs are tightly regulated by post-translational modifications, some of which lead to protein stabilisation or subsequent degradation (Caunt and Keyse, 2013). In general, this regulation controls an approximate half-life of 1 hour in many MKPs (Brondello et al., 1999; Katagiri et al., 2005; Marchetti et al., 2005). Interestingly, ERK-mediated phosphorylation is a common mechanism in MKP regulation and can form part of positive or negative feedback loops between ERK and its MKP targets (Caunt and Keyse, 2013). The ERK-mediated phosphorylation of DUSP16, DUSP1 and DUSP4 leads to increased protein stability in DUSP1 and DUSP4 and an increased half-life in DUSP16 (Brondello et al., 1999; Cagnol and Rivard, 2013; Katagiri et al., 2005). In contrast, ERK-mediated phosphorylation can also lead to decreased half-life of DUSP1 (Lin et al., 2003) and proteasomal degradation in DUSP6 (Marchetti et al., 2005).

1.3.3. Regulation of MAPKs by DUSP/MKPs

A number of mechanisms have been proposed as key regulatory functions of MKPs in relation to their MAPK substrates. MKPs that are induced by the MAPKs they subsequently target participate in direct negative feedback loops with their MAPK substrates. This form of autoregulatory feedback exists between DUSP5, DUSP6 and their singular target, ERK and is temporally distinct from more immediate forms of down-regulation present upstream of ERK-induced transcription. Autoregulatory feedback may therefore be most important in the context of sustained ERK signalling (Caunt and Keyse, 2013). While less common, the constitutive expression of MKPs has been demonstrated in some contexts and could confer an alternate form of negative regulation. While the down-regulation of MAPKs by inducible MKPs is not likely to constitute an immediate form of negative feedback, MKPs that are present prior to MAPK activation could inactivate or sequester their targets during any signalling phase (Camps, *et al.*, 1998; Bhalla, Ram and Iyengar, 2002). A similar scenario could occur with inducible MKPs that are still present when subsequent signals are fired. In this way cells could retain a signalling “memory” of prior stimulations that are able to influence successive signals (Caunt and Keyse, 2013).

Intrinsic to the regulatory potential of MKPs, is their ability to bind both phosphorylated and dephosphorylated MAPK forms with high affinity (Karlsson et al., 2004; Mandl et

al., 2005). Together with the propensity of many MKPs to remain in either the cytoplasm or nucleus, this allows for the retention of their MAPK targets in either cellular compartment. The subcellular retention of MAPKs may have both positive and negative consequences on further MAPK signalling and could act to sequester MAPKs away from their upstream activators, or indeed concentrate them in regions where subsequent signals could lead to rapid reactivation (Caunt and Keyse, 2013; Karlsson et al., 2006).

In addition to their dynamic roles as feedback regulators and subcellular anchors various MKPs appear to be important mediators of crosstalk between different MAPK pathways. In particular, DUSP1, which is induced by either ERK or p38 MAPK (Brondello et al., 1997; Staples et al., 2010) appears to preferentially target JNK (Slack et al., 2001) and has been shown to circumvent JNK-induced apoptosis in fibroblasts (Staples et al., 2010) and neuron differentiation (Jeanneteau et al., 2010). In this way, activation of DUSP1 by either ERK or p38 MAPK is able to reduce signalling in parallel pathways. Through the implementation of these and other regulatory mechanisms, MKPs do not simply act as “on/off” switches in their function as MAPK regulators, but rather as dynamic feedback mediators that regulate MAPK signal magnitude, duration, localisation and crosstalk.

1.3.4. ERK-specific MKPs DUSP6 and DUSP5

Unlike their subfamily members, DUSP5 and DUSP6 are unique in their sole dedication to catalytic dephosphorylation of ERK. In addition to this, both DUSP5 and DUSP6 expression is dependent on ERK signalling and as such, they serve as classical negative feedback regulators of the ERK pathway. These regulatory functions, together with their ability to bind and anchor dephosphorylated ERK in the nucleus or cytoplasm are likely to confer prominent roles for DUSP5 and DUSP6 in the regulation of ERK activity and localisation.

Initially, DUSP6 appeared to target multiple MAPK substrates, however it is now apparent that DUSP6 shows little catalytic activity towards p38 MAPK, JNK or ERK5 (Arkell et al., 2008; Groom et al., 1996). This could in part be due to the disorientation of the DUSP6 catalytic site prior to ERK binding (Camps *et al.*, 1998). While DUSP6 function has been shown to be constitutive in some contexts, its expression has predominantly been associated with growth factor-induced ERK. ERK is able to promote DUSP6 transcription through its targets ETS-1 and ETS-2, which bind to conserved *DUSP6* promoter regions (Ekerot et al., 2008; Li et al., 2007; Nunes-Xavier et al., 2010; Zhang et al., 2010). As mentioned, the nuclear export of DUSP6 is mediated by its NES region and the exportin-1-dependent nuclear export pathway. While DUSP6 is capable of shuttling between the nucleus and the cytoplasm, its NES directs its cytoplasmic location, where it is able to retain bound ERK (Karlsson et al., 2004).

Multiple studies have demonstrated that the expression of DUSP5 leads to the inactivation and nuclear accumulation of ERK, a phenomenon that is coincident with prolonged exposure to growth factor simulation (Volmat *et al.*, 2001; Mandl, Slack and Keyse, 2005; Kucharska *et al.*, 2009; Buffet *et al.*, 2015). The upregulation of DUSP5 appears to be mediated by ERK-targeted transcription factors such as Elk-1, that bind to distinct sequences in the promoter region of the *DUSP5* gene (Buffet et al., 2015). Once expressed, the accumulation of DUSP5 protein is regulated by rapid proteasomal degradation. This degradation may be influenced by stable association of DUSP5 with ERK, which was shown to enhance the half-life of DUSP5. Interestingly, phosphorylation of DUSP5 by ERK does not affect its stability (unlike several other MKPs) and the biological relevance of this post-translation modification is unclear (Kucharska *et al.*, 2009).

In response to serum and growth factors, the nuclear accumulation of dephosphorylated ERK has also been associated with nuclear DUSP2 and DUSP4 proteins in addition to DUSP5 (Caunt *et al.*, 2008a; Caunt *et al.*, 2008b), however the limited tissue distribution of DUSP2 may indicate that it is not critical for the nuclear regulation of ERK in many biological contexts. It is currently unclear how DUSP4 and DUSP5 may co-operate or indeed alternate in their roles as modulators of nuclear ERK activity, however recent studies in MEF cells derived from DUSP5 knockout mice

indicate that DUSP5 may have a non-redundant function in the control of ERK signalling duration and localisation (Kidger et al., 2017). Using vectors containing an ERK-responsive EGR1 immediate early gene promoter to drive DUSP5-Myc expression, the authors showed that the inactivation and anchoring of ERK in the nucleus could cause a paradoxical increase in cytoplasmic ERK activity, which may result from reduced negative feedback from active ERK to RAF (Kidger et al., 2017). It is unclear how other MKPs like DUSP4 and DUSP6 may influence this response, but this and other mechanisms are likely to form part of a complex and context-dependent system of ERK regulation.

The discovery and characterisation of multiple tiers of negative ERK regulation has led to the understanding that RAF/MEK/ERK signalling output is largely dependent on the balance of opposing positive and negative regulatory mechanisms. This implies that robust signalling is critical for the faithful delivery of numerous and often conflicting cellular signals. This fine balance of upstream and downstream ERK pathway activity is especially critical for navigating biological decisions in cells that are close to cell fate boundaries. The next section details multiple examples of ERKs pivotal role in determining cell fate.

1.4. ERK in the determination of cell fate

1.4.1. ERK substrates

Like its protein kinase relatives, the fundamental structure of the ERK protein is optimised for specific and efficient substrate binding and catalysis. In addition to the core catalytic domains described previously (Figure 1.1) the ERK protein structure consists of multiple regulatory and binding motifs. The docking groove, which binds a D domain or kinase interacting motif (KIM) in many MAPK substrates is comprised of the common docking (CD) domain and Glu-Asp (ED) pockets (Tanoue et al., 2001, 2000). Variations in the number of positively charged residues and hydrophobic regions in the D domains of MAPK targets contribute to the specificity of substrate binding between different MAPKs and the resulting docking interactions increase the efficiency of catalytic protein interactions (Jacobs et al., 1999; Tanoue et al., 2000). In a number of ERK targets a second docking site has been identified and is referred to as the DEF domain. These domains are generally comprised of a Phe-Xaa-Phe-Pro sequence near the phosphoacceptor site of the substrate and bind specifically to a DEF-binding pocket adjacent to the catalytic site of ERK (Jacobs et al., 1999).

A proteomics screen performed by von Kriegsheim *et al.* (2009) revealed at least 270 ERK-interacting proteins. Far fewer ERK-substrate interactions have been well characterised, however they still comprise a diverse and extensive list (Table 1.1). In general ERK has been shown to phosphorylate and or associate with multiple transcription factors, protein kinases, signalling receptors, cytoskeletal proteins, phosphatases and numerous other proteins in both the nucleus and cytoplasm (Yoon and Seger, 2006). It is through the activation or repression of these varied targets that ERK is able to exert its regulatory influence on multiple cell fate decisions. Of these, ERK is best known for its central role in cell cycle progression.

Table 1.1. Substrates of ERK. This table was adapted from Lu and Xu, 2006, with permission from Life.

Transcription factors	Kinases and phosphatases	Cytoskeletal proteins	Signaling proteins	Apoptotic proteins and proteinases	Other proteins
AML1 (RUNX1)	DAPK	Annexin XI	EGFR	Bad	Amphiphysin 1
Androgen receptor	ERK1/2	Caldesmon	ENaCβ/γ	Bim-EL	CPSII/CAD
ATF2	FAK1	Calnexin	Fe65	Calpain	CR16
BCL6	GRK2	CENP-E	FRS2	Caspase 9	GRASP55
BMAL1	Inhibitor-2	Connexin-43	Gab1	EDD	GRASP65
CBP	Lck	Cortactin	Gab2	IEX1	HABP1
C/EBPβ	MAPKAP3	Crystallin	GAIP	MCL-1	Histone H
CRY1/2	MAPKAP5	DOC1R	Grb10	TIS2	HnRNP-K
E47	MEK1/2	Dystrophin	IRS1	TNFR CD120a	KIP
Elk1	MKP1/2	Lamin B2	LAT		MBP
ER81	MKP3	MAP1	LIFR		PHAS-I (4E-BP1)
ERF	MKP7	MAP2	MARCKS		CPLA2
Estrogen receptor	MLCK	MAP4	Naf1α		Rb
c-Fos	MNK1/2	MISS	PDE4		SAP90/PSD95
Fra1	MSK1/2	NF-H	PLCβ		Spinophilin
GATA1/2	PAK1	NF-M	PLCγ		Topoisomerase II
HIF1α	PTP2C	Paxillin	Potassium channel Kv 4.2		Tpr
HSF1	Raf1	Stathmin	KSR1		TTP (Nup47)
ICER	B-Raf	SWI/SNF	Rab4		Tyrosine hydroxylase
c-Jun	RSK1-4	Synapsin 1	SH2-B		Vif
Microphthalmia	S6K	Tau	ShcA		Vpx
c-Myc	Syk	Vinexin β	Sos1		
N-Myc			Spin90		
Net (Sap2)			TSC2		
NFATc4					
NF-IL6					
NGFI-B/TR3/Nur77					
Pax6					
PPARγ					
P53					
Progesterone receptor					
RNA Pol. II					
PUNX2					
Sap1					
Smad1					
Smad2/3					
SP1					
SRC1					
SREBP1/2					
STAT1/3					
STAT5a					
TAL1/SCL					
TFII-I					
TFIIIB					
TGIF					
TIF1A					
Tob					
UBF					

1.4.2. ERK in the promotion of cell cycle progression

The cell cycle is a tightly controlled process that is primarily regulated by a family of cyclin-dependent kinases (CDKs) and their cognate cyclins. A key regulatory step in the cell cycle occurs at the transition from Gap 1 (G_1-) phase to the DNA synthesis (S-phase), where cells commit to cell cycle entry and subsequent DNA replication and division. In response to mitogenic signals this transition is driven by an accumulation of D-type cyclins, which bind and activate their catalytic partners Cdk4 and Cdk6 (Bertoli et al., 2015). Active Cdk4 and 6 are able to phosphorylate and inactivate retinoblastoma protein (RB), a critical cell cycle repressor. Prior to S-phase, RB is bound to E2F, a transcriptional activator of a number of cyclins, CDKs and check point regulators. Once inactivated, RB releases E2F which is now free to mediate the transcription of numerous genes necessary for entry into S-phase (Harbour & Dean, 2000). Specifically, these genes include Cdc6, cyclin E and CDK2 as well as DNA polymerase α, proliferating cell nuclear antigen (PCNA), ribonucleotide reductase and others (Leone *et al*., 1998).

ERK has been described as the 'master regulator' of the G_1- to S-phase transition (Meloche and Pouysségur, 2007). This is due to the discovery that sustained ERK activation throughout G_1-phase is required for successful S-phase entry *(*Meloche *et al*., 1992; 1995; Yamamoto *et al.*, 2006) and the numerous mechanisms through which ERK impinges on the cell cycle. ERK expression has been shown to promote the transcription and accumulation of Cyclin D1 during G1-phase through activation of the transcription factors ETS and AP-1 and inactivation of a transcriptional repressor of Cyclin D1, Transducer of ERBB2 (TOB) (Meloche and Pouysségur, 2007). Some studies have demonstrated that in addition to these mechanisms, ERK can influence the expression of Cyclin D1 at the post-transcriptional level by promoting the nuclear export and stabilisation of Cyclin D mRNA (Rousseau et al., 1996). Another cell cycle-related ERK target is c-myc, a transcription factor that plays a critical role in cell cycle progression through its ability to promote or repress important cell cycle regulators (Sears et al., 2000). Targets of c-myc include Cyclin D2 (Bouchard et al., 1999), Cdk4 (Hermeking et al., 2000) and $p21^{CIP1}$ (Claassen and Hann, 2000). ERK has been shown to directly phosphorylate c-myc, which enhances protein stability.

In addition to the promotion of positive cell cycle regulators, continuous ERK expression has been shown to downregulate anti-proliferative genes throughout G_1-phase, such as *Tob1,* which encodes a transcriptional repressor of Cyclin D1, and the pro-apoptotic transcription factor gene *Ddit3* (Yamamoto et al., 2006). ERK expression has also been linked indirectly to multiple other cellular processes required for cell proliferation, including the synthesis of pyrimidine nucleotides (Graves et al., 2000), chromatin remodelling (Soloaga et al., 2003), transcription of ribosomal RNA genes (Stefanovsky et al., 2006) and protein translation (Waskiewicz et al., 1999).

1.4.3. ERK in cell survival and apoptosis

Another major cell fate decision influenced by ERK regulation is whether to continue surviving or alternatively, commit to programmed cell death or apoptosis. Apoptosis can occur through either the extrinsic or intrinsic cell death pathway, the latter of which is induced by internal stress signals and is largely governed by the BCL2 protein family (Sale and Cook, 2013). The BCL2 proteins control the integrity of the outer mitochondrial membrane (OMM), a central determinant of cell survival (Jin and El-Deiry, 2005). During the initiation of apoptotic program, pro-apoptotic cellular signals promote permeabilization of the OMM (referred to as MOMP) which releases various intermembrane proteins into the cytosol. Cytochrome c release from the intermembrane space is a critical step in apoptosis initiation as this small hemeprotein is able to bind and promote the oligomerisation of APAF1, a key component of the apoptosome. The apoptosome is then able to activate caspase-9 a cysteine protease, which goes on to activate other caspase family members caspase-3 and caspase-7. These executioner caspases are responsible for the cleavage of various cellular substrates which ultimately leads to cell death (Pop and Salvesen, 2009).

The BCL2 family members can be divided into two classes; those that promote apoptosis such as BAX and BAK and the BH3-only proteins BIM, BID, NOXA, BMF and PUMA, and those that promote cell survival, such as BCL2, BCL-X_L and MCL1 (Chipuk *et al.*, 2010). The balance between this pro-apoptotic and anti-apoptotic or pro-survival BCL2 family members determines the fate of the cell. In healthy cells, there is an excess of pro-survival proteins which associate with the OMM and inhibit pro-apoptotic effector proteins such as BAX and BAK (Chipuk et al., 2010). When

apoptosis is induced, BH3-only proteins are able to target pro-survival proteins and displace effector proteins BAX and BAK, resulting in the activation of MOMP. Additionally, some pro-apoptotic BH3-only proteins can directly activate BAX and BAK (Chipuk et al., 2010).

ERK has been shown to directly or indirectly influence the expression or function of at least six BCL2 family members. In general, ERK promotes cell survival by repressing pro-apoptotic BH3-only proteins and positively regulating pro-survival BCL2 proteins. A repressive effect of ERK on BMF and PUMA BH3-only proteins has been demonstrated in ERK inhibition studies, where these pro-apoptotic proteins are significantly upregulated (Sale and Cook, 2012). The mechanism through which ERK disrupts BMF expression is unclear but may involve direct BMF phosphorylation (Shao and Aplin, 2012) and/or cellular translocation (VanBrocklin et al., 2009). It has been suggested that active ERK may downregulate PUMA expression through its target FOXO3, a transcriptional activator of PUMA (Sale and Cook, 2013). Indeed, ERK-mediated phosphorylation and subsequent degradation of FOXO3 (Yang et al., 2008) may contribute to ERKs' regulatory control of the most abundant isoform of BIM, BIM_{EL}. Like with PUMA, FOXO3 is a transcriptional activator of BIM_{EL} and therefore its degradation is likely to repress BIM_{EL} expression (Dijkers et al., 2000). In addition to transcriptional regulation of BIM_{EL}, ERK is able to directly phosphorylate the BIM_{EL} protein, which ultimately leads to its degradation (Ley et al., 2003). BAD, a third pro-apoptotic BH3-only protein, is also regulated by ERK-dependent phosphorylation (Scheid et al., 1999) which is catalysed by two well-known ERK substrates, RSK and MSK1 (She et al., 2002).

In contrast to its negative regulation of pro-apoptotic BCL2 family members, ERK signalling promotes the transcription of pro-survival proteins BCL2, BCL-X_L and MCL1 (Sale and Cook, 2013). This is mediated by RSK and MSK kinases, both targets of ERK, which activate the cAMP responsive element binding protein (CREB), a transcriptional activator that promotes BCL2, BCL-X_L and MCL1 expression (Bonni et al., 1999; Boucher et al., 2000). ERK can also upregulate MCL1 expression through the Elk1 transcription factor (Domina et al., 2004), as well as stabilise its protein structure through phosphorylation (Townsend et al., 1999). Interestingly, in addition to these pro-survival BCL2 proteins, ERK signalling has been shown to induce the

upregulation of a pro-apoptotic BH3-only protein, NOXA. This too is likely to be through ERK-directed activation of CREB, which may bind a CREB-binding site in the 5'-UTR region of NOXA (Elgendy et al., 2011; Liu et al., 2014; Sheridan et al., 2010). The biological function of this seemingly opposing regulation of NOXA in normal cells is unclear, but does appear to be particularly relevant in oncogenic contexts where ERK hyperactivation can have anti-proliferative effects (Cook et al., 2017; Elgendy et al., 2011).

More commonly, ERK positively regulates oncogenesis and is implicated in many, if not all of the major processes involved in cancer development. This is most likely due to ERKs' pivotal role in determining cell fate (Dhillon et al., 2007; Deschênes-Simard et al., 2014).

1.5. ERK signalling in cancer

1.5.1. RAS and RAF oncogenes

Cancer is a disease that is characterized by a set of defining features that lead to uncontrolled cell division and the formation of tumours. Most prominent of these features are their ability to sustain proliferative signalling, evade growth suppression and resist apoptosis (Hanahan and Weinberg, 2011). The ERK signalling pathway regulates many of these events and as such, has long been implicated in tumorigenesis (Dhillon *et al*., 2007; Deschênes-Simard *et a*l., 2014; Torii *et al*., 2006).

Abnormalities in ERK signalling pathways have been detected in a variety of human cancers with oncogenic mutations in *RAS* and *RAF* being especially frequent (Davies et al., 2002; Deschênes-Simard et al., 2014; Dhillon et al., 2007). *RAS* has an overall mutation incidence of up to 30% in all human tumours making it among the most common human oncogenes (Deschênes-Simard *et al*., 2014). Oncogenic mutations in *RAF*, although somewhat less frequent overall (8% of all human tumours) are found in a staggering 66% of malignant melanomas (Davies *et al*., 2002). In general, these mutations lead to constitutive activation of the respective proteins, resulting in increased signalling output through downstream ERK kinases (Dhillon *et al.*, 2007).

Mutant forms of the KRAS, NRAS and HRAS family members in various cancers have been frequently discovered over the last 30 years. Of the RAS isoforms, KRAS is the most commonly mutated (more than 20% of all human cancers), followed by NRAS (8.0%) and HRAS (3.3%) (Samatar and Poulikakos, 2014). Single base mutations that lead to oncogenic RAS isoforms are invariably found at codons 12, 13 or 61 and affect GTP hydrolysis, such that RAS remains in a GTP-bound, constitutively active state (Karnoub and Weinberg, 2008; Samatar and Poulikakos, 2014). The high frequency of *RAF* mutations in cancers such as melanoma was more recently discovered (Davies et al., 2002) and typically involves the BRAF isoform. In more than 90% of BRAF-mutant tumours, a single nucleotide substitution of valine to glutamic acid (V600E) in the BRAF activation loop accounts for its oncogenic properties i.e. persistent activation of BRAF catalytic activity (Wan et al., 2004). While *CRAF* and *ARAF* mutations have been identified in human cancers, it is with low incidence, which may be due to the lower basal activity of these RAF isoforms relative to BRAF, as well as the increased

complexity of their activation (Samatar and Poulikakos, 2014). Oncogenic forms of other signalling components of the ERK pathway such as MEK1 and MEK2 have been detected in various cancers, albeit at a much lower frequency (Caunt *et al.*, 2015). The high incidence of oncogenic RAS and RAF mutants in numerous cancers suggests that the RAS-RAF axis can determine the overall activation profile of ERK, a concept that has been confirmed by mathematical modelling (Orton et al., 2005).

The precise mechanisms through which amplified ERK signalling contributes to the development of tumourigenesis are complex, varied and highly context-dependent, however generally rely on ERKs central role in cell cycle entry, cell survival and evasion of apoptosis (Balmanno and Cook, 2009; Torii et al., 2006). Several common mechanisms of oncogenic ERK signalling have been identified in various colorectal cancers (CRCs) and melanomas, where tumourigenesis is often driven by either mutant KRAS or BRAF.

1.5.2. ERK signalling in colorectal cancer and melanoma

Colorectal cancer

Cancer of the colon and/or rectum is the third most common type of cancer worldwide and is the fourth leading cause of cancer-related deaths (Arnold et al., 2017). Colorectal carcinogenesis occurs through multiple steps and involves the prevailing survival and proliferation of abnormal intestinal epithelial cells (Fang and Richardson, 2005). In healthy cells, the ERK signalling pathway is important in the promotion of growth and differentiation of intestinal epithelium, however has been found to be frequently perturbed in colorectal cancer where tumourigenic intestinal cells are able to invade surrounding tissues (Fang and Richardson, 2005).

Increased signalling through the RAF/MEK/ERK pathway has been linked to colorectal cancer for some time and evidence of its tumourigenic relevance lies in the high incidence of RAS and RAF mutants in colorectal cancer patient samples (36% for RAS and 9-11% for RAF) (Andreyev et al., 1998; Davies et al., 2002). Importantly, mutation of RAS or RAF appears to be associated with early stages of carcinogenesis, and is coincident with increased ERK activation, implicating these oncogenes in ERK-mediated tumour initiation (Bos, 1989; Davies *et al.*, 2002; Fang and Richardson,

2005). Studies with ERK pathway inhibitors have illustrated a strong dependency of various CRC lines on high ERK activity for sustained proliferation and survival (Balmanno et al., 2009) and have revealed mechanisms through which ERK could promote colorectal tumourigenesis through the regulation of proliferation (Tetsu and McCormick, 2003) and apoptosis (Wickenden et al., 2008).

Work by Tetsu and McCormick (2003) demonstrated that various colon cancer cell lines enter G_1-arrest following treatment with selective MEK inhibitors. This cell cycle arrest was coincident with striking reductions in cyclin D1 and D3, CDK4 and $p21^{CIP1}$ after 12 hours of MEK inhibition and reductions in cyclin A and E and CDK1 after 48 hours of MEK inhibition. The reduction in CDK4 protein was paralleled by inhibition of CDK4 kinase activity, and subsequent inhibition of CDK4 phosphorylation sites on RB. The authors concluded that growth arrest in colon cancer cells exposed to ERK pathway inhibition was mediated by downregulation of critical effectors of cell cycle progression such as CDK4 (Tetsu and McCormick, 2003). Other work in CRC cell lines investigated the mechanism through which $BRAF^{V600E}$-driven cells were able to evade cell death associated with growth factor withdrawal (Wickenden et al., 2008). In this study, treatment of CRC cell lines with MEK inhibitors led to increased levels of dephosphorylated pro-apoptotic BCL2 protein BIM and subsequent cell death, an event that was reversed by disruption of BIM expression. This provided evidence that the repressive phosphorylation of BIM by active ERK in $BRAF^{V600E}$-driven CRC cells was sufficient to ensure growth factor-independent survival (Wickenden et al., 2008).

Melanoma

The discovery of BRAF mutants in up to 66% of malignant melanomas exposed RAF as a crucial regulator of oncogenic ERK signalling and emphasised the predominant role the ERK pathway plays in this aggressive, potentially lethal form of skin cancer (Davies et al., 2002). The tumourigenic potential of the most common BRAF mutant, $BRAF^{V600E}$, has been validated in a number of *in vitro* and *in vivo* melanoma models (Cartlidge et al., 2008; Dankort et al., 2009; Dhomen et al., 2009). One such model provided insights into a potential mechanism through which $BRAF^{V600E}$-driven ERK signalling could underpin resistance to apoptosis in melanoma cells.

In work performed by Cartlidge *et al*. (2008), the expression of BIM was shown to be important in conditions of trophic factor deprivation in mouse and human melanocytes and serum deprivation in human melanoma cells. Serum deprivation in human melanoma lead to apoptosis, a phenotype that was partially prevented by BIM knockdown. This work went on to show that oncogenic $BRAF^{V600E}$ inhibited BIM expression in these cell models and this inhibition was dependent on MEK and the proteasome. These results suggest that protein degradation of BIM following phosphorylation of ERK may protect melanoma cells from apoptosis in conditions of serum deprivation and thereby constitute a mechanism of resistance to cell death.

1.5.3. ERK pathway inhibitors in cancer treatment

In response to the discovery of the ERK pathway as a prominent cell cycle regulator and the frequent detection of mutant RAS, RAF and other ERK cascade-related oncogenes, the past decade has seen the development of multiple inhibitors of ERK signalling for use in chemotherapeutics (Caunt *et al.*, 2015). Inhibitors of BRAF (BRAFis), vemurafenib and dabrafenib, and inhibitors of MEK (MEKis) trametinib and cobimetinib (GDC-0973) have seen success in clinical use and are approved for the treatment of $BRAF^{V600E/K}$ melanoma (Holderfield *et al.*, 2014; Caunt *et al.*, 2015). The effectiveness of these inhibitors relies in part, on the phenomenon of “oncogene addiction”, where cancer cells become reliant upon specific oncogene-driven pathways for continued survival (Caunt *et al.*, 2015). When these pathways are successfully inhibited, cancer cells can no longer drive proliferation and cell survival signalling. However, the success of these strategies is often marred by the ability of cancer cells to reactivate the pathway upon which they have become reliant. This signalling reprogramming can occur through a number of mechanisms and commonly underlies the development of drug resistance (Sale and Cook, 2014).

Vemurafenib and dabrafenib are highly potent and selective ATP-competitive small molecule BRAF inhibitors and function by circumventing substrate binding. Both compounds preferentially bind active BRAF, which in the absence of stimulation is predominantly comprised of mutant $BRAF^{V600E}$ alone, thereby conferring a high therapeutic index (Holderfield et al., 2014). This specificity has led to success in treating tumours driven by $BRAF^{V600E}$, which are characteristically reliant on

RAF-MEK-ERK signalling (Davies et al., 2002; Holderfield et al., 2014; Joseph et al., 2010). However, in $BRAF^{WT}$ cells as well as cancer cells driven by RAS mutations, BRAF inhibition has been limited by a phenomenon whereby BRAFi causes the paradoxical reactivation of the ERK pathway, which can lead to increased proliferation and tumourigenesis (Heidorn *et al*., 2010; Poulikakos *et al*., 2010; Hatzivassiliou *et al*., 2010; Holderfield *et al*., 2013). Several different mechanisms have been proposed to account for this phenomenon but generally implicate wildtype BRAF and CRAF dimers in the reactivation of ERK. This homo- and hetero-dimerisation may be promoted by BRAFi-induced relief of the BRAF auto-inhibitory mechanism (Holderfield et al., 2013) and/or mediated by a RAS-dependent mechanism (Hatzivassiliou et al., 2010; Heidorn et al., 2010).

Feedback mechanisms have also been implicated in the inferior effectiveness of ERK pathway inhibitors vemurafenib and dabrafenib in colorectal cancers (CRC) harbouring $BRAF^{V600E/K}$ mutations (Corcoran et al., 2012). While these drugs have been associated with improved progression-free and overall survival compared with conventional chemotherapy in $BRAF^{V600E/K}$ melanoma, CRC patients with the same mutation appear to be markedly less sensitive to BRAF inhibition in early clinical trials (Chapman et al., 2011; Corcoran et al., 2015; Flaherty et al., 2010; Hauschild et al., 2012). A study by Corcoran and colleagues (2012) demonstrated that reactivation of ERK appeared to be mediated by EGFR, which was able to activate RAS and induce downstream ERK signalling, despite marked BRAF inhibition. Additionally, BRAF-mutant CRC cell lines appeared to maintain greater levels of EGFR than BRAF-mutant melanoma cell lines, possibly explaining why colorectal cancers are better able to resist ERK pathway inhibition (Corcoran et al., 2012).

Unlike prototypic BRAFis, most MEKis are allosteric inhibitors and bind to a unique pocket near the MEK ATP binding site. As MEK kinases are the sole activators of ERK, they constitute a theoretically ideal target for effecting downstream ERK suppression in both RAS- and BRAF-driven tumours. Unfortunately, like BRAF-inhibitors vemurafenib and dabrafenib, aside from clinical success in BRAF-mutant cancers, the scope of MEKi clinical efficacy has been limited by small therapeutic windows in RAS-mutant cells (where preliminary studies showed the ability of MEKis to successfully inhibit ERK) and the emergence of ERK pathway reactivation in BRAF

wildtype cancer cells and BRAF-mutant colorectal cancers, where the disruption of negative ERK feedback or the action of other feedback regulators such as EGFR drives upstream ERK signalling (Kidger et al., 2018).

Interestingly, combination therapies with MEK inhibitors, BRAF inhibitors and/or EGFR inhibitors have proved very successful and have become the standard of care in patients with $BRAF^{V600E}$-mutated advanced melanoma (Holderfield et al., 2014; Kidger et al., 2018). This is due in part, to their synergistic function in promoting robust inhibition of ERK activation and the ability of MEKis to curtail BRAFi-induced MEK activity (Kidger et al., 2018). Despite the clinical success of these regimes, the development of resistance to both combination and monotherapies appears at present to be unavoidable and invariably leads to disease relapse. The revelation that targeted ERK pathway inhibition frequently leads to the emergence of drug resistance has led to detailed investigations of the mechanisms that underpin this phenomenon. These can include both intrinsic and extrinsic processes and appear to be largely dependent on the specific context of oncogenic signalling.

1.5.4. Drug resistance

Intrinsic and extrinsic mechanisms of drug resistance

Studies have revealed that negative feedback regulators of ERK constitute an important class of signalling proteins that can mediate intrinsic resistance to ERK inhibition (Holderfield *et al.*, 2014; Sale and Cook, 2014; Caunt *et al.*, 2015). In general, the principle of inhibitor-induced ERK pathway reactivation is simple and relies on ERKs powerful and extensive control of signalling attenuation. As discussed previously, the RAF/MEK/ERK pathway is subject to multiple tiers of negative regulation which co-ordinate to restrain ERK activation within biologically relevant thresholds. Many of these negative feedback loops are initiated by active ERK itself, and include downregulation of upstream SOS and RAF, as well as upregulation of Sprouty family members and multiple MKPs. When ERK is successfully inhibited, the activity of various ERK substrates is restored and can inevitably lead to pathway reactivation. This mechanism of ERK reactivation has been observed with the use of a number of MEKis, including AZD6244 (selumetinib) and cobimetinib (Friday *et al*., 2008; Hatzivassiliou *et al*., 2013). Interestingly, some MEKis are able to reduce this

reactivation and as such have been termed “feedback busters” (Caunt *et al.*, 2015; Sale and Cook, 2014). This is due to their ability to reduce the phosphorylation of MEK by RAF by displacing the MEK activation loop (Hatzivassiliou et al., 2013; Lito et al., 2014).

Another mechanism of intrinsic resistance to MEK inhibition has been demonstrated in colorectal cancer (CRC) cell lines exposed to AZD6244. Of a panel of 19 CRC cell lines, those that showed resistance to AZD6244 exhibited low ERK activation or coincident activation of ERK and AKT, a downstream target of the PI3K signalling pathway. These results suggest that the tumour suppressive effects of ERK pathway inhibition can be offset by increased signalling through parallel pro-survival cascades such as the P13K pathway, which like ERK signalling, is activated by RAS (Balmanno et al., 2009).

In addition to mechanisms of innate drug resistance, RAF and RAS-driven cancer cells can become resistant to BRAFis and MEKis through the acquisition of de novo signalling pathway modifications. Such mechanisms can include the emergence of mutations in the drug targets (BRAF or MEK) and the amplification of the driving oncogene through various genetic abnormalities (Sale and Cook, 2014). The latter phenomenon has been thoroughly characterised in colorectal cancer cell lines harbouring mutations in *BRAF* or *KRAS*, where acquired resistance to the MEKi AZD6244 was modelled (Little *et al*., 2011). In this study, drug-resistant BRAF-driven COLO205 and HT29 cell lines and KRAS-driven HCT116 and LoVo cell lines were found to be refractory to AZD6344-induced cell cycle arrest and death. Resistance to targeted inhibition of ERK activation was mediated by intrachromosomal amplification of the respective driving oncogenes, *BRAF* or *KRAS*. The resulting oncogenic upregulation lead to a larger pool of activated MEK, essentially “diluting” the effect of inhibited MEK in the presence of AZD6244. The activity of this MEK was sufficient to induce ERK phosphorylation and subsequent proliferation (Figure 1.7, A and B).

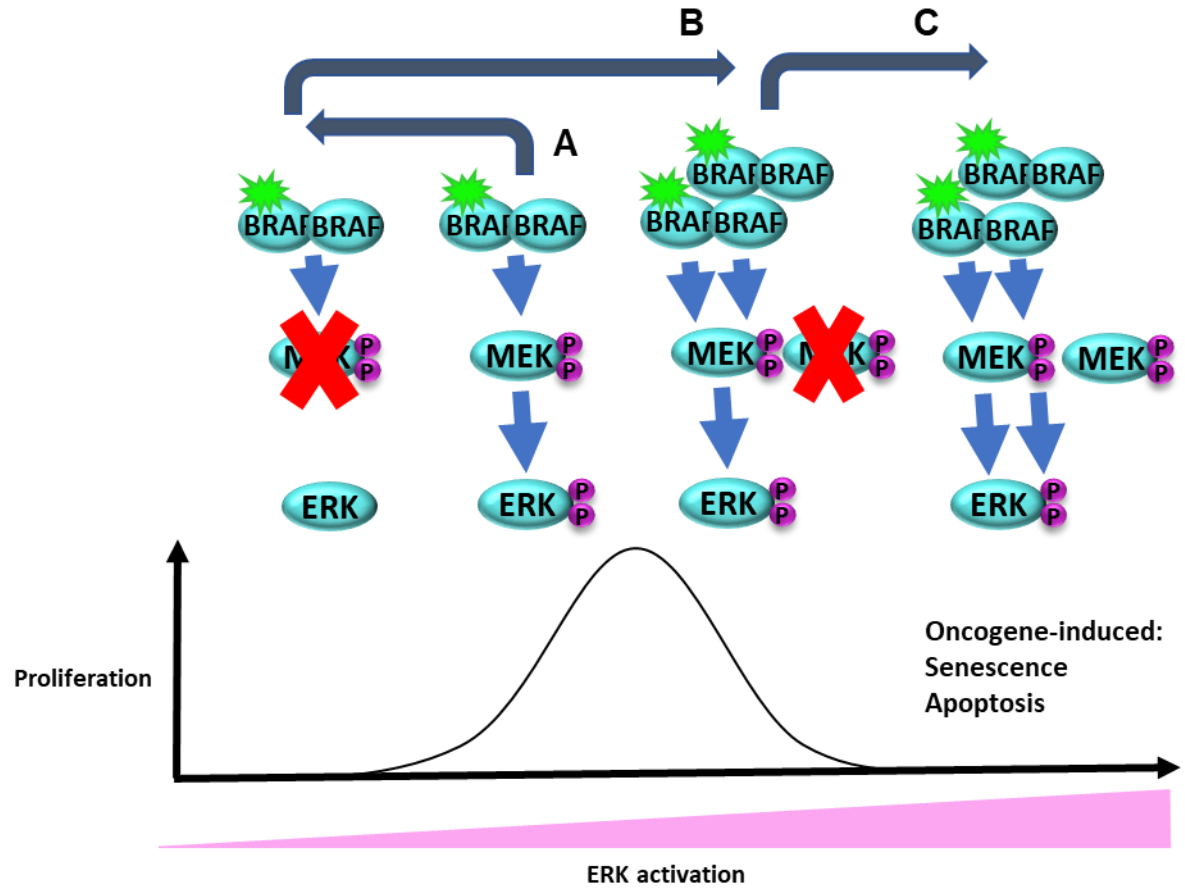

Figure 1.7. The emergence of drug resistance through amplification of the driving oncogene. A) When BRAF-mutant cancer cells are exposed to drug, ERK activation is inhibited and proliferation is reduced. B) Cancer cells reactivate ERK by amplifying the upstream driving oncogene, BRAF, leading to increased proliferation. C) Removing drug from resistant BRAF-driven cells leads to ERK hyperactivation and reduced proliferation.

Combination therapies and drug holidays

A similar mechanism of drug resistance to the RAFi vemurafenib was characterised in primary human melanoma xenograft models (Das Thakur *et al*., 2013). In this model resistant tumours were shown to rely on constitutive ERK signalling driven by elevated $BRAF^{V600E}$ expression. Importantly, this study showed that when the administration of vemurafenib was suspended, drug-resistant tumours began to regress. Coincident with tumour regression was an elevation in phosphorylated- (*p*-)ERK levels and a decrease in proliferation (Figure 1.7 C). These results concur with multiple studies that have shown a correlation between high ERK activity and anti-proliferative effects

(Cagnol and Chambard 2010; Wang *et al*. 2000; Bacus *et al*. 2001; Sewing *et al*. 1997; Woods *et al*. 1997). For instance, apoptosis induced by chemotherapeutic drugs, including cisplatin (Wang *et al*. 2000) and taxol (Bacus *et al*. 2001), is mediated by the induction of high intensity ERK activation and may be prevented using specific inhibitors of ERK signalling.

The discovery of “oncogene-induced senescence” and other anti-proliferative effects of high ERK activity has led to the concept of an ERK “sweet spot” - a narrow range of ERK activation that promotes cell survival and proliferation (Figure 1.7) (Das Thakur *et al*. 2013; Woods *et al*. 1997; Moriceau *et al*. 2015; Shojaee *et al*. 2015). When cellular levels of phosphorylated ERK are too low, they are not sufficient to induce cell cycle entry and proliferation, conversely, when cellular levels of phosphorylated ERK are too high this can lead to senescence and even cell death. This concept is of central importance in the design of specific inhibitors of the ERK pathway, as it suggests that inhibiting ERK may lead to different cellular outcomes depending on the context.

These findings, together with the discovery of multiple intrinsic drug resistance mechanisms highlight the importance of understanding how endogenous signalling pathways may adapt to circumvent changes in cell fate in response to targeted inhibition. They also emphasise the importance of negative regulators of ERK, such as the MKPs, that function to maintain active ERK levels at biologically relevant thresholds.

1.6. ERK-specific MKPs in cancer and drug resistance

Not surprisingly, due to their prominent role in MAPK regulation, MKPs have been shown to play an influential role in cancer progression where MAPK signalling has become deregulated (Seternes et al., 2019). While it may at first seem that MKPs would act as natural tumour suppressors in cancers driven by amplified ERK signalling, insights from various drug-resistance models as well as explicit investigations suggest that the effects of MKP expression in tumourigenesis and drug-resistance are highly context-dependent (Seternes et al., 2019). As such, observations of MKP deregulation in malignant disease has associated both reductions as well as increases in MKP expression with tumour progression (Kidger and Keyse, 2016; Seternes et al., 2019). While much of this work has relied on MKP-overexpression models and historical correlation studies more recent investigations using pharmacological and genetic manipulation of MKP expression in ERK-driven human cancers has provided clear demonstrations of MKP-specific roles in these contexts. For the purpose of this study, we will focus on work that has investigated ERK-specific MKPs.

Studies in pancreatic cancer cell lines (Furukawa et al., 2005, 2003) and lung tumours (Okudela *et al*., 2009) have demonstrated a tumour suppressor role for DUSP6, where DUSP6 expression levels were reduced in more invasive tumours. However in human glioblastoma cell lines, upregulation of DUSP6 conferred an increased propensity of cells to form colonies in agar and increased growth rate, suggesting that DUSP6 may be oncogenic in this context (Messina *et al*., 2011). An oncogenic role for DUSP6 has been demonstrated in other cell cancer models, such as papillary thyroid carcinoma (Degl'Innocenti *et al*., 2013) where DUSP6 overexpression was associated with increased cell migration and invasion and acute lymphoblastoid leukaemia (Shojaee *et al*., 2015). In the latter malignancy, survival and cell growth of human pre-B cells were shown to be dependent on the increased expression of DUSP6 and other negative ERK regulators, which acted to restrain ERK signalling hyperactivation and cell death.

Like DUSP6, DUSP5 has been found to be downregulated in a number of MAPK-driven tumours and cancer cell lines, suggesting that it may confer tumour suppressive effects (Cai et al., 2015; Haigis et al., 2008; Packer et al., 2009; Shin et al., 2013; Vartanian et al., 2013). A *bona fide* tumour suppressor function for DUSP5 was recently demonstrated in a DUSP5 mouse knockout model, where the $HRAS^{Q61L}$ mutation drove skin carcinogenesis (Rushworth *et al*., 2014). In this study, loss of DUSP5 lead to increased sensitivity to HRAS-driven papilloma formation, which was shown to be mediated by an ERK-dependent increase in SerpinB2 expression. In contrast to its anti-tumourigenic role in this model, the retention or overexpression of DUSP5 has been detected in $BRAF^{V600E}$-driven colorectal cancer, melanoma and thyroid cancer suggesting that DUSP5 can have both oncogenic and tumour-suppressive properties (Montero-Conde et al., 2013; Pratilas et al., 2009; Yun et al., 2009).

In addition to its various roles in tumourigenesis, DUSP6 has been shown to influence the sensitivity of different cancers to chemotherapeutic drugs. Downregulation of the ERK-specific DUSP6 has been associated with drug resistant mechanisms in non-small cell lung cancer (NSCLC). Mutations in the epidermal growth factor receptor (EGFR) or expression of a fusion protein, ELM4-ALK, drive tumour development through downstream ERK activation in a large proportion of cases (Lampaki *et al*., 2015; Soda *et al*., 2007; Russo *et al*., 2015). The success of specific inhibitors designed to target EGFR and ALK has been limited by the development of drug resistance, where cells are able to reactivate ERK signalling in the presence of drug. Biochemical analysis of these cells revealed that in both cases, loss of DUSP6 played a major role in this process (Phuchareon *et al*., 2015; Hrustanovic *et al*., 2015). Similarly, loss of DUSP6 has been linked to cisplatin resistance in ovarian cancer (Chan *et al*., 2008) and is observed in gastric cancer cell lines in response to prolonged use of an RTK inhibitor (Lai *et al*., 2014).

Results from multiple studies summarised above demonstrate that the tumour suppressive or oncogenic nature of DUSP5 and DUSP6 is highly dependent on the context of upstream oncogenic signalling. These effects could also depend on tissue-specific thresholds of ERK activity that correlate to either proliferative or anti-proliferative cell fate decisions. Despite this, experimental evidence has demonstrated

a key role of the ERK-specific phosphatase DUSP6 in influencing the efficacy of chemotherapeutic strategies targeting oncogenic ERK signalling pathways. To date, the potential influence of the nuclear ERK-specific MKP DUSP5 on ERK pathway inhibition in cancer has not been reported. However, the direct and highly specific nature of the negative feedback loop that exists between DUSP5 and ERK, together with the discovery of abnormal DUSP5 regulation in several oncogenic settings suggests that changes in DUSP5 expression may contribute to the signalling reprogramming events that occur in the development of ERK pathway-inhibitor resistance.

Further investigation into MKP function in ERK-related oncogenesis and drug resistance may contribute to improved chemotherapeutic strategies and may even generate novel drug targets. In this study we will address this task by assessing the influence of MKPs DUSP5, DUSP6 and others on the efficacy and potency of the MEKi AZD6244, in parental and drug-resistant colorectal cancer cell lines, COLO205, HT29 and HCT116.

1.7. Aim and objectives

Using parental CRC cell lines (COLO205, HT29 and HCT116) and their AZD6244-resistant derivatives as a model, the primary aim of this thesis was to establish whether MKP function influenced the regulation of oncogenic KRAS and BRAF cell signalling and acquired drug resistance to ERK pathway inhibition. We first sought to characterise the spatiotemporal responses of ERK to AZD6244 administration and establish whether correlative patterns in active and inactive ERK subcellular compartmentalisation existed using high content imaging and analysis. Then, by quantifying the mRNA and protein levels of prominent MKPs we aimed to evaluate MKP expression patterns in parental and drug resistant CRC cell lines in varying AZD6244 conditions. We hoped that these experiments would elucidate which, if any MKPs were potentially important in each cell line and condition. Our focus began with the ERK-specific MKPs DUSP5 and DUSP6. Not only have these MKPs been implicated in mechanisms of tumour development and chemotherapeutic resistance, but their exquisite specificity for ERK suggests an important role for these MKPs in specifically regulating oncogenic ERK signalling.

Following preliminary assessments that indicated that DUSP5 may be upregulated in AZD6244-resistant CRC cells, we hoped to further characterise the influence of DUSP5 in CRC models by assessing the effects of DUSP5 loss in parental HCT116 and HT29 cells and their AZD6244-resistant derivatives. Our approach involved the development of a flexible viral-based siRNA delivery system that could be used across both cell lines. Once an effective DUSP5 knockdown strategy was established, we aimed to assess signalling and cell fate events that occurred in response to AZD6244 administration or cessation with DUSP5 loss through conventional biochemical approaches such as RT-PCR and western blotting as well as high-throughput immunofluorescent-based microscopy. Finally, we hoped to determine whether DUSP5-targeting could be harnessed to maximise the anti-proliferative effects of withdrawal of MEK inhibition in AZD6244-resistant CRC cells.

Chapter 2. Materials & Methods

2.1. Materials

2.1.1. Solutions

TBE

1.08 % (w/v) Tris, 0.55 % boric acid, 2 mM Na_2EDTA (pH 8.0)

Tris-buffered saline (TBS)

10mM Tris.Cl, pH7.4, 154mM NaCl

TBS-Tween (TBST)

10mM Tris.Cl, pH7.4, 154mM NaCl, 0.1% Tween-20

Phosphate-buffered saline (PBS)

154mM NaCl, 12.5mM Na2HPO4.12H2O, pH7.2

PBS–Tween (PBST)

0.2% Tween–20 in 1X PBS

Lysogeny broth (LB)

1% (w/v) Bacto–tryptone, 0.5% (w/v) Yeast extract, 1% (w/v) NaCl

LB agar

1% (w/v) Bacto–tryptone, 0.5% (w/v) Yeast extract, 1% (w/v) NaCl, 1.5% (w/v) Agar, 50 µg/ml kanamycin

2X Hank's buffered salt solution (HBSS)

280mM NaCl, 10mM KCl, 1.5mM Na2HPO4.12H2O, 12mM D+glucose, 50mM 4(2-hydroxyethyl)-1-piperazineethanesulphonic acid (HEPES)

TG lysis buffer

20 mM Tris-HCl (pH 7.4), 137mM NaCl, 1 mM EGTA, 1% (v/v) Triton X-100, 10% (v/v) glycerol, 1.5 mM $MgCl_2$, 50 mM NaF, 1 mM Na_3VO_4, 5 $\mu g.mL^{-1}$ aprotinin, 10 $\mu g.mL^{-1}$ leupeptin, 1 mM phenylmethylsulfonyl fluoride (PMSF)

1 × Laemmli sample buffer

50 mM Tris-HCl (pH 6.8), 2% (w/v) SDS, 10% (v/v) glycerol, 1% (v/v) β-mercaptoethanol, 0.01% (w/v) bromophenol blue

Resolving gel buffer

1.5 M Tris.Cl, pH 8.8

Stacking gel buffer

0.5 M Tris.Cl, pH 6.8

SDS–PAGE running buffer

0.2 M glycine, 25mM Tris, 0.1% (w/v) SDS

Transfer buffer

0.2 M glycine, 25 mM Tris, 20% (v/v) methanol

2.2. Methods

2.2.1. Molecular Biology

Generation of pGSH1–GFP shRNA expression vectors

In order to generate pGSH1–GFP shRNA expression vectors for DUSP5 knockdown, shRNA oligonucleotides were subcloned into the pGSH1–GFP (BamHI/NotI) Expression Vector (Genlantis, USA). Plasmid maps and analytical digests are presented in the Appendix (Figures A1 and A2). Successful subcloning was confirmed by sequencing provided by Source Biosciences (Nottingham, UK).

Small hairpin RNA sequences (shRNA) targeting the DUSP5 coding sequence and 3' untranslated region (UTR), were synthesized by Invitrogen as forward and reverse complementary oligonucleotide sequences (Table 2.1). These sequences were pre-validated for successful DUSP5 knockdown by Sigma using MISSION® shRNA constructs.

Table 2.1 shRNA oligonucleotide sequences. The luciferase shRNA control sequence was obtained from Genlantis. Enzyme restriction sites underlined. Each 5' end contains a restricted BamHI site (GATCC), followed by a target–specific sequence spanning 19 base pairs. The hairpin loop contains a HindIII restriction sequence (AAGCTT), and is followed by the antisense target and a RNA polymerase III termination signal. A restricted NotI sequence (GC) is located at the 3' end.

Number	Target Region	Sequence
1	DUSP5 CDS	5'–GATCCGCAGCTCCTGCAGTACGAATCTGAAGCTT GAGATTCGTACTGCAGGAGCTGTTTTTTGGAAGC–3'
2	DUSP5 3'UTR	5'–GATCCGCCTGTCCTTCTGTGTGCTTATGAAGCTT GATAAGCACACAGAAGGACAGGTTTTTTGGAAGC–3'
3	DUSP5 CDS	5'–GATCCGAGCATGGTCTCGCCCAACTTTGAAGCTT GAAAGTTGGGCGAGACCATGCTTTTTTTGGAAGC–3'
4	DUSP5 CDS	5'–GATCCGACCCACCTACACTACAAATGGAAGCTT GCATTTGTAGTGTAGGTGGGTCTTTTTTGGAAGC–3'
5	Luciferase (Control)	5'–GATCCGATTATGTCCGGTTATGTAGGAGCTTGTA CATAACCGGACATAATCTTTTTTGGAAGC–3'

Forward and reverse oligonucleotides were annealed according to manufacturer's instructions (Genlantis, pGSH1–GFP siRNA Expression Vector Kit, P100300). Following the annealing reaction, annealed oligonucleotides were ligated into the pGSH1–GFP (BamHI/NotI) Expression Vector using T4 DNA Ligase (NEB, M0202S), according to the manufacturer's instructions. A "no insert" reaction was included to control for the efficiency of target vector digestion and self–ligation.

A vector:insert molar ratio of 1:3 was used to optimise ligation efficiency, and was calculated using the following equation:

$$\text{Insert mass (ng)} = 3 \times \frac{\text{Insert length (bp)}}{\text{Vector length (bp)}} \times \text{Vector mass (ng)}$$

Transformation of competent E.coli

Ligation reactions were used to transform DH5α competent *E.coli* cells (NEB, C2987H). 2.5µl of ligation reaction mix was aliquoted into Eppendorf tubes on ice. DH5α competent *E.coli* cells were thawed on ice, then dispensed into each tube containing plasmid solution at 25 µl per tube. Samples were incubated on ice for 30 minutes, heat–shocked at 42 °C for 30s and then placed on ice for 2 minutes. 250 µl of prewarmed SOC medium (New England Biolabs) was added and samples were incubated at 37 °C for 1 hour with vigorous shaking. Bacteria were pelleted by brief centrifugation at 10,000 x g and resuspended in 100µl SOC medium. The bacterial solution was then spread onto LB agar plates containing 50 $\mu g.ml^{-1}$ kanamycin. Spread plates were incubated at 37 °C overnight to allow colony formation, after which 3 to 4 colonies from each transformation were selected for overnight liquid culture.

Plasmid purification

Plasmid DNA was isolated from the overnight bacterial culture using the using either the Wizard Plus SV Minipreps DNA Purification System (Promega) or the GenElute™ HP Maxiprep Kit (Sigma–Aldrich) according to the manufacturers' instructions. Purified plasmid DNA was quantified on a NanoDrop–1000 spectrophotometer.

Restriction digestions

Restriction digests were used with analytic DNA gels to screen plasmids for the presence of desired inserts. Double digests were performed with *XhoI* and *HindIII* fast digest enzymes (ThermoFisher, FD0694 and FD0504) according to the manufacturer's instructions.

DNA agarose gel electrophoresis

Digested DNA samples were combined with bromophenol blue loading buffer and loaded onto 1 % (w/v) agarose TBE gels containing SYBR® Safe DNA Gel Stain (Thermo Fisher) alongside 5µl of 1kB DNA Ladder (Promega, Southampton, UK). DNA gels were run at 100 V for 45 minutes and were visualised using a non–UV Dark Reader Transilluminator (Clare Chemical Research, CO, US).

Generation of CRISPR/Cas9 gRNA constructs

CRISPR/Cas9 gRNA constructs were established through molecular cloning, following a standard protocol detailed in Ren *et al*. (2013). This work was carried out by Megan Cassidy at the Babraham institute (UK) and made use of the pSpCas9(BB)-2A-GFP genome-editing vector, illustrated in the Appendix (Figure A3). gRNAs (Table 2.2) were designed using Zhang lab's gRNA generator, which calculates "scores" based on on-target activity offset by off-target activity. These sequences were synthesised as oligonucleotides by Sigma-Aldrich (Dorset, UK). Recombinant CRISPR/Cas9 gRNA plasmids were sequenced by Genewiz (UK) to confirm successful cloning.

Table 2.2 DUSP5 gRNA sequences. GS1, GS2 and ZH1 gRNAs target exon 1 and the ZH1 gRNA targets exon 2. All gRNAs were synthesised with *BbsI* restriction site overhangs to facilitate cloning.

gRNA identifier	gRNA sequence
GS1	5'-GAGCGAGCCGCGCACGTTCG-3'
GS2	5'-ATGAAGGTCACGTCGCTCGA-3'
GS5	5'-TCACGTACCTGGTCATAAGC-3'
ZH1	5'-CTACTCGCTTGCCTACCCGC-3'

Amplification of adenoviral shRNA constructs

Replication-incompetent recombinant adenoviral constructs containing either a DUSP5-targeting shRNA sequence or a non-targeting shRNA sequence were purchased from VectorBuilder in the form of purified virus particles at an approximate titre of $\geq 1 \times 10^{10}$ PFU.mL^{-1}. The custom-designed vector maps and shRNA sequences can be found in the Appendix (Figure A4). The expression of each shRNA sequence is driven by a U6 promoter, while expression of the flanking EGFP coding sequence is driven by a PGK promoter.

Replication-incompetent recombinant adenoviral particles are able to infect mammalian cells, allowing for the entry of viral DNA and subsequent expression of genes encoded by this genetic material. However, due to the absence of genetic elements that encode the E1 and E3 proteins, these adenoviruses are only able to replicate and package new viral particles in an E1-expressing packaging cell line such as HEK293, allowing for tight regulation of adenovirus propagation.

Stocks of each adenovirus were established through the large-scale infection of HEK293 cells and subsequent viral purification. For each virus, a T75 flask of semi-confluent (~75%) HEK293 cells was inoculated with 2 µL purified virus and incubated at 37 °C, 5% CO_2. After 24 hours, the culture medium was removed from each flask, aliquoted into 5 mL bijou tubes and snap frozen in liquid nitrogen. Once this viral suspension was generated, 10 T175 flasks of HEK293 cells were each infected with 400 µL thawed viral suspension, for each adenovirus to be amplified. Cells were incubated at 37 °C, 5% CO_2 for between 1 and 3 days, until the appearance of viral plaques. At this stage, cells were easily dislodged from the flasks and collected in several 50 mL falcon tubes. Cell suspensions were centrifuged at 1000g for 10 minutes after which the supernatant was decanted, and the cell pellet was resuspended in 3 mL of 100 mM Tris.Cl, ph7.5 and snap frozen in liquid nitrogen.

After thawing on ice, cells were lysed through three consecutive freeze thaw cycles. The samples were centrifuged (3000 rpm for 10 minutes at 4 °C) to pellet cell debris and the viral supernatant was transferred to an ultracentrifuge tube (Beckman Coulter). 0.6 volumes of CsCl-saturated 100mM Tris-HCl was added to each tube, followed by a solution of 1 volume 100mM Tris : 0.6 volumes CsCl-saturated 100mM Tris (until full). Tubes were balanced to within 0.03 g of each other and heat sealed, in preparation for ultracentrifugation at 65000 rpm in a Beckman Coulter VTi65 rotor for 6 hours.

After ultracentrifugation, adenovirus was visible as a white band, which was carefully removed with a syringe and 21G needle. The viral suspension was placed in a new ultracentrifuge tube and was topped up with the solution of 1 volume 100mM Tris : 0.6 volumes CsCl-saturated 100mM Tris, before weighing and sealing. Samples were subjected to ultracentrifugation as before, but for 12 hours. After ultracentrifugation, the white viral band was removed from each tube and inserted into a 10kDa cut-off

Slide-A-Lyzer™ dialysis cassette (Pierce) in preparation for the removal of CsCl from each sample. This was accomplished through dialysis in 3% (w/v) sucrose in PBS over a 3-hour period at 4 °C. Each cassette was dialysed against 1 L of sucrose solution, which was replaced hourly. After dialysis, purified virus was removed from each cassette and dispensed into 20 or 50 µL aliquots, before snap freezing and storing at -80 °C.

2.2.2. Cell culture

COLO205, HT29, HCT116 and their AZD6244-resistant derivative cell lines C6244–R, HT6244–R and H6244–R were a kind gift from Simon Cook (Babraham Institute, Cambridge). HCT116 and H6244–R cells were maintained at 37 ºC, 5% CO_2 in Dulbecco's modified Eagle's medium (DMEM), COLO205 and C6244–R cells were cultured in RPMI 1640 and HT29 and HT6244–R cells were cultured in McCoy's 5A. All medium was supplemented with 10% (v/v) fetal bovine serum (FBS), penicillin (100 $U.mL^{-1}$), streptomycin (100 $mg.mL^{-1}$) and 2 mM glutamine. For routine culture, AZD6244–resistant cells were grown in 1 µM (C6244–R and HT6244–R) or 2 µM (H6244–R) AZD6244. Cells were passaged twice weekly as follows; plated cells were washed in PBS prior to incubation in 1% trypsin–EDTA for 5 minutes at 37 °C, 5% CO_2. Cells were then resuspended in complete medium, split according to experimental demand, diluted in fresh medium and replated. All reagents were purchased from Gibco, Thermo Fisher Scientific.

Cell transfections

pGSH1–GFP shRNA plasmid transfection

HCT116 and H6244-R cells were transfected using Lipofectamine® LTX (with Plus™ Reagent) according to manufacturer's instructions.

siRNA transfection

siGENOME siRNA oligonucleotides targeting human DUSP5 mRNA (#D-003566-01-0002 and #D-003566-03-0002) and ON-TARGETplus non-targeting siRNA #2 (#D-001810-02-05) were purchased from Dharmacon. For siRNA transfection, HCT116 cells were transfected using Lipofectamine® RNAiMAX Transfection Reagent. Approximately 18-24 hours prior to transfection, HCT116 and H6244-R cells were seeded into 6 well plates at a density of 1.25 $x10^5$ cells per well, in medium free of penicillin and streptomycin. Forward transfection was performed using a final siRNA concentration of 10 nM and 2.2 µL of lipofectamine reagent per well. Transfection medium was replaced with fresh complete medium 18-24 hours after transfection.

CRISPR/Cas9 shRNA plasmid transfection and generation of DUSP5 knock-out cell lines

For CRISPR/Cas9 plasmids, HCT116 cells were transfected using Lipofectamine® LTX (with Plus™ Reagent) or Lipofectamine® 2000. Approximately 18-24 hours prior to transfection, HCT116 and H6244-R cells were seeded into 10cm dishes at a density of 1.25$x10^5$ cells per dish, in medium free of penicillin and streptomycin. For each forward transfection, 15 µg of plasmid DNA and 25-50 µL of lipofectamine reagent was used. Transfection medium was replaced with fresh complete medium 18 hours after transfection.

The success of transfection was monitored by GFP expression using an EVOS microscope. 24 to 48 hours after transfection cell cultures were trypsinised, resuspended in complete media and centrifuged for 3 minutes at 1500 g. Cell pellets were resuspended in 250 µL of 2% FBS in PBS and filtered through a 40 µm cell strainer (CellTrics). GFP-positive cells were single-cell sorted into 96-well plates containing 75 µL of filter sterilised conditioned complete medium using a 100 µm nozzle on a BD FACSARIA III cell sorter (BD Biosciences, Oxford, UK). Each well was topped up with 75 µL fresh complete medium and incubated at 37 °C, 5% CO_2. 96 well cell culture plates were incubated for approximately 2 to 4 weeks, with frequent media changes and inspections for cell colony growth. Once large enough, colonies were expanded into larger tissue culture vessels until enough cells were present to prepare frozen cell stocks as well as protein lysates for preliminary western blot screening.

Adenoviral transfection

HT29 and HT6244-R cell lines were plated 18h before viral addition. DUSP5-targeting shRNA adenovirus 1 and 3 and non-targeting shRNA adenovirus were diluted in complete medium to give a final concentration of 45 pfu/nL. Culture medium was discarded from plates and replaced with diluted virus. Viral medium was replaced with fresh medium after a 24-hour incubation at 37 °C, 5% CO_2.

Lentiviral transfection and generation of inducible lentiviral shRNA stable cell lines

Stable shRNA-expressing HT6244-R cell lines were established using Dharmacon™ SMARTvector™ Inducible Lentiviral shRNA vectors. These lentiviral vectors make use of the Tet-On 3G bipartite induction system which is comprised of an inducible RNA polymerase promoter (TRE3G) and the Tet-On 3G transactivator protein, both encoded within the DNA vector (Loew et al., 2010; Zhou et al., 2006). When bound by doxycycline, the Tet-On 3G transactivator protein is able to bind to the TRE3G promoter and induce the expression of the downstream reporter gene and shRNA sequence. This system enables tightly regulated shRNA expression at low doses of doxycycline and can work effectively in many cell lines where transfection of DNA and RNA is not possible.

Purified Lentiviral shRNA vector DNA was kindly given to us by Professor Stephen Keyse (University of Dundee, UK). Details of these constructs as well as the DUSP5-targeting, GAPDH-targeting and non-targeting shRNA sequences can be found in the Appendix (Figure A5 and Table A1). Replication-incompetent lentiviral particles were generated with the Dharmacon™ Trans-Lentiviral Packaging System (GE Healthcare, #TLP5917), according to manufacturer's instructions.

18 hours prior to infection, CRC cells were seeded into 6 well plates at a density of approximately 2.5 – 3x10^5 cells per well in 1 mL complete medium. For each lentiviral stable cell line to be established, 1 mL of lentiviral suspension was added to each well, as well as 8 µg.mL^{-1} polybrene solution (#TR-1003, Sigma-Aldrich). Cells were incubated at 37 °C, 5% CO_2 for 24 hours, after which the culture medium was replaced, and cell cultures were expanded into larger tissue culture flasks as necessary. After 48 hours, transfected cells were selected with the addition of puromycin (#P8833-10,

Sigma-Aldrich). Concentrations of puromycin appropriate for selection were pre-determined for each cell line with dose-tolerance experiments. After approximately 2 weeks in selection media stocks of each cell line were trypsinised, frozen down and stored at -80 °C.

Immunofluorescent cell-staining

After each experimental incubation, the culture medium was discarded from culture plates and cells were fixed with 4% paraformaldehyde for 10 minutes at room temperature. Cells were then permeabilised with ice cold methanol at –20 ºC for 2 minutes and washed three times with PBS. For experiments quantifying the proportion of cells in S-phase, an EdU fluorescent thymidine analog (5–ethynyl–2'–deoxyuridine, EdU) (Click–iT® EdU HCS Assays, Invitrogen) was diluted in complete medium and added to cells at a final concentration of 10 μM 1 hour prior to fixation. The EdU label was detected with the Click–iT® EdU HCS Assay kit according to manufacturer's instructions.

For all immunofluorescent staining experiments, non–specific binding sites were blocked using 2.5 % (v/v) normal goat serum (NGS) in PBS with 0.01 % sodium azide or 2% BSA in PBS for 1 to 2 hours. Primary antibodies were diluted in blocking solution and cells were incubated in primary antibody overnight at 4 ºC. Cells were washed three times in PBS and incubated in secondary antibody dilutions for 1 to 2 hours at room temperature. After three PBS washes, nuclei were stained with a 300 nM solution of DAPI (Sigma, D9542) in PBS and stored at 4 ºC until required for imaging. All primary and secondary antibodies used in immunofluorescent cell-staining experiments are described in Table 2.3 and Table 2.4 below.

Table 2.3 Primary antibodies used in immunofluorescent microscopy experiments.

Primary Antibody	Supplier	Catalogue #	Dilution	Buffer
ERK (Rabbit mAb)	CST	4695	1:250	2% BSA/ 2.5% NGS
ERK (Mouse mAb)	CST	4696	1:250	2% BSA/ 2.5% NGS
p-ERK (Thr202/Tyr204) (Mouse mAb)	Sigma Aldrich	M9692	1:250	2% BSA/ 2.5% NGS
p-ERK (Thr202/Tyr204) (Rabbit mAb)	CST	4370	1:250	2% BSA/ 2.5% NGS

Table 2.4 Secondary antibodies used in immunofluorescent microscopy experiments.

Secondary Antibody	Supplier	Catalogue #	Dilution	Buffer
Alexa Fluor® 488-Conjugate, Goat anti-mouse IgG	Invitrogen	A-11001	1:300	2% BSA/ 2.5% NGS
Alexa Fluor® 568-Conjugate, Goat anti-rabbit IgG	Invitrogen	A-11011	1:300	2% BSA/ 2.5% NGS
Alexa Fluor® 680-Conjugate, Goat anti-rabbit IgG	Invitrogen	A-21244	1:300	2% BSA/ 2.5% NGS

2.2.3. Microscopy

High–content microscopy and analysis

Cells stained with fluorescent antibodies were imaged using an INCell Analyzer 2000 (GE Healthcare, Buckinghamshire, UK) using a 10x or 20x objective lens, typically acquiring 500–2000 individual cells (3 fields) per well in duplicate or triplicate wells per condition. Images were analysed using INCell Developer Toolbox software. A custom protocol was designed to identify nuclear and cytoplasmic regions and to detect the protein immunostaining intensity within these regions on a per cell basis. For *p*-ERK and total ERK expression profiles, the mean intensity of immunostaining for all cells in each condition was calculated and used to represent the population trend. For EdU staining, a minimum threshold for "positive" staining was established, and all cells with EdU signal higher than this threshold were counted as "S-phase positive".

EVOS cell imaging

Cells transfected with pGSH1-GFP shRNA constructs were imaged on an EVOS microscope (EVOS fl, AMG). Images were taken in the normal light channel as well as the GFP channel. Composite images were generated on ImageJ software (http:// rsb.info.nih.gov/ij/; W. Rasband, National Institutes of Health, Bethesda, USA) to assay transfection efficiency.

2.2.4. Western blotting

Preparing samples for SDS-PAGE

Cell medium was discarded, and culture plates were placed on ice. Cells were washed with ice cold PBS after which 50 - 100 µl of lysis buffer was added directly to each well. Cell lysates were transferred to Eppendorf tubes and were snap frozen in liquid nitrogen. Lysates were stored at –80 ºC until required.

Once thawed, lysates were centrifuged at 12000 g for 5 minutes at 4 ºC. Each supernatant was transferred to a new tube and diluted with 4× Laemmli sample buffer to a final ratio of 1:4 (4× Laemmli sample buffer to sample). Samples were boiled at 95 °C and stored on ice. Approximately 10 µl of undiluted sample was retained for protein concentration determination using the Bradford protein assay. Standard

solutions of bovine serum albumin (BSA) between 0 and 2mg.ml^{-1} were generated by diluting BSA in lysis buffer. In a clear 96-well plate, 2 µL of each standard BSA solution as well as each undiluted experimental sample were aliquoted into separate wells. A 1:5 dilution of Biorad protein assay dye reagent was prepared in water, and 198 µl of this solution was added to each well. After a 10-minute incubation at room temperature absorbance readings were taken at 565nm using a PHERAstar FSX plate reader (BMG Labtech). Protein concentrations were determined using the PHERAstar analysis software. The concentration of protein in each sample was normalised by diluting in appropriate amounts of 1× Laemmli sample buffer.

SDS–PAGE

Proteins were separated according to molecular weight by sodium dodecyl sulphate – polyacrylamide gel electrophoresis (SDS–PAGE) using the Laemmli discontinuous buffer system (Laemmli, 1970) and the Mighty small II gel apparatus (Hoefer). 1mm thick mini–gels were prepared with resolving and stacking gels according to the recipes provided in Table 2.5 and Table 2.6.

Table 2.5 Recipe for SDS–PAGE 10% resolving gel. Volumes provided are sufficient for four mini–gels.

Reagent	Volume (mL)
1.5 M Tris.Cl, pH 8.8	15
30% acrylamide:bisacrylamide (37:5:1)	19.8
H_2O	24
10% (w/v) SDS	0.6
10% (w/v) APS	0.6
TEMED	0.06

Table 2.6 Recipe for SDS–PAGE 6% stacking gel. Volumes provided are sufficient for four mini–gels.

Reagent	Volume (mL)
0.5 M Tris.Cl, pH 6.8	5
30% acrylamide:bisacrylamide (37:5:1)	4
H_2O	10.6
10% SDS	0.2
10% APS	0.2
TEMED	0.02

The Mighty small II gel apparatus was assembled according to manufacturer's instructions. Samples were loaded onto the gel alongside the Chameleon 800 protein ladder (Licor). Electrophoresis was carried out at 80 mA for 3 hours.

Protein transfer

Gels were blotted onto methanol-activated PVDF membrane (Immobilon-FL Membrane, Merck Millipore) using the Criterion blotter System (Bio-Rad) at a current of 300 mA for 90 min.

Immunoblotting

Immobilon-FL PVDF membranes were blocked in 5% milk/PBST for 30 minutes at room temperature. Primary antibodies were diluted in either 5% BSA/PBST or 5% milk/PBST and membranes were incubated in primary antibody solution at 4 ºC overnight. Following this incubation, membranes were washed in PBST three times for 5 minutes each and then incubated in secondary antibody, diluted in 5% milk/PBST for 1 hour at room temperature. Finally, immunoblots were washed in PBST as before and once in ddH2O to remove residual Tween, followed by imaging on the Licor Odyssey® CLx Imaging System. All primary and secondary antibodies used in immunoblotting experiments are described in Table 2.7 and Table 2.8 below.

Table 2.7 Primary antibodies used in immunoblotting experiments.

Primary Antibody	Supplier	Catalogue #	Dilution	Buffer
β-Tubulin	Sigma-Alrich	T8328	1:5000	5% BSA
Bim	CST	2933	1:1000	5% BSA
E-cadherin	CST	3195	1;1000	5% BSA
DUSP4	Abcam	ab216576	1:1000	5% BSA
DUSP5	Abcam	ab200708	1:1000	5% BSA
DUSP6	Abcam	ab76310	1:1000	5% BSA
ERK	CST	9107	1:2000	5% BSA
KRAS	Proteintech	12063-1-AP	1:1000	5% Milk
p-ERK (Thr202/Tyr204)	CST	4370	1:2000	5% BSA
$p21^{CIP1}$	CST	2947	1:1000	5% BSA
PARP	CST	9542	1:1000	5% Milk

Table 2.8 Secondary antibodies used in immunoblotting experiments.

Secondary Antibody	Supplier	Catalogue #	Dilution	Buffer
DyLight™ 680 Conjugate, Goat anti-rabbit IgG	CST	5366	1:30000	5% Milk
DyLight™ 800 Conjugate, Goat anti-rabbit IgG	CST	5151	1:30000	5% Milk
DyLight™ 800 Conjugate, Goat anti-mouse IgG	CST	5257	1:30000	5% Milk
680 Goat anti-mouse IgG	Licor	92632220	1:10000	5% Milk

2.2.5. RT–PCR

RNA extraction

After experimental incubation, cell culture medium was discarded from tissue culture plates and cells were washed in cold PBS. Cells were lysed directly in the wells and RNA was subsequently extracted using the RNEasy mini kit, according to manufacturer's instructions (Qiagen). RNA samples were subjected to an on–column DNA digestion with the RNase–Free DNase Set (Qiagen, 79254) according to the manufacturer's instructions.

Reverse transcription

RNA was converted into cDNA using the High–Capacity cDNA Reverse Transcription Kit (Applied Biosystems), according to manufacturer's instructions. A total of 1 µg RNA was used in each reaction. All samples were accompanied by control reactions that did not contain reverse transcriptase to confirm the absence of contaminating genomic DNA. cDNA was stored at –20 ºC until required for experimental use.

Quantitative real-time PCR

Relative mRNA levels were assessed in experimental samples using quantitative PCR. Forward and reverse primers used in these experiments are listed in

Table 2.9. The standard reaction used in all the RT–PCR performed was as follows; 1X Power SYBR Green PCR Master Mix (Applied Biosystems), 100 nM reverse and forward primer, 100 ng cDNA and nuclease–free water made up to 20 µl. Reactions were loaded into MicroAmp fast 96–well reaction plates (Applied Biosystems, 10670986) and the plates were sealed with MicroAmp Optical adhesive film (Applied Biosystems, 4360954). The cycling conditions used in all RT–PCR reactions are detailed in **Table 2.10**. All RT–PCR experiments were performed on the StepOnePlus RealTime PCR System (Applied Biosystems) and threshold cycles (C_T) were calculated using the instrument software.

Table 2.9 Forward and reverse primer sequences used in RT–PCR to determine relative mRNA levels of DUSP5 and β–Actin.

Target	Forward primer	Reverse primer
DUSP2	5'-AAAACCAGCCGCTCCG AC-3'	5'-CCAGGAACAGGTAGGGCAAG-3'
DUSP4	5'-CTGGTTCATGGAAGCCAT AGAGT-3'	5'-CGCCCACGGCAGTCC-3'
DUSP5	5'-CCGCGGGTCTACTTCCT CA-3'	5'-GGGTTTTACATCCACGCAA CA-3'
DUSP6	5'-CTGCCGGGCGTTCTAC CT-3'	5'-CCAGCCAAGCAATGTACCA AG-3'
β–Actin	5'-CCCCTGAACCCCAAG GC-3'	5'-CAGAGGCGTACAGGGATAG CAC-3'

Table 2.10 Standard RT–PCR cycling conditions. Initial denaturation was performed once, followed by 40 cycles of denaturation and annealing.

Step	Temperature (˚C)	Duration	Number of cycles
Initial denaturation	95	10 minutes	1
Denaturation	95	15 seconds	40
Annealing	60	60 seconds	40

For experimental samples, C_T values were normalised to those obtained for the reference gene, β–Actin. These ΔCT values were used to calculate the relative change in mRNA expression as the ratio of mRNA expression in treated cells versus mRNA expression in the control condition, using the Livak method (Livak & Schmittgen, 2001). The final normalised ratio is calculated by the following formula:

Normalised relative ratio = $2^{-\Delta\Delta CT}$

Where $\Delta C_T = C_T$ (target) – C_T (reference)
and $\Delta\Delta C_T = \Delta C_T$ (sample) – ΔC_T (calibrator)

Chapter 3. Characterisation of ERK pathway signalling in MEKi-resistant HCT116, COLO205 and HT29 colorectal cancer cell lines

3.1. Introduction

Mutant forms of RAS and RAF have been detected in various colorectal cancers (CRCs) with high incidence and frequently drive colorectal tumourigenesis through sustained ERK signalling (Fang and Richardson, 2005). While BRAF and MEK inhibitors have shown some success in inhibiting the proliferation and/or survival of $BRAF^{V600E}$-mutant cancers, especially in melanoma where the incidence of $BRAF^{V600E}$-driven oncogenesis is striking, success in treating colorectal cancers driven by mutant RAS has been highly limited (Kidger et al., 2018).

Initially, MEKis appeared to be promising candidates for combating ERK-addicted KRAS-driven and BRAF wildtype CRC, due to their specific targeting of the ERK "gatekeepers" MEK1 and MEK2. One such MEKi, AZD6244 is a highly-selective allosteric inhibitor of MEK1 and MEK2. Since its *in vitro* biological characterisation in 2008, AZD6244 has formed the focus of numerous phase I and II trials (Maloney *et al.*, 2008; Bennouna *et al.*, 2011; Catalanotti *et al.*, 2013 and others). However, like other MEKis, narrow therapeutic windows and ERK pathway reactivation are problems that continue to restrict the extent of their clinical efficacy. Despite this, AZD6244 has proven to be effective in combination therapies and continues to hold promise in phase III trials (Carvajal et al., 2018; Dombi et al., 2016; Jänne et al., 2017). In the wake of this, continued research into the inevitable development of drug-resistance to MEK and BRAF inhibition is of great clinical importance.

The astonishing prevalence of drug-resistance in ERK-addicted cancers has led to the investigation of various intrinsic and extrinsic adaptive mechanisms that can arise in the face of ERK pathway inhibition, many of which were characterised in cancer cell line models (Sale and Cook, 2014). A number of these models have been shown to faithfully recapitulate clinical outcomes and as such are highly valuable in the investigation of chemotherapeutic resistance (Lai et al., 2014b; Song et al., 2007; Villanueva et al., 2013). The use of CRC lines to investigate clinically-relevant cell

signalling adaptions is supported by findings that an entire spectrum of CRC subtypes previously defined in patients was represented in a large CRC line compendium, which reiterates the prevailing value in, and relevance of the use of cancer cell line models for this purpose (Picco et al., 2015).

In line with this work, a 2011 study by Little *et al*. modelled the development of resistance to the anti-proliferative effects of AZD6244 in $BRAF^{V600E}$-driven COLO205 and HT29 cell lines as well as the $KRAS^{G13D}$-driven HCT116 cell line. Results from this investigation revealed intrachromosomal amplification of the driving oncogenes $BRAF^{V600E}$ and $KRAS^{G13D}$ and subsequent ERK reactivation as the driving forces behind this resistance. While amplified mutant BRAF or KRAS is selected for its effects in reinstating active ERK levels in these cell models, these levels remain within a tight optimal range. Microarray data revealed that concomitant with the development of resistance, is a myriad of ERK pathway-related signalling changes, including the upregulation of several downstream negative ERK regulators.

Previous studies have shown that the influence of negative ERK feedback regulation in tumourigenesis, drug efficacy and the development of drug-resistance is profound (Holohan et al., 2013; Kidger and Keyse, 2016). A prominent tier of this feedback is regulated by the MAP kinase phosphatases (MKPs) which are solely dedicated to the spatiotemporal regulation of their MAPK targets. Since the discovery of their unique regulatory role, MKPs have been investigated in the context of a number of ERK pathway-driven cancers, and several MKPs have been implicated in tumour suppression and oncogenesis as well as drug resistance, including the ERK-specific MKPs DUSP5 and DUSP6 (Kidger and Keyse, 2016).

Using the parental and AZD6244-resistant CRC cell lines developed by Little *et al.* (2011) we aimed to investigate the potential role of MKPs in the evolution of drug-resistance in these CRC models. To begin with, we set out to establish whether any differences in expression of relevant MKPs were visible between parental and AZD6244-resistant CRC cells and whether patterns of MKP expression were coincident with AZD6244 administration.

3.2. Work preceding this thesis

3.2.1. Establishment and genetic characterisation of AZD6244-resistant derivatives of COLO205 (C6244-R), HT29 (HT6244-R) and HCT116 (H6244-R) cells

In their 2011 paper, Little *et al.* investigated the development of resistance to the anti-proliferative effects of MEK inhibition in three human colorectal cancer (CRC) cell lines and their AZD6244-resistant derivative cell lines (Little *et al.*, 2011). HCT116, COLO205 and HT29 are CRC cell lines that drive uncontrolled proliferation through abnormal activation of ERK. This is a result of a $BRAF^{V600E}$ mutation in COLO205 and HT29 cells, and a $KRAS^{G13D}$ mutation in HCT116 cells. All three lines have previously been found to be sensitive to AZD6244 treatment in proliferation assays, due to their reliance on the ERK signalling pathway for cell cycle entry and cell survival (Balmanno et al., 2009; Davies et al., 2007). Across assays, HCT116 cells demonstrated a higher tolerance for AZD6244 than the $BRAF^{V600E}$-driven COLO205 and HT29 lines, which is likely due to the ability of oncogenic $KRAS^{G13D}$ to activate other proliferative signalling cascades, such as the PI3K pathway, which could effectively compensate for reduced ERK signalling (Caunt *et al.*, 2015).

To establish AZD6244-resistant derivatives of COLO205, HT29 and HCT116 drug-naïve “parental” cells were cultured in increasing concentrations of AZD6244 until they were able to grow, without noticeable defects, in 1 μM drug for COLO205 and HT29 cells and 2 μM drug for HCT116 cells (Little *et al.*, 2011). Stable cell populations were established without clonal selection and were designated C6244-R (AZD6244-resistant COLO205), HT6244-R (AZD6244-resistant HT29) and H6244-R (AZD6244-resistant HCT116). Following this, AZD6244-resistant cells were routinely cultured in 1 or 2 μM AZD6244 to maintain selective pressure. These AZD6244 concentrations were approaching the maximum achievable and tolerable dose of AZD6244 *in vivo* (2 μM) and were approximately 10 times the IC50 for inhibition of proliferation for each parental CRC cell line (Banerji *et al.*, 2010; Little *et al.*, 2011).

Analysis of whole cell extracts revealed a marked increase in BRAF protein levels as well as genomic copy number in C6244-R cells compared to their parental counterparts, while a similar amplification in KRAS was seen in H6244-R cells relative to parental HCT116 cells. In situ hybridisation of these cells revealed intrachromosomal amplifications of the oncogenic $BRAF^{V600E}$ allele in C6244-R cells and the oncogenic $KRAS^{G13D}$ allele in the H6244-R cell line as the underlying cause of increased BRAF/KRAS abundance. Further analysis of downstream signalling targets of BRAF and KRAS demonstrated that the increased levels of oncogenic protein in each instance were functionally relevant and successfully increased the activation of downstream targets (Little *et al.*, 2011).

3.2.2. C6244-R and H6244-R cells exhibit increased ERK pathway signalling and are refractory to AZD6244-induced cell cycle arrest and cell death

Little *et al*. (2011) went on to further substantiate and characterise the observed ability of C6244-R and H6244-R cell lines to survive and proliferate in AZD6244 conditions previously shown to inhibit corresponding parental CRC lines. [^{3}H] thymidine-incorporation assays revealed the IC50 for inhibition of proliferation in C6244-R and H6244-R cells to be at least 20 times higher than that of corresponding parental lines (COLO205 and HCT116, respectively) (Figure 3.1, a and b). This was coincident with the ability of AZD6244-resistant cells to form colonies in AZD6244 conditions (1 μM AZD6244 for C6244-R/COLO205 cells and 10 μM AZD6244 for H6244-R/HCT116 cells) that inhibited colony formation of parental lines by ~85% (Figure 3.1, d and e). In [^{3}H] thymidine-incorporation assays performed with HT29 and HT6244-R cell lines, HT6244-R cells thrived in concentrations of AZD6244 up to 1 μM, without any reduction in proliferation (Figure 3.1, c). In flow cytometry experiments performed to assess cell cycle distribution, C6244-R and H6244-R cells showed little to no cell death in AZD6244 concentrations between 1 and 10 μM, the same conditions that were able to induce sub-G1 cell populations in parental COLO205 and HCT116 lines (Figure 3.2). These experiments clearly demonstrate that C6244-R, HT6244-R and H6244-R cells are resistant to the anti-proliferative and death-inducing effects of the maximum tolerable *in vivo* dose of AZD6244.

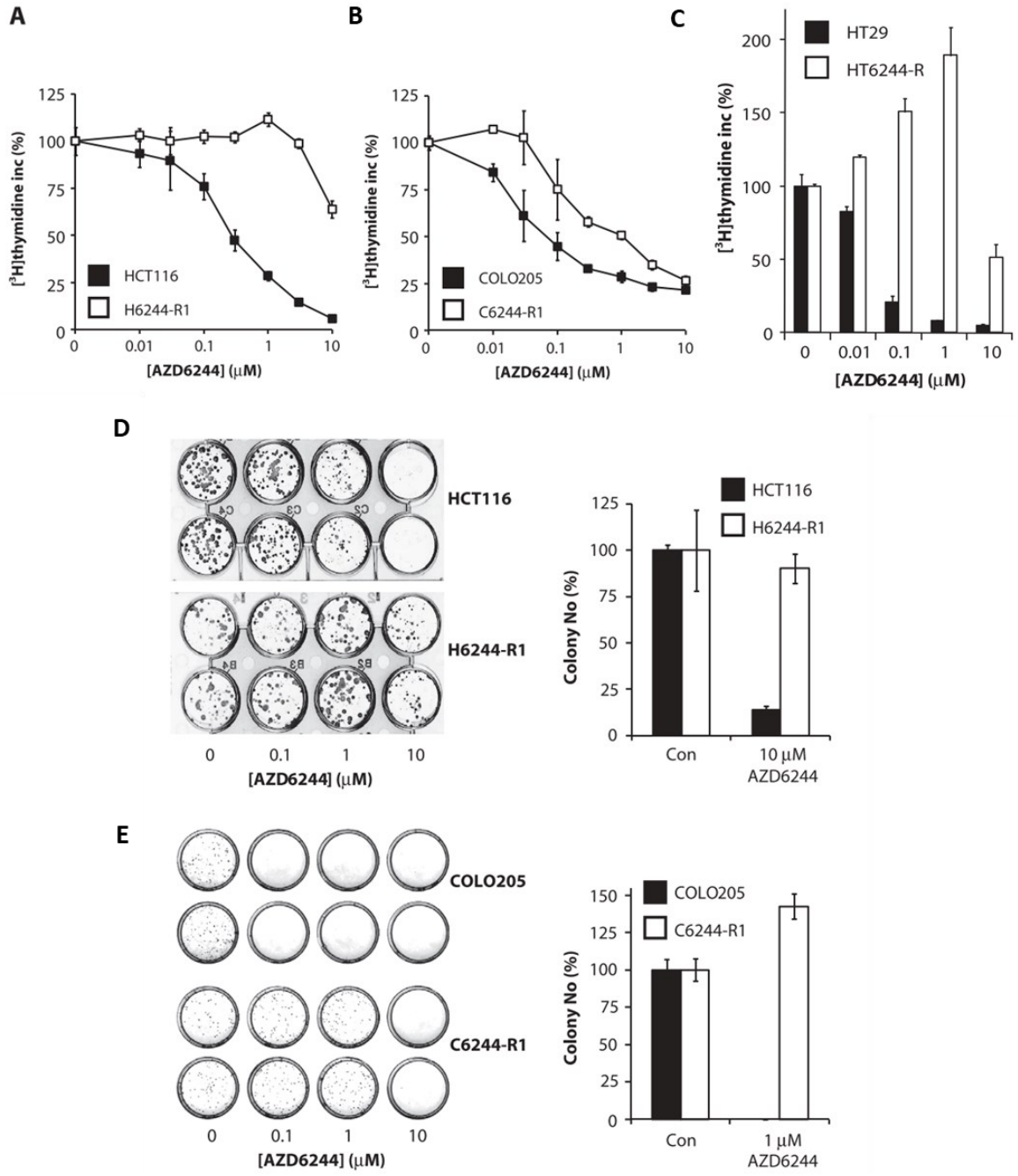

Figure 3.1. H6244-R1 and C6244-R1 cells are resistant to the anti-proliferative effects of AZD6244. (A) HCT116 and H6244-R1 cells, (B) COLO205 and C6244-R1 or (C) HT29 and HT6244-R1 cells were treated with increasing concentrations of AZD6244 for 24 hours, and DNA synthesis was assayed by [^{3}H]thymidine incorporation. Data points represent means ± CV (coefficient of variation) of biological triplicates. (D) HCT116 and H6244-R1 cells or (E) COLO205 and C6244-R1 cells were treated with AZD6244, as indicated, and their ability to grow in colony-forming assays was assessed after 2 weeks in culture. The mean number of colonies formed ±SD (right panel) and photographic images (left panel) from a representative experiment of three are shown. Adapted from Little *et al*. 2011. Copyright 2008 by the American Association for the Advancement of Science.

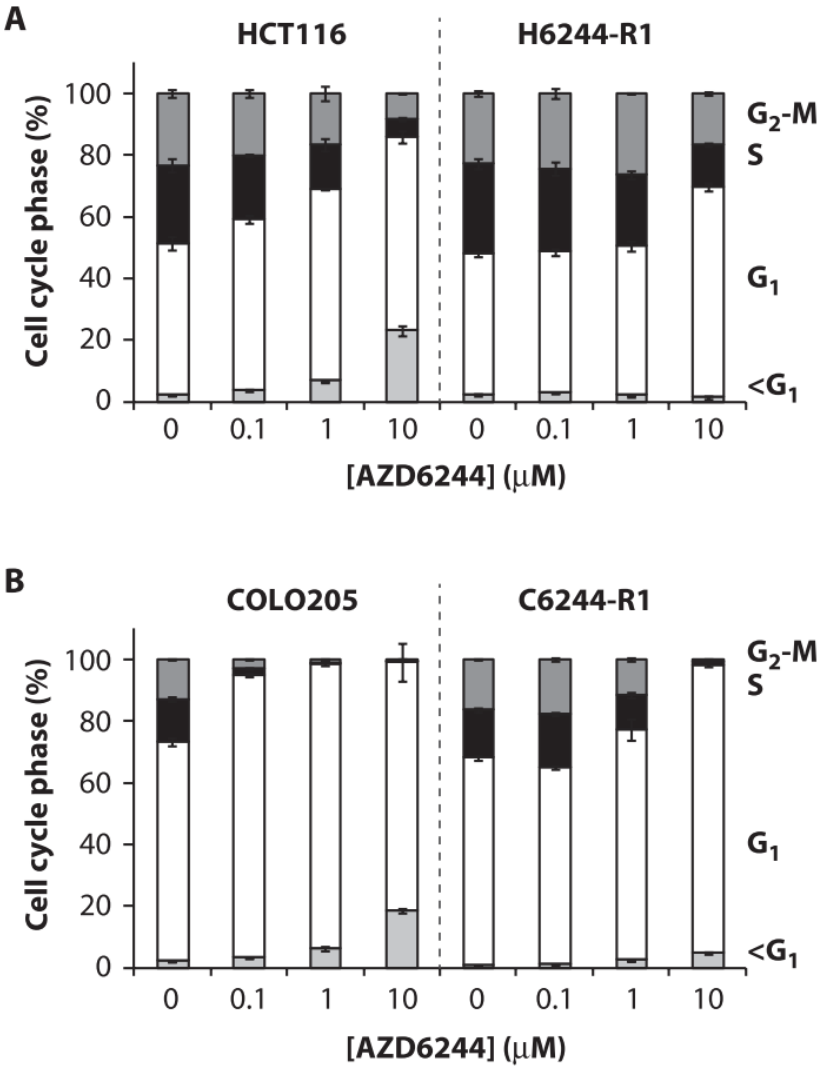

Figure 3.2. H6244-R1 and C6244-R1 are resistant to AZD6244-mediated cell cycle arrest and cell death. After treatment for 48 hours with the indicated concentrations of AZD6244, subconfluent cultures of (A) HCT116 and H6244-R1 cells or (B) COLO205 and C6244-R1 cells were harvested and stained with propidium iodide, and their cell cycle distribution was assessed by flow cytometry. All data are taken from a single experiment representative of three giving similar results. Adapted from Little *et al*. (2011). Copyright 2008 by the American Association for the Advancement of Science.

In order to delineate the signalling events that caused or were coincident with the development of resistance to AZD6244, the presence and activation of major ERK pathway components and targets were assessed at the protein level (Figure 3.3). As expected, levels of phosphorylated- (*p*)-ERK in parental COLO205 and HCT116 cells decreased in response to increasing AZD6244 concentrations. This was evident from 100 nM AZD6244 (COLO205) and 200 nM AZD6244 (HCT116) and upward and was accompanied by decreased abundance of cyclin D1 and phosphorylated (*p*-)RB, and increased levels of cyclin-dependent kinase inhibitor $p27^{KIP1}$. In contrast, substantial inhibition of *p*-ERK in AZD6244-resistant lines was only evident in 10 μM AZD6244, which corresponded to a marked reduction in cyclin D1 and *p*-RB in C6244-R cells but not H6244-R cells (Little *et al.*, 2011).

Under routine culture conditions for resistant CRCs (1 or 2 μM AZD6244), the *p*-ERK levels detected were similar to those seen in parental cell lines cultured in the absence of AZD6244 (Figure 3.3). This, together with the karyotyping experiments discussed previously, suggest that increased signalling flux driven by upstream amplification of $BRAF^{V600E}$ or $KRAS^{G13D}$ protein enables drug-resistant cells to sustain levels of active ERK within a suitable range for cell cycle entry and cell survival, despite considerable MEK inhibition. This hypothesis is substantiated by experiments showing resensitisation of C6244-R and H6244-R cells to the anti-proliferative effects of AZD6244 when the abundance of either active BRAF or KRAS were restored to “normal” parental levels. This was achieved with combination treatment of AZD6244 and a pan-RAF inhibitor AZ628 in C6244-R cells and targeted inhibition of KRAS with siRNA in the presence of AZD6244 in H6244-R cells (Little *et al.*, 2011).

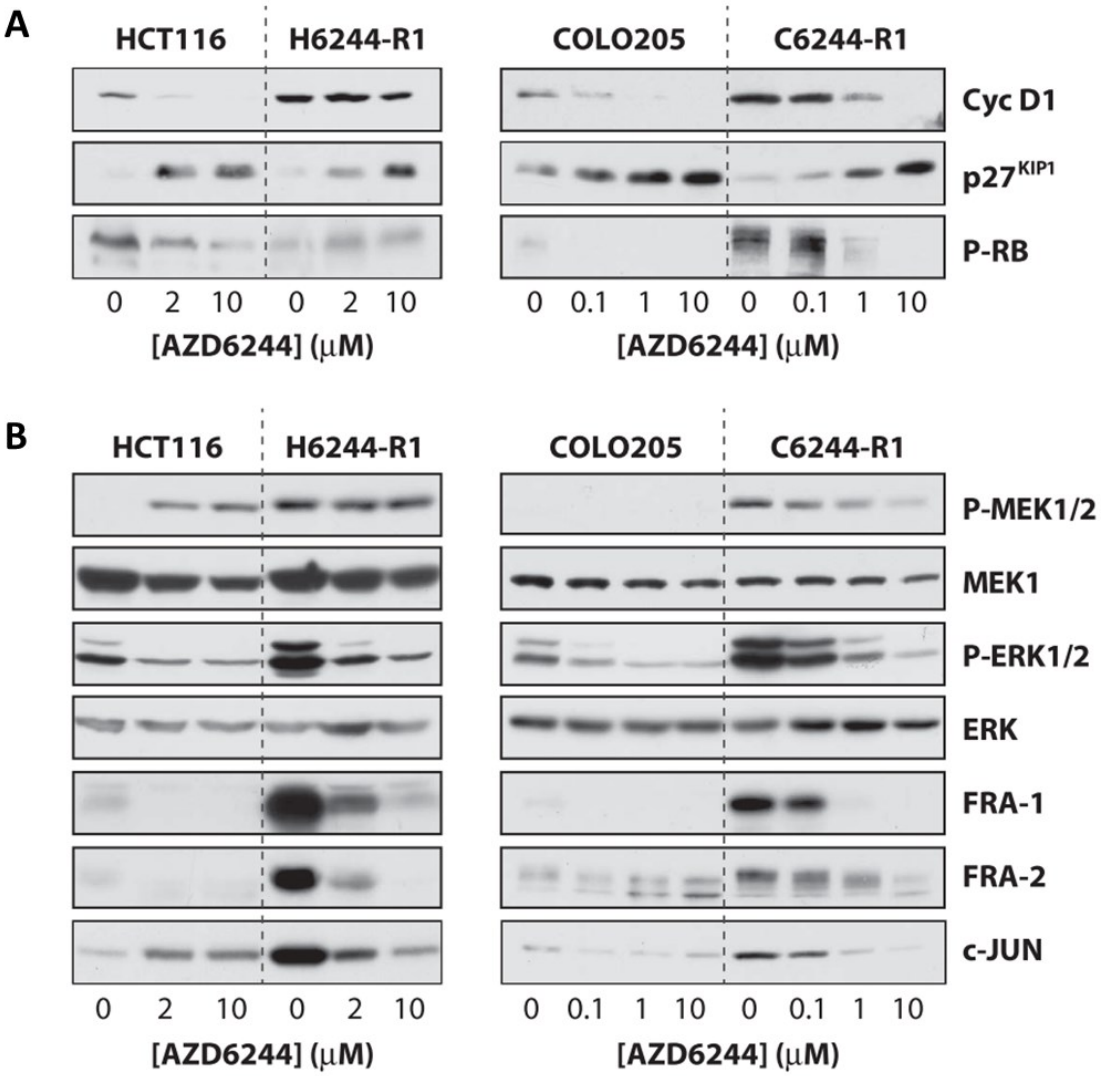

Figure 3.3. H6244-R1 and C6244-R1 exhibit increased basal MEK-ERK activation and ERK pathway output. (A and B) CyclinD1 (CycD1), $p27^{KIP1}$, *p*(S^{795})-RB, *p*-MEK, total MEK, *p*-ERK, total ERK1, FRA-1, FRA-2 and c-jun levels were determined by Western blot analysis of whole-cell extracts from HCT116, H6244-R1, COLO205 and C6244-R1 cells treated with vehicle control [dimethyl sulfoxide (DMSO)] or AZD6244 for 24 hours. All data are taken from a single experiment representative of three giving similar results. Adapted from Little *et al*. 2011. Copyright 2008 by the American Association for the Advancement of Science.

3.2.3. Transient removal of AZD6244 from C6244-R and H6244-R cells leads to ERK hyperactivation

After demonstrating adaptive ERK pathway reprogramming in response to long-term MEK inhibition, Little *et al*. (2011), and subsequently Sale *et al*. (2019), explored how C6244-R and H6244-R cells would respond to the removal of AZD6244. Long-term study (up to 20 weeks) of drug withdrawal from C6244-R cells demonstrated that resistance to the anti-proliferative effects of AZD6244 was reversible and was correlated with decreased BRAF and *p*-ERK protein levels (Little *et al.*, 2011; Sale *et al.*, 2019). The exact mechanism through which these cells transition back to parental levels of oncogenic BRAF is unclear, however it does involve the loss of chromosome 7 and/or BRAF amplicons, indicating that BRAF amplification in the absence MEK inhibition may elicit a fitness disadvantage.

Experiments that assessed the transient withdrawal of AZD6244 from C6244-R and H6244-R cells (up to 24 hrs) revealed that in the absence of drug, *p*-ERK levels in AZD6244-resistant CRCs were markedly increased compared to their parental counterparts and to those seen under routine culture conditions (1 or 2 μM AZD6244) (Figure 3.3). This suggests that when AZD6244 is removed from AZD6244-resistant cells the combination of amplified upstream signalling and the release of MEK leads to hyperactivation of ERK. This increase in abundance of active ERK appears to be functionally relevant, inducing increased protein levels of downstream ERK targets FRA-1, FRA-2, and c-jun (Figure 3.3).

In parental and AZD6244-resistant CRC lines cultured in maintenance conditions (AZD6244-free media and 1 or 2 μM AZD6244, respectively), the expression of another set of ERK target genes previously defined as a “signature” for MEK output (Dry et al., 2010) was assessed using genome-wide mRNA expression analysis. Results showed an overall increase in expression of ERK target genes in C6244-R and H6244-R cells compared to their parental lines, again indicating increased signalling flux through ERK. These ERK targets included negative feedback regulators of the ERK pathway, SPRY2 and the MAPK phosphatases DUSP4 and DUSP6.

Later work performed by Andrew Kidger (Cook laboratory, Babraham Institute, Cambridge, UK) assessed levels of DUSP5 and DUSP6 protein in several drug-naïve KRAS- and BRAF-driven cell lines including COLO205, HT29 and HCT116 as well as HEK293 and HeLa cell lines (Figure 3.4). These western blots revealed that DUSP6 was relatively highly expressed in COLO205, HT29 and HCT116 cells grown in routine culture conditions. Additionally, the expression of another MKP, DUSP5, was quite prominent in HCT116 cells, but not others. This work illustrated substantial variation in different MKP levels, which correlated to some extent, with the amount of *p*-ERK present.

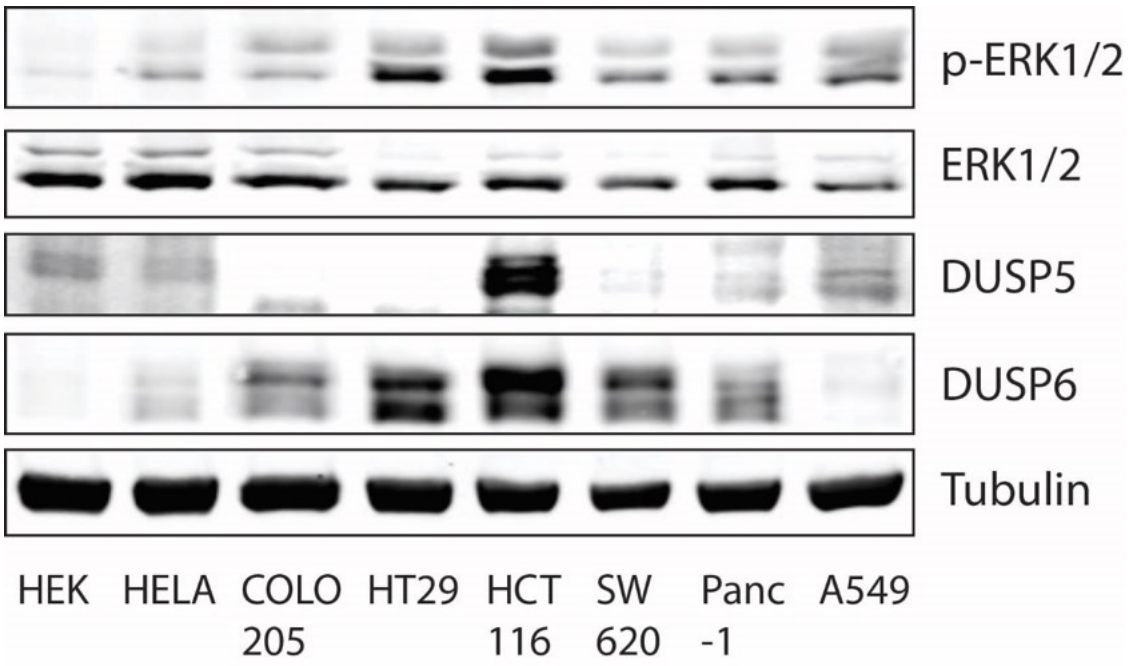

Figure 3.4 Relative expression levels of DUSP5 and DUSP6 in HEK293, Hela and mutant KRAS- and BRAF-driven cancer cell lines. Cells were maintained in routine culture conditions prior to lysis and western blotting. Protein concentration was normalised across samples. Western blot analysis was carried out by Andrew Kidger (Cook laboratory, Babraham Institute, Cambridge, UK).

Based on these findings, and previous work demonstrating the influence of MKPs in tumourigenesis and drug-resistance, we aimed to investigate whether MKP expression levels differed between parental and AZD6244-resistant CRC cell lines in different AZD6244 conditions. As MKPs function as important ERK-induced negative feedback regulators in the ERK signalling pathway we reasoned that this may be likely, and that trends in MKP expression in response to AZD6244 could reflect the nature of their regulatory influence in these cell models.

3.3. Results

3.3.1. MEKi–resistant CRC cells maintain proliferation through sustained ERK activation

Previous work by the Cook laboratory assessed average cell population changes in levels of phosphorylated ERK and other key pathway components in parental and AZD6244-resistant cells through western blot analysis of whole-cell extracts. Additionally, cell fate responses were evaluated primarily through flow cytometry and [^{3}H]thymidine incorporation assays (Little *et al.*, 2011). Western blot analysis remains an invaluable tool in the investigation of protein expression, however most chemiluminescent-based techniques are unable to provide quantitative results. Similarly, while [^{3}H]thymidine incorporation assays are able to reliably demonstrate changes in the proportion of cells in a population undergoing DNA replication and proliferation, the definitive and comparative quantification of cell proliferation is restricted by an inability to account for cell number between different population samples.

Using high content microscopy, a sensitive confocal imaging platform that is able to provide high resolution images as well as detailed signal quantification data, we were able to visualise and quantify changes in levels of total and phosphorylated ERK on a per-cell basis. We aimed to corroborate findings from Little *et al*. (2011) while also allowing for new investigations into signalling and cell fate responses on the single cell level. For these experiments, parental COLO205, HT29 and HCT116 cells and their AZD6244-resistant derivatives were used as cell models. The driving mutations and respective maintenance culture conditions for each of these cell lines are detailed in Table 3.1.

Table 3.1. Driving mutations and maintenance culture conditions of CRC cell model

Cell line	Driving mutation	Maintenance culture conditions
COLO205	$BRAF^{V600E}$	Complete medium
C6244-R AZD6244-resistant COLO205 derivative	$BRAF^{V600E}$	Complete medium with 1 μM AZD6244
HT29	$BRAF^{V600E}$	Complete medium
HT6244-R AZD6244-resistant HT29 derivative	$BRAF^{V600E}$	Complete medium with 1 μM AZD6244
HCT116	$KRAS^{G13D}$	Complete medium
H6244-R AZD6244-resistant HCT116 derivative	$KRAS^{G13D}$	Complete medium with 2 μM AZD6244

In our experiments, parental and drug-resistant cells incubated with increasing concentrations of AZD6244 were subjected to pulse EdU labelling for S-phase detection, prior to cell fixation. This was followed by immunofluorescent protein staining and image acquisition on a high content microscope. Signal intensity data was collected on a per-cell per-compartment basis which allowed for single cell data as well as population data analysis.

Results from these experiments showed that in all parental cell lines, the mean whole-cell intensity of immunofluorescent staining for *p*-ERK decreased in an AZD6244 dose-responsive manner. This paralleled a dose-responsive decrease in proliferation, interpreted as the percentage of cells entering S-phase in a 1h pulse label window (Figure 3.5). These results corroborated findings from previous work characterising cellular responses to AZD6244 in these cell lines (Balmanno et al., 2009; Davies et al., 2007; Yeh et al., 2007). In comparison, drug-resistant CRC lines demonstrated the

ability to maintain relatively high levels of *p*-ERK in the presence of AZD6244 (Figure 3.5). This sustained ERK phosphorylation correlated with the ability of AZD6244-resistant lines to continue proliferating in conditions of up to 1 μM (C6244-R and HT6244-R) or 2 μM (H6244-R) AZD6244 (Figure 3.5), supporting previous results found by western blot analysis and [^{3}H]thymidine incorporation assays (Little *et al.*, 2011).

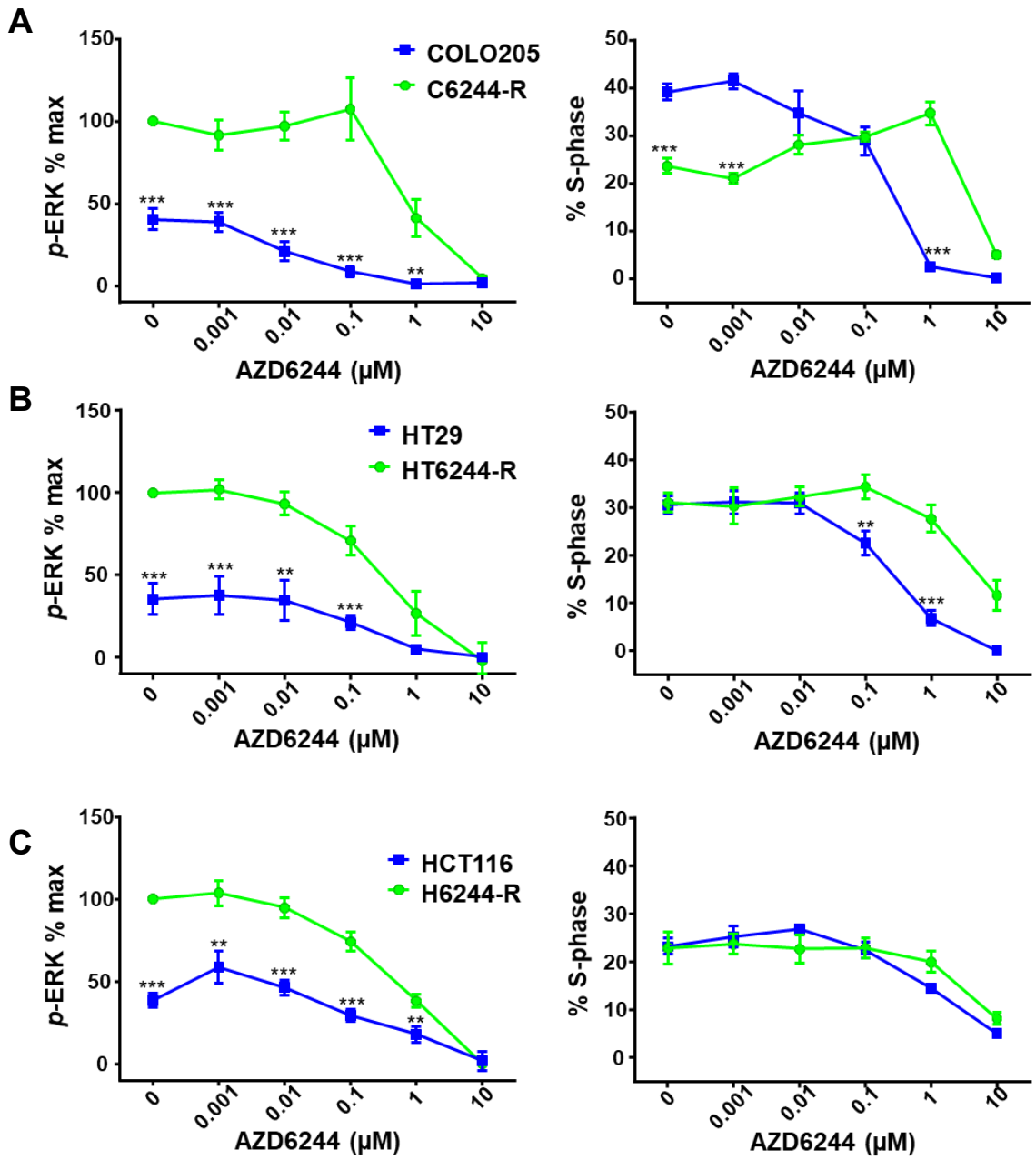

Figure 3.5. Drug-resistant CRCs maintain proliferation through sustained ERK activation. Quantitative HCM summary data of *p*-ERK levels (shown as a percentage of the maximum) and percentage of S-phase cells in the total cell population counted in (A) COLO205 and C6244-R (B) HT29 and HT6244-R and (C) HCT116 and H6244-R samples. Cells were maintained in indicated concentrations of AZD6244 for 48 hours prior to fixation and immunostaining. n=3-6 biological replicates, ± SEM. Statistically significant differences between parental and AZD6244-resistant cell lines in the same AZD6244 concentration were determined using the Holm-Sidak method, where (*) denotes a p-value less than 0.05, (**) denotes a p-value less than 0.01 and (***) denotes a p-value less than 0.001. All assays; 3 fields/well, 2-4 wells (~2000 individual cells) per condition per experiment.

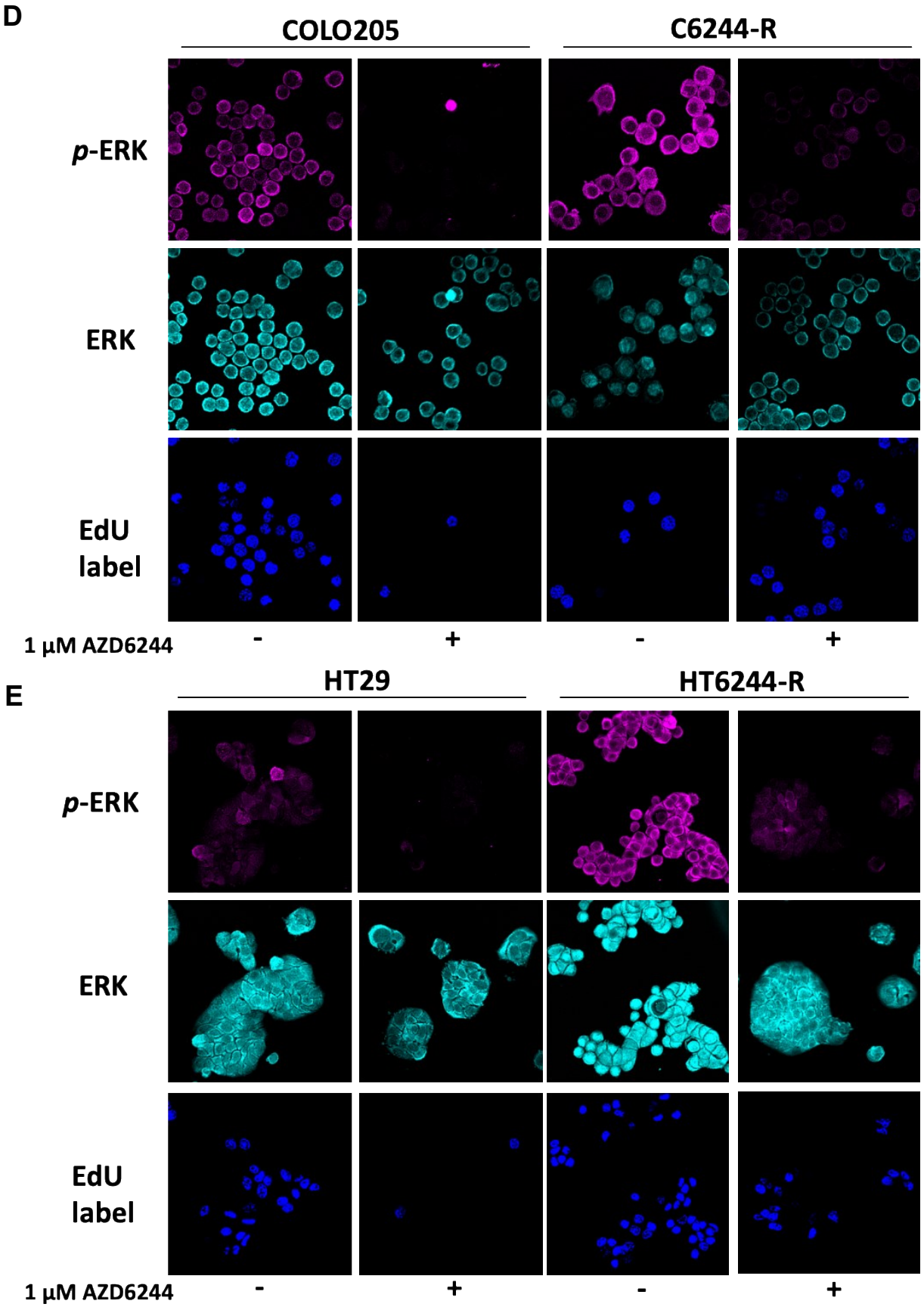

Figure 3.5 continued.

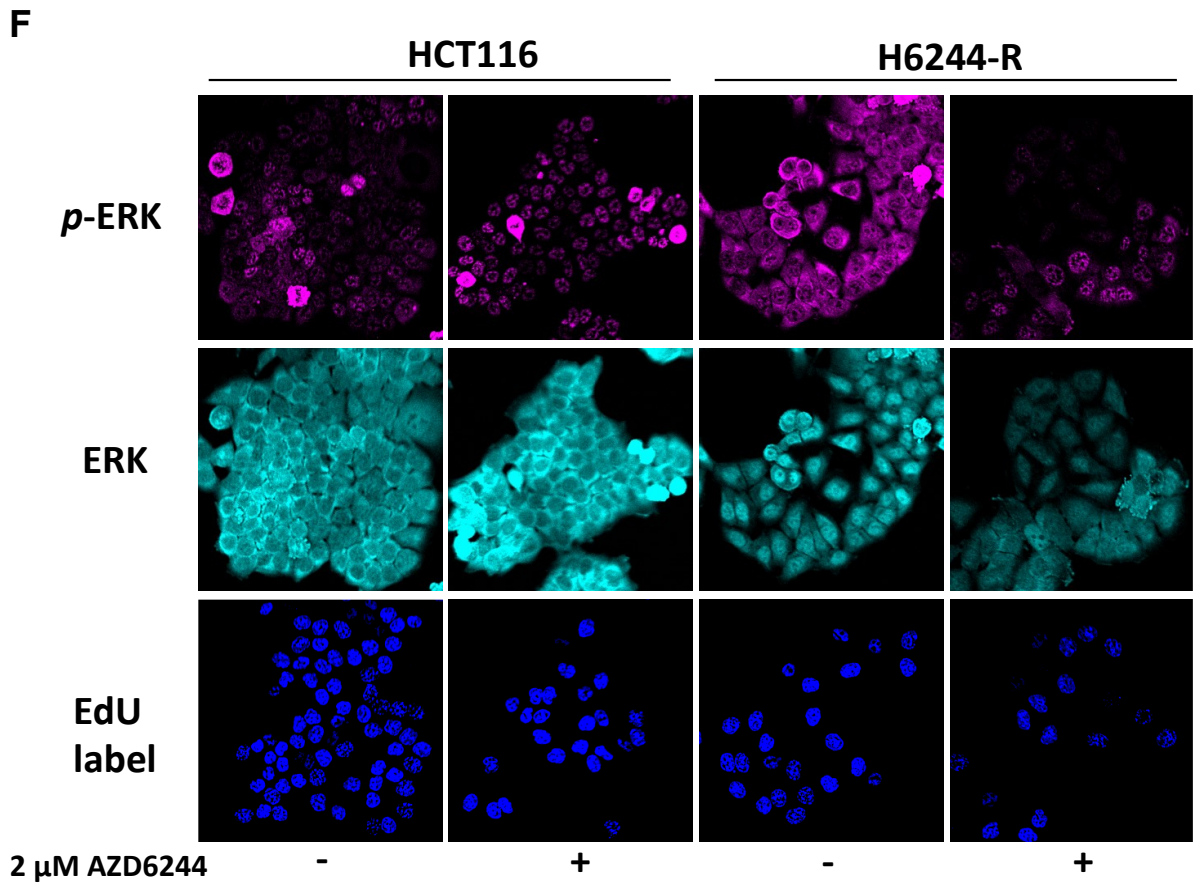

Figure 3.5 continued. Representative images of (A) COLO205 and C6244-R (B) HT29 and HT6244-R and (C) HCT116 and H6244-R cells in the absence or presence of 1 or 2 µM AZD6244.

When comparing the proliferation responses seen in Figure 3.5 to the results of similar experiments from Little *et al*. (2011) shown in Figure 3.1, some discrepancies could be seen in the response of C6244-R to the withdrawal of AZD6244 (i.e. in conditions where the AZD6244 concentration is lower than 1 μM used in routine culture conditions). Figure 3.5a illustrates that the proportion of C6244-R cells undergoing proliferation in all AZD6244 concentrations below routine culture conditions (1 μM AZD6244) was lower than that in routine AZD6244 conditions and indeed less than the subset of proliferating cells in parental cells in routine culture conditions (no AZD6244). This was most apparent in C6244-R cultured in the absence of AZD6244, suggesting that withdrawal of drug from these cells may evoke an anti-proliferative effect.

While it is not possible to directly compare proliferation values between COLO205 and C6244-R cells in Figure 3.1b from Little *et al*. (2011), C6244-R cells demonstrated a dose-responsive decrease in proliferation in the presence of AZD6244, with peak proliferation conditions at 0 μM AZD6244, similar to parental COLO205 cells. This was consistent with cell cycle distribution data obtained by Little et al (2011), shown in Figure 3.2b, where the proportion of cells in G2/M and S-phase in C6244-R cells incubated in the absence of AZD6244 for 24 hrs was similar to or possibly higher than the proportion of these cells in C6244-R populations incubated with AZD6244 concentrations up to 1 μM. In more recent data published by Sale *et al*. (2019) and illustrated in Appendix Figure A6a and d, the proliferation profile and cell cycle distribution of C6244-R cells is more comparable to data shown in Figure 3.5a, displaying a similar anti-proliferative effect of AZD6244 withdrawal. Much like our assays, proliferation assays performed by Sale *et al.* (2019) made use of EdU-labelling and high content microscopy.

Cell cycle distribution data for HT6244-R cells exposed to increasing concentrations of AZD6244 published in Little *et al*. (2011) are shown in Figure 3.1c. These cells appeared to proliferate optimally in routine culture conditions of 1 μM AZD6244 and decreased in proliferative capacity upon drug removal. This trend was not replicated in our data (Figure 3.5b), instead the proportion of proliferating HT6244-R cells appeared to remain relatively constant across AZD6244 concentrations between 0 and 1 μM AZD6244, compared to a dose-responsive decrease in proliferation seen in

parental HT29 cells in the same conditions. Again, our data is consistent with cell cycle distribution data and S-phase data presented in Sale *et al*. (2019), shown in Figure 5.1a (Chapter 5) and in Appendix Figure A6b, respectively, where there was no marked difference in the proportion of cells in G2/M and S-phase between HT6244-R cells incubated with or without 1 μM AZD6244 for 24 hrs.

Finally, a dissimilarity observed when comparing our data set (Figure 3.5c) and results obtained both by Little *et al*. (2011) illustrated in Figure 3.1a, and Sale *et al*. (2019) illustrated in Appendix Figure A6c, was seen in the response of HCT116 and H6244-R cells to increasing AZD6244 concentration. Similar to previous dose response experiments with HCT116 cells and AZD6244 (Balmanno et al., 2009), Figure 3.1a and Appendix Figure A6c show a steady decrease in HCT116 proliferation from 100 nM AZD6244 onwards, reflecting an IC50 of approximately 200nM for inhibition of proliferation in these cells. In contrast, proliferation of H6244-R cells only began to decrease at AZD6244 concentrations higher than 2 μM, reflecting an IC50 of inhibition of proliferation that was approximately 10 times higher than that of parental cells. In our results, HCT116 cells had a proliferation profile that was not markedly different to H6244-R cells and was not indicative of a profound difference in sensitivity to AZD6244.

While the proliferation profiles of drug-resistant CRC cells in response to increasing AZD6244 concentrations showed some differences when compared to similar experiments in Little *et al*. (2011), we were able to quantitatively confirm the observation that drug-resistant CRC lines cultured under routine conditions (1 μM AZD6244 for C6244-R and HT6244-R cells and 2 μM AZD6244 for H6244-R cells) had similar *p*-ERK levels to parental CRC lines under “normal” conditions (no AZD6244), and these tended to be the conditions where proliferation was maximised. This finding supports key evidence found by Little *et al*. (2011), which suggested that AZD6244-resistant cells are able to adapt to MEK inhibition through ERK pathway reprogramming. It also supports the proposed existence of an optimal range of ERK activation that confers cell cycle entry, one which appears to be maintained with some extent of precision within a given cell line.

3.3.2. A narrow range of ERK activation is coincident with S–phase entry

Several methods have been used previously to measure the relative magnitude of active ERK and how this relates to cellular proliferation in response to drug treatment, including western blot analysis of total ERK and *p*-ERK levels, kinase activity assays and population-based proliferation assays. While data derived through these techniques is very useful in describing drug dosage-response trends in the cell population, they are not able to quantify *p*-ERK levels within a single cell and relate this value to the same cell's proliferation status. The ability to do this is important in validating responses to drug administration on a single cell level and ensuring that these trends are a true representation of the population majority and are not the sum of differing sub-populations. Additionally, by analysing cells that have *p*-ERK levels "maintained" by MEK inhibition we can assume with more confidence that the *p*-ERK levels detected at the time of cell fixation are those that were present when cells entered S-phase during the 1-hour pulse.

By using single cell data obtained from immunoflouresence staining experiments detailed above, we have demonstrated the relative frequency distribution of all S-phase positive cells in one AZD6244-dose response experiment across increasing levels of *p*-ERK intensity (Figure 3.6). This includes all cells, in all AZD6244 conditions (0 to 10 μM AZD6244). This frequency distribution data was generated by grouping whole cell *p*-ERK intensity values into bins of 20 grey-scales each. The number of cells that fell within each category that was also S-phase positive was summated and calculated as a percentage of all cells counted in each bin. This percentage value was plotted against the average *p*-ERK intensity value in each bin.

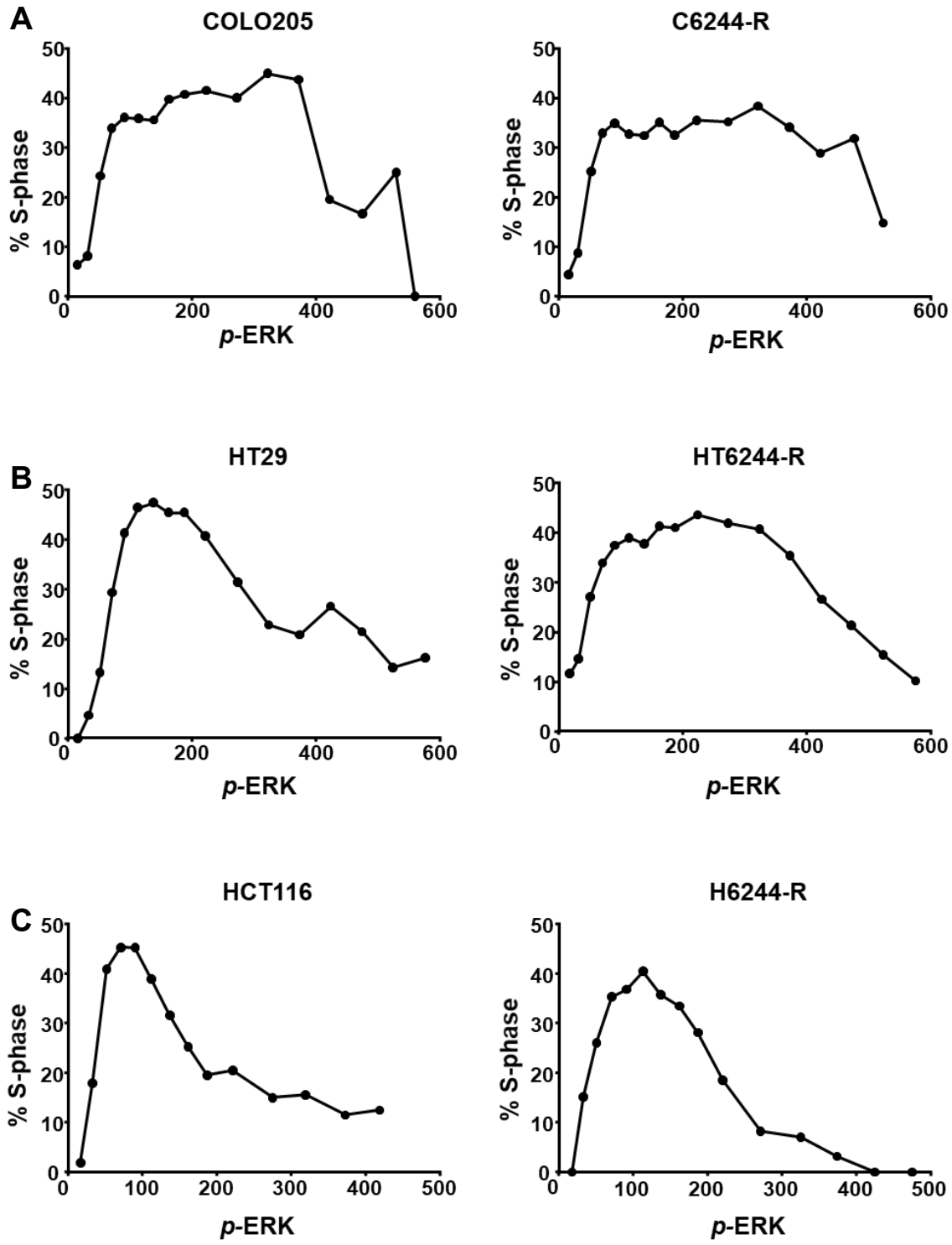

Figure 3.6. A narrow range of ERK activation is coincident with S–phase entry. Single cell HCM data showing p-ERK frequency distributions of the total S-phase positive parental (left) and AZD6244-resistant (right) cells counted in (A) COLO205 and C6244-R (B) HT29 and HT6244-R and (C) HCT116 and H6244-R samples. Cells were maintained in increasing concentrations of AZD6244 for 48 hours prior to fixation and immunostaining. Data obtained from 3 fields/well, 2-4 wells (~2000 individual cells) per condition.

The single-cell data illustrated in Figure 3.6 was obtained from CRC cell lines seeded into one 96 well plate, with comparable densities. While there may be cell line-specific variations in staining quality and image analysis due to different cell morphologies, by exposing all cells to the same increasing AZD6244 dosage, fixing, immunostaining, image acquisition and analysis at the same time, we hoped to enable some comparison between cell samples.

These curves generally show a modal distribution, where the majority of proliferating cells across all drug conditions had *p*-ERK levels that fall within a narrow range. This data suggests that both parental and AZD6244-resistant CRC cells show a similar range of *p*-ERK intensity that correlates with the highest proportion of S-phase positive cells, reinforcing the theory that there is a pre-existing and prevailing “sweet spot” for ERK activity. Parental HT29 and HCT116 curves appeared to be positively skewed, with the HT29 curve showing a potential “shoulder” right of the major peak (Figure 3.6b and c). In HT29, this may indicate a smaller sub-population of cells able to proliferate at higher *p*-ERK levels. The existence of such populations would seem more likely in AZD6244-resistant populations that have been continuously exposed to AZD6244, creating a potential selection pressure. However, while HT6244-R and H6244-R curves were positively skewed, similar to the relative frequency distribution of their parental counterparts, there were no obvious signs of secondary peaks.

In general, proliferating COLO205 and C6244-R cells appeared to tolerate higher levels of *p*-ERK over a larger range, relative to HT29, HCT116 and their derivative cell lines (Figure 3.6a). It is important to note however, that it is unclear whether these differences were biologically relevant or a result of variation in immunostaining capacity due to different cell-line characteristics and morphologies.

3.3.3. MEKi removal from MEKi-resistant CRC cells causes ERK hyperactivation and the nuclear accumulation of ERK

The concept of the ERK “sweet spot” becomes particularly relevant in the context of AZD6244-resistant cells, where removal of AZD6244 leads to ERK hyperactivation. This phenomenon was first demonstrated in Little *et al*. (2011) and was replicated in our data (Figure 3.5). Relative quantification of *p*-ERK protein abundance revealed that *p*-ERK levels were almost doubled in the absence of AZD6244 compared to their routine culture conditions containing 1 or 2 μM AZD6244 (Figure 3.5). Sustained

increases in endogenous *p*-ERK levels such as this are not commonly reported, presumably due to the robust and self-limiting nature of the ERK signalling pathway. These conditions could therefore serve as a unique and valuable model to investigate the mechanisms through which endogenous ERK hyperactivation can occur, and the cellular consequences that may follow.

In order to assess the population variation of cells exposed to the addition or removal of AZD6244 and to replicate the trends described in Figure 3.5 on a single cell level, we plotted the percentage of single cells in each concentration of AZD6244 (as a proportion of all cells in each condition) that fell within a 10 grey-scale *p*-ERK intensity bin against the minimum value of each bin. These frequency distributions were generated using GraphPad Prism. Figure 3.7 illustrates that in general, each cell population was normally distributed within a single peak, indicating that the majority of *p*-ERK values measured in each condition fell within a small distance of the mean value. The absence of multiple peaks suggests that the mean *p*-ERK value for each condition did in fact reflect the average response of all cells and not an average of two or more sub-populations.

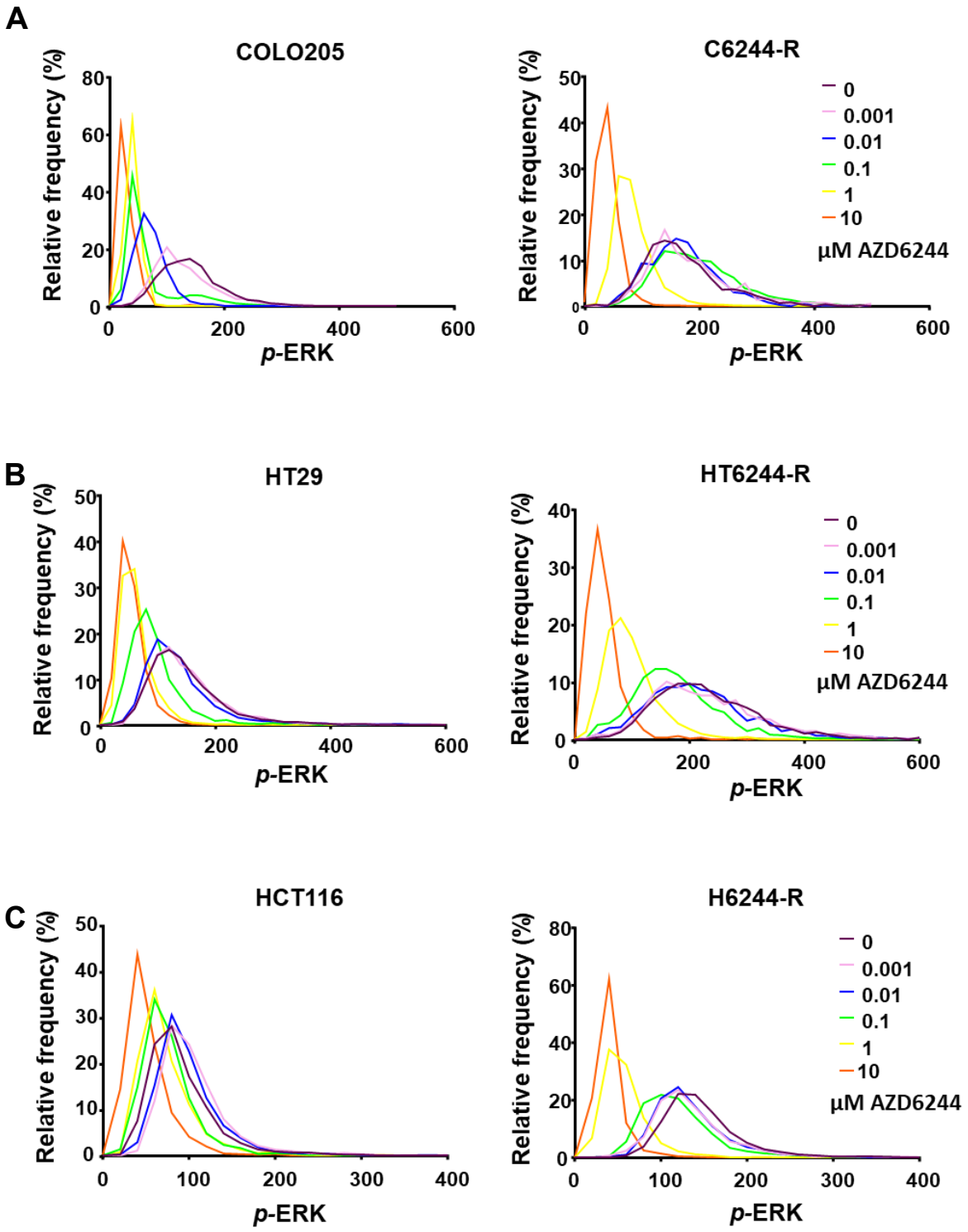

Figure 3.7. Drug-resistant CRCs shift to higher *p*-ERK levels following drug-removal. Single cell data showing *p*-ERK frequency distributions of cells in (A) COLO205 and C6244-R (B) HT29 and HT6244-R and (C) HCT116 and H6244-R samples at each drug concentration in parental (left) and AZD6244-resistant cells (right). Cells were maintained in indicated concentrations of AZD6244 for 48 hours prior to fixation and immunostaining. Data obtained from 3 fields/well, 2-4 wells (~2000 individual cells) per condition.

If the figures for parental cell lines COLO205, HT29 and HCT116 (Figure 3.7a, b and c) are viewed from right to left, the distributions of cells at each drug concentration showed a strong shift to lower *p*-ERK levels following AZD6244 addition. The trends seen in the AZD6244-resistant cell lines are markedly different, where the distribution of cells only shifted in AZD6244 conditions of 0.1 μM AZD6244 and higher. This clearly demonstrates the ability of AZD6244-resistant CRC cells to maintain higher levels of *p*-ERK in the presence of AZD6244, compared to their parental counterparts.

If the figures for AZD6244-resistant cell lines C6244-R, HT6244-R and H6244-R are viewed from left to right, each cell distribution showed a strong shift to higher *p*-ERK levels following AZD6244 removal (Figure 3.7a, b and c). The maximum *p*-ERK levels reached were substantially higher than those measured for each parental counterpart and represented conditions of ERK hyperactivation. The distribution of AZD6244-resistant cells under routine culture conditions (1 μM AZD6244) were comparable to each parental counterpart under normal culture conditions (no AZD6244). This paralleled results observed in the average population data (Figure 3.5) and those in Little *et al*. (2011). In both parental and AZD6244-resistant cells, the width of the peaks, and therefore spread of the data, tended to increase with decreasing AZD6244 concentration and increasing *p*-ERK values, indicating that variability in response increased in these conditions. This was most pronounced in drug-resistant CRCs in conditions of AZD6244 below routine culture concentrations, where *p*-ERK levels were greatly enhanced.

The analysis of the high content microscopy data obtained from AZD6244 dose-response experiments was performed in such a way that the relative immunofluorescent staining intensity for *p*-ERK and ERK in the cytoplasm and nucleus were quantified as separate measures. This made it possible to assess *p*-ERK and ERK compartmentalisation in response to AZD6244 in our parental and AZD6244-resistant cell models. Localisation of ERK is a key aspect of ERK pathway regulation that is not yet fully understood, specifically in the context of ERK pathway addiction and inhibition. Many studies have demonstrated that mitogenic activation of the ERK signalling pathway and subsequent nuclear accumulation of *p*-ERK is a prerequisite for cell-cycle entry in various cell lines. However, these studies tend to focus on short-

term activation of the ERK pathway and not on tumourigenic cell lines that rely on consistent ERK activation.

Using data derived from HCM imaging and analysis experiments we compared the ratio of nuclear to cytoplasmic ERK across increasing AZD6244 conditions in all 6 CRC cell lines. Figure 3.8 demonstrates that removing drug from drug-resistant CRC cells caused an increase in the ratio of nuclear to cytoplasmic ERK, while this ratio remained relatively constant in parental cell lines. In this data set a ratio of 1 would indicate an equal amount of ERK signal in the nucleus and cytoplasm. A number greater than 1 indicates a higher proportion of ERK in the nucleus, while a number less than 1 indicates a higher proportion of ERK in the cytoplasm. In AZD6244-free conditions, the nuclear to cytoplasmic ratio of all 3 parental lines approached 1, indicating that ERK levels were relatively consistent across the cell. A similar trend was seen in AZD6244-resistant cells in routine culture conditions (1-2 μM AZD6244). However, when AZD6244 concentration was decreased in AZD6244-resistant cells, total ERK appeared to shift predominantly to the nucleus in a dose-responsive manner.

In HT6244-R cells, the N:C ratio was significantly higher in cells cultured without AZD6244 than in cells cultured with 1 μM AZD6244. While the apparent increase in nuclear ERK in AZD6244-withdrawal conditions in C6244-R and H6244-R cells was not statistically significant, a trend is visible and an apparent increase in nuclear ERK in C6244-R, HT6244-R and H6244-R cells cultured in the absence of AZD6244 can be seen in representative cell images in Figure 3.5 (d-f). Interestingly, these images appeared to indicate that the proportion of ERK that moved into the nucleus was in the unphosphorylated state, as high intensity *p*-ERK signal appeared predominantly in the cytoplasm (Figure 3.5 d-f).

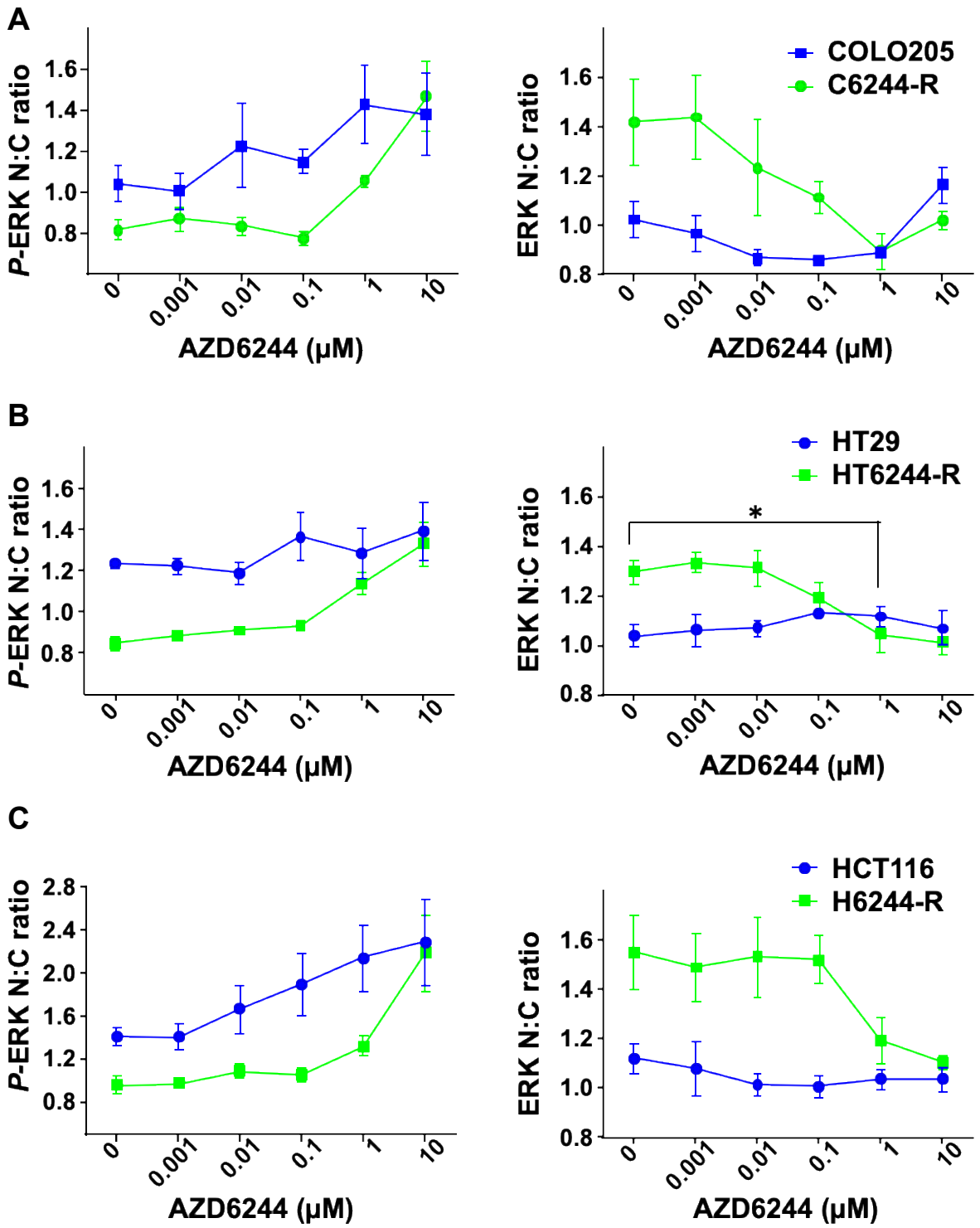

Figure 3.8. AZD6244 withdrawal from resistant lines causes nuclear accumulation of ERK. Quantitative HCM summary data. (A) COLO205 and C6244-R (B) HT29 and HT6244-R and (C) HCT116 and H6244-R cells were maintained in indicated concentrations of AZD6244 for 48 hours prior to fixation and immunostaining. n=3-4 biological replicates, ± SEM. A statistically significant difference in N:C ratio between HT6244-R cells cultured without AZD6244 and those cultured with 1 μM AZD6244 was determined using an unpaired t test, where (*) denotes a p value less than 0.05. All assays; 3 fields/well, 2-4 wells (~2000 individual cells) per condition per experiment.

The nuclear to cytoplasmic ratios shown for *p*-ERK in Figure 3.8 should be interpreted with caution, as the signal intensity for *p*-ERK drops towards background levels in concentrations above 1 μM in parental and AZD6244-resistant CRC cells as shown in Figure 3.5. In addition, non-specific or low-level background signal tends to stain brighter in the nucleus. Under such conditions, the nuclear to cytoplasmic ratio may appear higher, however these values are not biologically meaningful.

With the limitations of this data noted, it is still possible to assess the nuclear to cytoplasmic ratios in conditions where *p*-ERK signal is reliably detectable (between 0 and 1 μM AZD6244). Interestingly, in general, all three parental cell lines appeared to retain more *p*-ERK in the nucleus than their AZD6244-resistant derivatives in routine 1 or 2 μM AZD6244 conditions as well as in drug withdrawal conditions (Figure 3.8). The most consistent trend seen in AZD6244-resistant CRC cells was that relative to the distribution of *p*-ERK in maintenance conditions (either more or less equally present in the nucleus or cytoplasm or slightly more present in the nucleus than cytoplasm) *p*-ERK appeared to reside more predominantly in the cytoplasm than the nucleus when AZD6244 is removed from these cells (Figure 3.8) As mentioned, this was apparent in representative images illustrated in Figure 3.5 (d-f).

The results obtained thus far together with work performed by other groups have shown marked changes in the phosphorylation and location of ERK in response to the administration or withdrawal of AZD6244 in parental and drug-resistant CRC cells (Smith *et al.*, 2007; Yeh *et al.*, 2007; Balmanno and Cook, 2009; Little *et al.*, 2011). Most importantly, these experiments suggested that AZD6244 withdrawal and ERK hyperactivation in resistant CRC cells was consistent with the nuclear accumulation of ERK, which appeared to be largely unphosphorylated. As MKP proteins are key regulators of ERK activation and localisation, we went on to assess the relative abundance of these phosphatases in parental and drug-resistant CRC cell lines exposed to similar AZD6244 regimes.

3.3.4. DUSP4, DUSP5 and DUSP6 expression increases in a dose-responsive manner following MEKi removal from MEKi-resistant CRC lines

Dual-specificity MAPK phosphatases (MKPs) are a family of inducible signalling proteins that are solely dedicated to the regulation of their target MAP kinases. While ten catalytically active DUSPs have been identified in mammalian cells, we chose to focus on 3 nuclear MKP proteins, DUSP2, DUSP4 and DUSP5 as well as DUSP6, which is located in the cytoplasm. A predominant role of the nuclear MKP proteins, specifically DUSP5 which solely targets ERK, is to dephosphorylate and anchor ERK in the nucleus. We therefore reasoned that nuclear MKPs may play a role in the accumulation of dephosphorylated ERK that was coincident with AZD6244 removal in CRC cells (Figure 3.8). We also assessed DUSP6, which like DUSP5, specifically targets ERK. By comparing the expression of DUSP5 and DUSP6 we hoped to provide some insight into differing roles of nuclear and cytoplasmic MKPs in these cell models.

To begin investigating the role of transcriptionally-induced MKPs in the signalling responses of parental and drug-resistant CRC lines, relative DUSP2, DUSP4, DUSP5 and DUSP6 mRNA levels were assessed using quantitative RT-PCR in the absence or presence of AZD6244. The most prominent result visible in this data was a relative increase in DUSP5 mRNA in all three drug-resistant cell lines cultured in the absence of AZD6244, compared to the DUSP5 levels detected in samples from drug-resistant and parental cell lines cultured in maintenance conditions (Figure 3.9, a, b and c). A similar trend was seen for DUSP4 in AZD6244-resistant HT6244-R and H6244-R, where levels of DUSP4 mRNA increased upon AZD6244 removal (Figure 3.9b and c). While this difference in DUSP4 mRNA levels was not statistically significant in HCT116 and H6244-R cells (Figure 3.9c), a similar trend was apparent.

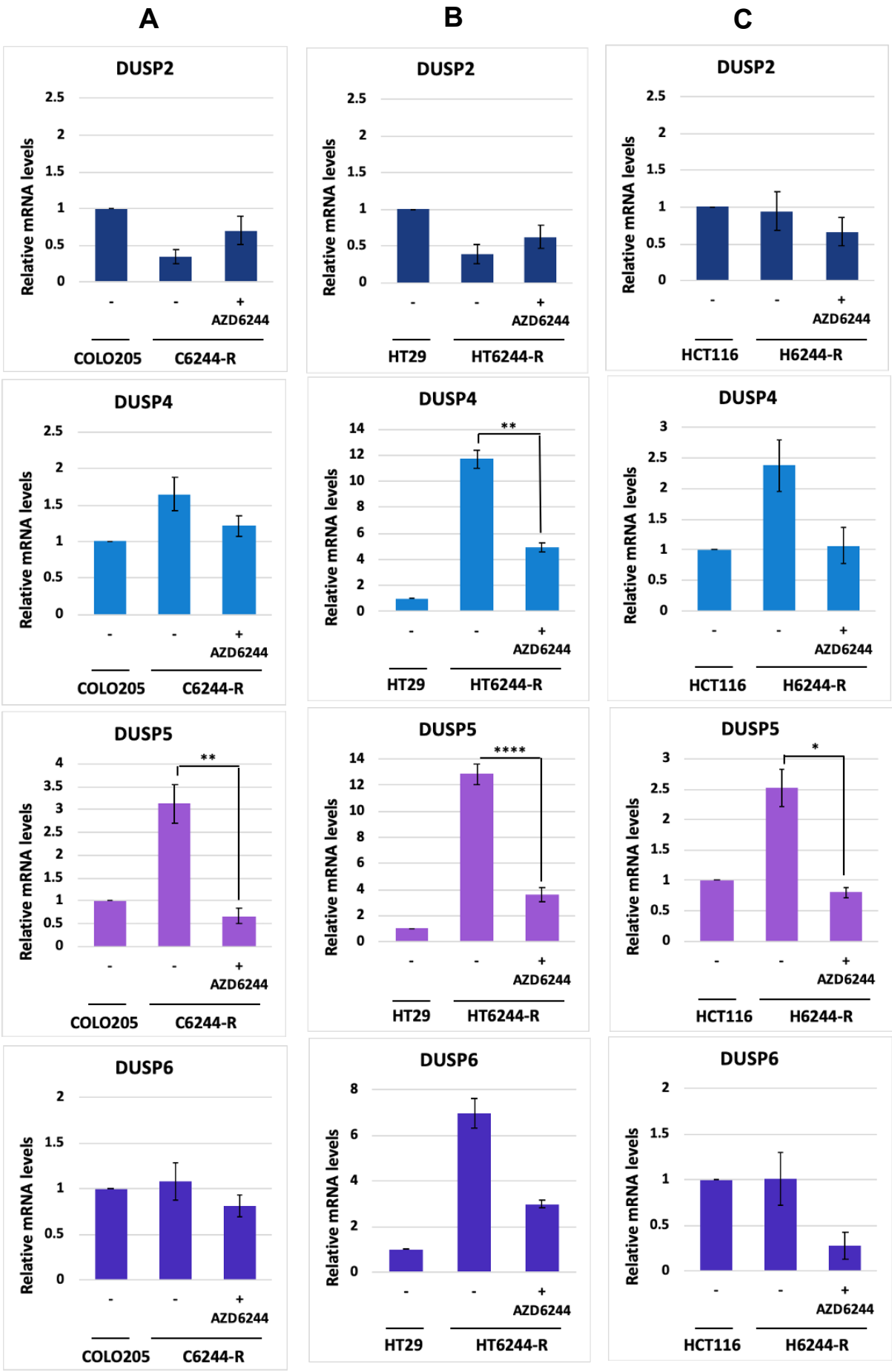
A
B
C
DUSP2
Relative mRNA levels
2.5
2
1.5
1
0.5
0
- - +
AZD6244
COLO205 C6244-R
HT29 HT6244-R
HCT116 H6244-R
DUSP4
14
12
10
8
6
4
3
**
DUSP5
****
*
DUSP6

Figure 3.9. Removal of AZD6244 from AZD6244–resistant CRC cells leads to increased DUSP4, 5 and 6 mRNA expression. Relative DUSP mRNA expression levels in (A) COLO205 and C6244-R (B) HT29 and HT6244-R and (C) HCT116 and H6244-R cells in the presence of 0, 1 (C6244-R AND HT6244-R) or 2 μM (H6244-R) AZD6244. Cells were maintained with or without AZD6244 for 48 hours prior to RNA extraction. n=3-4 biological replicates ± SEM. Statistical analysis performed using a One-way ANOVA and a post-hoc Tukey analysis, where (*) denotes a p-value less than 0.05, (**) denotes a p-value less than 0.01 and (****) denotes a p-value less than 0.0001.

Overall, no statistically significant differences in mRNA expression of DUSP2 or DUSP6 were detected across parental and AZD6244-resistant CRC lines in response to AZD6244. This is perhaps not surprising for DUSP2, which has primarily been shown to be expressed in hematopoietic tissue (Seternes et al., 2019). However, an interesting trend was seen in the expression of DUSP6 in HCT116 and H6244-R cells. In their respective maintenance conditions, DUSP6 expression was decreased in H6244-R cells compared to HCT116 cells, however, when AZD6244 was removed from H6244-R cells, DUSP6 levels were increased back to the levels seen in parental HCT116 cells.

In the interpretation of these results, it is important to highlight that the ΔΔCq method of data normalisation ensures that all Cq values detected are normalised to the those for the reference gene as well as to those in a calibrator sample within each experiment. Therefore, the resulting ratios calculated did not provide quantification data for the abundance of each transcript relative to any other transcript, but only a ratio of the transcript abundance in one sample compared to the calibrator sample. This means that a relative increase in mRNA levels in a sample does not necessarily reflect an abundance of transcript in this sample, as the levels of transcript in the calibrator could be very low.

MKP protein induction is predominantly controlled through de novo mRNA transcription, thus increases in mRNA levels are generally indicative of increases in protein abundance (Huang and Tan, 2012). However, regulation of MKP protein stability can occur at the post-translational level and may result in discrepancies in mRNA and protein abundance (Caunt and Keyse, 2013). In order to directly assess levels of MKP protein, western blot analysis of whole cell lysates harvested after a 48-

hour incubation with different AZD6244 concentrations were performed (Figure 3.10). These immunoblots revealed similar trends in MKP protein abundance to those seen for MKP mRNA levels, with some exceptions.

In HT6244-R and H6244-R cells, DUSP4 and DUSP5 protein levels increased in a dose-responsive manner to the withdrawal of AZD6244 (Figure 3.10b). In C6244-R cells, DUSP4 levels also appeared to increase with decreasing AZD6244 concentration, while DUSP5 protein was barely detectable in either COLO205 or C6244-R cells (Figure 3.10a). This may at first appear contrary to the mRNA results seen in COLO205 and C6244-R cells, however as mentioned, these results indicated that DUSP5 transcript levels were higher in C6244-R cells cultured in the absence of AZD6244 than those in C6244-R and COLO205 cells cultured in their respective maintenance conditions and not that they were generally abundant in these samples. These results were consistent with western blots performed by Andrew Kidger, showing an absence of DUSP5 protein expression in parental COLO205 cells (Figure 3.4).

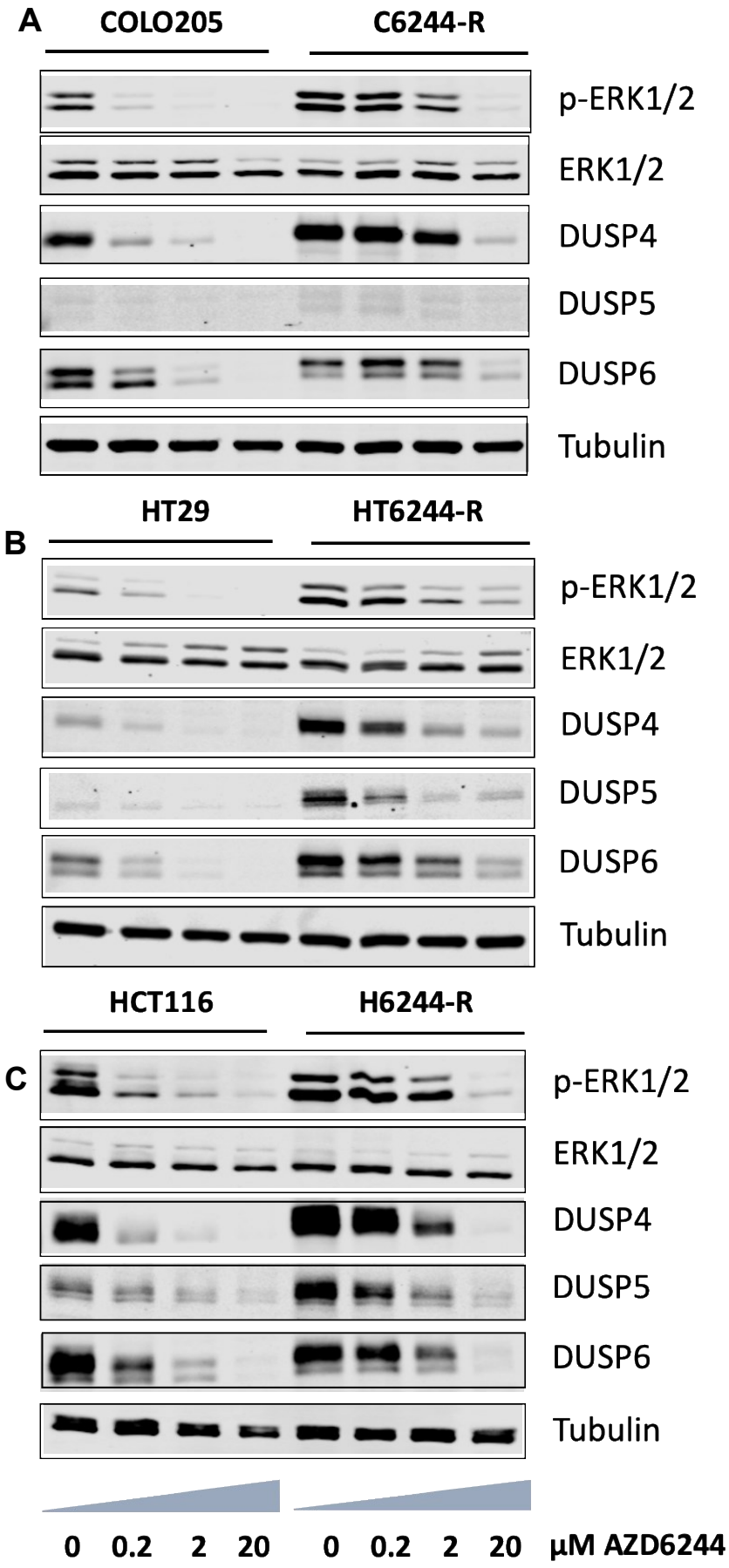
A
COLO205
C6244-R
p-ERK1/2
ERK1/2
DUSP4
DUSP5
DUSP6
Tubulin
B
HT29
HT6244-R
p-ERK1/2
ERK1/2
DUSP4
DUSP5
DUSP6
Tubulin
C
HCT116
H6244-R
p-ERK1/2
ERK1/2
DUSP4
DUSP5
DUSP6
Tubulin
0 0.2 2 20 0 0.2 2 20 μM AZD6244

Figure 3.10. Removal of AZD6244 from AZD6244-resistant CRC cells causes an increase in DUSP4, 5 and 6 protein expression. (A) COLO205 and C6244-R (B) HT29 and HT6244-R and (C) HCT116 and H6244-R cells were maintained with or without AZD6244 for 48 hours prior to cell lysis. Cell lysates were subject to SDS-PAGE and immunoblot. Images are representative of results from 3 independent experimental repeats.

Similar to mRNA results, DUSP4 and DUSP5 proteins were most highly expressed in AZD6244-resistent cells in the absence of drug and lower levels of DUSP4 and DUSP5 were seen in parental cells in 0 μM AZD6244 and their AZD6244-resistant derivatives in either 1 or 2 μM AZD6244 (with the exception of DUSP5 in COLO205 and C6244-R cells). This was coincident with a similar expression pattern seen for *p*-ERK in these conditions (Figure 3.10), suggesting a positive correlation between the expression of *p*-ERK and DUSP4 and 5 in response to AZD6244.

mRNA analysis did not reveal significant differences between DUSP6 expression in AZD6244-resistant cell lines cultured in AZD6244 compared to those cultured without AZD6244, however western blot images in Figure 3.10, b and c indicated that DUSP6 levels were increased in drug withdrawal conditions in HT6244-R and H6244-R cells relative to maintenance conditions. Interestingly, like in mRNA results, DUSP6 levels in untreated HCT116 cells appeared to be higher than in any other condition and DUSP6 levels in H6244-R cells cultured in maintenance conditions were reduced compared to their parental counterparts. Upon AZD6244 removal, these levels increased and were more similar to those seen in untreated HCT116 cells (Figure 3.10c). Similarly, high levels of basal DUSP6 expression were also evident in COLO205 cells in maintenance conditions compared to all other COLO205 and C6244-R samples. Unlike results seen in HT6244-R and H6244-R samples, it was unclear whether DUSP6 levels were increased in response to AZD6244 removal in C6244-R cells in these experiments (Figure 3.10a).

This data has clearly demonstrated that in AZD6244-resistant CRC cell lines, MKP levels become changed in response to AZD6244 removal, such that DUSP4, DUSP5 and DUSP6 are strongly induced by ERK hyperactivation. These findings are significant in establishing a correlation between strong ERK activation and increased expression of ERK-induced negative feedback regulators in the context of oncogenesis. It also indicates that MKPs may play an important role in restraining hyperactive ERK in the development of drug-resistance in these cell lines.

3.3.5. The induction of different MKPs upon MEKi removal is temporally distinct and cell-line dependent

After assessing whether there was any correlation between MKP and *p*-ERK levels and AZD6244 administration after a 48-hour incubation period, we went on to investigate shorter term signalling changes that may occur in AZD6244-resistant CRC cells directly after drug withdrawal. In these western blot experiments, AZD6244-resistant CRC cells routinely cultured in 1 μM AZD6244 (C6244-R and HT6244-R) or 2 μM AZD6244 (H6244-R) were incubated in the absence of AZD6244 according to a 48-hour time course protocol. These results revealed that phosphorylation of ERK was strongly induced within 30 minutes of AZD6244 withdrawal, a response that was consistent across all three AZD6244-resistant cell lines (Figure 3.11).

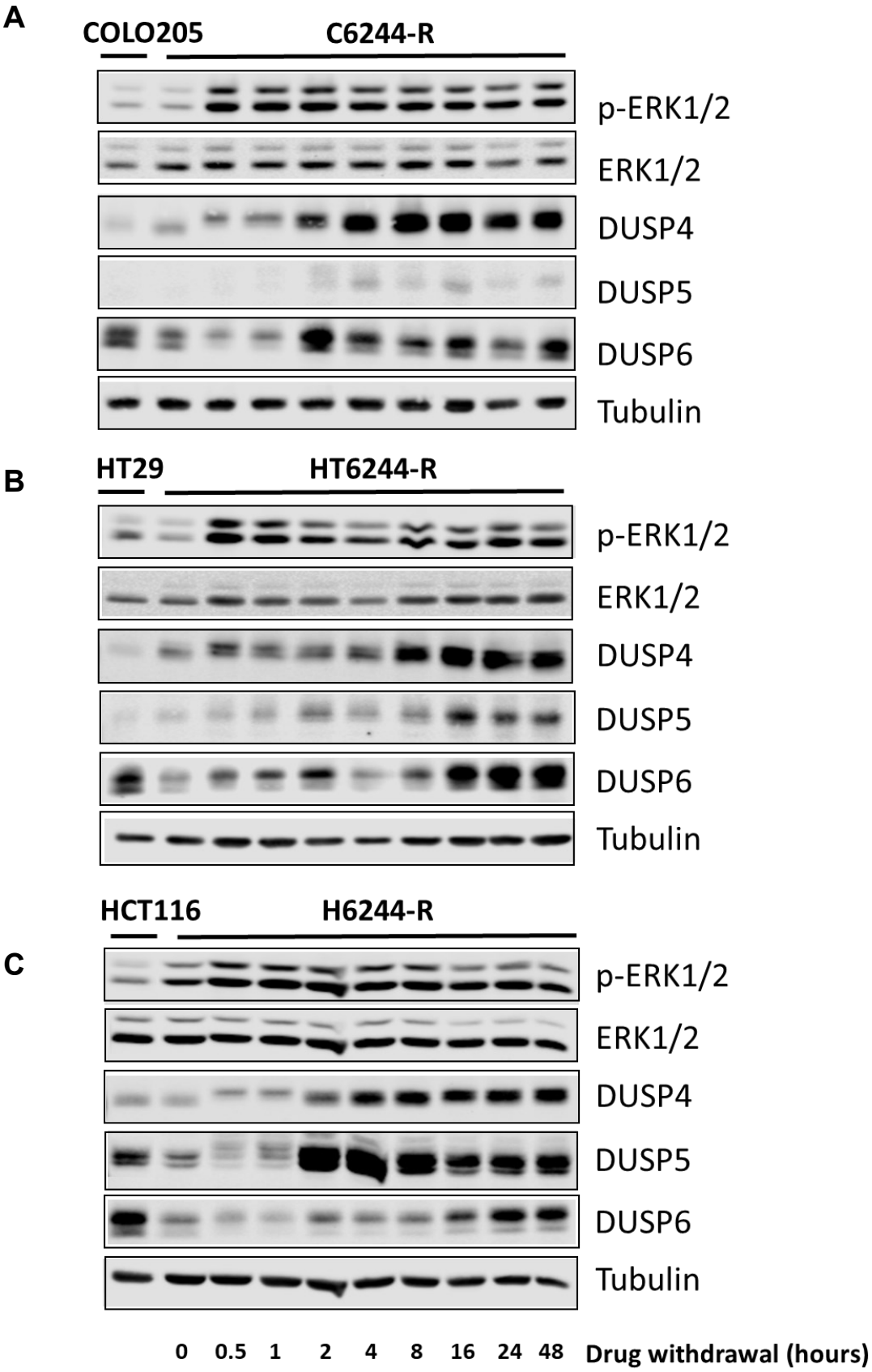
A
COLO205
C6244-R
p-ERK1/2
ERK1/2
DUSP4
DUSP5
DUSP6
Tubulin
B
HT29
HT6244-R
p-ERK1/2
ERK1/2
DUSP4
DUSP5
DUSP6
Tubulin
C
HCT116
H6244-R
p-ERK1/2
ERK1/2
DUSP4
DUSP5
DUSP6
Tubulin
0 0.5 1 2 4 8 16 24 48
Drug withdrawal (hours)

Figure 3.11. The induction of DUSP4, 5 and 6 protein expression in response to AZD6244 removal follows temporal and cell-specific patterns. (A) COLO205 and C6244-R (B) HT29 and HT6244-R and (C) HCT116 and H6244-R cells were maintained with or without AZD6244 for 48 hours prior to cell lysis. Cell lysates were subject to SDS-PAGE and immunoblot. Images are representative of results from 3 independent experimental repeats.

Within 30 minutes to an hour of drug withdrawal, DUSP4, DUSP5 and DUSP6 proteins appeared to undergo a shift to a higher molecular weight form (Figure 3.11b). In C6244-R cells this shift was followed by an increase in DUSP4 and DUSP6 protein abundance, which for DUSP4, was then sustained up to 48 hours (Figure 3.11a). Before DUSP4 expression peaked between 2 and 16 hours after AZD6244 removal in C6244-R cells, DUSP4 protein appeared to return to a lower molecular weight form. As mentioned before, DUSP6 protein was present in relatively high abundance in parental COLO205 cells as well as C6244-R cells in 1 μM AZD6244 (Figure 3.10 and Figure 3.11). These protein levels appeared to decrease within 1 hour of AZD6244 removal (coincident with a molecular weight shift) and then peaked at 2 hours post-AZD6244 removal. This was followed by a period within which DUSP6 abundance appeared to fluctuate (Figure 3.11a). While there was some indication that DUSP5 was induced in C6244-R cells, its expression was substantially lower than in HT6244-R and H6244-R cells, where equal amounts of total protein were loaded (Figure 3.11).

The molecular weight shifts in DUSP4, DUSP5 and DUSP6 proteins shifts are likely to reflect post-translational modifications of the MKP proteins, such as phosphorylation. The phosphorylation of DUSP6 by ERK has been shown to promote its ubiquitination and degradation (Marchetti et al., 2005). This is consistent with our findings that generally showed a decrease in DUSP6 expression at higher molecular weight forms. In light of strong ERK activation in these conditions, these molecular weight shifts and fluctuations in DUSP6 protein levels may be indicative of ERK-mediated DUSP6 turnover. In contrast, phosphorylation of DUSP4 by ERK has been shown to increase its stability, while phosphorylation of DUSP5 does not appear to affect its half-life (Brondello et al., 1999; Cagnol and Rivard, 2013; Kucharska et al., 2009b). Interestingly, our results showed that like DUSP6, DUSP4 and DUSP5 were most highly expressed in their lower molecular weight form.

Patterns of DUSP4, DUSP5 and DUSP6 expression in HT6244-R cells in response to AZD6244 removal (Figure 3.11b) were similar to those seen in C6244-R cells (Figure 3.11a), with the exceptions that DUSP5 induction was more prominent and DUSP6 expression seemed to be steady between 16 and 48 hours after treatment. DUSP4 and 6 protein expression in H6244-R cells followed similar response profiles to those seen in C6244-R and HT6244-R cells (Figure 3.11). Notably, the expression of DUSP5 in these cells was particularly robust, which suggests that DUSP5 may play an important role in the response of H6244-R cells to ERK pathway inhibition and release. While *p*-ERK levels were increased within 30 minutes of drug withdrawal in all AZD6244-resistant cell lines, the time of maximal induction of DUSP4, DUSP5 and DUSP6 differed between different MKPs and across the different cell lines. Once maximally induced, the expression of DUSP4 and DUSP5 was sustained and remained high at 48 hours post-AZD6244 withdrawal in all drug-resistant lines. In contrast, the levels of DUSP6 appeared to fluctuate over this time period.

Taken together, mRNA and protein analyses assessing changes in MKP expression in parental and AZD6244-resistant CRC lines have shown that the removal of AZD6244 from drug-resistant CRC cells induced the expression of DUSP4, DUSP5 and DUSP6, with the exception of DUSP5 in C6244-R cells. The expression of DUSP4 and DUSP5 in both parental COLO205, HT29, HCT116 cells and their AZD6244-resistant derivatives followed a similar expression pattern to *p*-ERK, suggesting a positive correlation between ERK activation and DUSP4 and DUSP5 induction. While DUSP6 expression was also increased in drug-resistant CRC cells in the absence of AZD6244 compared to its expression in C6244-R, HT6244-R and H6244-R cells cultured in maintenance conditions, these relatively higher levels were similar to those seen in untreated parental CRC cells, unlike coincident *p*-ERK levels.

3.4. Discussion

Using a mixture of conventional biochemical approaches and high content microscopy, we have compared changes in drug efficacy and signalling/cell fate response in mutant BRAF- and KRAS-driven colorectal cancer (CRC) cell lines and derivatives that have evolved resistance to the MEK inhibitor (MEKi), AZD6244, by KRAS or BRAF oncogene amplification. Our data firstly confirm quantitatively and on a single-cell level, the observation that CRC cells become MEKi-resistant by restoring ERK activity to levels that drive proliferation. We further show that removal of MEKi from drug-resistant CRC cells causes ERK hyperactivation, and the nuclear accumulation of ERK, leading to cell cycle arrest in BRAF- but not KRAS-driven cells. These changes are coincident with a large increase in transcription and expression of DUSP4, DUSP5 and DUSP6, dual specificity/MAPK phosphatases that dephosphorylate and anchor ERK in the nucleus and cytoplasm.

Immunofluorescent-staining and high content microscopy of colorectal cancer cells lines HCT116, HT29 and COLO205 and their drug resistant derivatives revealed that proliferation of drug-resistant CRCs in the presence of AZD6244 was maintained through sustained activation of ERK (Figure 3.5) and these levels of *p*-ERK were consistent with levels found in parental cells maintained in drug-free medium. This data provides quantitative evidence to support the theory proposed by Little *et al.* (2011) that resistant cells compensate for inhibited MEK by restoring signalling output through the ERK pathway, such that *p*-ERK levels remain in a range consistent with proliferation. Single cell distribution curves from our AZD6244 dose-response experiments further illustrated that the majority of proliferating cells in each population expressed levels of *p*-ERK that fell within a relatively narrow range (Figure 3.6). This and other work alludes to a “sweet spot” of ERK activity that is required for cell cycle entry *(Woods et al*., 1997; Sewing *et al*., 1997; Das Thakur *et al*., 2013). While single cell data was able to show the distribution of all proliferating parental and AZD6244-resistant cells relative to their respective *p*-ERK levels, quantification of *p*-ERK in these experiments was purely relative, and did not provide any information on the absolute levels of *p*-ERK. Work following this performed by Sale *et al*. (2019) was able to provide more definitive insight into the optimal range of ERK activation required for proliferation. In a series of mass spectometery analyses Sale and colleagues assessed the absolute levels of total and phosphorylated ERK present in proliferating

parental and AZD6244-resistant CRC cells and revealed that just 1-5% of total ERK was active in all cell lines, and was sufficient for continued cell division. These results were unexpected; not only did all CRC cell lines evaluated show very similar stoichiometry for active ERK, but this analysis revealed a substantial spare capacity for ERK activation.

Interestingly, while amplified KRAS or BRAF was likely established to counteract MEK inhibition in AZD6244-resistant C6244-R and H6244-R cells, microarray data from cell samples revealed coincident increases in downstream negative regulators of ERK signalling such as SPRY2 and DUSP4 and DUSP6 phosphatases relative to parental COLO205 and HCT116 cells (Sale et al., 2019). This suggests that despite considerable MEK inhibition, signalling downstream of amplified BRAF/KRAS needs to be further restrained by negative feedback regulation to elicit ERK levels coincident with cell cycle entry. The importance of negative feedback in this context is further emphasised by the discovery of the substantial spare capacity of ERK which is likely maintained by negative ERK regulators such as the DUSP/MKPs. With this understanding, it follows that large increases in active ERK, such as those seen in AZD6244-resistant CRC cells incubated without AZD6244 may induce concomitant increases in MKP expression.

Results from mRNA and protein quantification analyses were consistent with this hypothesis and demonstrated the expression of DUSP4 and DUSP6 in parental COLO205 and HT29 cells and their AZD6244-resistant derivatives and DUSP4, DUSP5 and DUSP6 in both HCT116 and H6244-R cells in maintenance conditions. When AZD6244 was removed from AZD6244-resistant cells, ERK hyperactivation was coincident with markedly increased levels of DUSP4 and DUSP5 in HT6244-R and H6244-R cells and DUSP4 in C6244-R cells. While DUSP6 was robustly expressed in AZD6244-withdrawal conditions across all resistant cells, these levels were not necessarily higher than those in parental conditions, and therefore were not directly correlated to the expression patterns of *p*-ERK in these conditions. In contrast, levels of DUSP4 and DUSP5 appeared to mirror those of *p*-ERK in the same conditions.

Concomitant with ERK hyperactivation and DUSP4 and DUSP5 induction in AZD6244-resistant cells deprived of AZD6244, was what appeared to be the nuclear accumulation of unphosphorylated ERK. This was reminiscent of results seen in experiments with intestinal epithelial crypt (IEC) cells where the ectopic expression of $KRAS^{G12V}$ and $BRAF^{V600E}$ led to sustained ERK activation and an accumulation of ERK in the nucleus (Cagnol and Rivard, 2013). Interestingly, high levels of *p*-ERK appeared to be localised primarily in the cytoplasm of these cells and this phenotype was associated with increased mRNA expression of the nuclear MKPs DUSP4 and DUSP5. When transformed IEC cells were treated with vanadate, a potent tyrosine phosphatase inhibitor, levels of nuclear *p*-ERK were increased (Cagnol and Rivard, 2013). This work went on to demonstrate that heightened DUSP4 expression and predominantly cytoplasmic expression patterns of *p*-ERK were evident in 19 CRC cell lines. In each case, nuclear *p*-ERK levels could be increased with vanadate treatment. The exclusion of DUSP5 in further investigations was due to the absence of a reliable DUSP5 antibody at this time, rather than its inferior relevance. While these experiments did not account for the relative contribution of other ERK phosphatases or suggest what the influence of the cytoplasmic ERK-specific MKP might be, it does clearly demonstrate a potential role for nuclear MKPs DUSP4 and DUSP5 in sustained ERK signalling in colorectal cells (Cagnol and Rivard, 2013).

The reason for the potentially increased biological relevance of MKP signalling in these contexts may be due to changes in MKP function in the presence of prevailing ERK activation. In transient ERK activations, signalling is commonly attenuated by immediate forms of negative regulation, such as the inhibitory effects of active ERK on its upstream activators. In these scenarios, feedback by MKPs is limited to later phases of the stimulus. When consistent oscillations of ERK activation continue to induce MKP expression, this may simulate a kind of signalling “memory” where MKPs that are still present from previous inductions can exert regulatory functions at any stage of consecutive activation cycles. In this way, inducible MKPs such as DUSP4 and DUSP5, may exert more immediate and profound control of ERK in scenarios where ERK activation is sustained.

In saying this, the potential relevance of different MKPs appears to be highly variable across different CRC cell lines. Not only do different cell lines express different DUSPs at varying levels, but the temporal induction of MKPs in response to ERK hyperactivation appears to be cell line specific too. This is likely to reflect substantial differences in the genotypic background of these lines that would have inevitably influenced the specific adaptions that occur during oncogenesis and the evolution of drug resistance, including the relative contributions of different MKPs.

In summary, these experiments have illustrated a correlative relationship between ERK hyperactivation and MKP expression in three AZD6244-resistant CRC cells. This provides strong preliminary evidence of a role of MKPs in the development of resistance to ERK pathway inhibition, where they likely function to restrain rampant ERK activation induced by upstream amplification of mutant BRAF or KRAS.

3.5. Limitations and future work

As previously discussed, our investigations into the correlation between *p*-ERK expression and proliferative status in single cell data were limited by the relative nature of immunofluorescent protein quantification as well as the innate inability to accurately measure cellular *p*-ERK levels at the time of cell cycle entry. Later work by Sale et al. (2019) used mass spectrometry to gather absolute quantification data that revealed the proportion of active ERK in the total ERK pool of proliferating cells, which provided valuable insight into the dynamics of the ERK “sweet spot”. It will be interesting to see if this work is replicated in other cell lines, and if the biological function of ERKs substantial “spare capacity” can be revealed.

Additionally, initial HCM experiments designed to investigate the dynamics of ERK phosphorylation and localisation in response to AZD6244 administration also aimed to assess proliferation, and so AZD6244 regimes typically lasted for 24 to 48 hours. While this provided valuable data illustrating sustained effects on the magnitude of *p*-ERK in relation to proliferation, it did not reveal any information on the more immediate spatiotemporal regulation of ERK. Time course experiments completed for western blot analysis revealed that *p*-ERK was induced within 30 minutes of AZD6244 withdrawal. HCM experiments assessing the intensity and location of *p*-ERK and ERK

signal within this initial response period could provide interesting insights into the precise subcellular mechanisms of ERK hyperactivation.

Finally, mRNA and protein expression analyses were able to show the robust induction of DUSP4, DUSP5 and DUSP6 in response to ERK hyperactivation, which provided important preliminary insights into the influence these proteins may have on oncogenic ERK signalling. However, through these analyses, we were not able to compare the levels of different MKPs to one another, or ascertain the relative abundance of these transcripts or proteins in each sample. In future, a more global and informative assessment of feedback at play in these cell models could be attained through the assessment of mRNA copy number variations in a high throughput RNA screen. Not only could this validate our current data, but it could provide further insights into kinome and phosphatome reprogramming that occurs in drug-resistant CRC cells cultured with and without MEK inhibition.

Chapter 4. DUSP5 loss in MEKi-resistant HCT116 cells enhances ERK hyperactivation and the reduction of E-cadherin expression upon AZD6244 withdrawal

4.1. Introduction

The analysis of MKP expression in parental CRC cell lines and their AZD6244-resistant derivatives has revealed cell-line specific nuances in DUSP4, DUSP5 and DUSP6 mRNA and protein levels. This is reminiscent of conflicting accounts of the potential tumour suppressive or oncogenic roles of various MKPs in different cancer models and likely reflects a dependence of MKP influence on the specific context it arises in. Even within a single cancer model, the impact of negative MKP-directed ERK regulation could differ before and after tumour development and again before and after the development of drug-resistance. This will depend on the signalling changes that are necessary to maintain the narrow “proliferative window” of ERK activation in each context. Most strikingly, our work demonstrated that when AZD6244 is withdrawn from resistant CRC cells and ERK is hyperactivated, a robust and sustained induction of DUSP4, DUSP5 and DUSP6 is evident. This observation implies that these ERK-targeting MKPs may act to restrain active ERK levels in these conditions. This hypothesis is supported by the observation that the relative expression profiles of the nuclear MKPs DUSP4 and DUSP5 correlated to ERK hyperactivation and the accumulation of dephosphorylated ERK in the nucleus, findings that were consistent with a previous study in colorectal cells (Cagnol and Rivard, 2013). While it would be interesting to explore the relevant impact of both nuclear MKPs in this model, the promiscuity of DUSP4 in its ability to inactivate ERK, JNK and p38 MAPKs would add untold complexity to the interpretation of any subsequent results. Particularly in the context of the anti-proliferative effects seen in AZD6244-deprived C6244-R and HT6244-R cells, where changes in ERK, JNK and p38 MAPK levels could have opposing effects.

In C6244-R cells, removal of AZD6244 leads to hyperactivation of ERK and senescence (Sale et al., 2019). A similar phenotype was demonstrated in a breast cancer cell line model, where exposure to the phorbol 12-myristate 13-acetate (PMA) led to increased active ERK levels and growth arrest (Nunes-Xavier et al., 2010). This work went on to show that coincident with this phenotype, was a substantial upregulation of DUSP5 and DUSP6 expression and silencing of either MKP led to the acceleration of growth arrest. Interestingly, when DUSP5 or DUSP6 was ectopically expressed in PMA-treated breast cancer lines, ERK levels were reduced and the proliferative capacity of these cells appeared to be reinstated (Nunes-Xavier et al., 2010). Additionally, these cells appeared to adopt a migratory phenotype. While the ectopic expression of MKPs has demonstrated similar results in other oncogenic models, it is important to note that the endogenous link between active ERK and MKP expression is seldom recapitulated in these studies which reduces the biological relevance of their use. Despite this caveat, these results suggested that similar to DUSP4 in oncogene-transformed IEC cells, DUSP5 and DUSP6 may be vital negative regulators of sustained ERK activity in breast cancer models.

Like breast cancer cell lines in the Nunes-Xavier *et al.* (2010) PMA model, changes in *p*-ERK levels in AZD6244-resistant H6244-R cells leads to increased cell mobility (Sale et al., 2019). While this was induced by a reduction of *p*-ERK in breast cancer lines, it was coincident with increased ERK activation in H6244-R cells in AZD6244-withdrawal conditions and correlated with an epithelial-to-mesenchymal transition (EMT). As mentioned before, ERK hyperactivation in these conditions was coincident with an accumulation of dephosphorylated ERK in the nucleus and marked increases in DUSP4, DUSP5 and DUSP6 expression. Interestingly, basal levels of DUSP5 were relatively high in HCT116 as well as H6244-R cells compared to CRC cell lines. Following these results and findings from previous studies, we aimed to evaluate the effects of DUSP5 loss in HCT116 and H6244-R cells and whether DUSP5 ablation was able to influence the signalling and phenotypic outcomes of AZD6244 administration.

4.2. Work preceding this thesis

4.2.1. AZD6244 withdrawal from resistant cells with KRAS^{G13D} amplification induces long-term hyperactivation of ERK

Following work published by the Cook laboratory in 2011 detailing the resistance mechanisms of four colorectal cancer cell lines to the MEK inhibitor AZD6244, Sale *et al*. (2019) went on to further explore the effects seen in AZD6244-resistant cells when AZD6244 was removed. This work revealed that hyperactivation of ERK induced by drug withdrawal demonstrated in Little *et al*. (2011) as well as this thesis (Figure 3.5), is maintained for 30 weeks in H6244-R cell lines and single cell clones, with 30 weeks being the maximum length of study performed (Figure 4.1a). This is coincident with sustained KRAS amplification as well as hyperactivation of PKB, the downstream effector of the PI3K signalling pathway. When exposed to AZD6244 after 30 weeks, H6244-R cells were not resensitised to the anti-proliferative effects of AZD6244 and showed similar proliferation profiles to that of H6244-R cells maintained in AZD6244 in dose response experiments (Figure 4.1b). This is contrary to the effects of prolonged drug withdrawal seen in BRAF^{V600E}-driven C6244-R andHT6244-R cells, where resistance to AZD6244 is reversed and a reduction in amplified BRAF leads to reduced levels of *p*-ERK (Sale et al., 2019).

In C6244-R and HT6244-R cells, AZD6244 withdrawal leads to cell-cycle arrest or cell death, demonstrating the anti-proliferative effects of ERK hyperactivation in these cells (Sale et al., 2019). In contrast, the hyperactivation of ERK and PKB upon AZD6244 withdrawal in H6244-R cells does not appear to have an effect on proliferation or cell survival (Figure 4.1c) when compared to parental HCT116 cells or H6244-R cells in the presence of drug. H6244-R cultured in the absence of AZD6244 for 9 to 12 days show similar cell numbers (Figure 4.1c) and cell cycle profiles (Figure 4.1d) to those cultured in AZD6244. Interestingly, similar results were observed in the KRAS^{G13D}-driven cell line LOVO. While the genetic mechanisms of amplified ERK signalling in AZD6244-resistant LOVO cells differs to that of H6244-R cells, similar increases in *p*-ERK are seen upon drug withdrawal, along with no quantifiable deficit in proliferation. While some AZD6244-resistant LOVO clones had partial reversion to AZD6244 sensitivity after prolonged withdrawal, others remained refractory to the anti-proliferative effects of AZD6244 (Sale et al., 2019).

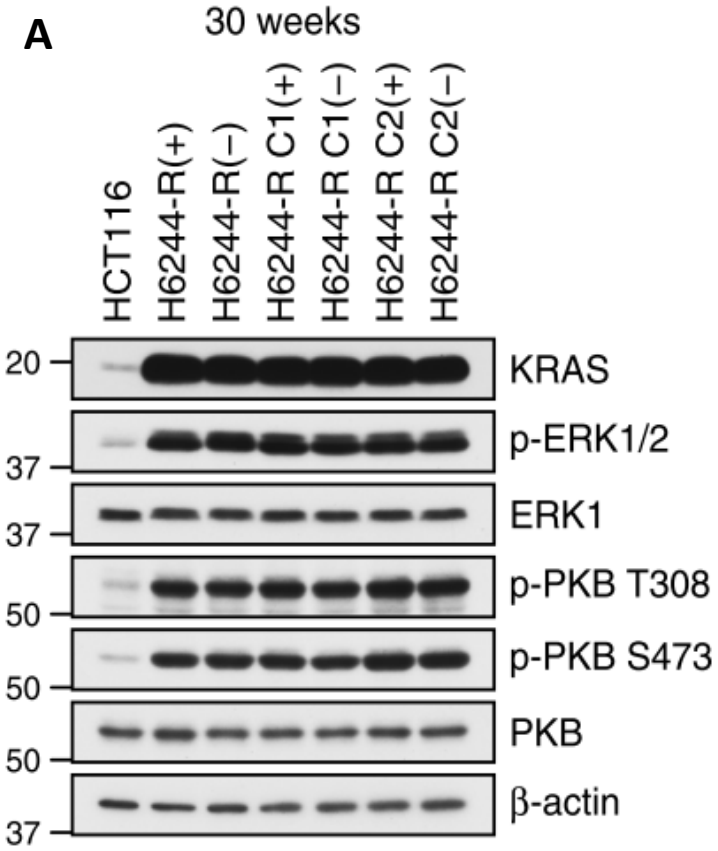

Figure 4.1. Acquired MEKi resistance driven by KRAS^{G13D} amplification is not reversible. A) Following 30 weeks culture in the presence (+) or absence (HCT116, (−)) of 2 μM AZD6244, cells were incubated in selumetinib-free medium for 24 hours and lysates were western blotted with the indicated antibodies. H6244-R C1 and C2 are single-cell clone derivative cell lines of H6244-R. This figure was adapted from Sale et al. (2019) with permission from Nature communications.

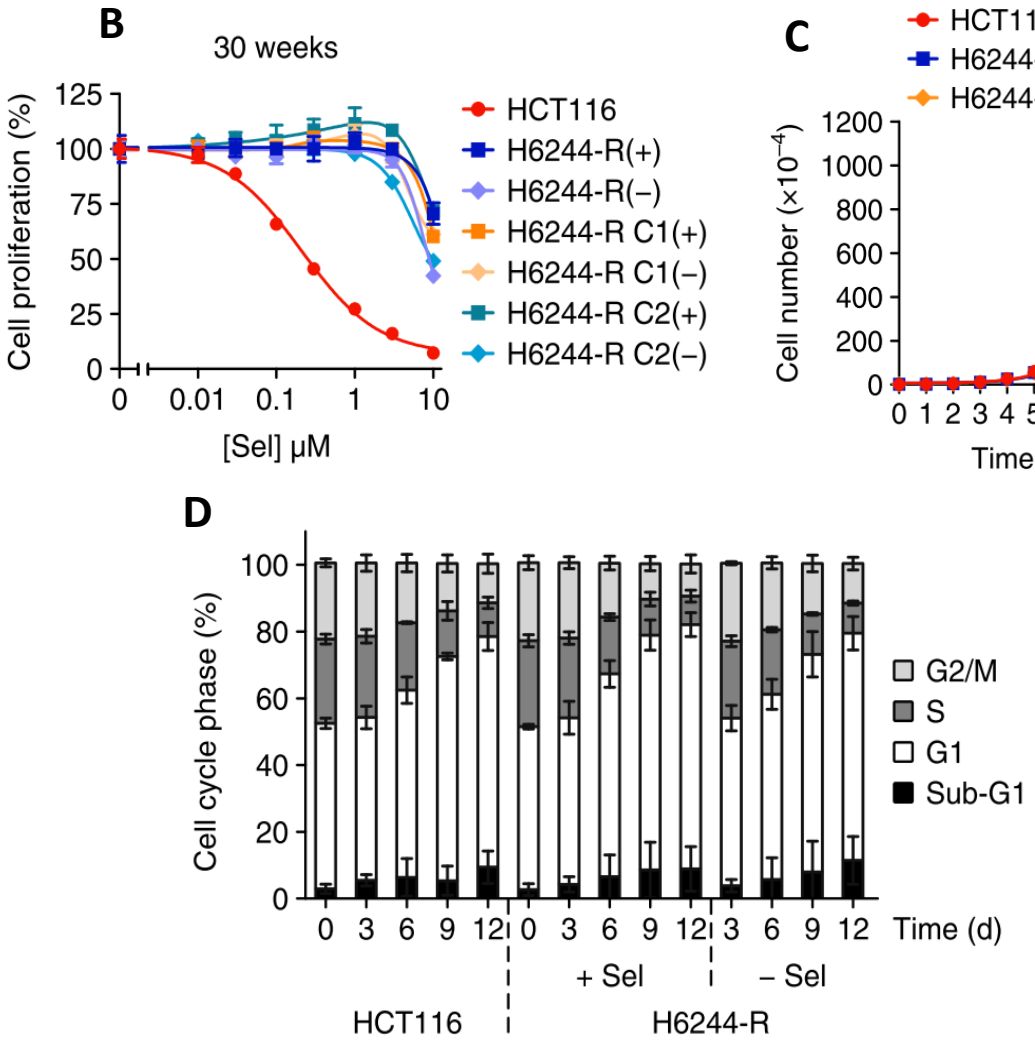

Figure 4.1 continued. B) Following 30 weeks culture in the presence (+) or absence (HCT116, (−)) of 2 μM AZD6244, cells were treated as indicated with AZD6244 for 24 hours, and DNA synthesis assayed by [3H]thymidine incorporation. C) HCT116 and H6244-R cells were treated with either 2 μM selumetinib (H6244-R+ Sel) or DMSO only (HCT116, H6244-R − Sel) and cell numbers counted over 9 days. Results are mean ± SD of cell culture triplicates, representative of three independent experiments. D) HCT116 and H6244-R cells were treated with either 2 μM selumetinib (H6244-R+ Sel) or DMSO only (HCT116, H6244-R − Sel) for the indicated times. Cell cycle distribution was determined by flow cytometry. This figure was adapted from Sale et al. (2019) with permission from Nature communications.

4.2.2. AZD6244 withdrawal from H6244-R cells promotes an ERK-dependent epithelial-to-mesenchymal transition

Proliferation assays investigating the phenotypic effects of AZD6244 removal from H6244-R cells did not reveal any anti-proliferative effects, however, upon visual inspection of H6244-R cells in AZD6244-free conditions, striking changes to the morphology of these cells were observed (Sale et al., 2019). HCT116 cells and H6244-R cells cultured in routine conditions grow in discrete patches with well-defined cell to cell contacts (Figure 4.2a). Confocal microscopy and immunofluorescent protein staining show distinct patterns of E-cadherin expression along the periphery of these cells, an epithelial-associated cell-cell adhesion molecule (Figure 4.2b). In contrast, H6244-R cells grown in the absence of AZD6244 showed a spindle-shaped morphology and reduced cell-cell contacts (Figure 4.2a). These cells also showed limited E-cadherin staining and the appearance of Vimentin protein inclusions (Figure 4.2b), both indications of an epithelial-to-mesenchymal (EMT) transition.

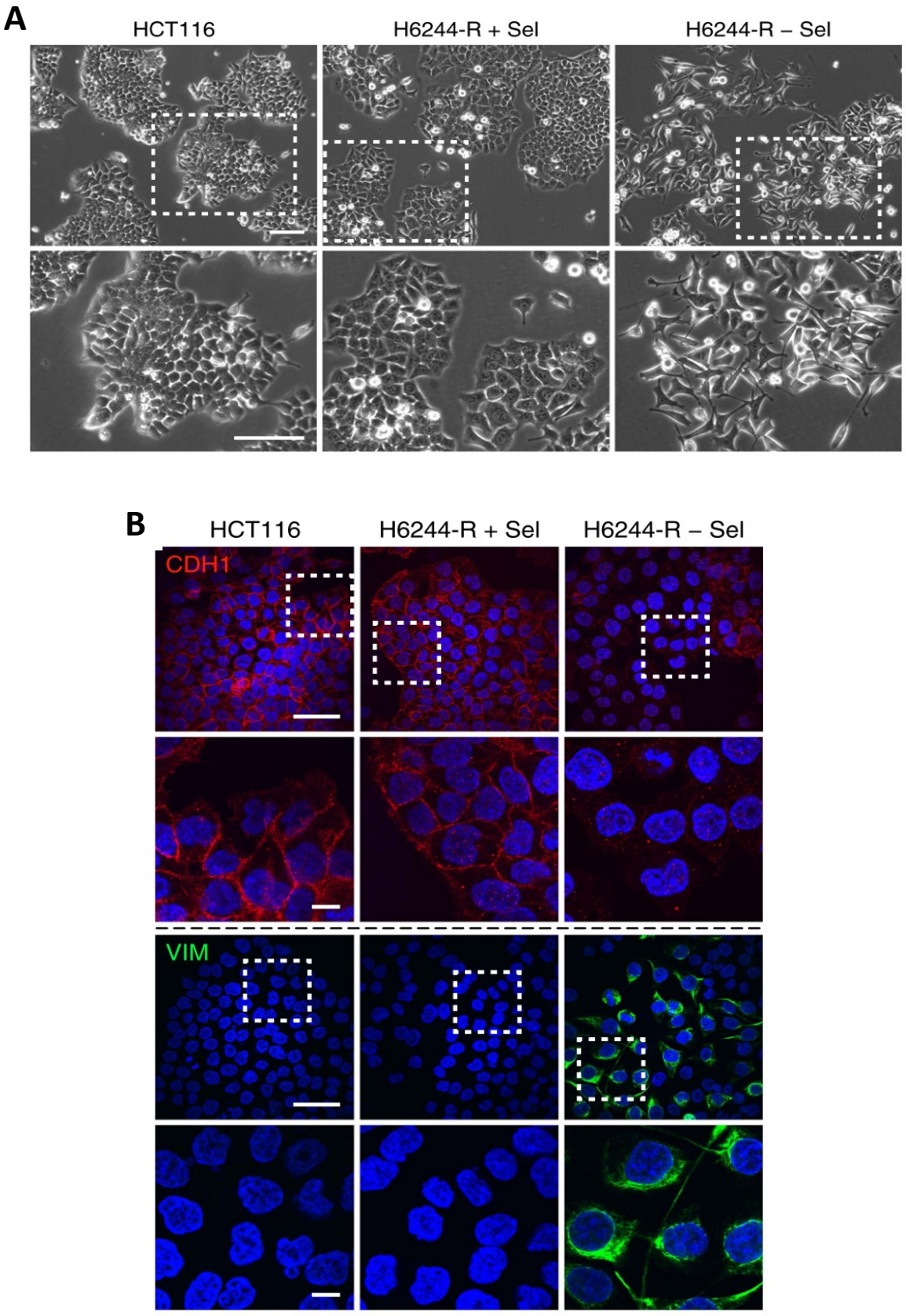
A
HCT116
H6244-R + Sel
H6244-R – Sel
B
HCT116
H6244-R + Sel
H6244-R – Sel
CDH1
VIM

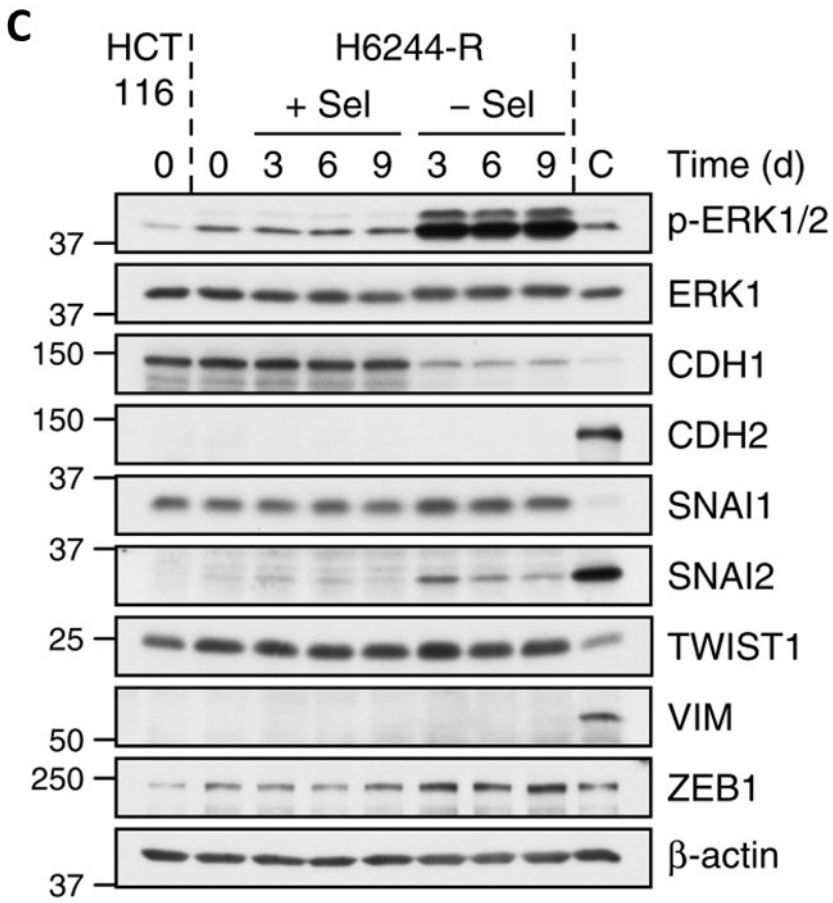

Figure 4.2. MEKi withdrawal from cells with KRAS^{G13D} amplification/upregulation induces a ZEB1-dependent EMT. A) HCT116 and H6244-R cells were treated with 2 μM selumetinib (H6244-R+ Sel) or DMSO only (HCT116, H6244-R − Sel) and imaged by brightfield phase contrast microscopy after 9 days. Scale bars indicate 100 μm. B) HCT116 and H6244-R cells were treated with 2 μM selumetinib (H6244-R+ Sel) or DMSO only (HCT116, H6244-R − Sel) for 9 days and stained for CDH1 (red) or VIM (green) and nuclei (blue). Scale bars indicate 50 μm (upper panels) and 10 μm (lower panels). C) HCT116 and H6244-R cells were treated with 2 μM selumetinib (+ Sel) or DMSO only (HCT116, − Sel) for the indicated times. This figure was adapted from Sale *et al*. (2019) with permission from Nature communications.

RT-PCR and western blotting revealed the upregulation of other mesenchymal markers in AZD6244-deprived H6244-R cells, including SNAI2 and ZEB1 (Figure 4.2c). siRNA- knockdown of ZEB1 in these cells reversed E-cadherin loss, indicating that the EMT observed upon drug withdrawal may be ZEB1-dependent. ERK has been shown to induce transcription of ZEB1 mRNA through its upregulation and stabilisation of FRA1 (Shin et al., 2010). It has also been shown to repress E-cadherin expression by promoting the interaction of ZEB1 and the CtBP co-repressor complex (Ichikawa et al., 2015). Together these provide a possible mechanism through which hyperactive ERK may promote EMT in H6244-R cells. Indeed, further experiments by Sale *et al*. (2019) demonstrated that administration of the ERK inhibitor SCH772984 and successful *p*-ERK reduction was able to reverse the upregulation of ZEB1 and SNAI2 and the loss of E-cadherin expression. Like KRAS-driven H6244-R cells, E-cadherin loss, upregulation of mesenchymal markers and a ZEB1-dependent EMT were found in AZD6244-resistant LOVO cells undergoing drug withdrawal. Similarly, ERK inhibition by SCH772984 was able to reverse this phenotype.

These results give an indication of the consequences of drug-cessation in BRAF- and KRAS-driven colorectal cells and illustrate the heterogenic response of genetically distinct cancer lines to changes and adaptations in ERK signalling. This work also emphasises the potential influence regulators of ERK may have on signalling adaptions that occur in response to chemotherapeutic inhibitors. Indeed, this study as well as others preceding it demonstrate that the tumour suppressive or oncogenic potential of negative regulators of ERK, such as the MKP proteins, may depend largely on the genetic landscape within which tumourigenesis has developed. (Rushworth *et al.*, 2014; Kidger *et al.*, 2017; Sale *et al.*, 2019). The AZD6244-resistant CRC models provide a unique opportunity to investigate the role of the MKPs in these differing oncogenic contexts, where the inhibition or indeed hyperactivation of ERK leads to distinct cell fates.

4.3. Results

4.3.1. Optimising DUSP5 knockdown in HCT116 and H6244-R cells

Analysis of DUSP mRNA and protein levels in AZD6244-resistant CRC lines identified DUSP4, DUSP5 and DUSP6 as being prominently expressed in response to AZD6244 withdrawal in HT6244 and H6244-R cell lines, indicating that these MAPK phosphatases may contribute to the signalling reprogramming that occurs during drug administration and cessation. Work performed by Sale *et al*. (2019) illustrated severe and irreversible effects of ERK hyperactivation induced by AZD6244 withdrawal in these cells, which emphasises the potential importance of negative regulators of ERK, such as the DUSPs, in this context. To further explore the role of DUSP proteins in MEKi-resistant CRC cells we sought to develop a versatile and efficient strategy for DUSP knockdown that could be used in all three cell lines - COLO205, HT29 and HCT116. As COLO205 and HT29 cells were not amenable to lipid-based transfection, it would be necessary to explore other options.

Recombinant adenovirus vectors are able to target a wide range of host cells (both replicative and non-replicative) and provide a method of highly efficient and reproducible gene delivery. Once established, adenovirus vectors can be amplified and reused at low cost, without the need for expensive consumable reagents. They also offer a flexible gene expression system where similar constructs could be used for both gene silencing and re-expression. For these reasons we aimed to develop shRNA adenovirus vectors that could be used to knockdown DUSP proteins in all three target cell lines. We began by targeting DUSP5, the MAPK phosphatase that showed the most pronounced protein induction upon AZD6244 withdrawal in HT6244-R and H6244-R cells. For optimisation of DUSP5 knockdown, we began work in HCT116 cells. These cells showed high basal levels of DUSP5 which would aid the interpretation of initial DUSP5 knockdown assessment. Additionally, they are amenable to lipid-transfection, which would allow for transfection and assessment of DUSP5-targeting shRNA constructs prior to the establishment of adenoviral vectors. Most importantly, AZD6244-resistant H6244-R cells showed robust DUSP5 induction in response to AZD6244 withdrawal (Figure 3.9, Figure 3.10 and Figure 3.11, Chapter 3), suggesting that this nuclear, ERK-specific MKP may play a unique and important role in this cell model.

In order to synthesise DUSP5-targeting shRNA adenoviral vectors, we planned to make use of the RAPAd® Adenoviral Expression System. This system consists of a pacAd5 9.2–100 adenoviral backbone plasmid vector as well as a pacAd5 CMV K-N pA shuttle vector containing the gene of interest. When co-transfected into the packaging cell line HEK293, a double recombination event between the two vectors occurs, creating a recombinant adenovirus that is able to produce mature, replication-competent virus particles. These particles are able to deliver the expression vector into target cells with high efficiency through viral infection. Before we could employ the RAPAd® Adenoviral system it was necessary to generate functional shRNA expression constructs that could be cloned into the pacAd5 CMV K-N pA shuttle vector. We chose to make use of the pGSH1-GFP vector from Genlantis which contains the H1 RNA polymerase III promoter as well as a GFP coding sequence (Figure A1). The vector is designed for easy insertion of shRNA sequences through BamHI and NotI restriction sites.

Previously validated DUSP5-targeting shRNA oligonucleotides were designed and synthesized with BamHI-NotI “sticky ends” to ensure successful ligation into the pGSH1–GFP Expression Vector (Figure A1). These sequences contained a hairpin loop structure, which facilitates the expression of fold-back stem-loop structures that are processed into functional siRNAs within the cell. Within the hairpin loop is a *HindIII* restriction site which allows for screening of recombinant plasmids (Figure A1). Recombinant plasmid DNA was prepared by plasmid midi preps and a sample of each stock was analyzed through *HindIII-XhoI* restriction digestions. The *XhoI* restriction site is just upstream of the GFP coding sequence, therefore a *HindIII-XhoI* enzyme digestion should produce two DNA bands - linear plasmid DNA (5318 bp) and the GFP-H1-shRNA construct (approx. 1250 bp). These results are illustrated in (Figure A2b) and indicate the presence of the shRNA coding sequence in each recombinant vector. The expected DNA sequence for each construct was confirmed by DNA sequencing.

Prior to the next sub-cloning step, the pGSH1–GFP-shRNA plasmid vectors were transfected into HCT116 cells to assess whether the expression cassette was able to induce DUSP5 knockdown. HCT116 cells transfected with each of the four constructs as well as the control luciferase targeting construct were imaged on an EVOS microscope prior to RNA extraction. Transfection efficiency was determined by the number of cells expressing the GFP protein, as determined by detection of GFP fluorescent signal (Figure A2a). In general, all constructs appeared to have been transfected efficiently. Using RNA extracted from each sample, RT-PCR was performed to assess relative DUSP5 mRNA levels. Subsequent analysis revealed no observable DUSP5 mRNA knockdown in samples transfected with shRNA constructs 1 to 4 when compared to samples transfected with the luciferase-targeting shRNA construct and an untreated control. These results indicated that the shRNA expression cassettes were not able to induce DUSP5 knockdown (Figure 4.3a). Successful transfection of each vector and subsequent expression of GFP suggests that the absence of effective DUSP5 knockdown is likely a result of non-functional or inefficient shRNA structures, or alternatively, a problem with the position or frame of these inserts relative to the H1 promoter. It is also possible that the H1 promoter is not highly functional in HCT116 cells.

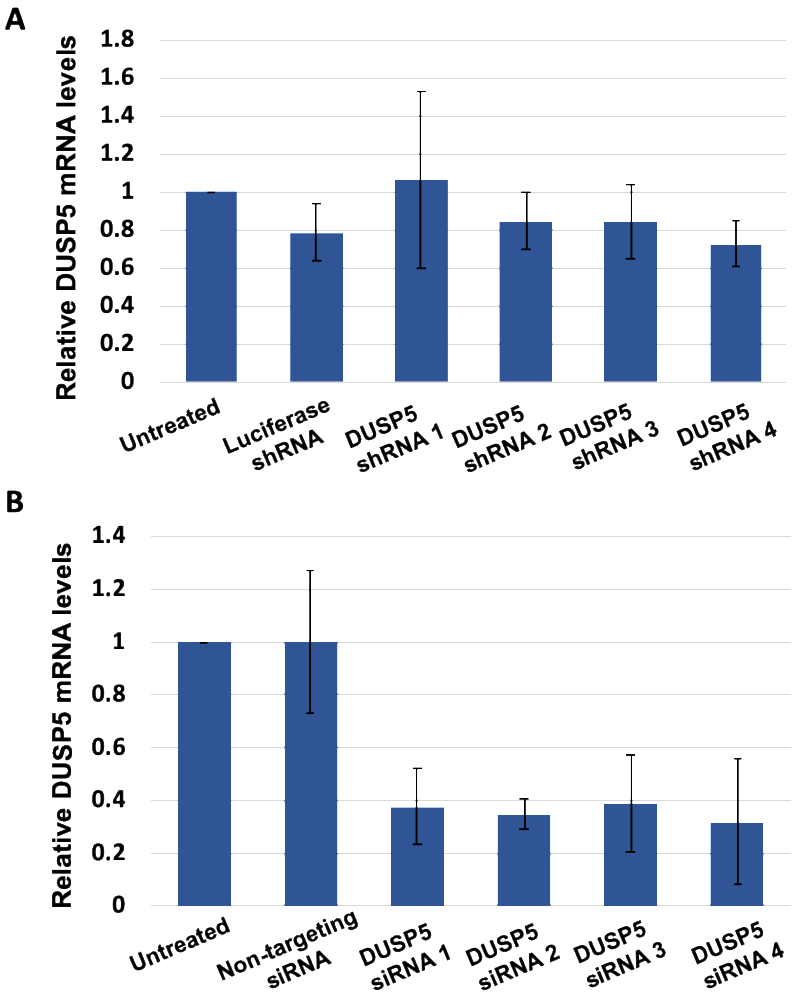

Figure 4.3. DUSP5-targeting pGSH1-GFP-shRNA constructs versus siRNA in HCT116 cells. A) Relative DUSP5 mRNA expression levels in HCT116 cells transfected with DUSP5- or luciferase-targeting pGSH1-GFP-shRNA vectors show no observable knockdown in DUSP5. n=3 biological replicates ± SEM. B) Samples transfected with siGENOME DUSP5-targeting siRNA (Dharmacon) show a relative knockdown of DUSP5 mRNA expression compared to non-targeting control siRNA and an untreated sample. n=3 biological replicates ± SEM.

Initially, previously validated DUSP5 siRNA sequences (Caunt et al., 2008a) were used as a side by side comparison for successful DUSP5 knockdown (Figure 4.3). However, as they presented a successful and efficient method of DUSP5 knockdown in HCT116 cells, as illustrated in Figure 4.4. we chose to use them in subsequent experiments while a new multi-purpose DUSP5 knockdown strategy was devised. While lipofectamine transfection had previously conferred successful siRNA delivery in HCT116 and H6244-R cells, it was necessary to optimize transfection conditions to reduce cellular stress (as was evidenced by cell death in conditions where the concentration of siRNA/lipofectamine complexes was too high) and ensure robust DUSP5 knockdown for the duration of each experiment. While HCT116 and H6244-R cells cultured in routine conditions (AZD6244-free media and 2 μM AZD6244, respectively) showed similar tolerance levels to lipofectamine, optimization experiments were performed on H6244-R cells as they were the primary focus for future investigations.

Figure 4.4 demonstrates that both siRNA sequences 1 and 3 caused a reduction in DUSP5 protein expression, with siRNA 3 being slightly more effective. Robust DUSP5 knockdown was evident at 48 hours and was maintained until at least 72 hours post-transfection. These results also revealed that knockdown of DUSP5 protein appeared to coincide with increased *p*-ERK levels. While Figure 4.4 shows the results of one experiment, results obtained from similar experiments reproduced these findings and are illustrated in Figure 4.8.

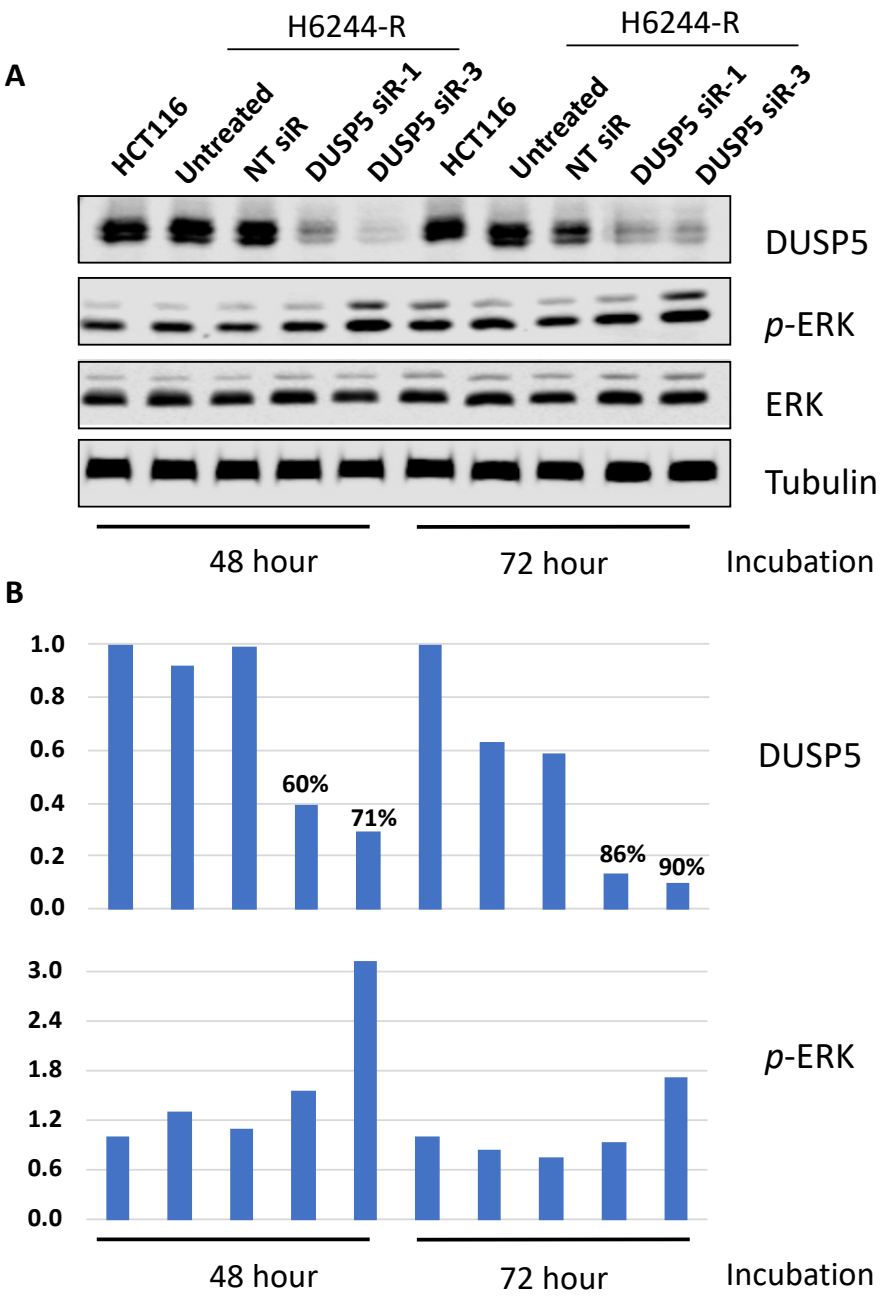

Figure 4.4. siRNA DUSP5 knockdown in HCT116 cells. Samples transfected with siGENOME DUSP5-targeting siRNA (Dharmacon) show a relative knockdown of DUSP5 protein expression compared to non-targeting control siRNA and an untreated sample. A) western blot image. B) Relative protein quantification. n=1 biological replicate.

4.3.2. DUSP5 reduction in the absence of MEKi enhances ERK hyperactivation and restricts nuclear accumulation of ERK

Similar to experiments completed previously (Figure 3.5) we aimed to assess the effects of AZD6244 administration and withdrawal in HCT116 and H6244-R cells but in conditions where DUSP5 expression was compromised. This strategy was implemented in HCT116 and H6244-R cell lines treated with increasing concentrations of AZD6244. HCM data revealed that knocking down DUSP5 appeared to enhance ERK hyperactivation seen in H6244-R cells cultured in the absence of drug (

Figure 4.5**). Not only this, but in normal H6244-R culture conditions (2 μM AZD6244), DUSP5 knockdown appeared to induce sustained ERK hyperactivation levels to a similar magnitude seen when drug is removed from these cells. This result is not commonly seen in "normal" cell types where *p*-ERK signalling is highly robust and resistant to sustained changes. The enhancement of ERK hyperactivation coincident with DUSP5 repression was correlated with a reduction in the proportion of S-phase positive cells as well as an overall decrease in cell numbers (**

Figure **4**.**5**). Cell count measures for each condition were normalised by choosing the minimum and maximum cell count values from each experimental data set to represent 0% and 100% and converting all other values to a proportion within this range. This is a crude assessment of potential cell death that would need to be validated by further experiments.

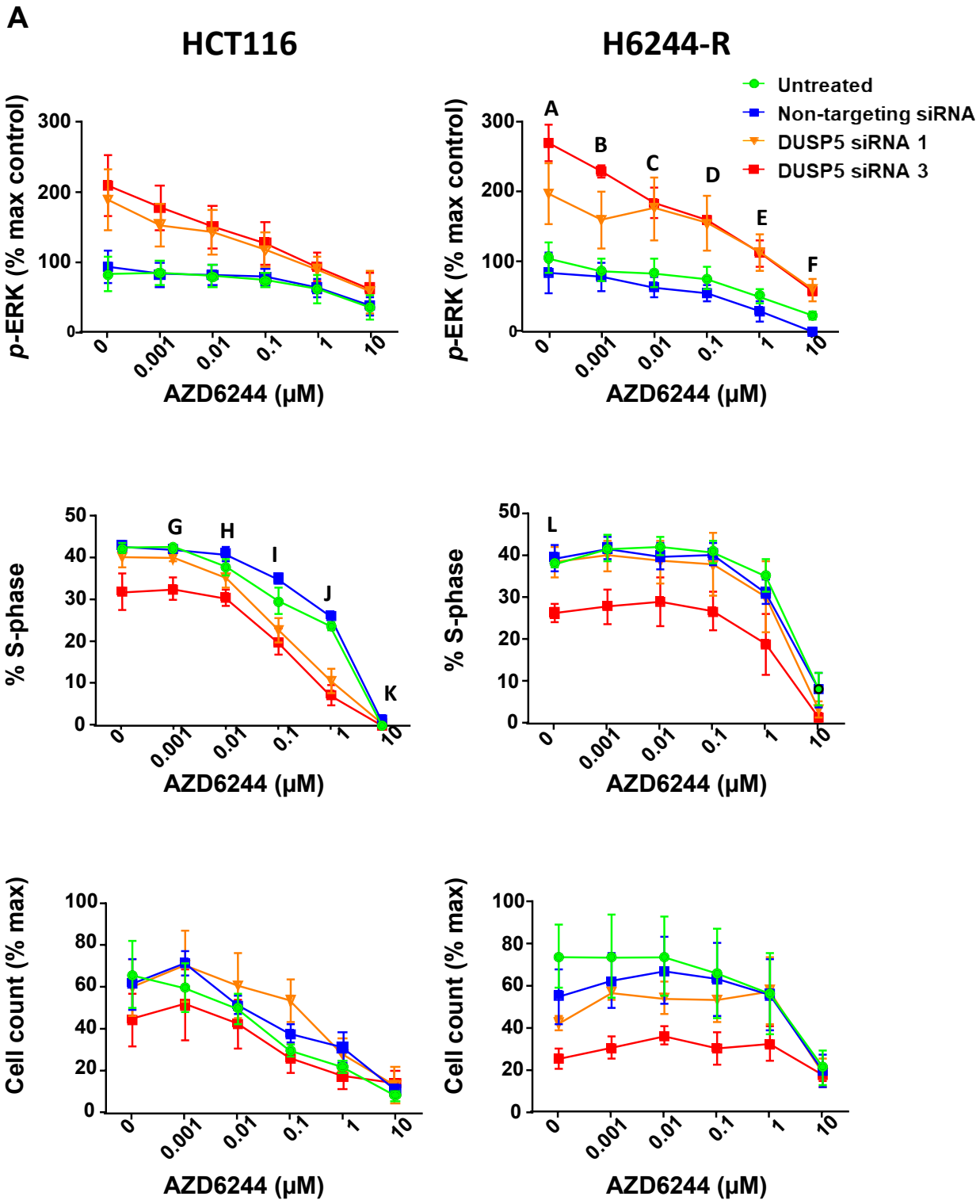
A
HCT116
H6244-R
Untreated
Non-targeting siRNA
DUSP5 siRNA 1
DUSP5 siRNA 3
p-ERK (% max control)
% S-phase
Cell count (% max)
AZD6244 (μM)
0
0.001
0.01
0.1
1
10
A
B
C
D
E
F
G
H
I
J
K
L

Figure 4.5**. DUSP5 knockdown enhances ERK hyperactivation and decreases proliferation and cell count in H6244-R1 cells.** A) Quantitative HCM summary data of *p*-ERK levels (normalised to a percentage of the maximum value in untreated HCT116 cells), percentage of S-phase cells and cell count (converted to percentage within minimum and maximum value range) in HCT116 and H6244-R samples. For siRNA treated samples, cells were transfected with DUSP-targeting siRNA 1, 3 or non-targeting siRNA 24 hours prior to AZD6244 treatment. Cells were maintained in indicated concentrations of AZD6244 for 24 hours prior to fixation and immunostaining. n=3-4 biological replicates, ± SEM. Symbols A to L highlight AZD6244 conditions where a statistically significant difference between siRNA-treated or untreated samples was determined using the Holm-Sidak method. Refer to Table A2 for statistical analysis. All assays; 3 fields/well, 2-4 wells (~2000 individual cells) per condition per experiment.

ges of HCT116 and H6244-R
bel is apparent in cells in S-ph

Interestingly, in the presence of 1 μM AZD6244, DUSP5 knockdown appeared to increase the anti-proliferative effects of MEK inhibition compared to untreated cells or cells treated with a non-targeting siRNA, despite any major difference in *p*-ERK levels under these conditions (Figure **4**.**5**). This might indicate that other measures of ERK regulation exerted by DUSP5 including directing ERK localisation, may account for the effects seen on proliferation. Thus, in conditions of DUSP5 knockdown, even when *p*-ERK levels were much reduced by increasing AZD6244 concentration, normal proliferation rates were not restored. Alternatively, effects on proliferation could be a result of an off-target event, which may explain why the reduction of ERK hyperactivation by AZD6244 seen in DUSP5 knockdown conditions did not reverse the effects seen on proliferation.

While the consistency between the results for two different siRNAs versus a non-targeting siRNA control makes this possibility appear unlikely in HCT116 cells, the effect on proliferation and cell numbers DUSP5 knockdown seems to confer in H6244-R cells was evident in only one of two siRNAs. While this may be a result of the superior knockdown efficiency of siRNA 3, it is not wise to exclude the possibility that an off-target effect on cell survival and proliferation exists in these conditions.

Major cell fate decisions such as proliferation or cell death are affected by various complex factors and are regulated by multiple signalling pathways, making it difficult to exclude the possibility that unexpected off-target effects contribute to or are responsible for the changes in the measures illustrated in

Figure **4.5**. However, the effects seen on *p*-ERK and ERK were consistent between two different DUSP5-targeting siRNA sequences when compared to a non-targeting siRNA sequence and an untreated control. In addition to ERK phosphorylation status, other factors important to the regulation of ERK activity are the timing and duration of its induction time and its cellular location. As MKP expression is likely to influence these factors, we went on to assess the impact of DUSP5 loss on the spatiotemporal activation of *p*-ERK in H6244-R cells cultured without AZD6244 for varying time periods.

Results in

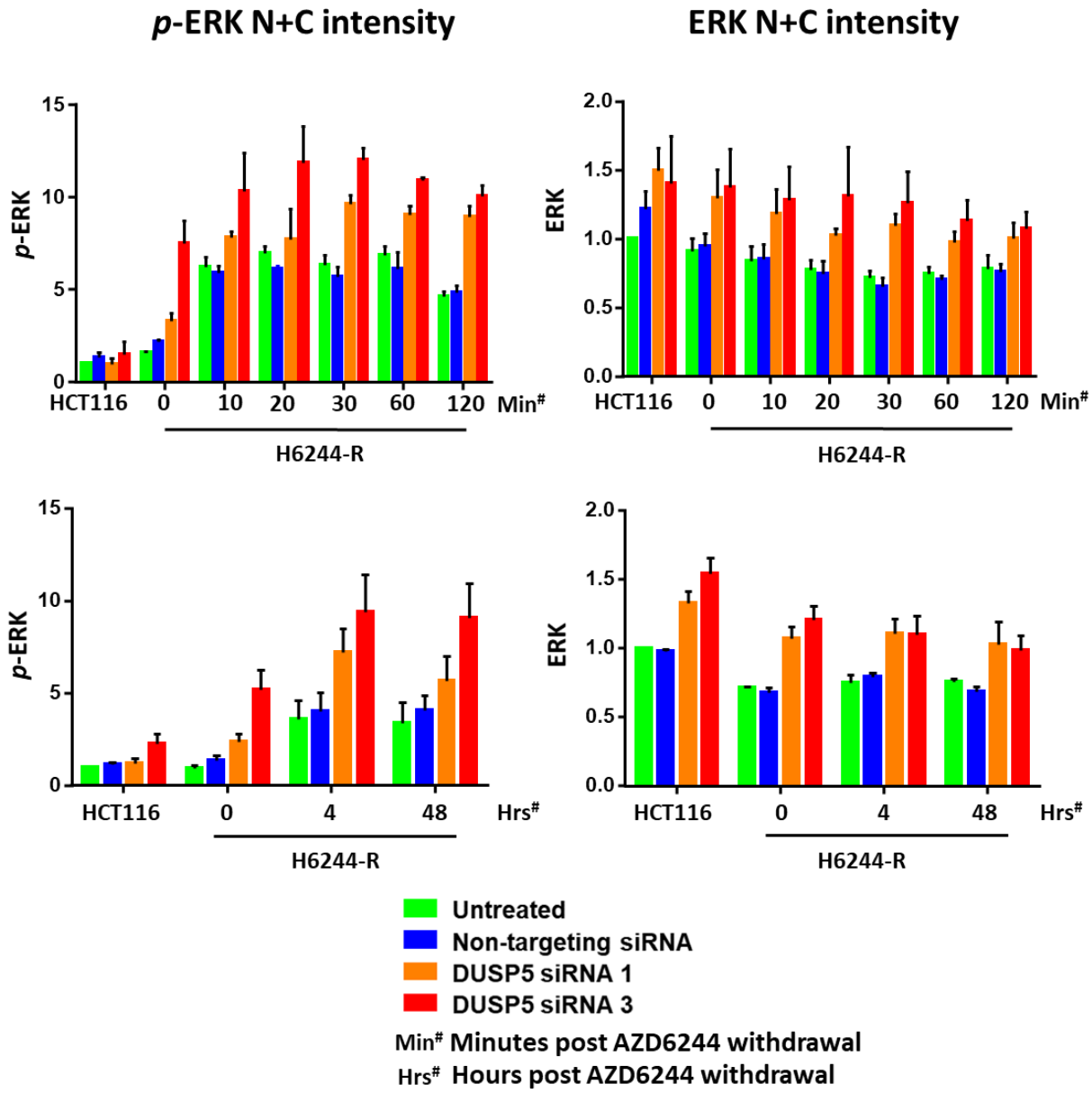

Figure 4.6 show that the increases in whole-cell *p*-ERK levels in response to AZD6244 withdrawal were induced as early as 10 minutes post-withdrawal both in DUSP5 knockdown and control samples. *p*-ERK induction appeared to peak between 10 and 120 minutes after AZD6244 removal, then decreased slightly and remained at relatively high levels thereafter. Like previous HCM data illustrated in

Figure **4.5**, these results demonstrated that DUSP5 knockdown increased levels of *p*-ERK in HCT116 and H6244-R cells relative to control samples. Upon AZD6244 withdrawal in H6244-R cells, a further increase in the magnitude of ERK hyperactivation was seen in DUSP5 knockdown conditions compared to control samples (

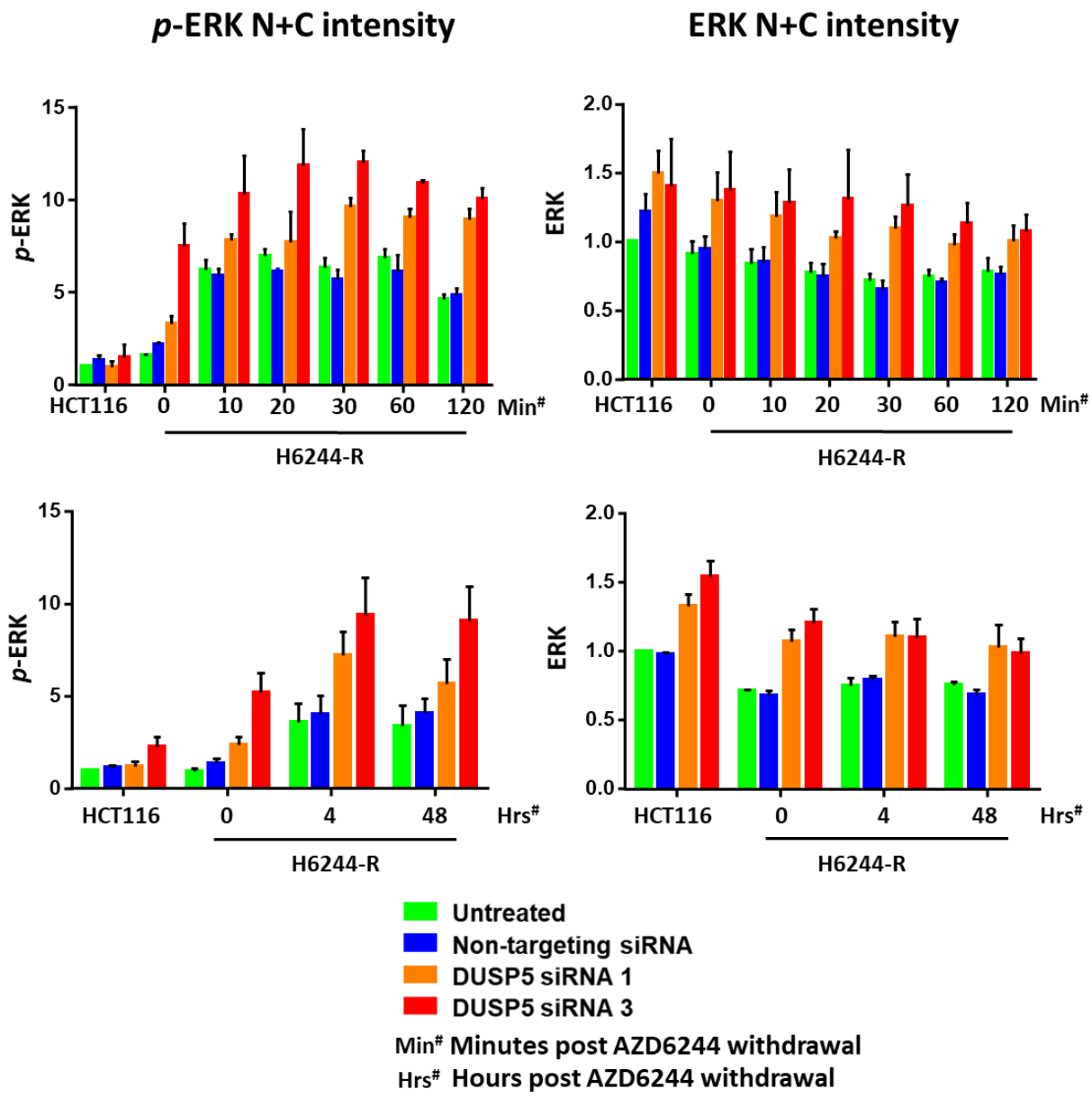

Figure 4.6). These results were consistent for both siRNAs, with the effects on *p*-ERK being more pronounced and statistically significant in cells treated with DUSP5 siRNA 3 (refer to table A3 in the Appendix for statistical analyses). Interestingly, in H6244-R cells, DUSP5 knockdown in cells cultured in maintenance conditions (2 μM AZD6244)

was able to induce levels of *p*-ERK similar to or higher than those seen in DUSP5-expressing H6244-R cells in AZD6244-free conditions.

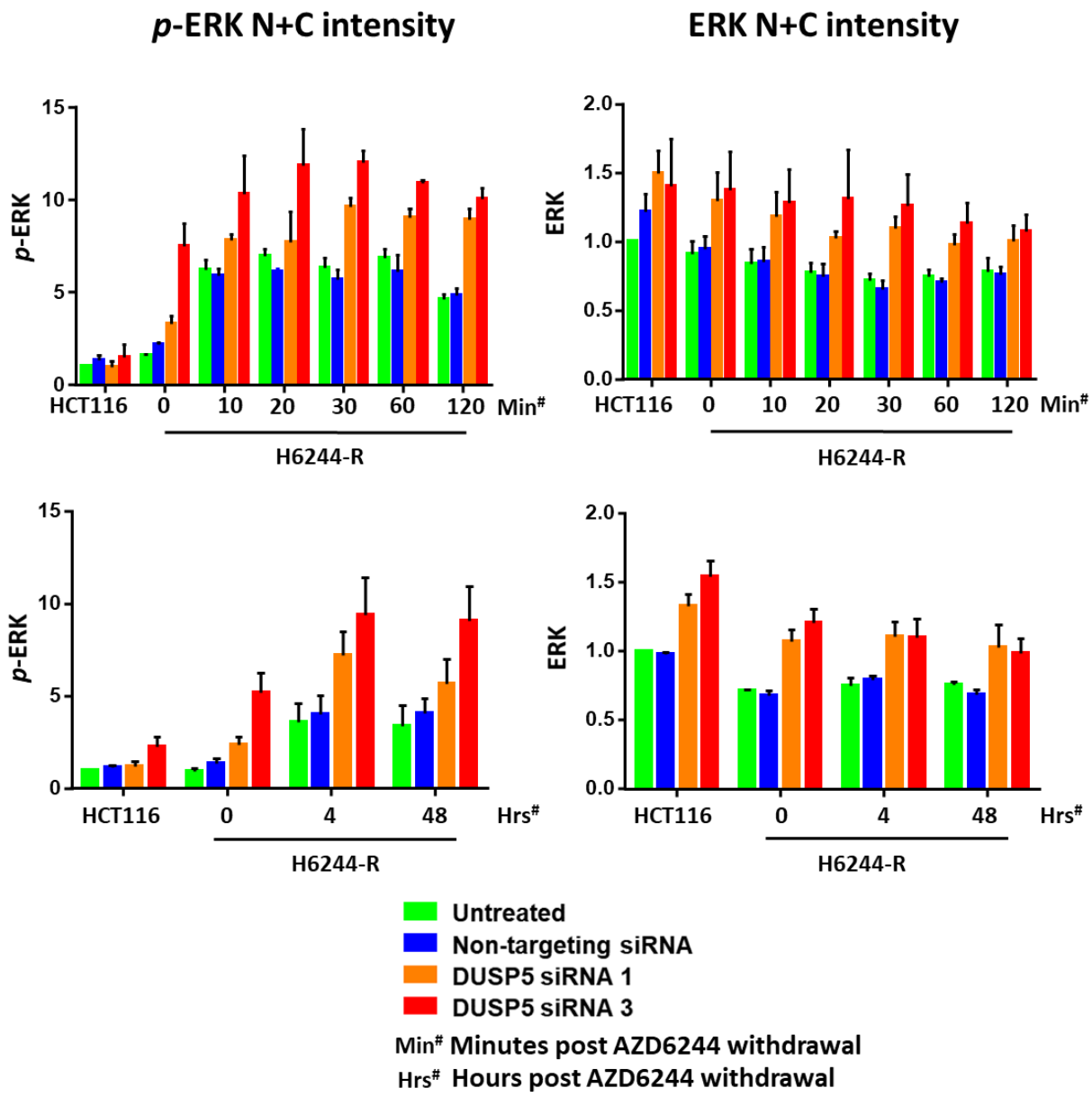

Figure 4.6. ERK hyperactivation in response to AZD6244 withdrawal and enhanced ERK hyperactivation coincident with DUSP5 knockdown is induced within 10 minutes of AZD6244 removal. Quantitative HCM summary data of *p*-ERK and ERK whole cell (nuclear and cytoplasmic) levels in HCT116 and H6244-R samples. For siRNA treated samples, cells were transfected with DUSP-targeting siRNA 1, 3 or non-targeting siRNA 24 hours prior to AZD6244 treatment. Cells were maintained in indicated concentrations of AZD6244 for varying time periods prior to fixation and immunostaining. n=3-4 biological replicates, ± SEM. Refer to A3 in appendix for statistical analyses.

The effects on whole cell *p*-ERK levels seen in HCT116 cells and H6244-R cells cultured in routine conditions (AZD6244-free or 2 μM AZD6244, respectively) were somewhat unexpected, as knockdown of DUSP5 under "normal" conditions, where *p*-ERK has not been induced has not been seen in experiments performed in HeLa cells (Caunt *et al.*, 2008) or MEFs (Kidger et al., 2017). In saying that, basal levels of DUSP5 measured in HCT116 cells were found to be markedly higher than a number of other cell lines assessed (Figure 3.4) which may indicate a unique importance of DUSP5 in these cells.

Interestingly, DUSP5-targeting siRNA 1 and 3 also appear to increase levels of ERK relative to a non-targeting siRNA and untreated H6244-R cells (

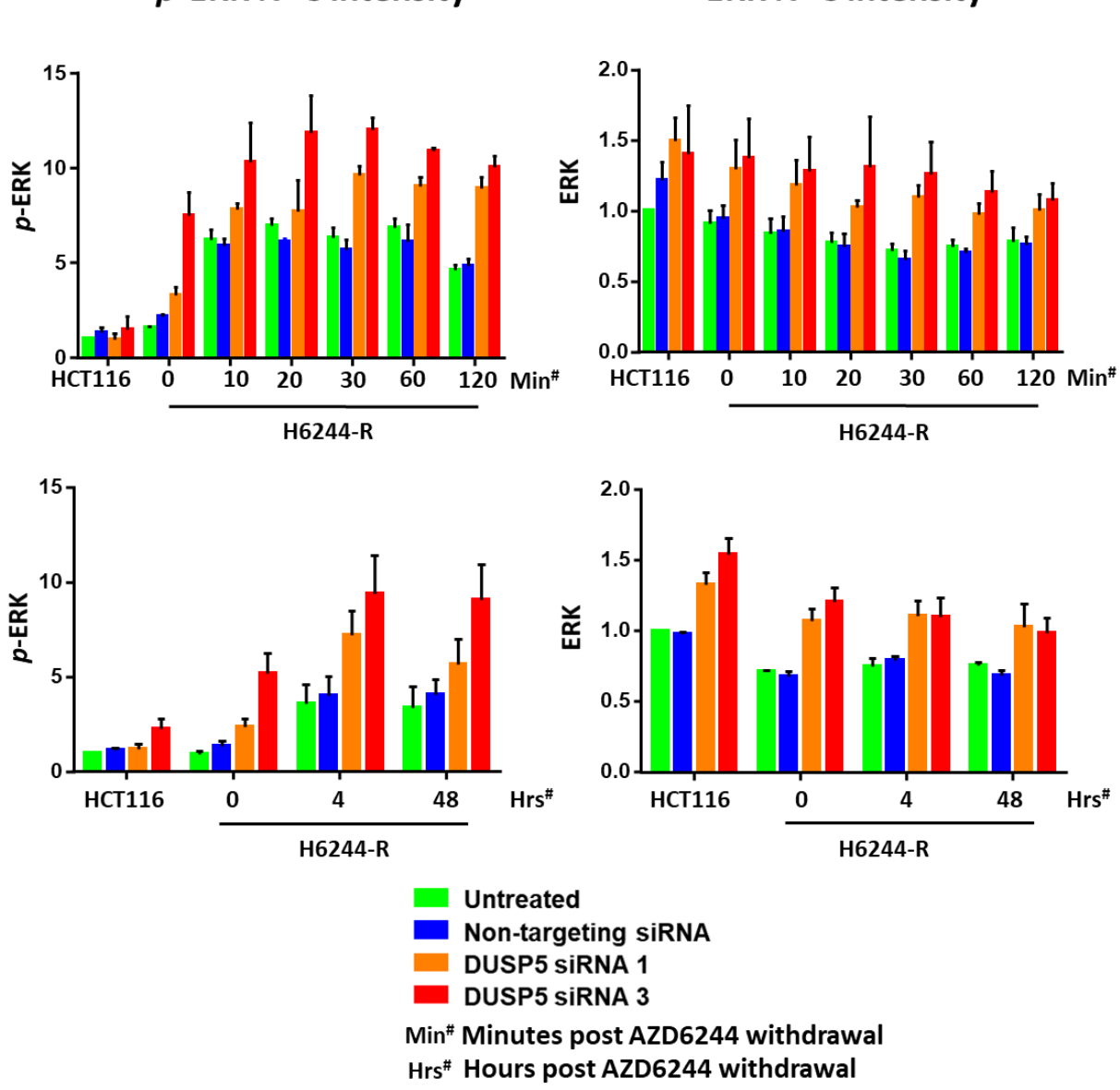

Figure 4.6 and Appendix Table A3). These results were also unexpected, as whole-cell ERK levels tend to remain relatively constant within the cell, with changes in ERK activity being regulated primarily through phosphorylation and dephosphorylation and movement between the cytoplasm and nucleus (Joe W Ramos, 2008). An increase in total ERK such as this would suggest a *de novo* increase in ERK protein transcription and translation or alternatively, a decrease in ERK protein degradation, both mechanisms that have not been thoroughly investigated due to the consensus that ERK levels remain stable. Another possible explanation for this observation is that the association of DUSP5 with ERK decreases antibody binding and in the absence of DUSP5, this inhibitory effect is relieved and ERK detection is increased.

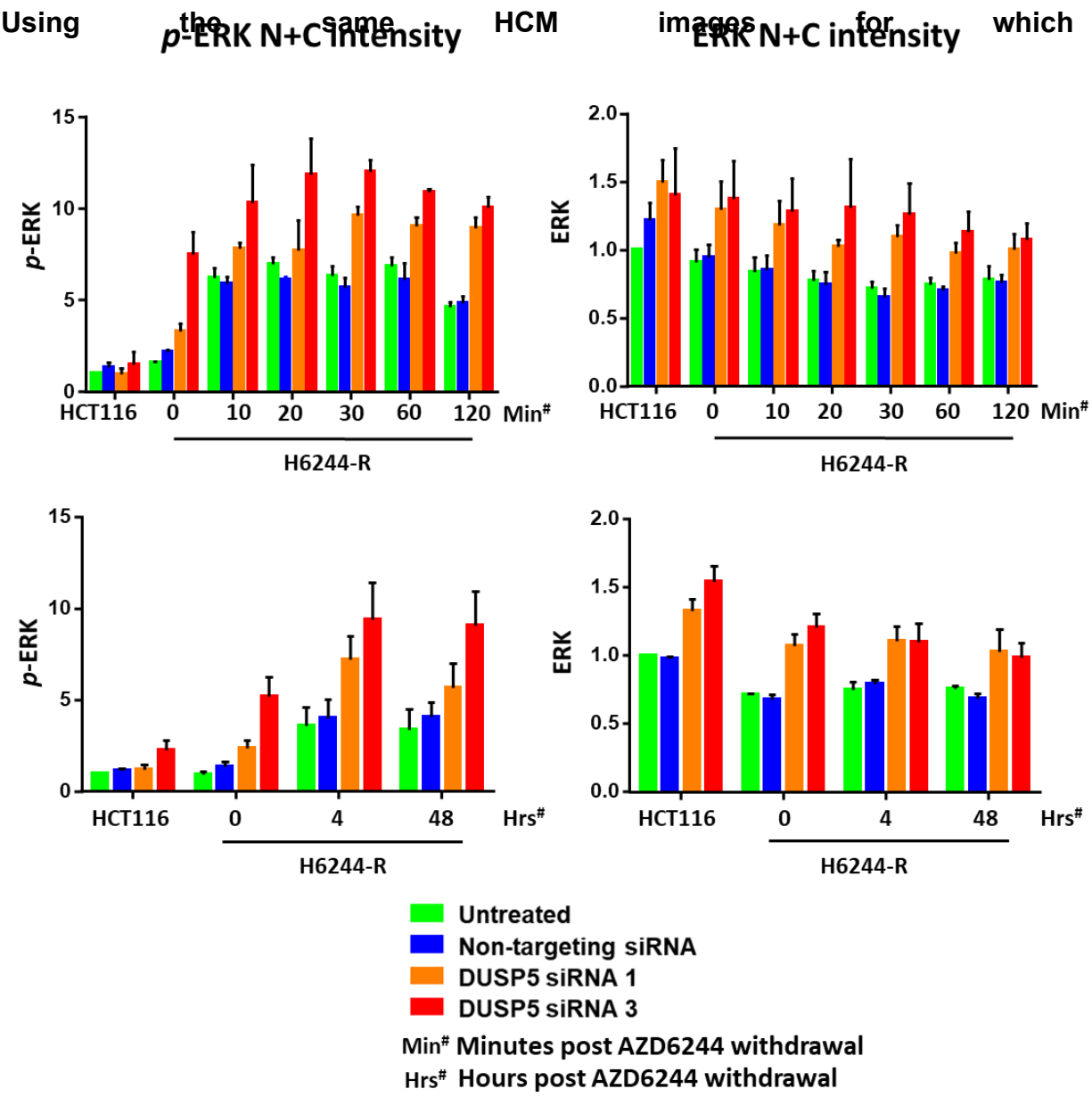

Figure 4.6 summary data was calculated, the *p*-ERK and ERK nuclear and cytoplasmic signal intensity data was quantified and used to calculate the nuclear to cytoplasmic ratio for each protein. These results confirm findings from previous experiments that looked at N:C ratios of ERK (Figure 3.8) where the distribution of ERK is relatively constant across the cell (indicated by a N:C ratio of ~1) in HCT116 and H6244-R cells cultured in their respective maintenance conditions (Figure 4.7). Removing drug from DUSP5-expressing control H6244-R cells caused an increase in the ratio of nuclear to cytoplasmic ERK, suggesting an accumulation of ERK in the nucleus. Interestingly, in DUSP5 knockdown conditions, the accumulation of ERK in the nucleus is less

pronounced, particularly in siRNA 3 knockdown conditions, where this relative decrease is statistically significant (Figure 4.7 and Appendix Table A4). This might suggest that DUSP5 knockdown limits ERK's ability to accumulate in the nucleus. As DUSP5 primarily functions to dephosphorylate and anchor ERK in the nucleus after it itself is induced by ERK activation, it seems plausible that a loss of DUSP5 function may lead to a decrease in the nuclear retention of ERK.

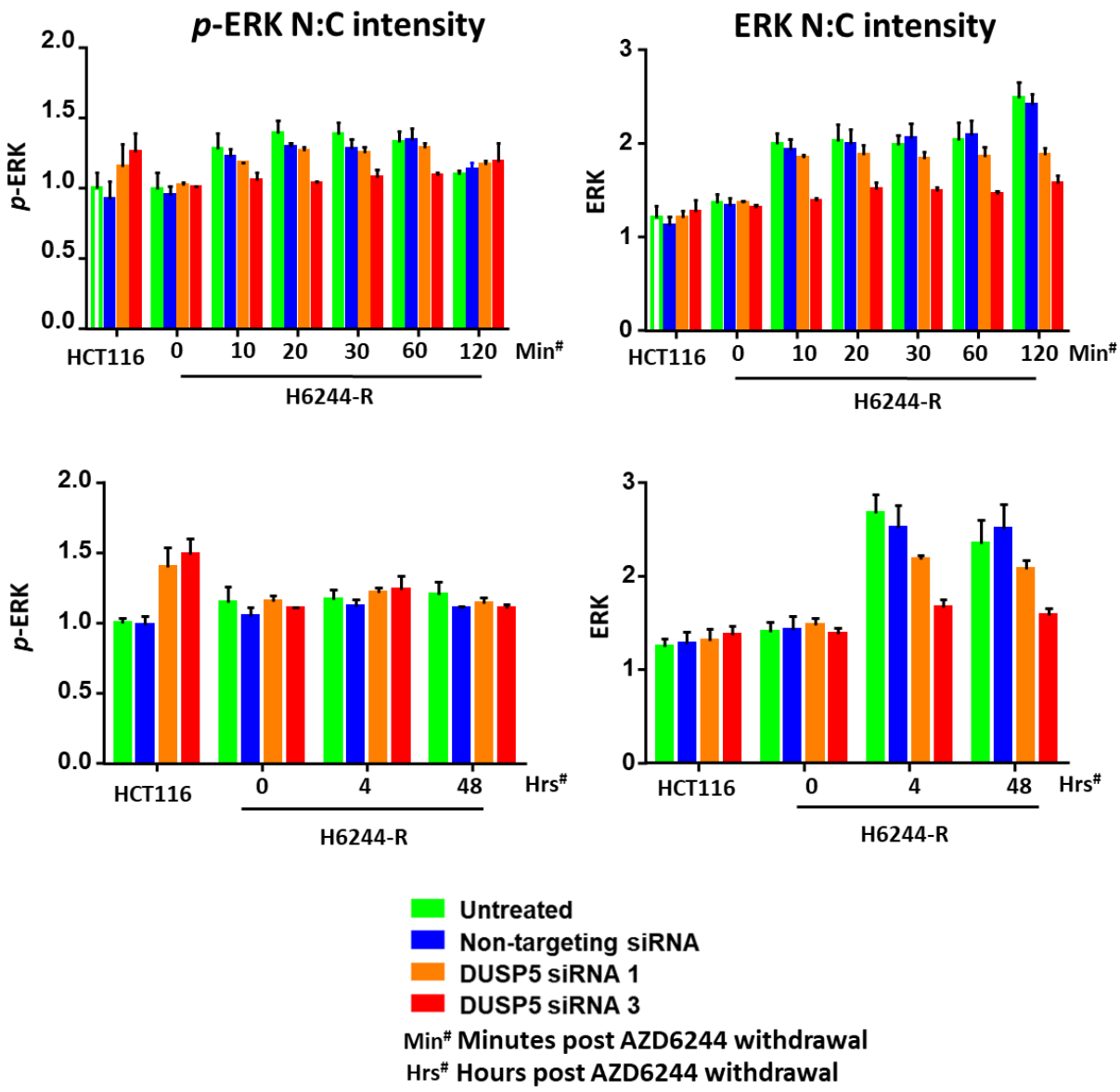

Figure 4.7. DUSP5 knockdown increases the nuclear accumulation of *p*-ERK in HCT116 cells and decreases the nuclear accumulation of total ERK in H6244-R cells in AZD6244-free conditions. Quantitative HCM summary data of nuclear to cytoplasmic (N:C) ratios of *p*-ERK and total ERK signal levels in HCT116 and H6244-R samples. For siRNA treated samples, cells were transfected with DUSP-targeting siRNA 1, 3 or non-targeting siRNA 24 hours prior to AZD6244 treatment. Cells were maintained in indicated concentrations of AZD6244 for varying time periods prior to fixation and immunostaining. n=3-4 biological replicates, ± SEM. Refer to A4 in appendix for statistical analyses.

In HCT116 and H6244-R DUSP5-expressing cells cultured in maintenance conditions, the N:C ratio of *p*-ERK is close to 1, reflecting an even distribution of *p*-ERK across the nucleus and cytoplasm in these conditions (Figure 4.7). The removal of AZD6244 from H6244-R cells causes a subtle increase in the N:C ratio of *p*-ERK from ~1 to ~1.3 within 60 minutes. This trend is consistent between DUSP5 knockdown and control H6244-R cells. Surprisingly, in HCT116 samples DUSP5 knockdown is coincident with significantly increased nuclear accumulation of *p*-ERK compared to control samples (Figure 4.7 and Appendix Table A4). While this is consistent with the hypothesis that removing a nuclear, ERK-specific phosphatase may lead to increased levels of *p*-ERK in the nucleus, it is unclear why this trend would not be replicated in H6244-R cells and enhanced upon AZD6244 removal.

4.3.3. Enhanced ERK hyperactivation is coincident with a further reduction in E-cadherin expression over time

Preliminary results investigating DUSP5 knockdown in HCT116 and H6244-R cells have revealed that loss of DUSP5 in these cells leads to increased ERK phosphorylation. In H6244-R cells where AZD6244 is removed, ERK hyperactivation is further enhanced by DUSP5 knockdown and leads to a reduction in proliferation and cell numbers in one of two DUSP5-targeting siRNA sequences. As this phenotype is not consistent between both DUSP5-targeting siRNA sequences, despite similar levels of *p*-ERK levels in both conditions, it is difficult to establish whether this is an "on-target" effect.

Sale *et al*. (2019) have clearly demonstrated an ERK-dependent phenotype induced by AZD6244 removal and subsequent ERK hyperactivation in H6244-R cells. To further investigate likely on-target effects of DUSP5 knockdown we chose to expand on work by Sale *et al*. (2019) which characterised the epithelial-to-mesenchymal transition that took place in H6244-R cells exposed to prolonged AZD6244 withdrawal. As DUSP5 is highly specific for ERK and the increase in *p*-ERK levels coincident with DUSP5 knockdown appear to be on-target, we aimed to investigate whether the EMT observed in H6244-R cells cultured without AZD6244 would be affected by DUSP5 knockdown.

Figure 4.8A illustrates the relative levels of *p*-ERK, ERK, DUSP5 and E-cadherin in protein lysates harvested from HCT116 cells and H6244-R cells that had been cultured in AZD6244-R media for varying time periods. Western blot images (Figure 4.8a) and relative protein signal quantification data (Figure 4.8) firstly confirms robust and reproducible knockdown of DUSP5 by siRNA 1 and 3. It also illustrates the greater efficacy of siRNA 3 in repressing DUSP5 expression in response to ERK activation. While siRNA 1 is successful in reducing DUSP5 protein levels relative to those seen in “untreated” or non-targeting siRNA H6244-R samples, at what appears to be the peak of DUSP5 expression at 4 hours, some DUSP5 protein induction is still evident. In siRNA 3 samples, DUSP5 protein induction is almost entirely ablated, even at 4 hours post-AZD6244 withdrawal.

A

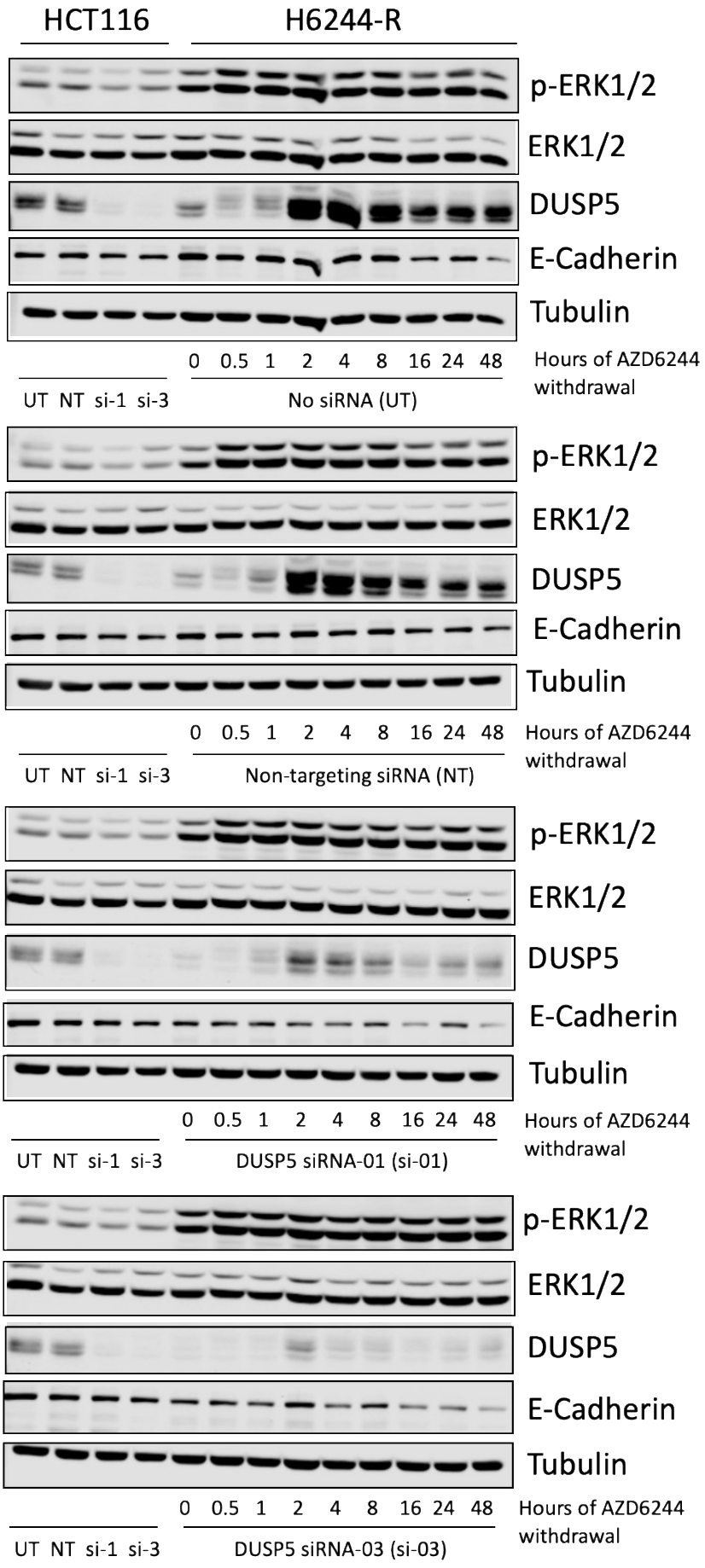
HCT116
H6244-R
p-ERK1/2
ERK1/2
DUSP5
E-Cadherin
Tubulin
0 0.5 1 2 4 8 16 24 48
Hours of AZD6244 withdrawal
UT NT si-1 si-3
No siRNA (UT)
p-ERK1/2
ERK1/2
DUSP5
E-Cadherin
Tubulin
0 0.5 1 2 4 8 16 24 48
Hours of AZD6244 withdrawal
UT NT si-1 si-3
Non-targeting siRNA (NT)
p-ERK1/2
ERK1/2
DUSP5
E-Cadherin
Tubulin
0 0.5 1 2 4 8 16 24 48
Hours of AZD6244 withdrawal
UT NT si-1 si-3
DUSP5 siRNA-01 (si-01)
p-ERK1/2
ERK1/2
DUSP5
E-Cadherin
Tubulin
0 0.5 1 2 4 8 16 24 48
Hours of AZD6244 withdrawal
UT NT si-1 si-3
DUSP5 siRNA-03 (si-03)

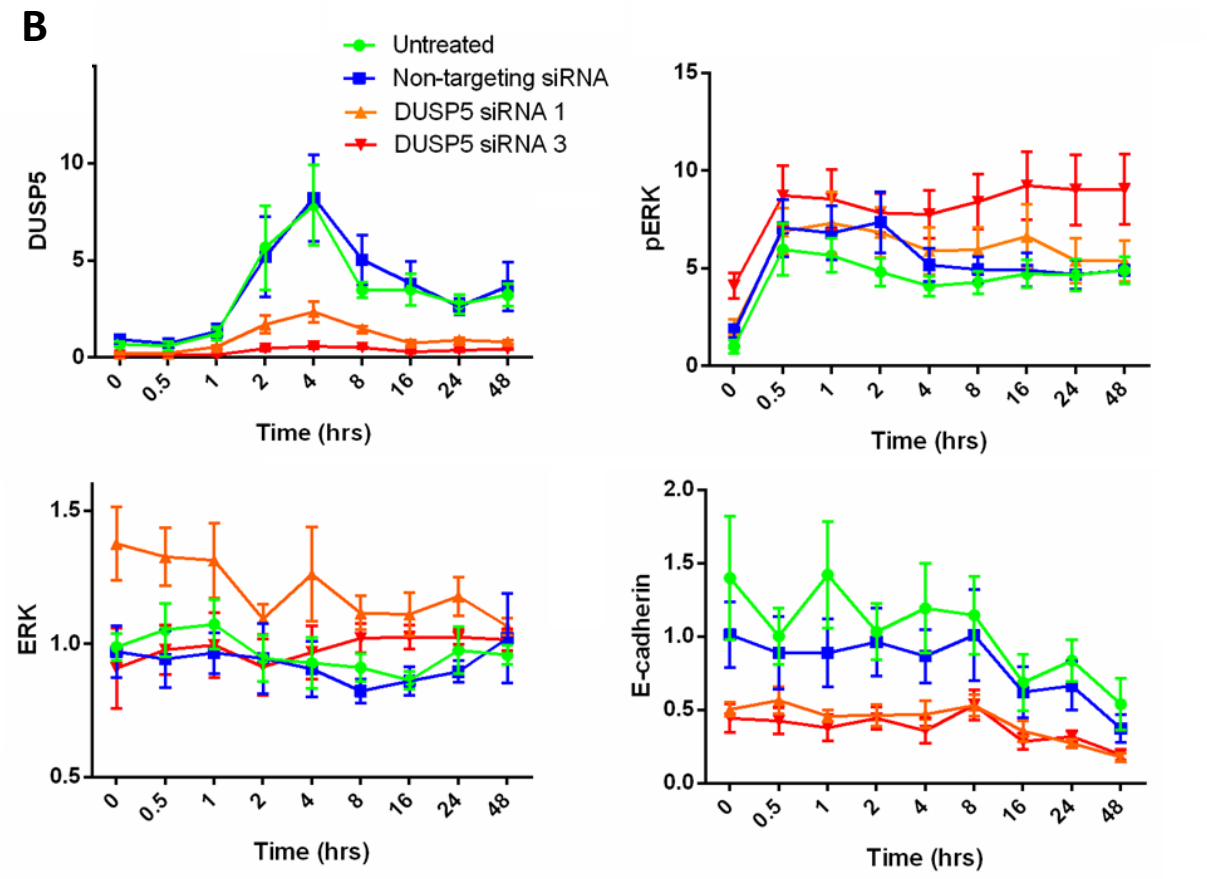

Figure 4.8. Enhanced ERK hyperactivation is coincident with a further reduction in E-cadherin expression over time. For siRNA treated samples, cells were transfected with DUSP-targeting siRNA 1, 3 or non-targeting siRNA 24 hours prior to AZD6244 treatment. H6244-R cells were maintained in indicated concentrations of AZD6244 for 24 hours prior to cell lysis, HCT116 cells were cultured without AZD6244 for 24 hours prior to cell lysis. A) Western blot images. B) relative quantification of protein levels calculated with Licor imaging software. n=3 biological replicates, ± SEM.

As expected, these experiments show an increase in *p*-ERK levels in response to AZD6244 withdrawal in "untreated" H6244-R cells as well as a decrease in protein levels of E-cadherin from 16 hours onwards (Figure 4.8). This correlated with data found by Sale *et al*. (2019) in similar experiments illustrated in Figure 4.2. Unexpectedly, these results do not illustrate a clear enhancement of *p*-ERK levels in DUSP5 knockdown H6244-R samples relative to untreated and non-targeting siRNA H6244-R samples seen in previous HCM experiments (

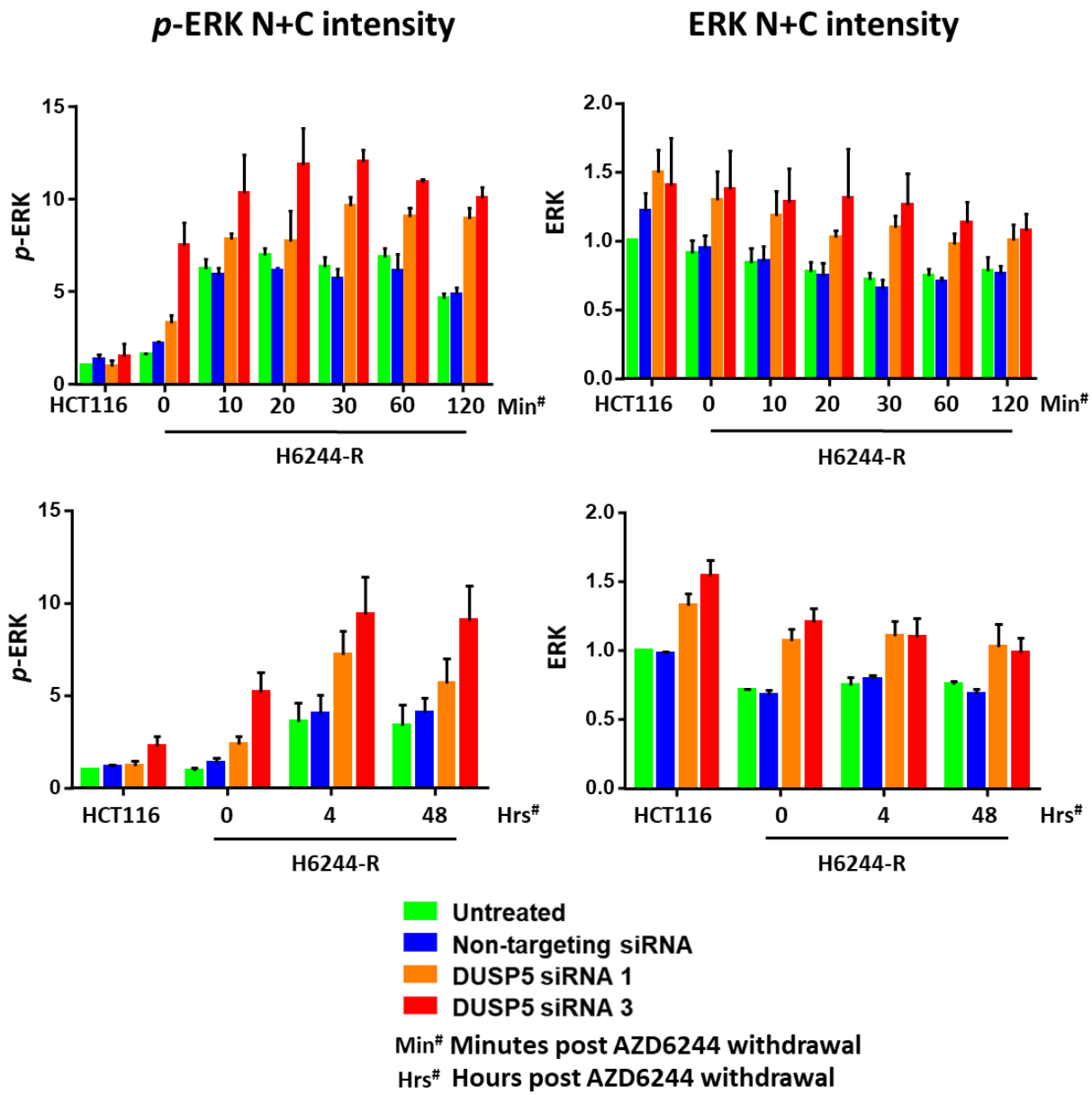

Figure 4.6). However, despite the absence of an obvious increase in ERK activation in these immunoblots, a clear reduction in E-cadherin can be seen in DUSP5 knockdown H6244-R samples (Figure 4.8). This relative decrease is present in H6244-

R cells cultured in AZD6244, is further reduced in H6244-R cells cultured in AZD6244-free media and becomes progressively more reduced with prolonged AZD6244 withdrawal. The substantial and consistent effect of DUSP5 disruption on E-cadherin expression suggests that through its regulatory influence on *p*-ERK, DUSP5 is able to modulate the cellular consequences of AZD6244 withdrawal in drug-resistant H6244-R cells. This is a significant finding that clearly demonstrates an important role for DUSP5 in the regulation of oncogenic ERK signalling in a MEK-inhibitor resistant cell model.

4.3.4. Establishing DUSP5 knockout HCT116 and H6244-R single cell clones

While investigating and optimising different knockdown strategies it became clear that variability in the extent of DUSP5 knockdown achieved may present challenges in reproducing our preliminary data. Additionally, variability in the results observed for two different DUSP5-targeting siRNA sequences (

Figure **4.5**) led us to question whether off-target effects were taking place. Using a CRISPR/Cas9 genome editing technique we could eliminate any ambiguity about residual DUSP5 function by selecting complete DUSP5 knockout clones for downstream functional studies. Naturally, plasmid transfection and single cell outgrowth can induce off-target cellular stress, but we hoped to avoid this by analysing stable DUSP5 knockout (KO) and control cell lines that had been given several passages to recover.

We made use of a customised Type II CRISPR/Cas9 system, described in detail by Ran *et al*. (2013). The pSpCas9(BB)-2A-GFP vector developed by the Zhang group contains a chimeric guide RNA (gRNA), an EGFP coding sequence and a human codon-optimized Cas9 coding sequence. The plasmid is designed such that a 20-nucleotide target-specific guide sequence can be easily ligated into a *BbsI* cloning site, just upstream of the sgRNA scaffold. Four guide sequences designed for targeting DUSP5 were cloned into the pSpCas9(BB)-2A-GFP vector and subsequently transfected into HCT116 and H6244-R cells, alongside a control transfection with empty vector (EV) Cas9 DNA as detailed in Chapter 2.

After single cell-sorting and the expansion of multiple colonies transfected with each gRNA and EV Cas9 DNA in both HCT116 cells and H6244-R cells, clones were incubated for 2 to 6 weeks. The frequency of colony outgrowth was unexpectedly low, specifically in H6244-R cells (for cells transfected with EV as well as gRNA plasmid) suggesting that one or more parts of the protocol had led to cell stress and subsequent death or senescence. The rate of colony outgrowth was variable among clones, with some forming large colonies within 2 weeks, and others forming colonies within 6 or more weeks. Another noteworthy observation was pronounced variability in cell morphology and size among different clonal populations. The cell morphology of most of the clonal populations were comparable to the parental populations (HCT116 and H6244-R), growing in tightly packed, epithelial-like colonies. However, some populations contained cells that appeared enlarged with pronounced nuclei (results not shown). These cells did not grow in compact colonies but tended to be more sparsely distributed across the tissue culture vessel. Variability in growth rate and cell morphology was seen across cells expressing DUSP5-targeting guides as well as EV clones and so were not likely to be a phenotype associated with DUSP5 knockout.

A preliminary western blotting screen for DUSP5 knockout was performed on a selection of EV clones and all clones established for each gRNA for both HCT116 and H6244-R (Figure 4.9). This screen showed that all four gRNA targets gave rise to knockout clones. These clones were named according to the gRNA they expressed and the order in which each colony originally arose. In HCT116 clonal populations (Figure 4.9a), clones EV1, EV2 and ZH1-4 showed pronounced levels of DUSP5 while GS1-1, GS1-3, GS1-4, GS5-1, GS5-4, ZH1-2 and ZH1-3 appeared to be DUSP5 knockouts. GS1-2, GS5-2, GS5-3 and ZH1-1 clones appeared to be "partial" DUSP5 knockouts showing low levels of DUSP5 protein expression.

In H6244-R clonal populations (Figure 4.9b), GS1-1, GS1-2, GS2-1, ZH1-2, ZH1-3, ZH1-4, ZH1-5 and GS5-1 appeared to be DUSP5 knockouts. Interestingly, the levels of DUSP5 in all other clones including EV clones EV-1, EV-2 and EV-4 appeared to have variable levels of DUSP5 protein expression. This suggested that reduced levels of DUSP5 shown in these blots may not necessarily reflect "partial" DUSP5 knockouts, but rather variability in DUSP5 protein levels resulting from other factors. In fact, as single clone assays for DUSP5 expression in untreated HCT116 and H6244-R cells have not been carried out, it is possible that this variability is biologically normal. While variation in levels of phosphorylated ERK is evident in these preliminary western blot results, there is no obvious correlation between DUSP5 knockout and enhanced levels of *p*-ERK. This is contrary to results seen with siRNA knockdown of DUSP5 in HCT116

and H6244-R cells (

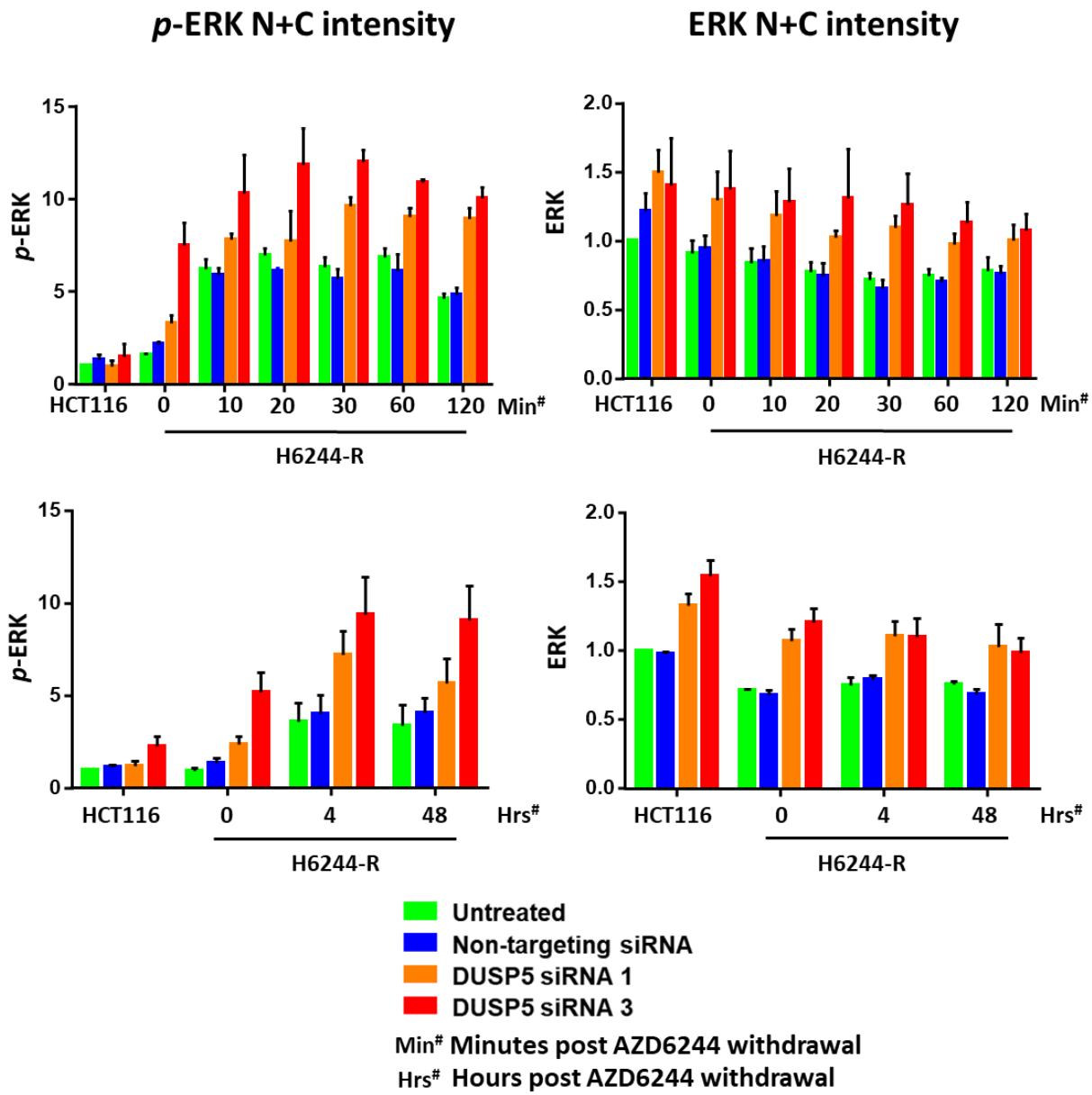

Figure 4.6).

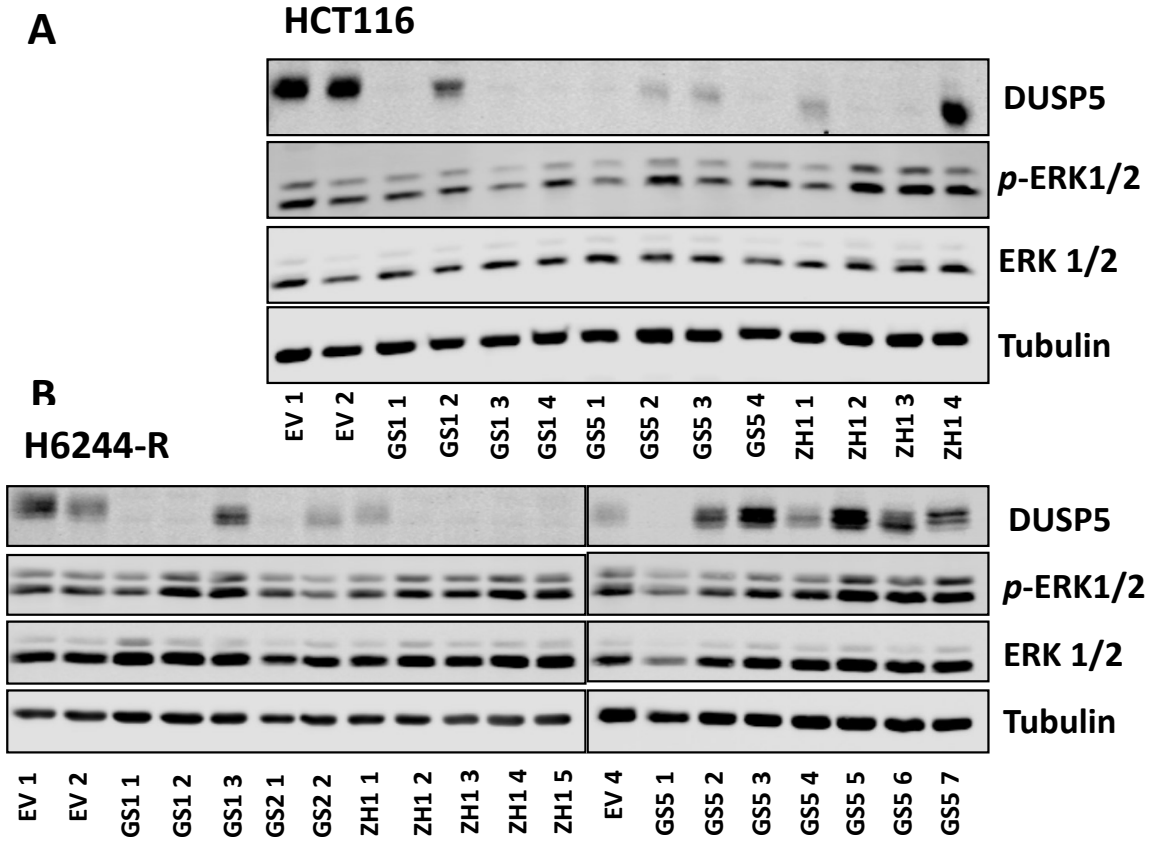

Figure 4.9. Preliminary western blot screening for DUSP5 knockout clones. HCT116 or H6244-R clonal populations were grown in routine culture conditions for a period of 2 to 6 weeks. Protein lysates were generated from semi-confluent 10 cm TC dishes and were normalised for protein content. Lysates were fractioned by SDS-PAGE and Western blotted with DUSP5 antibody to confirm the absence or presence of expressed DUSP5 protein. (EV) denotes “empty vector” transfected clones. GS1, GS2, GS5 and ZH1 are assigned names of clones transfected with one of four DUSP5-targeting CRISPR/Cas9 plasmids containing each gRNA. A) HCT116 clones. B) H6244-R clones.

One DUSP5 KO clone and one DUSP5-expressing clone generated with each of gRNAs GS1, GS5 and ZH1 was chosen for further characterisation. DUSP5-expressing or “uncut” clones together with EV clones were used as controls to account for off-target effects associated with each gRNA plasmid and/or the transfection, single cell-sorting and expansion protocol. Table 4.1 and **Table 4.2** list these clones and describe their nomenclature going forward.

Table 4.1 HCT116 clones chosen for further study.

Name of clone	DUSP5 genotype	New nomenclature
EV-1	DUSP5-expressing	EV
GS1-1	DUSP5 KO	GS1 KO
GS1-2	DUSP5-expressing	GS1 WT
GS5-4	DUSP5 KO	GS5 KO
GS5-3	DUSP5-expressing	GS5 WT
ZH1-2	DUSP5 KO	ZH1 KO
ZH1-4	DUSP5-expressing	ZH1 WT

Table 4.2 H6244-R clones chosen for further study.

Name of clone	DUSP5 genotype	New nomenclature
EV-1	DUSP5-expressing	EV
GS1-2	DUSP5 KO	GS1 KO
GS1-3	DUSP5-expressing	GS1 WT
GS5-1	DUSP5 KO	GS5 KO
GS5-5	DUSP5-expressing	GS5 WT
ZH1-1	DUSP5 KO	ZH1 KO
ZH1-2	DUSP5-expressing	ZH1 WT

4.3.5. DUSP5 knock-out AZD6244-resistant H6244-R cell lines exhibit similar active ERK levels, but reduced E-cadherin expression compared to DUSP5 wildtype cells

Preliminary results from HCT116 and H6244-R clones cultured in routine conditions did not reveal any correlation between DUSP5 KO and enhanced *p*-ERK levels. We speculated that the prolonged period between pSpCas9(sgRNA)-2A-GFP transfection and the first screening experiments may have allowed sufficient time for the development of compensatory mechanisms that could restrain the effects of DUSP5 knockout in these conditions. If this were the case, we reasoned that exposing H6244-R DUSP5 KO and WT clones to conditions of AZD6244 withdrawal, potential differences in their signalling responses may be revealed.

To this end, we probed protein lysates obtained from experiments were HCT116 and H6244-R clones were incubated in 2 μM AZD6244 or AZD6244-free media for 4 or 48 hours. Previous experiments revealed that peak DUSP5 expression is apparent approximately two hours post AZD6244 withdrawal in H6244-R cells (Figure 3.11). We chose to probe samples at 4 hours post-AZD6244 withdrawal to assess any in signalling changes coincident with DUSP5 KO within 2 hours of a timepoint where DUSP5 expression would have normally peaked. We also assessed samples 48 hours post-withdrawal to investigate any potential changes in E-cadherin expression over time.

Figure 4.10a illustrates that all DUSP5 KO clones chosen for further characterisation appear to have a lack of detectable DUSP5 protein. The H6244-R ZH1 WT clone appears to have similar basal levels of ERK to the H6244-R EV clone as well as an HCT116 EV clone. Levels of DUSP5 induced upon AZD6244 withdrawal also appear to be similar between the H6244-R ZH1 WT clone and the H6244-R EV clone, suggesting that these clones serve as reliable DUSP5 WT controls. In contrast, H6244-R GS1 and GS5 “WT” clones appear to have reduced DUSP5 protein levels compared to HCT116 EV, H6244-R EV or H6244-R ZH1 WT clones in all conditions. Similar variation in DUSP5 levels is apparent in HCT116 “WT” clones. As mentioned, this may be indicative of partial DUSP5 knockout in these clones or natural variation in DUSP5 expression levels. For the sake of ease, these intermediate DUSP5 clones were labelled “DUSP5 WT” in Figure 4.10 but are better described as DUSP5-

expressing clones. Figure 4.10d illustrates that across all HCT116 and H6244-R "DUSP5 WT" clones (re. clones that had been transfected with DUSP5-targeting CRISPR/Cas9 constructs but still showed some DUSP5 expression) an overall reduction in DUSP5 protein levels relative to EV clones. In light of this, these clones may better represent partial DUSP5 loss conditions than "wildtype" DUSP5 conditions.

Interestingly, despite marked variation in DUSP5 expression across the clones studied in this experiment (from robust to intermediate to un-detectable levels of DUSP5 protein) detected levels of *p*-ERK appeared relatively consistent across all clones in each condition (Figure 4.10d). This is similar to results in siRNA studies where correlations between DUSP5 disruption and relative changes in *p*-ERK levels were not seen in western blot analyses. Despite the absence of visible changes in *p*-ERK, in conditions where cells were cultured in the absence of AZD6244 for 48 hours, a marked difference in E-cadherin was observed between DUSP5 KO clones and clones that expressed DUSP5 protein (Figure 4.10b, c and d). This suggests that similar to H6244-R cells treated with DUSP5-targeting siRNA (Figure 4.8), the prevention of DUSP5 protein expression is coincident with reduced levels of E-cadherin compared to control samples. Like results seen DUSP5 siRNA knockdown experiments, the reduction in E-cadherin levels is most pronounced after 48 hours of AZD6244-withdrawal, but is also evident prior to AZD6244 withdrawal (Figure 4.10b). The reduction of E-cadherin seen in experiments with AZD6244-deprived H6244-R cells performed by Sale *et al*. (2019) was shown to be ERK-dependant. This, together with the knowledge that DUSP5's only known target is ERK implies that any targeted effects of DUSP5 knockout are likely to be ERK-dependant.

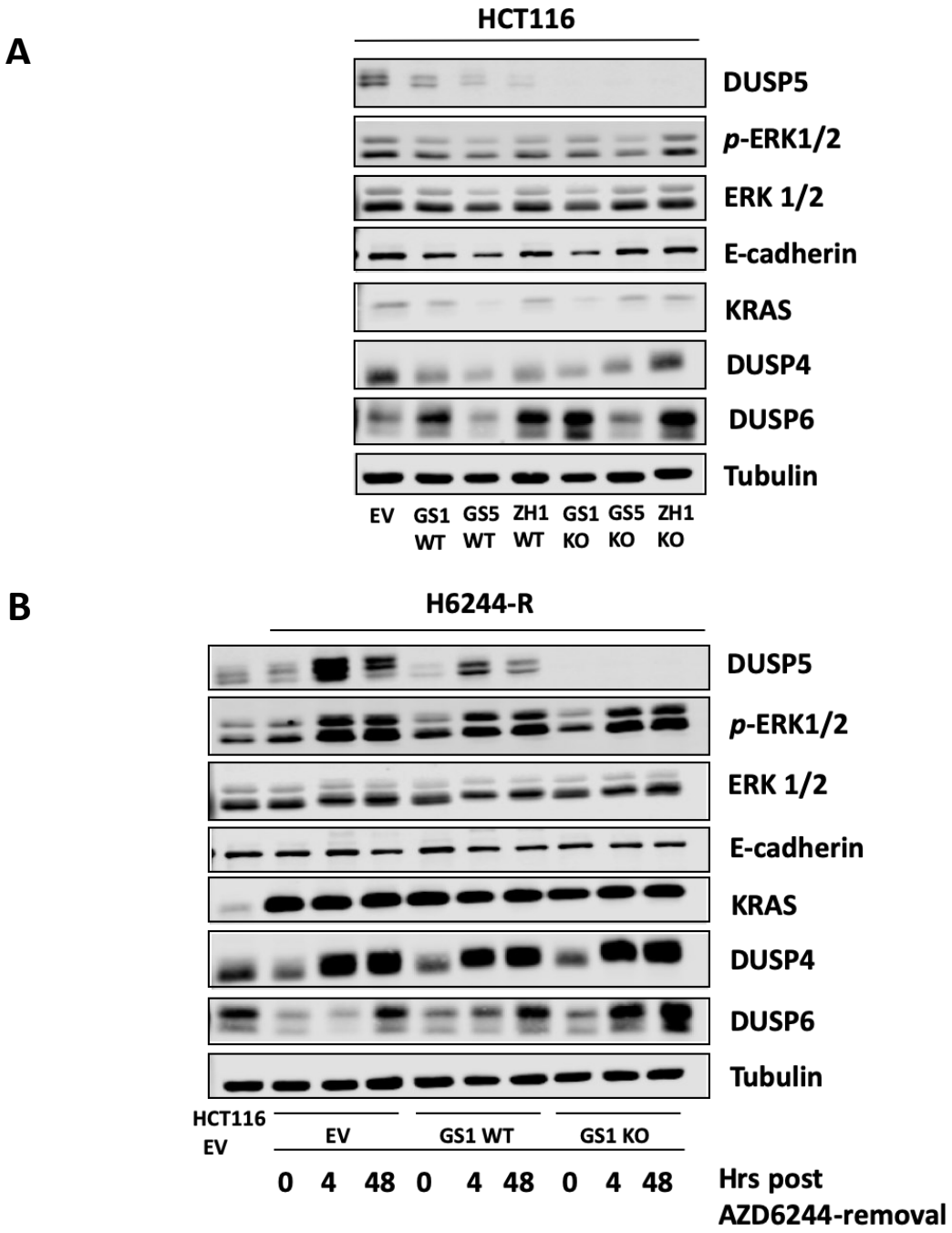

Figure 4.10. DUSP5 knock-out H6244-R cell lines exhibit similar active ERK levels, but reduced E-cadherin expression compared to DUSP5 wildtype cells. HCT116 or H6244-R clonal populations were grown with or without AZD6244 for 4 or 48 hours. (EV) denotes “empty vector” transfected clones. GS1, GS5 and ZH1 are assigned names of clones transfected with one of four DUSP5-targeting CRISPR/Cas9 plasmids containing each gRNA. (WT) denotes DUSP5-expressing clones. (KO) denotes DUSP5 knock out clones. A-C) Lysates were fractioned by SDS-PAGE and Western blotted with the indicated antibodies. Western blot images are representative of three separate experiments.

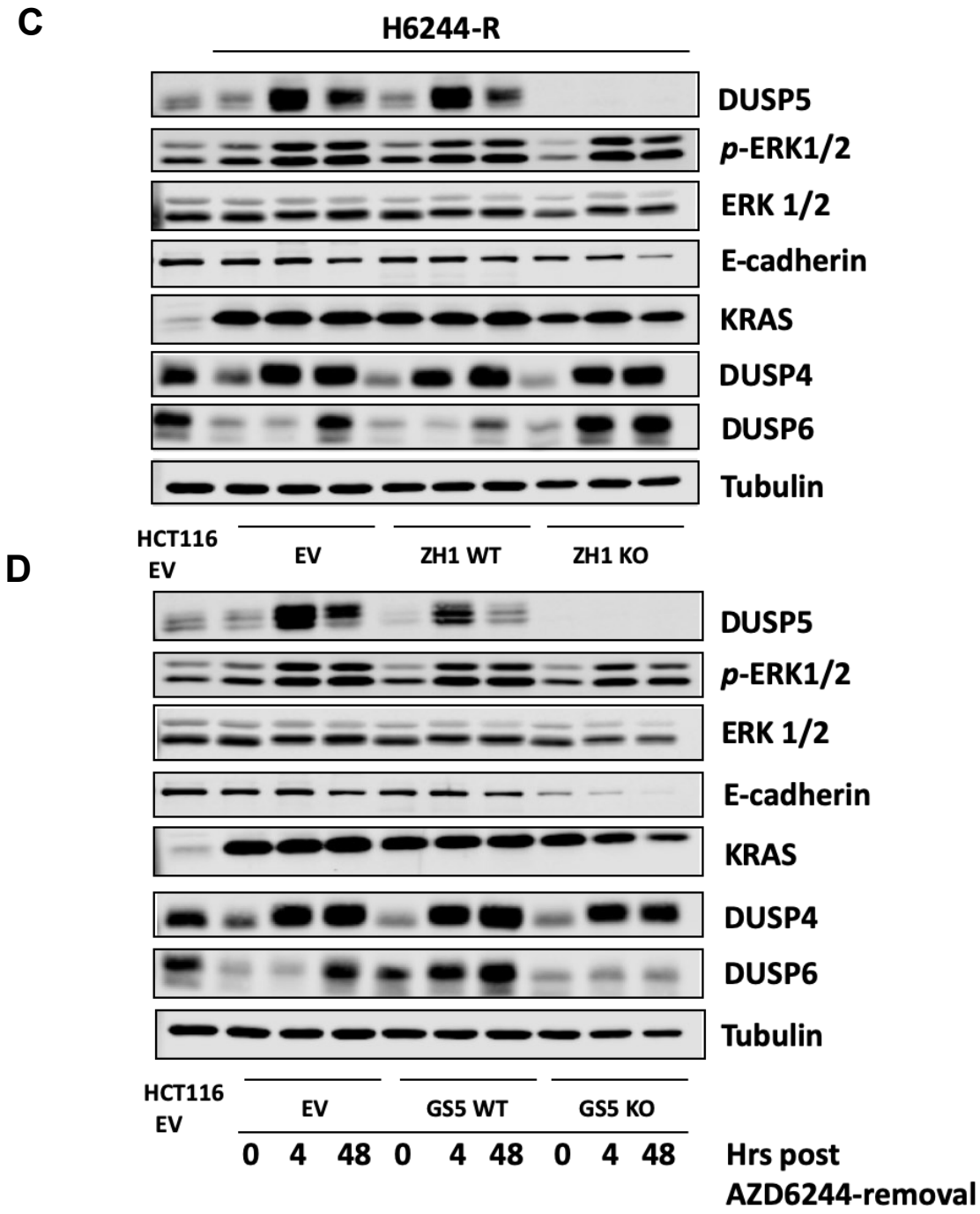

Figure 4.10 continued.

E

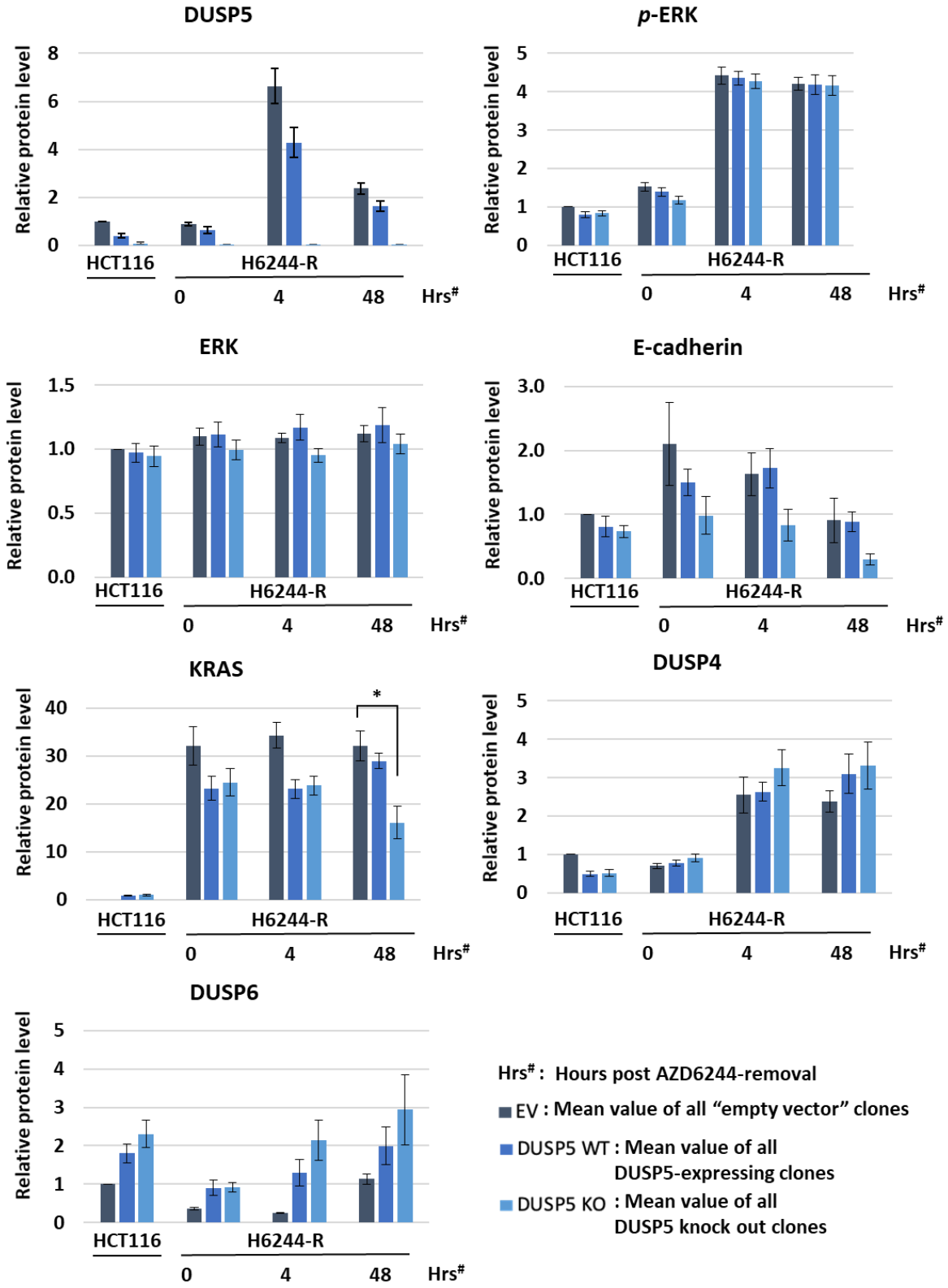
DUSP5
p-ERK
ERK
E-cadherin
KRAS
DUSP4
DUSP6
Relative protein level
HCT116
H6244-R
0
4
48
Hrs#
*
Hrs# : Hours post AZD6244-removal
EV : Mean value of all "empty vector" clones
DUSP5 WT : Mean value of all DUSP5-expressing clones
DUSP5 KO : Mean value of all DUSP5 knock out clones

Figure 4.10 continued. D) Licor quantification of western blot results. Average mean values were calculated from data from 3 experimental repeats and 3 clonal populations for each clonal category; empty vector-treated HCT116 or H6244-R cells, DUSP5-expressing HCT116 or H6244-R cells and DUSP5 knock out HCT116 or H6244-R cells, ± SEM. Statistical analysis was performed using a One-way ANOVA and a post-hoc Tukey analysis, where (*) denotes a p-value less than 0.05.

As DUSP5 knockout clonal populations had been through several passages we were eager to investigate whether any basic compensatory signalling mechanisms had occurred within this time period. We assessed protein levels of the upstream oncogene KRAS as well as DUSP4 and DUSP6, MAPK phosphatases that have previously been shown to be induced in H6244-R cells when AZD6244 was removed (Figure 3.9, Figure 3.10 and Figure 3.11, Chapter 3). Experiments in Sale *et al*. (2019) showed highly consistent levels of amplified KRAS across 12 separate H6244-R clones after 24 hours of AZD6244 withdrawal. In longer term experiments, both a heterogenous population of H6244-R cells as well as two separate H6244-R clones showed the same consistent levels of amplified KRAS after 30 weeks of AZD6244 removal.

In our H6244-R clones cultured in AZD6244, both the DUSP5-expressing clones and the DUSP5 KO clones appear to have reduced levels of KRAS relative to those seen in the EV clone (Figure 4.10d). A similar trend is seen in conditions where H6244-R clones have been cultured in AZD6244-free media for 4 hours. Interestingly, after 48 hours of drug withdrawal, KRAS levels in DUSP5 KO clones are significantly reduced compared to the levels seen in the EV clone (Figure 4.10d). This observation appeared unlikely to reflect an actual decrease in KRAS expression as this is would likely require a profound and highly efficient mechanism of KRAS silencing, which at present, is not conceivable.

Analysis of changing DUSP4 levels in response to AZD6244 withdrawal in H6244-R cells did not reveal any differences between trends in EV clones, DUSP5-expressing clones and DUSP5 KO clones (Figure 4.10d). In contrast, DUSP6 levels appeared slightly increased in both HCT116 and H6244-R DUSP5-expressing and DUSP5 KO clones compared to levels in HCT116 and H6244-R EV clones across all AZD6244 conditions. These results suggest that DUSP6 protein may be upregulated in response to DUSP5 loss in these cells and could reflect a potential compensatory mechanism.

4.4. Discussion

Using siRNA knockdown of DUSP5, we have demonstrated that DUSP5 ablation leads to enhanced ERK activation in HCT116 and H6244-R cells. This was coincident with a higher proportion of *p*-ERK in the nucleus compared to the cytoplasm in HCT116 but not H6244-R cells. In conditions where AZD6244 was removed from H6244-R cells, DUSP5 knockdown was coincident with reduced accumulation of total ERK in the nucleus. In addition to this, disruption of DUSP5 by siRNA or CRISPR/Cas9-mediated gene knockout in H6244-R cells led to accelerated and enhanced reduction of E-cadherin in H6244-R cells cultured without AZD6244. Together these results implicate DUSP5 in modulating the cellular effects of AZD6244 withdrawal in an AZD6244-resistant CRC cell line and highlight the potentially influential role of MKPs in restraining oncogenic ERK signalling.

Previous experiments revealed a robust induction of DUSP5 in response to AZD6244 withdrawal and ERK hyperactivation in H6244-R cells. To further explore the role of DUSP5 in this cell model, we used targeted DUSP5 siRNA and high content microscopy to explore the consequences of disrupting DUSP5 protein expression in similar experimental conditions. Results from these experiments demonstrate that DUSP5 ablation leads to a further enhancement of ERK activation in H6244-R cells cultured in the absence of AZD6244. This enhancement was most apparent after 2 hours of drug withdrawal, the point at which DUSP5 induction is evident in control samples. Together these results suggest an important role for DUSP5 in restraining amplified ERK signalling in this cell model. Interestingly, DUSP5 knockdown was also coincident with increased *p*-ERK levels in HCT116 and H6244-R cells cultured in maintenance conditions, where *p*-ERK expression remains within a “normal” oncogenic range. This implies that negative regulation of active ERK is also required under these conditions, despite the absence of upstream $KRAS^{G13D}$ amplification in HCT116 cells and the presence of MEK inhibition in H6244-R cells cultured in 2 μM AZD6244.

The requirement of DUSP5s' negative influence on ERK activation in conditions outside of AZD6244 withdrawal and ERK hyperactivation may at first seem contradictory, as H6244-R cells amplify upstream $KRAS^{G13D}$ to combat MEK inhibition and decreased ERK activation. However, microarray data from H6244-R samples cultured in maintenance conditions showed an upregulation in other negative ERK regulators of the Sprouty family as well as DUSP4 and DUSP6, indicating that negative feedback is still critical to maintain suitable levels of ERK in these cells (Little *et al.*, 2011). Interestingly, upregulated DUSP5 levels were not detected in this assay.

Surprisingly, in western blot analyses that illustrated the relative levels of *p*-ERK in HCT116 cells and H6244-R cells in varying AZD6244 conditions, DUSP5 ablation with either siRNA or gene knockout did not appear to coincide with marked increases in *p*-ERK. These results were perturbing and seemed to conflict with those derived from HCM experiments. While it is not clear why similar effects of DUSP5 disruption on *p*-ERK levels were not visible in western blot analyses, because these effects were significant and consistent in high content studies we reasoned that despite using semi-quantitative Licor imaging and analysis, the linear range of detection in western blot experiments may not have been sensitive enough to capture these more subtle quantitative differences.

In addition to quantitative intensity data for *p*-ERK expression, high content imaging experiments in H6244-R cells were also able to provide information on the spatiotemporal aspects of ERK activation in response to AZD6244 withdrawal, which had not yet been explored. We hoped that by characterising these trends we could assess whether disruption of DUSP5 in these conditions could lead not only to changes in *p*-ERK magnitude, but potentially in the subcellular location and relative duration of ERK activation.

Time course experiments that assessed the relative magnitude and location of active ERK at after varying periods of AZD6244 withdrawal revealed that hyperactivation of ERK in response to the removal of AZD6244 was evident within 10 minutes and maximal levels of ERK activation were sustained for approximately 1 hour. Interestingly, this *p*-ERK response profile is similar to those seen for prototypic growth-factor induced *p*-ERK, with the exception that levels of *p*-ERK remain high after maximal induction (Caunt et al., 2008b; Kidger et al., 2017). This initial reduction in *p*-

ERK levels precedes the induction of DUSP4, DUSP5 and DUSP6 in H6244-R cells (~2 hours after drug withdrawal) and is still evident in DUSP5 knockdown conditions, so may be a result of more immediate upstream negative feedback mechanisms. Hyperactivation of ERK within 10 minutes of drug removal was coincident with the nuclear accumulation of *p*-ERK. Again, this is consistent with conventional growth factor-induced ERK activation that shows increased ERK phosphorylation and nuclear entry in response to stimulation (Caunt et al., 2008b; Kidger et al., 2017). The ratio of nuclear to cytoplasmic *p*-ERK appears to once again approach 1 after ~60 minutes, indicating that sustained *p*-ERK is present in similar levels in both the nucleus and cytoplasm for the remainder of the response duration assessed. These results differ to those seen in AZD6244 dose-response experiments in Chapter 3, that showed higher *p*-ERK N:C ratios in parental HCT116 cells compared with H6244-R cells in maintenance conditions and decreased *p*-ERK N:C ratios in H6244-R cells cultured without AZD6244 for 48 hours, compared to H6244-R cells in maintenance conditions. The reasons for these discrepancies are unclear, however could indicate that comparing ratios of N:C *p*-ERK between conditions where *p*-ERK levels differ substantially (and reach the minimum threshold of detection) may not be as robust a measure as comparing the same ratios of a relatively consistent signal like ERK.

In H6244-R cells, DUSP5 disruption did not appear to affect the subcellular distribution of *p*-ERK and active ERK accumulated in the nucleus to a similar extent and duration that it did in control samples. Unexpectedly, knockdown of DUSP5 did appear to affect *p*-ERK nuclear accumulation in HCT116 cells. It is unclear why DUSP5 disruption would have different effects on the subcellular location of *p*-ERK in parental and AZD6244-resistant HCT116 cells, but it may be a result of ERK pathway reprogramming events that occur in the evolution of drug-resistance. For example, DUSP6, a cytoplasmic anchor of ERK, appears to be downregulated in H6244-R cells relative to HCT116 cells. These results imply that the interplay between DUSP5, DUSP6 and other ERK regulators that control ERK localisation may become altered in drug-resistant H6244-R cells.

In response to AZD6244 withdrawal in H6244-R cells, the nuclear accumulation of *p*-ERK appears to be transient, and *p*-ERK is more or less once again evenly distributed in the cell after ~ 60 minutes. In contrast, total ERK shifts predominantly to the nucleus within 10 minutes of AZD6244 withdrawal (where its intensity is twice as strong as that for total ERK) and this subcellular distribution appears to be maintained for the duration of the response evaluated (48 hours). The biological relevance of this prolonged nuclear ERK retention is not entirely clear, however, DUSP5 knockdown appeared to disrupt the accumulation of total ERK in the nucleus. Again, these effects were most apparent after 2 hours of ERK hyperactivation, where robust DUSP5 expression is induced in control conditions. These findings are in line with experiments performed by Kidger *et al*. (2017), that showed decreased nuclear accumulation of ERK in response to FBS stimulation in DUSP5 knockout MEFs compared to DUSP5 wildtype MEFs and supports an important role for DUSP5 in anchoring ERK in the nucleus.

Surprisingly, decreased nuclear retention of ERK in DUSP5 knockdown conditions coincided with increased whole-cell ERK levels in both HCT116 and H6244-R cells in maintenance conditions and H6244-R cells in drug withdrawal conditions. While it is not impossible that DUSP5 could affect ERK protein turnover, this is not something that has been reported (Ramos, 2008). It is possible that these results are an artefact of the immunofluorescent staining protocol, wherein binding of DUSP5 to ERK may reduce ERK-specific antibody binding. The detection of total ERK levels in denaturing conditions, such as in western blot analyses, would not be affected by DUSP5 binding and could therefore explain discrepancies in HCM and western blot results for total ERK levels. If this were the case, it is still a striking result and could illustrate the extent of DUSP5 and ERK association in these cells. It is important to note that DUSP5 binding is unlikely to affect the detection of *p*-ERK as DUSP5 dephosphorylates *p*-ERK upon binding and remains associated with its dephosphorylated form.

Proliferation assays performed in conjunction with the assessment of DUSP5 knockdown on *p*-ERK and ERK responses to AZD6244 indicated that DUSP5 disruption in HCT116 and H6244-R may have anti-proliferative effects. ERK hyperactivation was shown to induce senescence and cell death in C6244-R and HT6244-R as well as other cell lines (Sale 2019, others) so these results were initially deemed plausible. However, in HCT116 cells, reduced proliferation was not rescued by increasing AZD6244 concentration and reduced *p*-ERK levels and in H6244-R cells, decreased proliferation and cell numbers was seen in only one of two DUSP5-targeting siRNAs. These observations led us to speculate whether these effects were truly ERK-mediated and induced by DUSP5 ablation and not by other factors at play.

Going forward, we chose to explore the effects of DUSP5 disruption on the undoubtedly ERK-mediated EMT phenotype described by Sale *et al.* (2019) in H6244-R cells deprived of AZD6244. This EMT was characterised by distinct changes in cell morphology and colony growth and decreased expression of the cell-cell adhesion molecule E-cadherin. Based on the observation that DUSP5 knockdown led to enhanced ERK hyperactivation in H6244-R cells cultured without AZD6244, we reasoned that this effect could enhance or accelerate the EMT phenotype see in these conditions.

Consistent with findings in Sale *et al*. (2019) we demonstrated that E-cadherin expression is reduced in H6244-R cells after approximately 48 hours of AZD6244 withdrawal. In both H6244-R DUSP5 siRNA knockdown conditions and DUSP5 knockout clones, reduced E-cadherin was not only enhanced, but it was apparent prior to AZD6244 withdrawal. These findings are significant and clearly demonstrate a role for DUSP5 in influencing the cellular effects of oncogenic ERK signalling. Additionally, the appearance of reduced E-cadherin levels in conditions where DUSP5 expression is disrupted but MEK inhibition is still present, suggests that DUSP5 is critical in restraining ERK activation in both the context of “normal” oncogenic ERK signalling and hyperactive ERK signalling.

While the observation that western blot analyses did not show comparative increases in *p*-ERK to those seen in HCM data in siRNA work could be due to a lack of sensitivity in this technique, in DUSP5 KO clones a similar absence of obvious differences in *p*-ERK levels, despite a marked effect on E-cadherin, could be influenced by other factors too. Specifically, over multiple clonal passages that occurred post-DUSP5 knockout, compensatory mechanisms may have evolved to restrain potential increases in *p*-ERK levels caused by DUSP5 ablation. Therefore, initial *p*-ERK induction may have occurred as an early event which induced an EMT and despite later compensation for hyperactive ERK this EMT was sustained.

Despite some queries over the precise detection and quantification of changing *p*-ERK levels and potential compensatory differences elicited by DUSP5 knockdown versus knockout, the correlation between DUSP5 ablation and enhanced E-cadherin reduction in H6244-R cells was clear and consistent. Based on work by Sale *et al*. (2019) this enhanced downregulation of E-cadherin is likely to coincide with the general enhancement or acceleration of EMT in these cells.

In C6244-R and H6244-R cells, AZD6244 withdrawal and ERK hyperactivation led to decreased proliferation and cell survival, both events that could confer clinical advantages in the treatment of colorectal tumourigenesis (Sale et al., 2019). This work highlighted the potential effectiveness of “drug holiday” regimes in ERK-driven cancers that have acquired similar oncogene amplifications. In these cancers, the anti-proliferative effects of ERK hyperactivation induced by removing ERK pathway inhibitors could be harnessed, leading to better clinical outcomes. In contrast, ERK hyperactivation in H6244-R cells does not have anti-proliferative consequences and instead promotes an epithelial-to-mesenchymal transition. In cancer development and progression, EMT is often associated with metastasis and increased invasiveness (Thiery et al., 2009) and has also been correlated with cross-resistance to chemotherapeutic agents (Zheng et al., 2015).

Experiments performed by Sale *et al*. (2019) demonstrated that while H6244-R cells cultured in the absence of AZD6244 showed enhanced cell motility and faster wound closure, subcutaneous xenograft models did not show increased invasiveness of these cells compared to controls. However, AZD6244 withdrawal and subsequent EMT did reduce the sensitivity of H6244-R cells to oxaliplatin and 5-FU, chemotherapeutic agents widely used in colorectal cancer. Together, work by Sale and colleagues emphasises how the genetic idiosyncrasies of a specific cancer can lead to diverse outcomes in response to drug administration. Our results have shown that these genetic idiosyncrasies include variations in the expression and function of negative ERK regulators such as DUSP5, which in H6244-R cells, is able to modulate the cellular effects of AZD6244 withdrawal. Our work therefore suggests an important role for DUSP5 and other MKPs in the regulation of oncogenic ERK signalling and ERK pathway inhibitor-resistance.

4.5. Limitations and future work

While we attempted to employ DUSP5 knockdown/ knockout strategies that achieved robust/ complete DUSP5 loss without exerting unknown off-target effects, both siRNA and CRISPR/Cas9-mediated strategies had limitations in this respect.

The development of DUSP5 knockout clones was a lengthy process that had various caveats. Firstly, plasmid transfection followed by single cell sorting and outgrowth are processes that can induce cellular stress. This stress could promote natural variations and adaptions in different clones that were not be accounted for. Indeed, variations in cell morphology and growth rate were apparent in different clones and appeared to be independent of initial transfection with empty vector or DUSP5-targeting constructs. Secondly, marked natural variation could exist in each clone prior to single cell outgrowth. As mentioned, variation in DUSP5 expression was observed amongst clones and it is unclear whether this variation was “natural” or a result of partial gene knockout. The latter concern could be addressed relatively easily through DNA sequencing of selected H6244-R clones.

In siRNA knockdown of DUSP5 the appearance of an anti-proliferative phenotype with one of two DUSP5 siRNAs led us to question whether off target effects were at play. Additionally, discrepancies in the effects of DUSP5 knockdown on the relative expression of *p*-ERK were seen using two different quantitative techniques. While the coincident reduction of E-cadherin and DUSP5 ablation was consistent and appeared targeted, future DUSP5 rescue experiments could be performed in order to exclude any doubts on the specificity of the effects demonstrated in our experiments. In work completed by Kidger *et al.* (2017), adenoviral constructs containing the DUSP5 coding sequence downstream of an Egr1 promoter were used to recapitulate ERK-mediated DUSP5 expression in DUSP5 knockout MEFs. A similar strategy could be useful in assessing whether enhanced ERK hyperactivation and E-cadherin reduction are reversed in the presence of homeostatic levels of DUSP5 expression.

This work could be coupled with experiments that further characterised the potential influence of DUSP5 on the EMT in H6244-R cells. Experiments in Sale *et al.* (2019) revealed that decreases in E-cadherin in response to AZD6244 withdrawal in H6244-R cells were coincident with increased expression of the mesenchymal markers SNAI2 and ZEB1. It is possible that ERK mediates these changes by promoting the expression of ZEB1 through its regulation of FRA1 (Shin et al., 2010) and the downregulation of E-cadherin through the subsequent repressive effects of ZEB1 on E-cadherin expression (Ichikawa et al., 2015). mRNA and protein quantification experiments that assessed whether DUSP5 loss lead to an increase in ZEB1 and SNAI2 expression could further establish DUSP5 effects on the EMT in these conditions.

In addition to these experiments, it would be interesting to further explore potential compensatory mechanisms that may occur when DUSP5 expression is disrupted, both transiently (through siRNA knockdown) and permanently (through CRISPR/Cas9-mediated knockout), in HCT116 and H6244-R cells. Preliminary experiments in DUSP5 KO clones revealed possible compensatory upregulation of DUSP6 and downregulation of KRAS in response to AZD6244 withdrawal in H6244-R cells. These results could be further investigated through the assessment of KRAS and MKP expression in DUSP5 knockdown conditions or in more individual DUSP5 KO clones, and could include DUSP5 rescue experiments to ensure the specificity of these

effects. It is worth noting that the above objectives could be addressed in part, through targeted high throughput RNA screens performed on samples derived from H6244-R cells with or without DUSP5 loss, in various relevant experimental conditions. This would offer a more global overview of the signalling changes that occur in response to DUSP5 loss and could provide further insight into the mechanism of the ERK-mediated EMT seen in H6244-R cells.

Chapter 5. Sustained DUSP5 loss in MEKi-resistant HT29 cells leads subtle changes in cellular responses to AZD6244 withdrawal

5.1. Introduction

Experiments that investigated the impact of DUSP5 loss on HCT116 and H6244-R cells demonstrated that DUSP5 is able to modulate the effects of sustained ERK signalling. In H6244-R cells where ERK hyperactivation is induced upon AZD6244 removal, disruption of DUSP5 led to an enhancement of hyperactive ERK and of reduced E-cadherin levels, both associated with EMT in this cell model. Characterisation of the EMT in H6244-R cells showed that these phenotypic changes were correlated with increased resistance to both 5-fluorouracil and oxaliplatin, standard of care chemotherapies used to treat colorectal cancer (Sale et al., 2019). In this instance, the potential enhancement and acceleration of EMT through DUSP5 targeting could have a detrimental impact on clinical outcome. In light of this, we hoped to explore an avenue where the regulatory effects of MKP could be harnessed, such as in HT6244-R cells, where AZD6244 deprivation and ERK hyperactivation lead to cell death.

Cell survival and cell death are two opposing cell fate trajectories, the outcome of which is determined by the balance of pro-apoptotic and pro-survival regulatory mechanisms. These mechanisms are largely comprised of the BCL2 family members which control the intrinsic apoptotic pathway. The regulation of various BLC2 family members by ERK is ubiquitous and while active ERK commonly acts to promote cell survival, it can induce anti-proliferative and apoptotic cell fates (Cagnol and Chambard, 2010; Cook et al., 2017). The ability of ERK to mediate these effects has frequently been linked to its downstream targets $p21^{CIP1}$ and p53 and less commonly, NOXA and is largely associated with ERK hyperactivation (Cagnol and Chambard, 2010; Elgendy et al., 2011; Sewing et al., 1997; Woods et al., 1997b). It follows that negative regulators of ERK activity such as the MKPs, are likely to have enhanced influence in these contexts and may be employed in adaptive strategies to restrain hyperactive ERK. Indeed, in a recent study using ERK-regulated DUSP5 expression constructs in DUSP5 knock out MEFs, amplified DUSP5 was shown to facilitate

$BRAF^{V600E}$-driven proliferation and transformation in MEF cells, while the absence of DUSP5 caused ERK hyperactivation and cellular senescence (Kidger et al., 2017).

Like results seen in H6244-R cells, robust DUSP5 induction was associated with ERK-hyperactivation in AZD6244-deprived HT6244-R cells. Using similar experimental approaches to those implemented in our previous work, we aimed to assess whether DUSP5 loss in HT6244-R cells affected the cell death phenotype observed in conditions of AZD6244 withdrawal.

5.2. Work preceding this thesis

5.2.1. AZD6244 withdrawal from HT6244-R cells promotes ERK-dependent activation of pro-apoptotic BH3-only proteins NOXA and BID, leading to cell death

Work by the Cook laboratory (Little et al., 2011; Sale et al., 2019), has demonstrated that unlike KRAS-driven H6244-R cells, AZD6244-resistant C6244-R and HT6244-R cells exhibit a proliferation defect when cultured in the absence of AZD6244. This was first established in work with C6244-R cells, where ERK hyperactivation induced by AZD6244 withdrawal promoted cell cycle arrest within 24 hours of AZD6244 removal (A. S. Little et al., 2011b) and was confirmed in similar experiments in this thesis (Figure 3.5, Chapter 3). Later work revealed that this response is mediated by upregulation of the CDK inhibitor $p57^{KIP2}$ and results in resensitisation of C6244-R cultures to the anti-proliferative effects of AZD6244 after prolonged drug withdrawal (Sale et al., 2019).

In early AZD6244-withdrawal experiments where HT6244-R cells were cultured in AZD6244-free media for 24 to 48 hours, cell cycle data and proliferation assays did not reveal any effects of ERK hyperactivation on proliferation Figure 3.4, Chapter 3). However recent work by the Cook group has revealed that AZD6244 withdrawal leads to a transient G1 arrest in HT6244-R cells (16 hours post-withdrawal) followed by cell death after 6 or more days of AZD6244 deprivation (Sale et al., 2019).

Figure 5.1 illustrates cell cycle distribution profiles for HT6244-R cells cultured both in the presence and absence of AZD6244 (a and b) as well as western blot images of multiple ERK-associated signalling proteins from similar experiments (c). The data shows a temporary G1 arrest in HT6244-R cells deprived of AZD6244 for 16 hours, which was coincident with the expression of Cyclin D1 and $p21^{CIP1}$ (Figure 5.1, a and c). However, by 48 hours, expression of these proteins appeared to decrease and the proportion of cells in G2/S phase in HT6244-R cells deprived of AZD6244 were similar to those in HT6244-R cells cultured in 1 μM AZD6244 (Figure 5.1a).

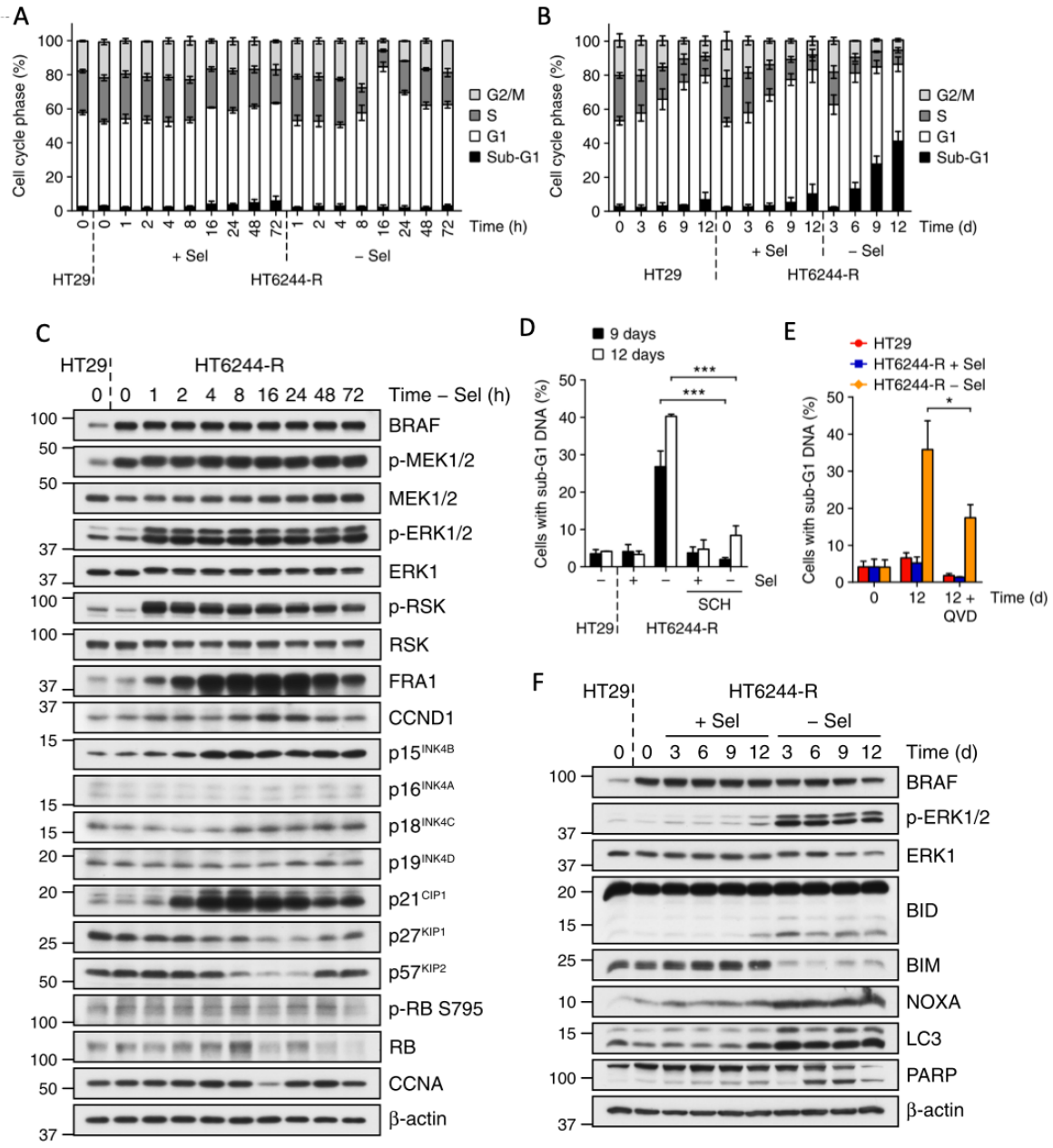

Figure 5.1 MEKi withdrawal from BRAFV600E-amplified MEKi-resistant HT29 cells causes a transient G1 arrest followed by cell death. A.B,C,F) HT29 and HT6244-R cells were treated with either 1 μM AZD6244 or DMSO only for the indicated times. A,B) Cell cycle distribution was determined by flow cytometry. C,F) Lysates western blotted with the indicated antibodies. Results are representative of at least two experiments giving equivalent results. D, E) HT29 or HT6244-R cells were treated with 1 μM AZD6244 or DMSO only, with or without D) 0.1 μM SCH772984 (SCH) for 9 or 12 days E) 10 μM Q-VD-OPh (Q-VD) for up to 12 days. sub-G1 fraction was determined by flow cytometry. A, B, D, E) Results are mean ± SD of three independent experiments. This figure was adapted from Sale et al. (2019) with permission from Nature communications.

The most striking results in these experiments occurred between 6 and 12 days of AZD6244 withdrawal where cells began to detach from the culture plate, indicating that cell death was taking place. Flow cytometry data showed that under these conditions, the proportion of cells exhibiting sub-G1 DNA became markedly increased in AZD6244-deprived HT6244-R cells, also an indication of cell death (Figure 5.1b). This increase was approximately 20 to 35 % higher in AZD6244-deprived HT6244-R cells than HT6244-R and HT29 cells cultured in their maintenance conditions (Figure 5.1d). Further experiments determined that this cell death was both caspase- and ERK-dependent as it was decreased by the ERK inhibitor SCH772984 (Figure 5.1d) and the pan-caspase inhibitor Q-VD-OPH (Figure 5.1e).

As previously discussed, ERK is able to promote cell survival as well as cell death through its regulation of the BCL2 family members (Cook et al., 2017). In healthy cells, ERK has been shown to activate pro-survival proteins such as BCL2 and BCL-xL and repress pro-apoptotic proteins such as BIM and PUMA, thus promoting cell survival (Balmanno and Cook, 2009). However, in some contexts, ERK activation can lead to the autophagy and/or apoptosis through the upregulation of NOXA, a pro-death BH3-only protein (Elgendy et al., 2011; Sheridan et al., 2010). Naturally, following the discovery that ERK activation upon AZD6244 withdrawal in HT6244-R cells lead to cell death, Sale *et al*. (2019) went on to investigate the expression of several BCL2 family members in cells exposed to these conditions.

Figure 5.1f illustrates the effects of AZD6244 removal and ERK hyperactivation on relevant cell death-associated markers in HT6244-R cells. As expected, ERK hyperactivation was coincident with a reduction in the pro-apoptotic BIM protein. This is likely to occur through ERKs ability to phosphorylate and inhibit a transcriptional activator of BIM, FOXO3A (Yang et al., 2008) and/or phosphorylate BIM itself, leading to increased proteasomal degradation of this protein (Ley et al., 2003). Reduction in BIM protein levels was evident from 3 days of drug withdrawal onwards. Between 6 and 12 days of AZD6244 deprivation an increase in both BID and PARP cleavage was evident (Figure 5.1f). The cleavage of BID, a pro-apoptotic BCL2 family member, and of PARP a DNA-binding polymerase involved in DNA repair, is commonly associated with caspase-mediated apoptosis. These changes were coincident with increased levels of NOXA as well as increased LC3-II (Figure 5.1f). The amount of LC3-II present

in a sample is correlated with the number of autophagosomes, thus indicative of the occurrence of autophagy. As mentioned, upregulation of NOXA has been shown to play a role in autophagy, through its ability to bind the pro-survival BCL2 protein MCL1, thereby freeing a major autophagic effector Beclin-1 from repressive MCL1/Beclin-1 complexes (Cook et al., 2017).

While the mechanisms through which hyperactive ERK induces apoptosis and features of autophagy in this model have not yet been fully delineated, this work contributes to a growing body of evidence that implicates ERK signalling in oncogene-induced cell death and senescence (Cagnol and Chambard, 2010). As demonstrated in work by Sale *et al.* (2019) where ERK hyperactivation induced by inhibitor-withdrawal lead to the death of previously drug-resistant H6244-R cancer cells, a thorough understanding of the regulatory power of ERK signalling in combination with therapeutic manipulation of this pathway can lead to clinically advantageous outcomes. By investigating the effects of MKP expression in this context, we hoped to add further insight into the regulatory mechanisms that could be of potential clinical relevance in similar “drug holiday” regimes.

5.3. Results

5.3.1. Transient DUSP5 loss in MEKi-resistant HT29 cells has subtle effects on the spatiotemporal regulation of ERK

HT29 cells are not readily transfected through lipid-based methods and our early attempts at developing in-house DUSP5-targeting shRNA adenoviral constructs were unsuccessful, so we aimed to induce DUSP5 loss in HT29 and HT6244-R cells through DUSP5-targeting shRNA adenoviral constructs purchased from VectorBuilder (detailed in Chapter 2). Similar adenoviral constructs used routinely in our laboratory were able to infect MEF cells and induce robust DNA expression at viral titres between 0.3 and 3 $pfu.nL^{-1}$ (Kidger et al., 2017). Following these guidelines, experiments were performed to reveal the lowest titre of DUSP5-targeting shRNA adenovirus that could achieve robust DUSP5 knockdown. These experiments were initially performed in H6244-R cells in AZD6244-free conditions, where DUSP5 was highly expressed and easily detected by western blotting. Figure 5.2 illustrates one of these experiments, where a marked reduction of DUSP5 protein was seen in cells incubated with 5 $pfu.nL^{-1}$ of either DUSP5-targeting shRNA adenovirus 3 or 5.

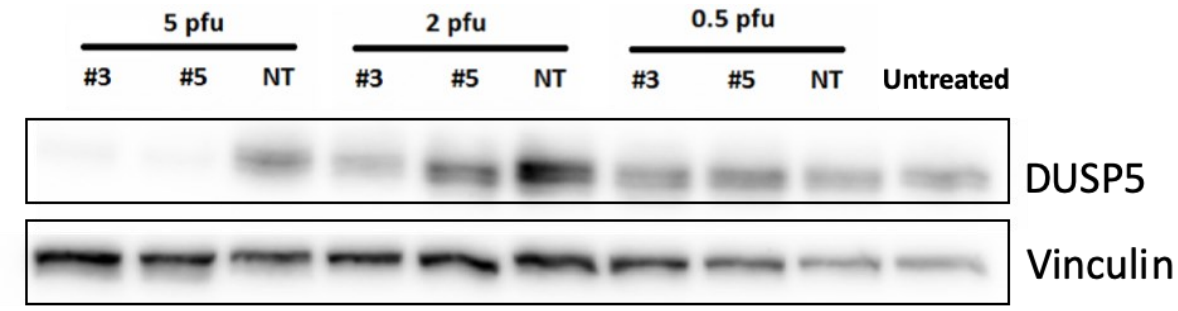

Figure 5.2 Optimising DUSP5 protein knockdown with VectorBulider DUSP5-targeting shRNA adenovirus in H6244-R cells. H6244-R cells were incubated with the indicated concentrations (in pfu.nL^{-1}) of VectorBuilder DUSP5-targeting shRNA adenovirus 3, 5 (#3 and #5) or non-targeting shRNA adenovirus (#NT) overnight. Viral media was washed from the culture plates and replaced with AZD6244-free complete media. Cells were incubated for a further 48 hours prior to cell lysis and SDS-PAGE. Samples were Western blotted with DUSP5 antibody to confirm the absence or presence of expressed DUSP5 protein. Image is representative of results from 3 separate experiments.

While using the same viral concentration (calculated as pfu.nL^{-1}) in repeated experiments is a reliable method of ensuring consistent amounts of virus being present in each condition, it does not take into account changing cell numbers across different cell culture formats. An increase or decrease in the ratio of viral particles to number of cells could affect the efficiency of viral infection and so should be kept as consistent as possible in order to reduce variability between experiments. In an attempt to keep both these measures consistent, we calculated the MOI of virus in conditions where DUSP5 knockdown was achieved and used a consistent pfu.nL^{-1} and MOI of virus in all future experiments. Based on the pfu.nL^{-1} and MOI used in successful DUSP5 knockdown experiments with H6244-R cells, similar conditions were employed in experiments assessing DUSP5 knockdown efficiency in HT6244-R cells. Similar to results in H6244-R cells, DUSP5 protein appears to be markedly reduced after transfection with either DUSP5-targeting shRNA adenovirus 3 or 5 compared to controls, at a MOI of 150 and higher (Figure 5.3).

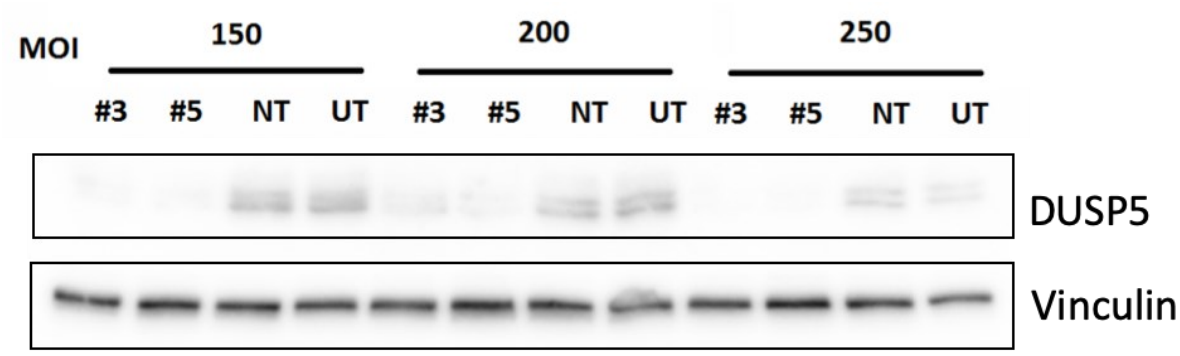

Figure 5.3 Optimising DUSP5 protein knockdown with VectorBulider DUSP5-targeting shRNA adenovirus in HT6244-R cells. HT6244-R cells were incubated with the indicated MOI of VectorBuilder DUSP5-targeting shRNA adenovirus 3, 5 (#3 and #5), non-targeting shRNA adenovirus (#NT) or remained untreated (UT) overnight. Viral media was washed from the culture plates and replaced with AZD6244-free complete media. Cells were incubated for a further 48 hours prior to cell lysis and SDS-PAGE. Samples were Western blotted with DUSP5 antibody to confirm the absence or presence of expressed DUSP5 protein. Image is representative of results from 3 separate experiments.

Once the conditions for DUSP5 knockdown were established in HT6244-R cells we went on to investigate whether DUSP5 repression had any effect on the spatiotemporal regulation of ERK and/or other ERK signalling-related targets associated with cellular stress and cell death. Similar to experiments completed in H6244-R cells in Chapter 4, AZD6244-withdrawal time course experiments were performed and assessed through quantitative immunoblotting and high content microscopy. Previous experiments in HT6244-R cells revealed peak DUSP5 expression 2 hours post AZD6244 withdrawal (Figure 3.11, Chapter 3). Therefore, we chose to investigate the relative expression of our proteins of interest at this time point, as well as 48 hours post-withdrawal to assess any longer-term changes (Figure 5.4).

In addition to evaluating DUSP5, *p*-ERK and ERK protein levels, levels of $p21^{CIP1}$ and BIM proteins were assessed as "early" (detectable within 48 hours) markers of biologically relevant increases in active ERK. $p21^{CIP1}$ induction has previously been correlated with sustained increases in *p*-ERK (Balmanno and Cook, 1999; Sewing et al., 1997; Woods et al., 1997a), and was found to be increased in response to AZD6244 removal in HT6244-R cells (Sale et al., 2019). Conversely, BIM is repressed by active ERK (Cook et al., 2017; Ley et al., 2003; Sale and Cook, 2012) and was found to decreased in AZD6244 withdrawal conditions (Sale et al., 2019).

As expected, HT6244-R cells in control conditions (untreated or transfected with non-targeting shRNA adenovirus) showed an increase in *p*-ERK levels following AZD6244 withdrawal, coincident with DUSP5 and $p21^{CIP1}$ induction and a reduction in protein levels of BIM (Figure 5.4). In DUSP5 knockdown conditions where DUSP5 protein levels were reduced by approximately 80% relative to controls (in conditions of peak DUSP5 expression) no observable or quantifiable effects on levels of *p*-ERK, BIM or $p21^{CIP1}$ were seen, however a subtle decrease in ERK levels was evident in HT6244-R shRNA 5 lines compared to all other lines (Figure 5.4).

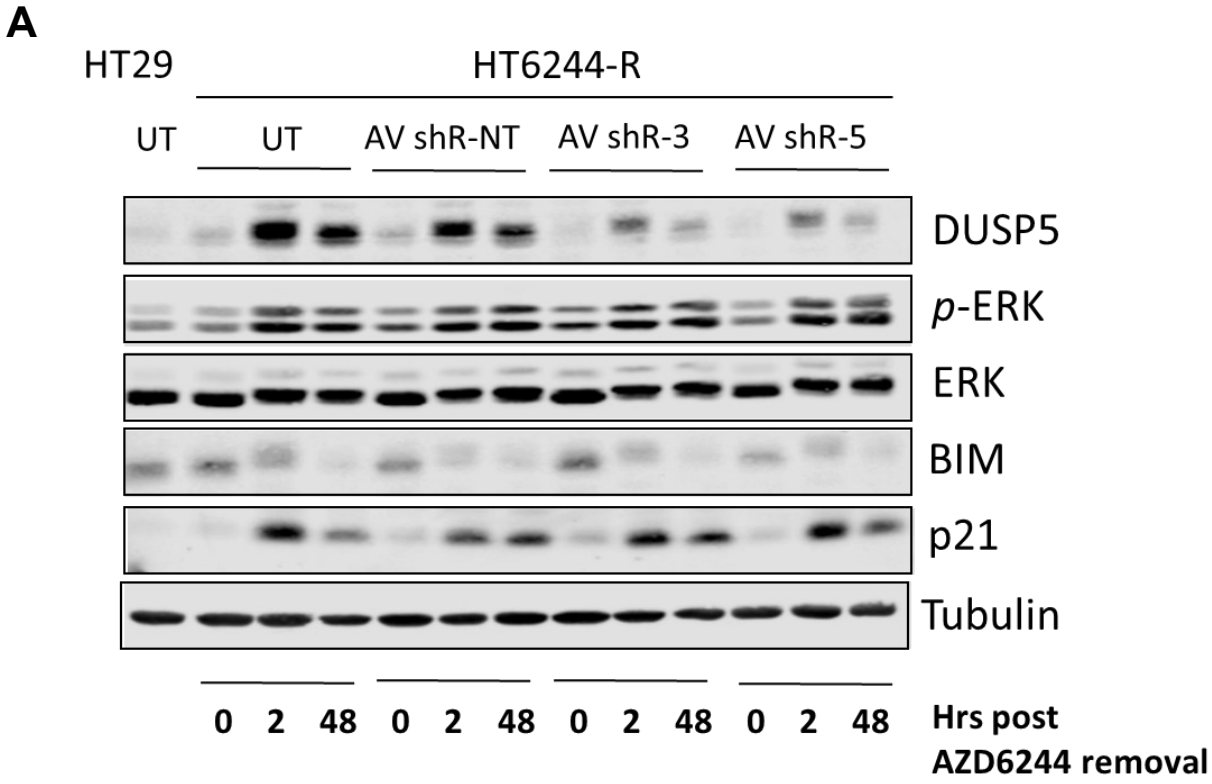

Figure 5.4 Transient adenoviral knockdown of DUSP5 in HT6244-R cells does not affect relative levels of *p*-ERK, p21^{CIP1} or BIM protein. HT29 and HT6244-R control cells were incubated alongside HT6244-R cells treated with VectorBuilder DUSP5-targeting shRNA adenovirus 3, 5 (#3 and #5) or non-targeting shRNA adenovirus (#NT) overnight. Viral media was washed from the culture plates and replaced with AZD6244-free complete media for the period of time indicated. Cells were lysed and fractioned by SDS-PAGE. Samples were Western blotted with the indicated antibodies to assess relative protein levels. A) Western blot images. Images are representative of results from 3 separate experiments.

B

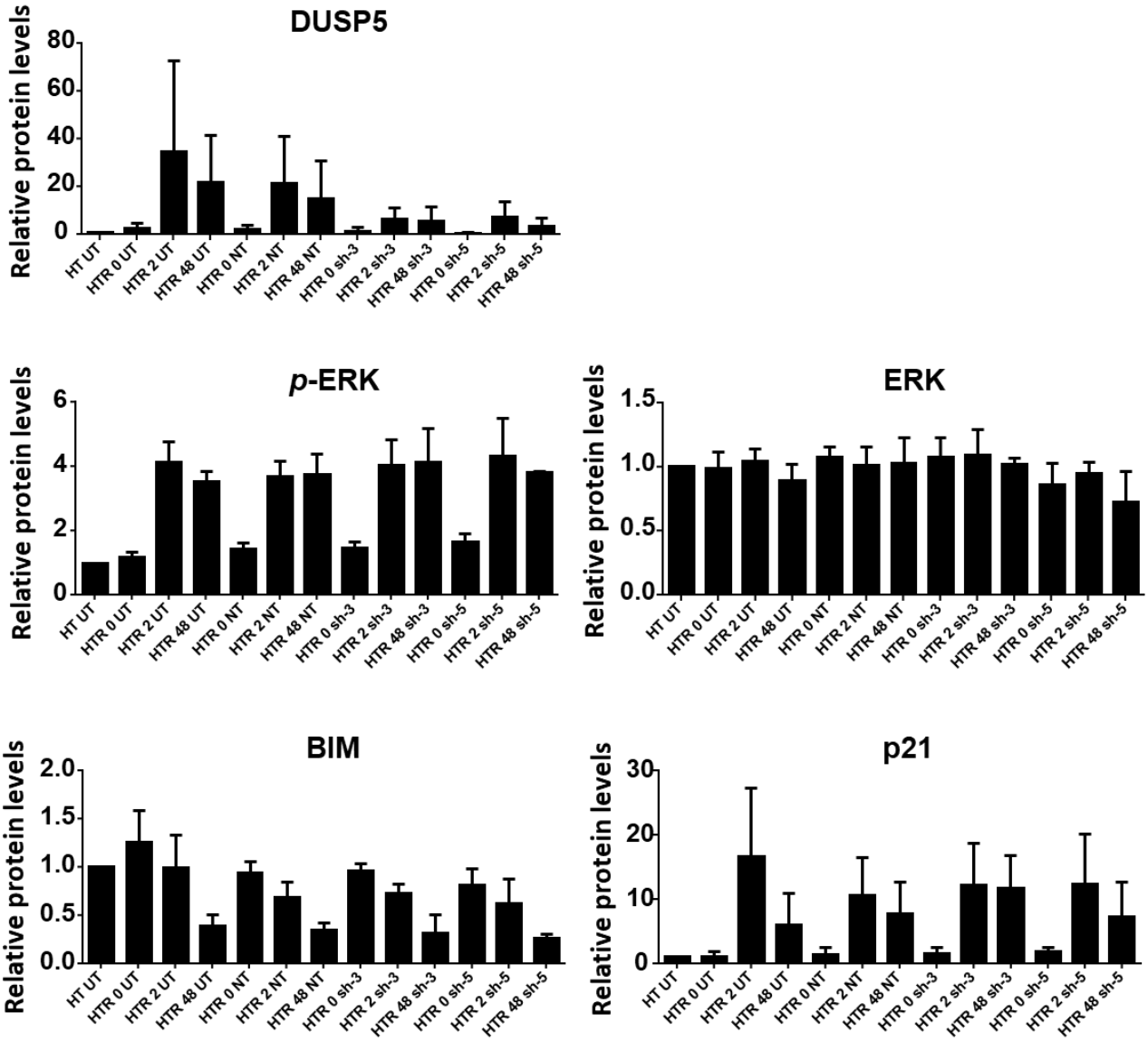

Figure 5.4 continued. B) Protein quantification. Relative intensities of protein bands were quantified using Liquor's Image Studio Lite software. DUSP5: Percentage DUSP5 knockdown relative to the untreated control shown. n=3 biological replicates, ± SEM.

Previous experiments in HCT116 and H6244-R cells that blotted for *p*-ERK protein in an effort to assess potential changes in these levels (Figure 4.8, Chapter 4) showed relatively uniform levels of *p*-ERK across DUSP5 knockdown and control conditions. These results were not consistent with quantative data derived from high content microscopy experiments (

Figure **4.5** and

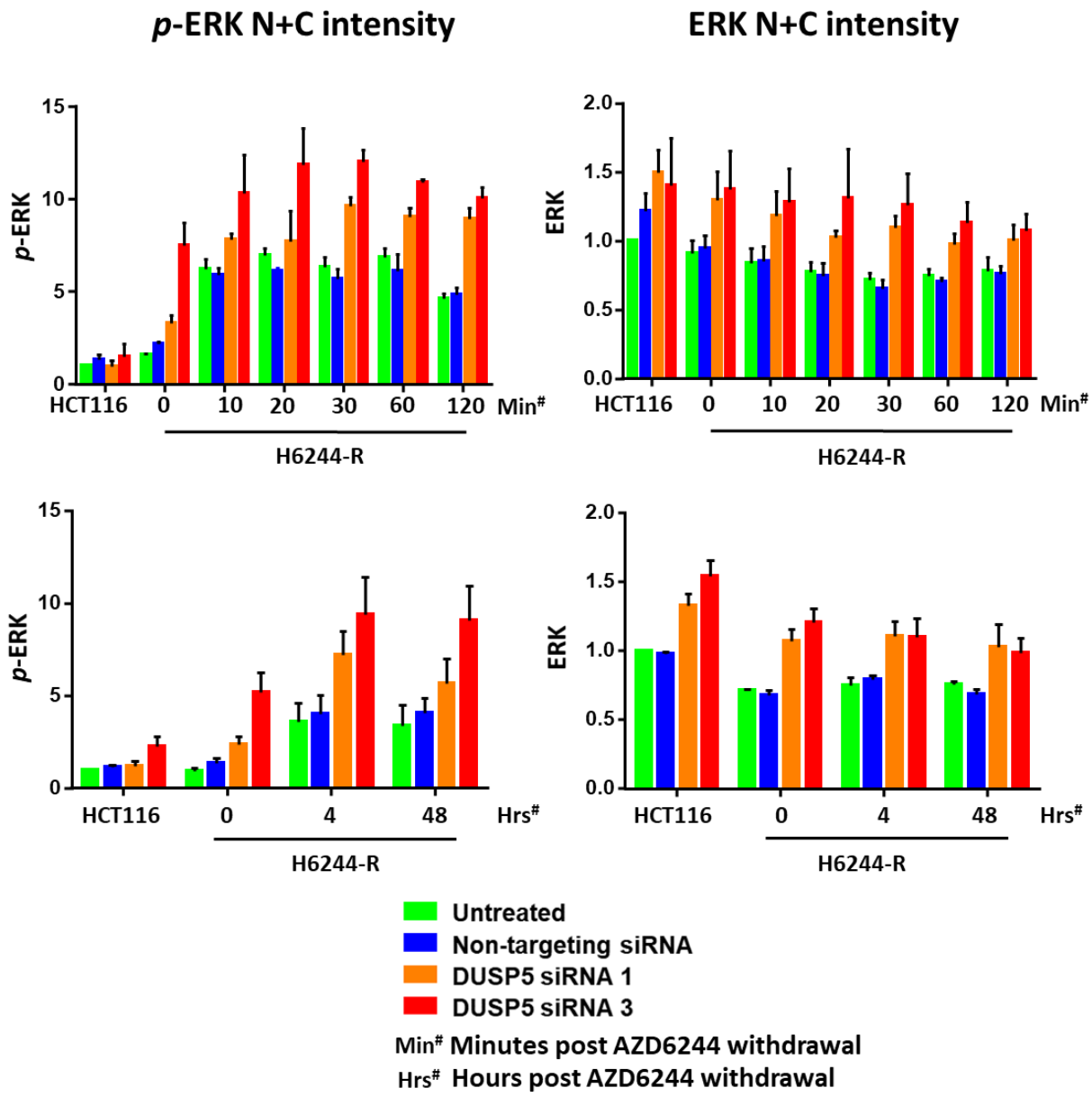

Figure 4.6), which showed significantly increased *p*-ERK levels in DUSP5 KD conditions compared to controls. In light of this, we performed parallel HCM experiments assessing similar experimental conditions as those illustrated in Figure 5.4, as well as shorter time course experiments to examine the relative magnitude and location of *p*-ERK and ERK directly following AZD6244 withdrawal.

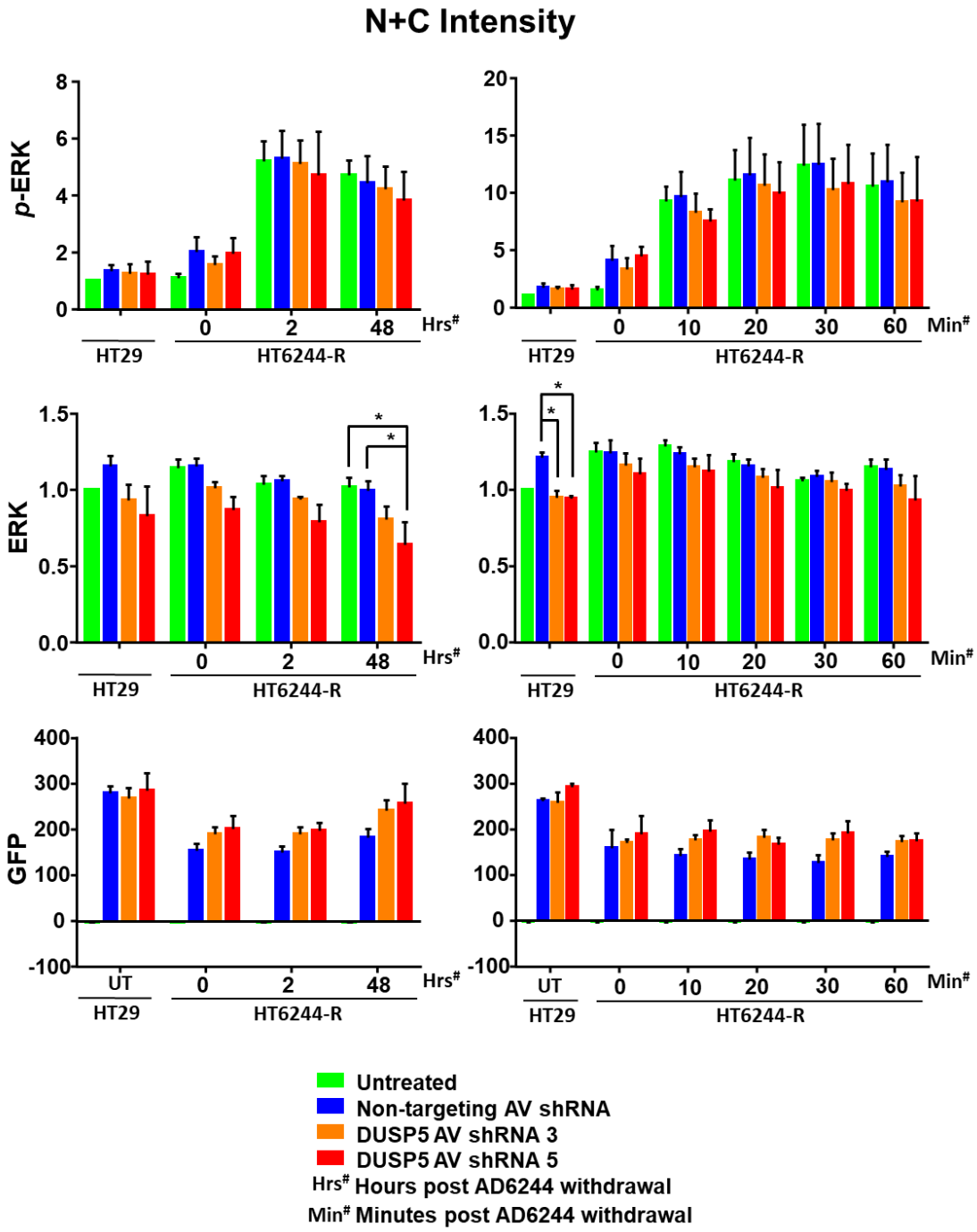

Figure 5.5 illustrates whole-cell GFP, *p*-ERK and ERK signal intensity data in experiments where H6244-R cells were cultured in the absence of AZD6244 for varying time periods. Relative to *p*-ERK levels in HT29 cells and HT6244-R cells cultured in maintenance conditions, enhanced ERK activation was apparent within 10 minutes of AZD6244 removal, peaked at 30 minutes after AZD6244 removal and then

decreased slightly thereafter (

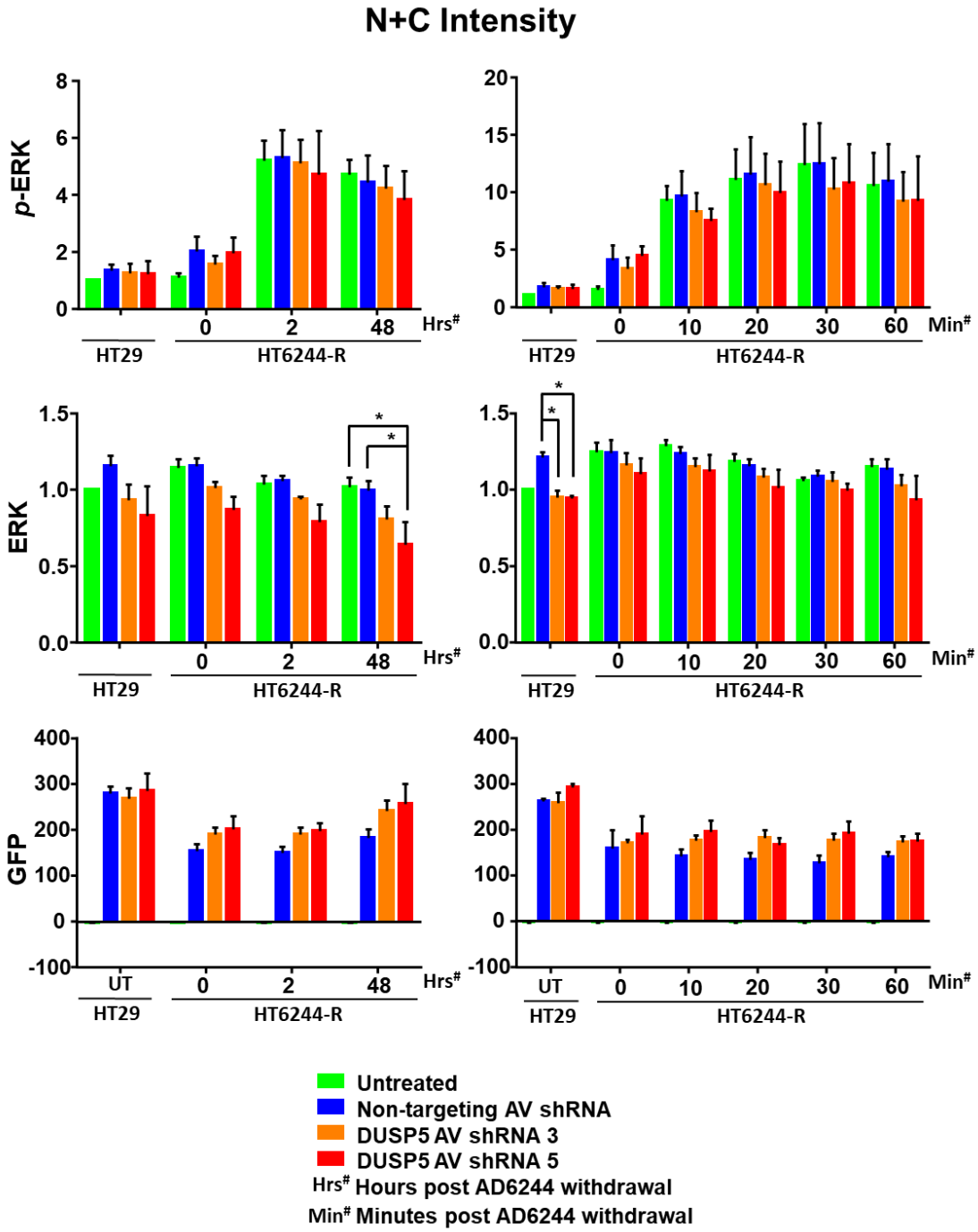

Figure 5.5, top left). At 2 hours and 48 hours post-AZD6244 removal, *p*-ERK remained higher in AZD6244-free conditions relative to control conditions (

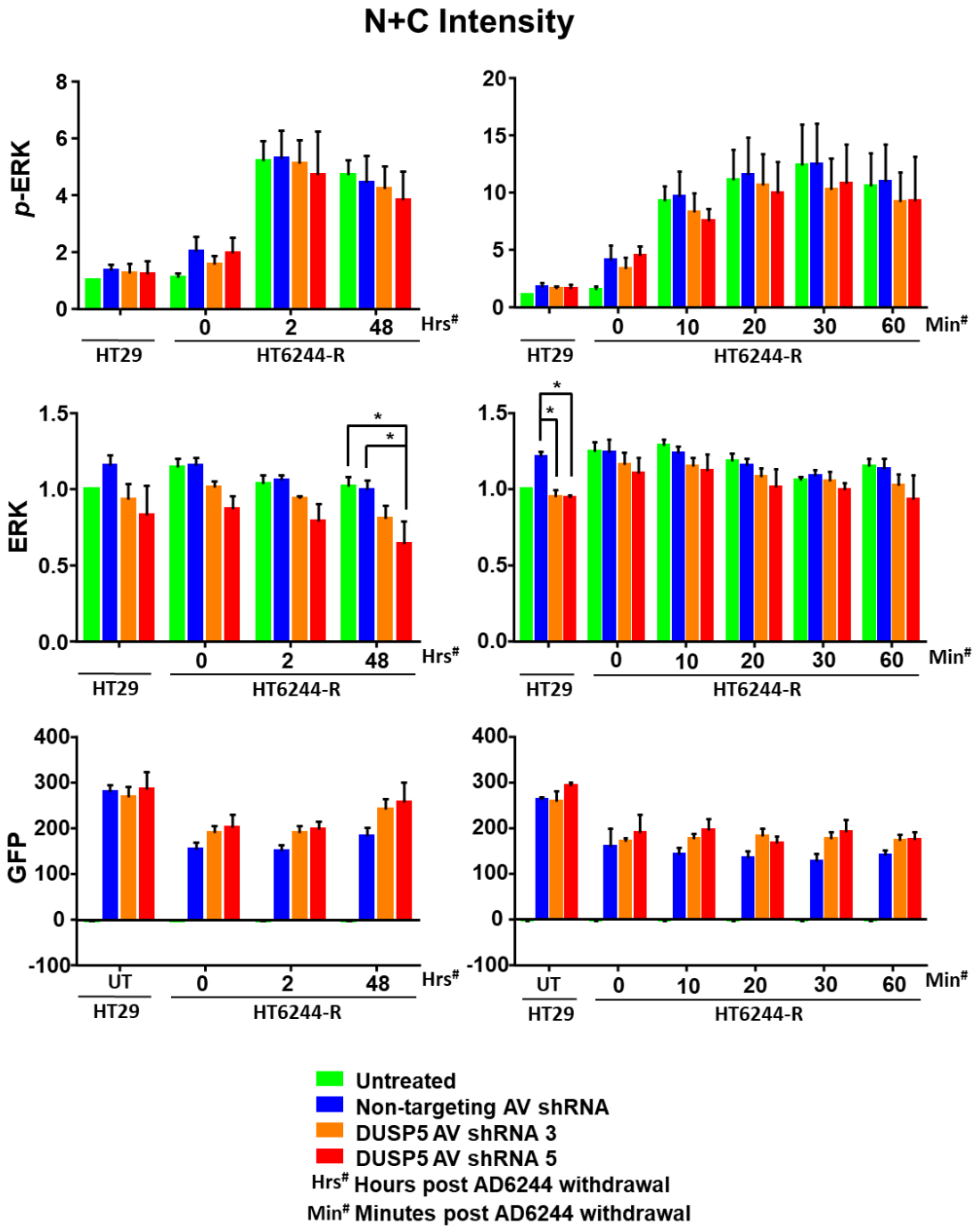

Figure 5.5, top right). This was consistent with western blot results dillustrated in Figure 3.11 (Chapter 3) for HT29 and H6244-R cells as well as *p*-ERK profiles

seen in H6244-R cells (

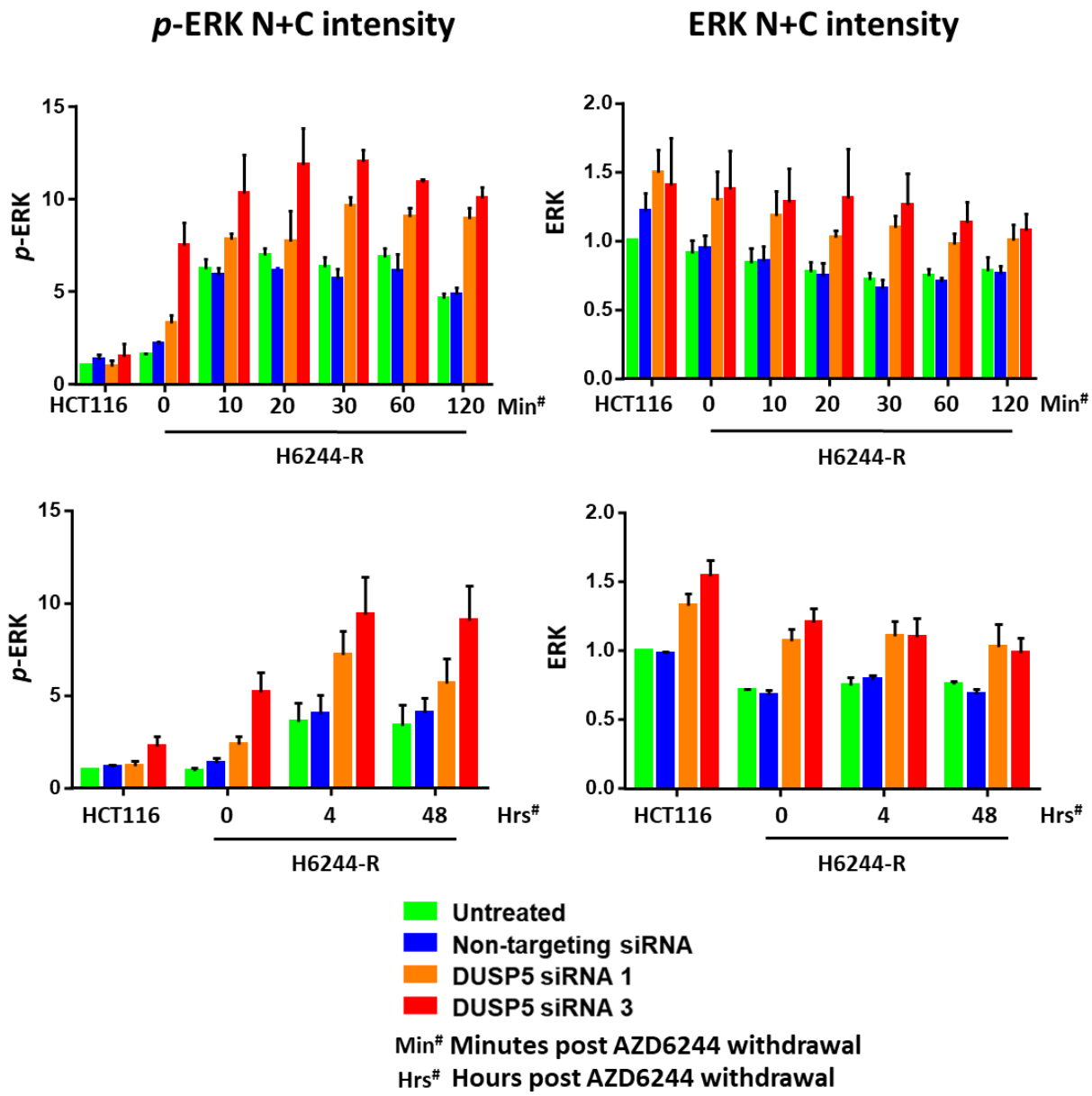

Figure 4.6, Chapter 4). In thes eexperiments, GFP levels were assessed in order to confirm that similar levels of adenovirus were present in transfected cells. While it may appear that non-targeting shRNA adenovirus-treated samples exhibited less GFP expression, there were no statisitically siginificant differences between any of these

samples (

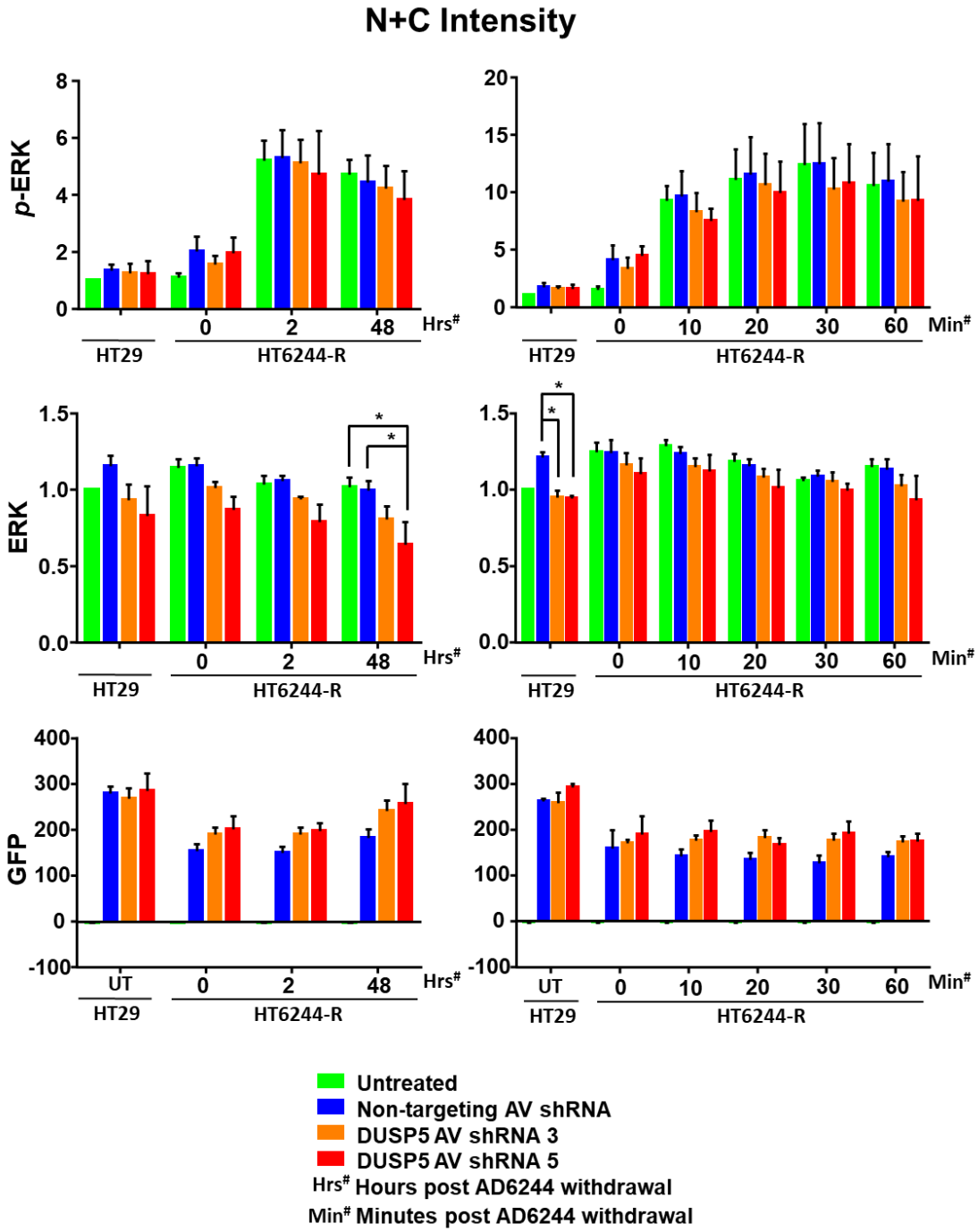

Figure 5.5, bottom image panel).

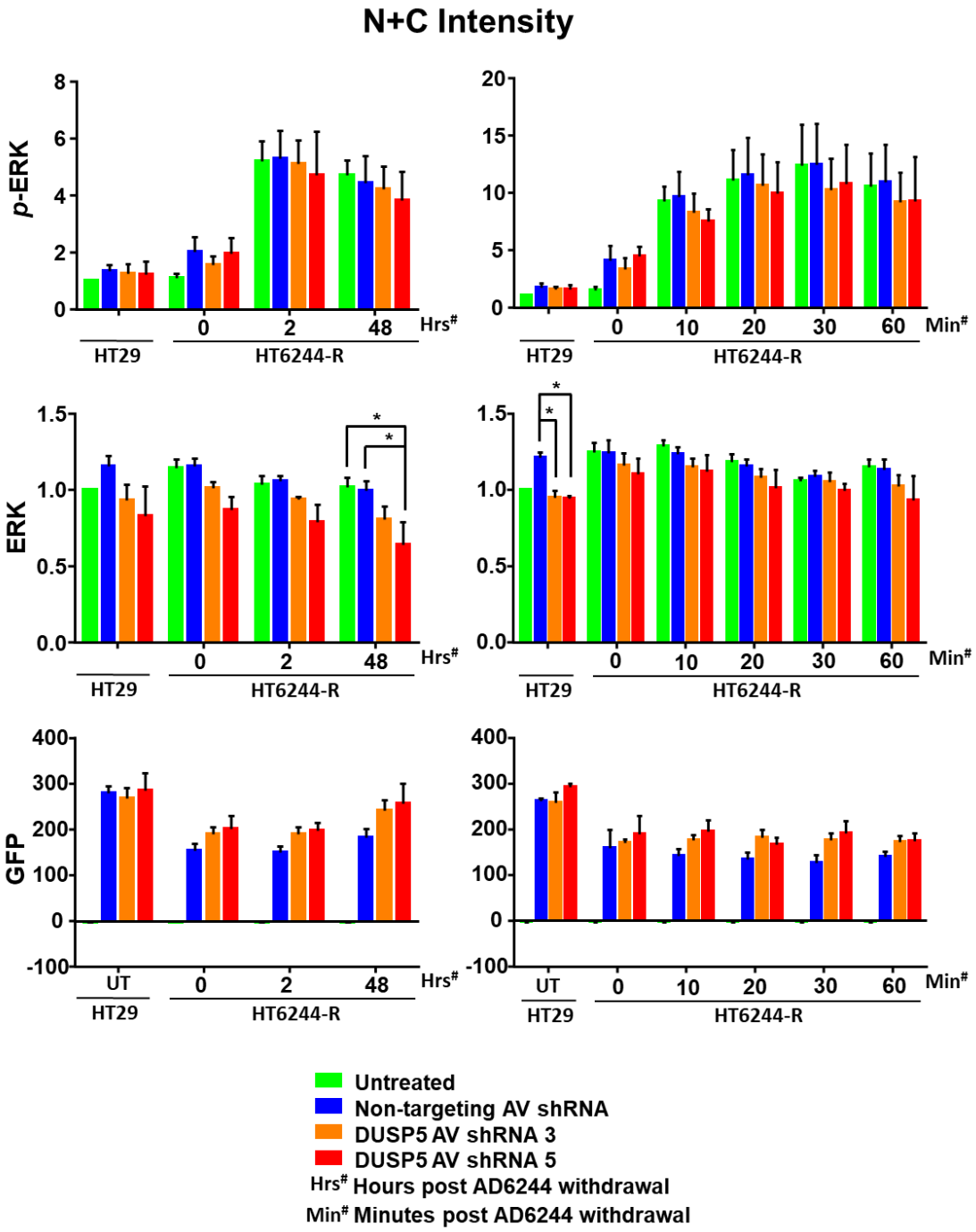

Figure 5.5 Transient adenoviral knockdown of DUSP5 in HT6244-R cells leads to reduced whole-cell levels of ERK. HT29 and HT6244-R control cells were incubated alongside HT6244-R cells treated with VectorBuilder DUSP5-targeting shRNA adenovirus (AV) 3, 5 or non-targeting shRNA adenovirus hours 18 prior to AZD6244 treatment. Cells were maintained in indicated concentrations of AZD6244 for varying time periods prior to fixation and immunostaining. n=3 biological replicates, ± SEM. Statistical analysis performed using a One-way ANOVA and a post-hoc Tukey analysis, where (*) denotes a p-value less than 0.05.

A comparison of relative *p*-ERK protein levels in DUSP5 knockdown conditions versus control conditions in HT29 and HT6244-R cells revealed no significant differences in these measures (

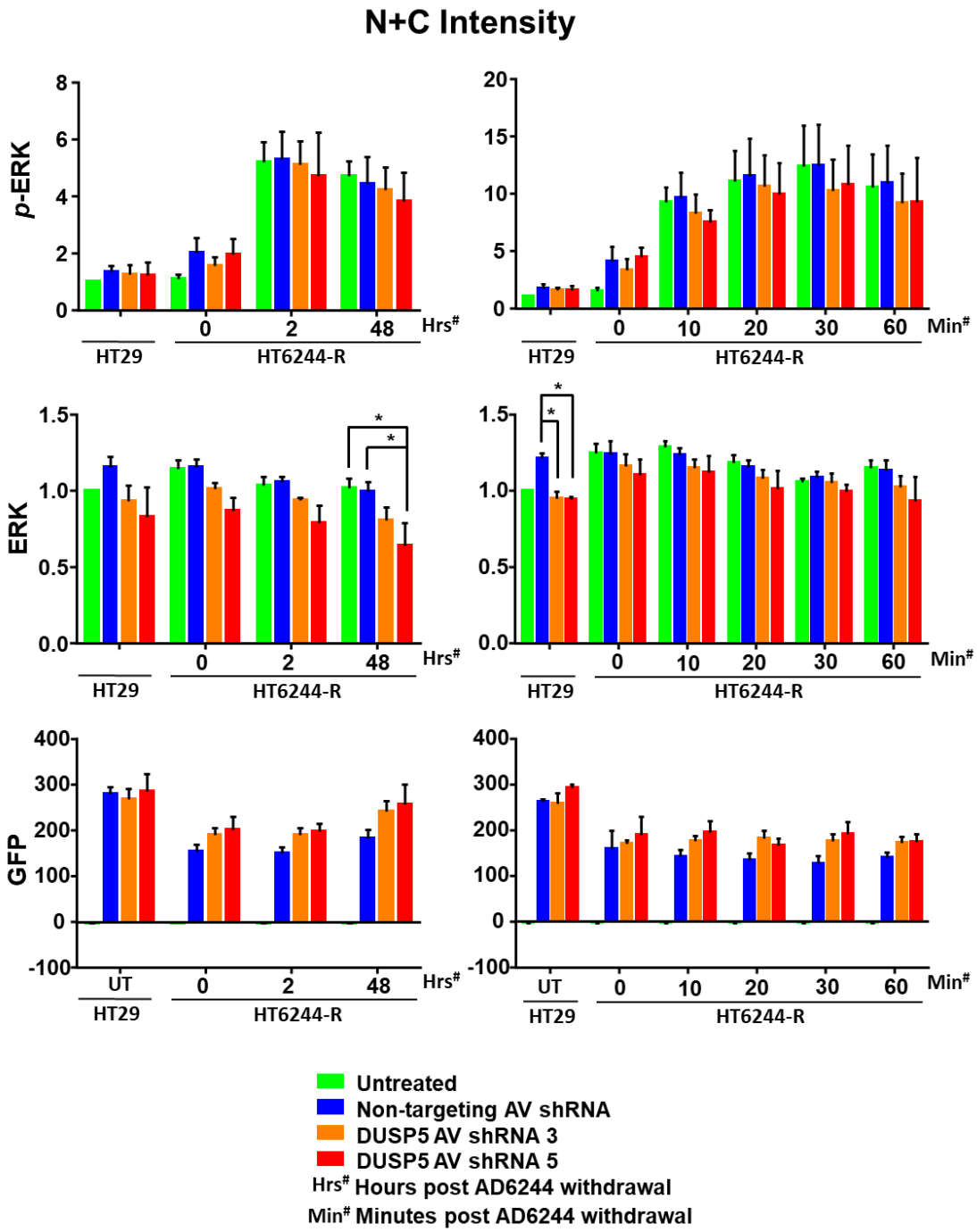

Figure 5.5 top image panel). These results contrasted the marked increase in *p*-ERK seen in HCT116 and H6244-R cells with reduced DUSP5 expression compared to

controls (

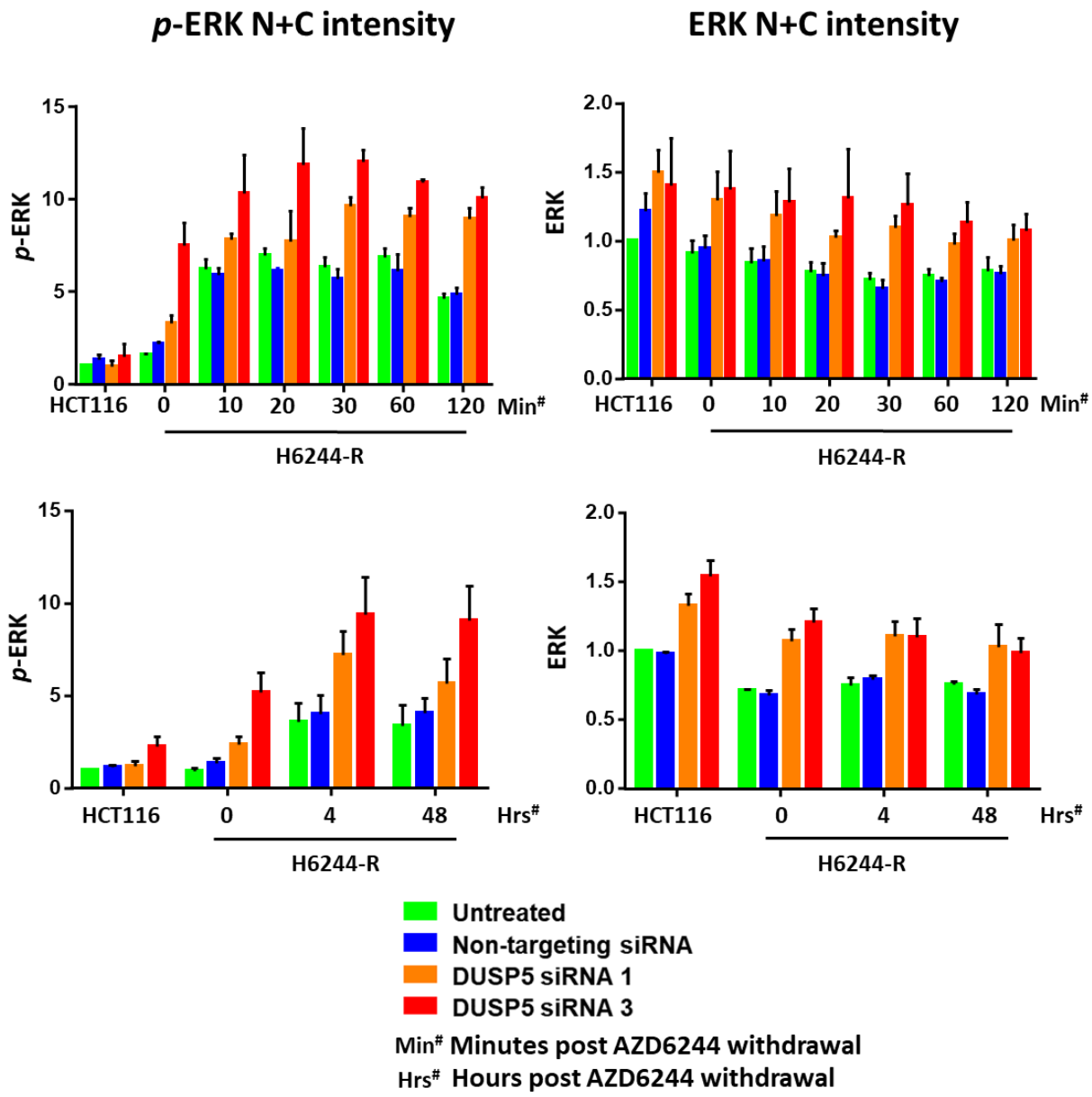
p-ERK N+C intensity
ERK N+C intensity
p-ERK
ERK
HCT116
0
10
20
30
60
120
Min#
H6244-R
4
48
Hrs#
Untreated
Non-targeting siRNA
DUSP5 siRNA 1
DUSP5 siRNA 3
Min# Minutes post AZD6244 withdrawal
Hrs# Hours post AZD6244 withdrawal

Figure 4.6, Chapter 4). Results summarised in

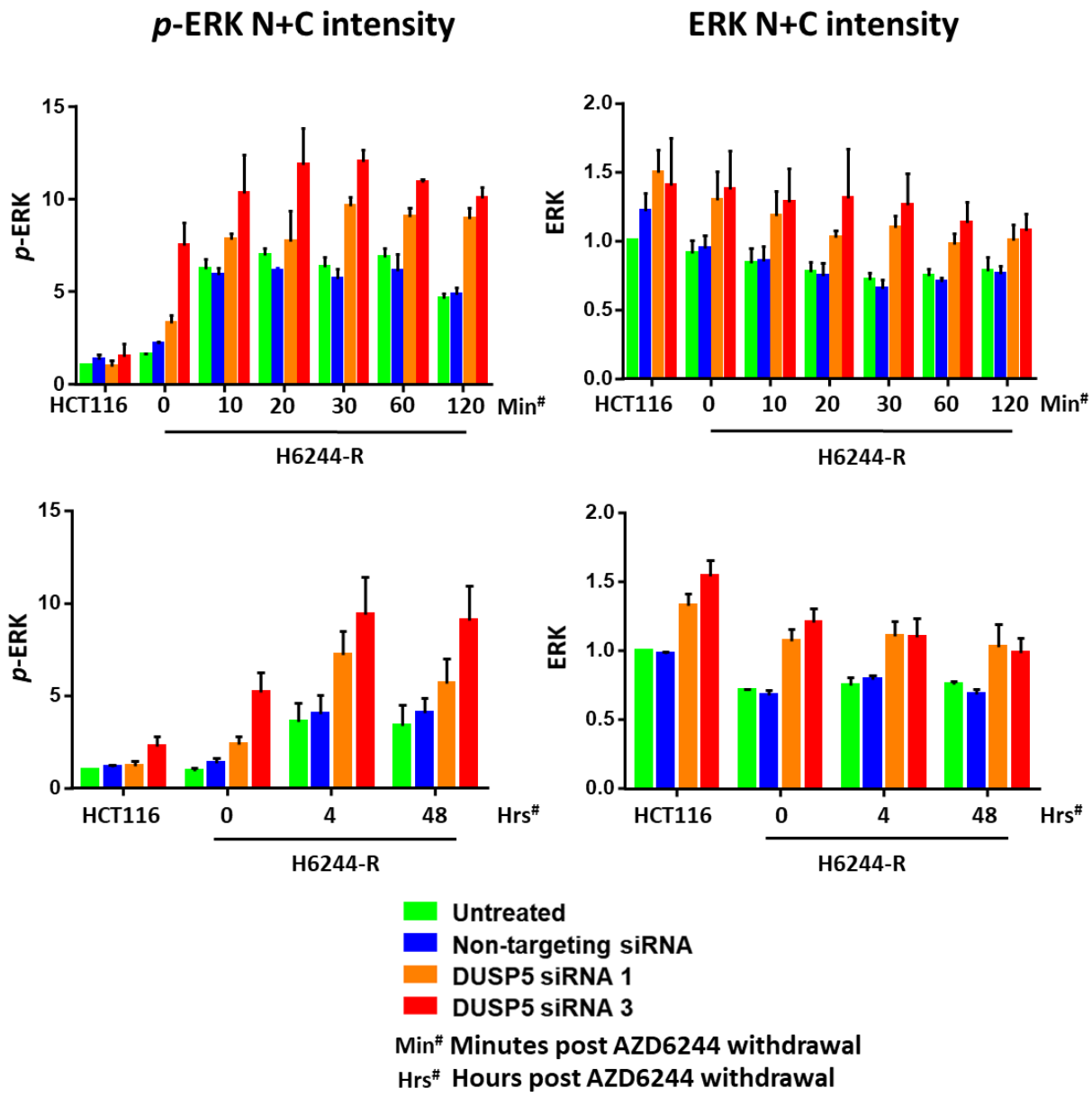

Figure 4.6 also demonstrated an increase in ERK protein levels coincident with DUSP5 knockdown, however this may have been an artefact of the immunofluorescenct-staining protocol. Contrary to this, ERK levels in HT29 and

HT6244-R cells appeared to be slightly reduced in DUSP5 knockdown conditions (

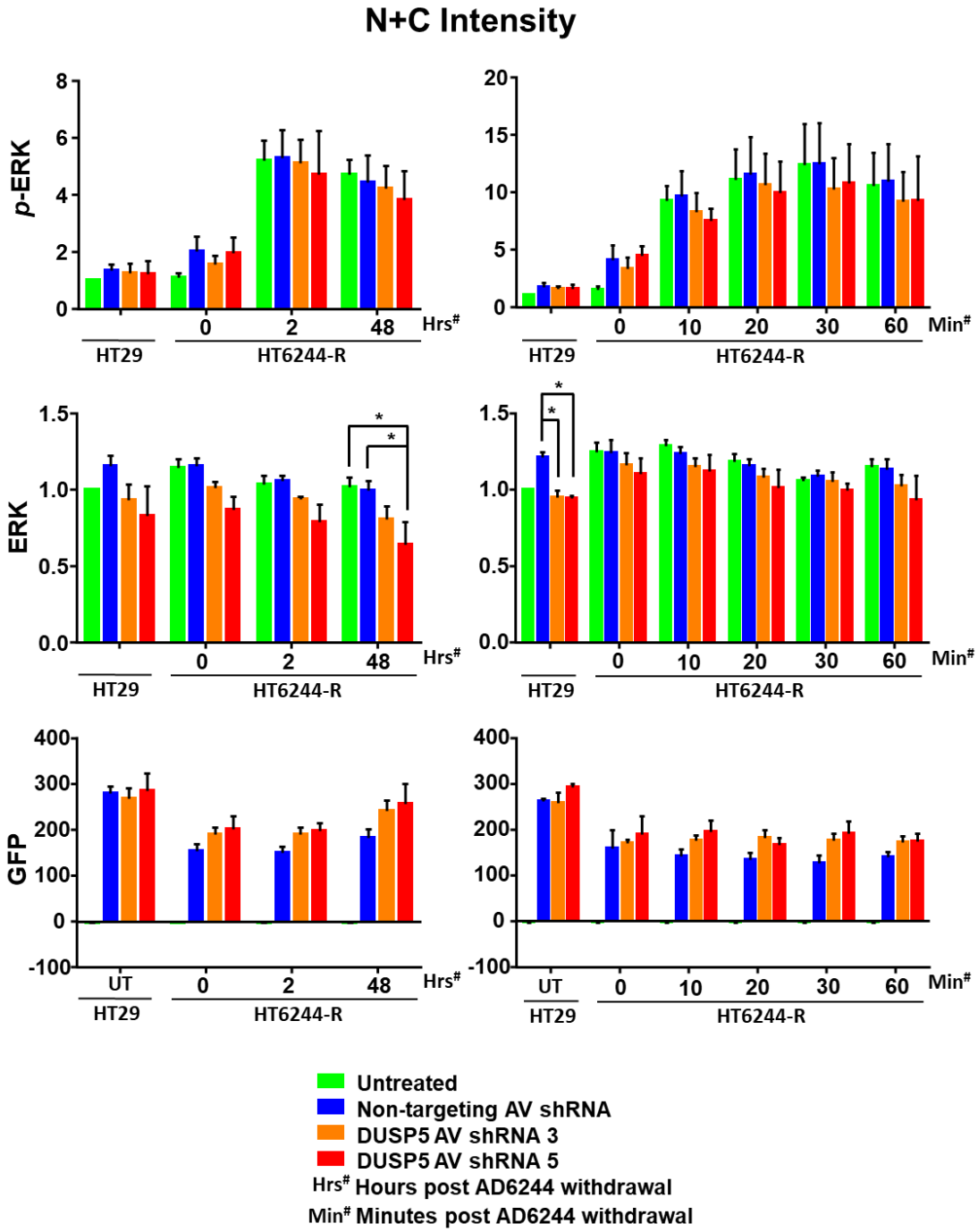

Figure 5.5, middle image panel). This reduction was most noticeable 48 hours after the removal of AZD6244, where ERK levels detected in samples transfected with DUSP5-targeting shRNA 5 adenovirus were significantly different to those transfected

with non-targeting shRNA adenovirus or untreated H6244-R cells (

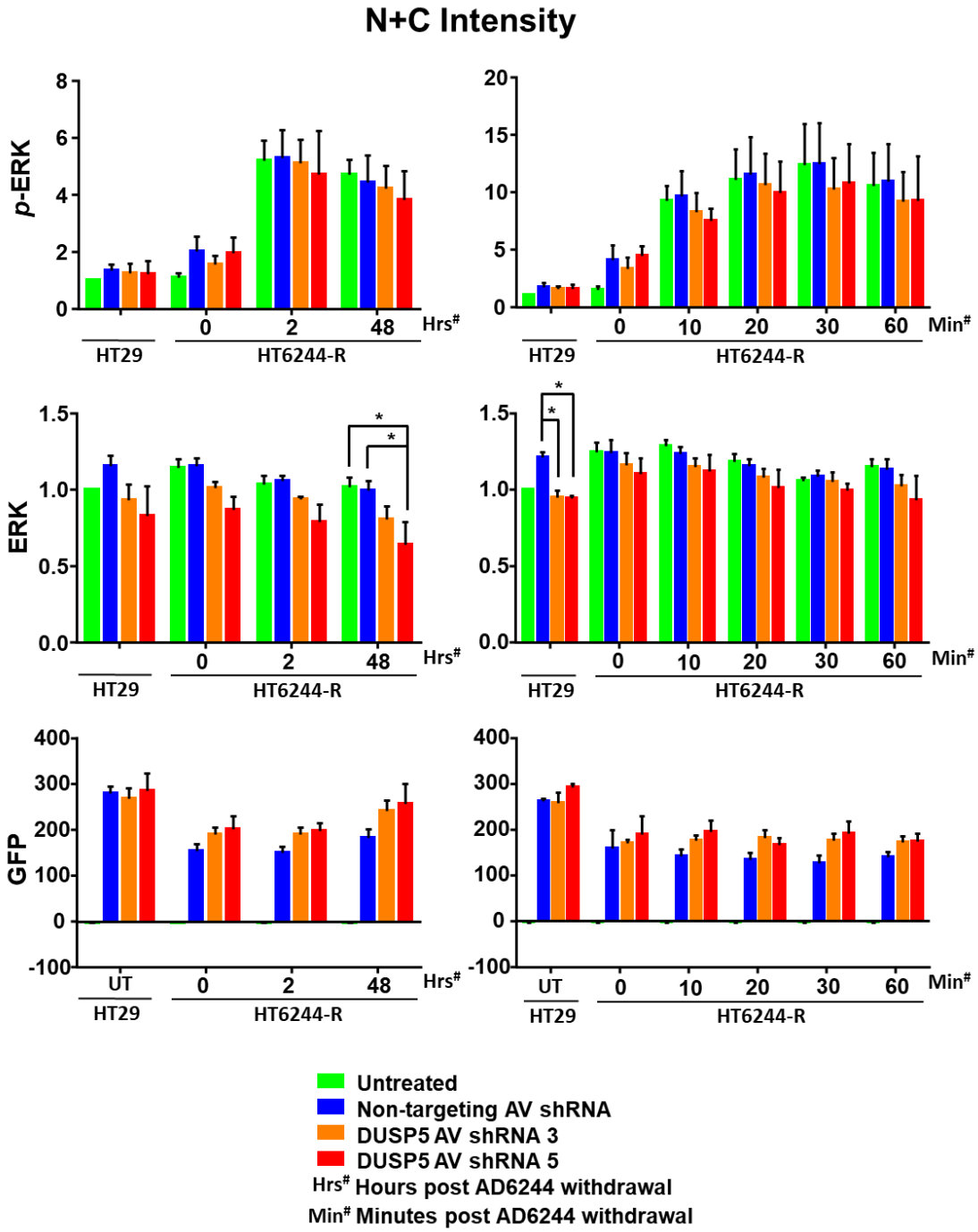

Figure 5.5, middle left). This was consistent with subtle decreases in total ERK visible in western blot images in samples exposed to the same conditions (DUSP5-targeting shRNA 5 adenovirus and 48 hour AZD6244 withdrawal). These results also showed a statistically significant increase in ERK levels between HT29 cells treated with DUSP5-targeting shRNA adenovirus 3 and 5 and HT29 cells treated with non-targeting shRNA

adenovirus, but not untreated HT29 cells (

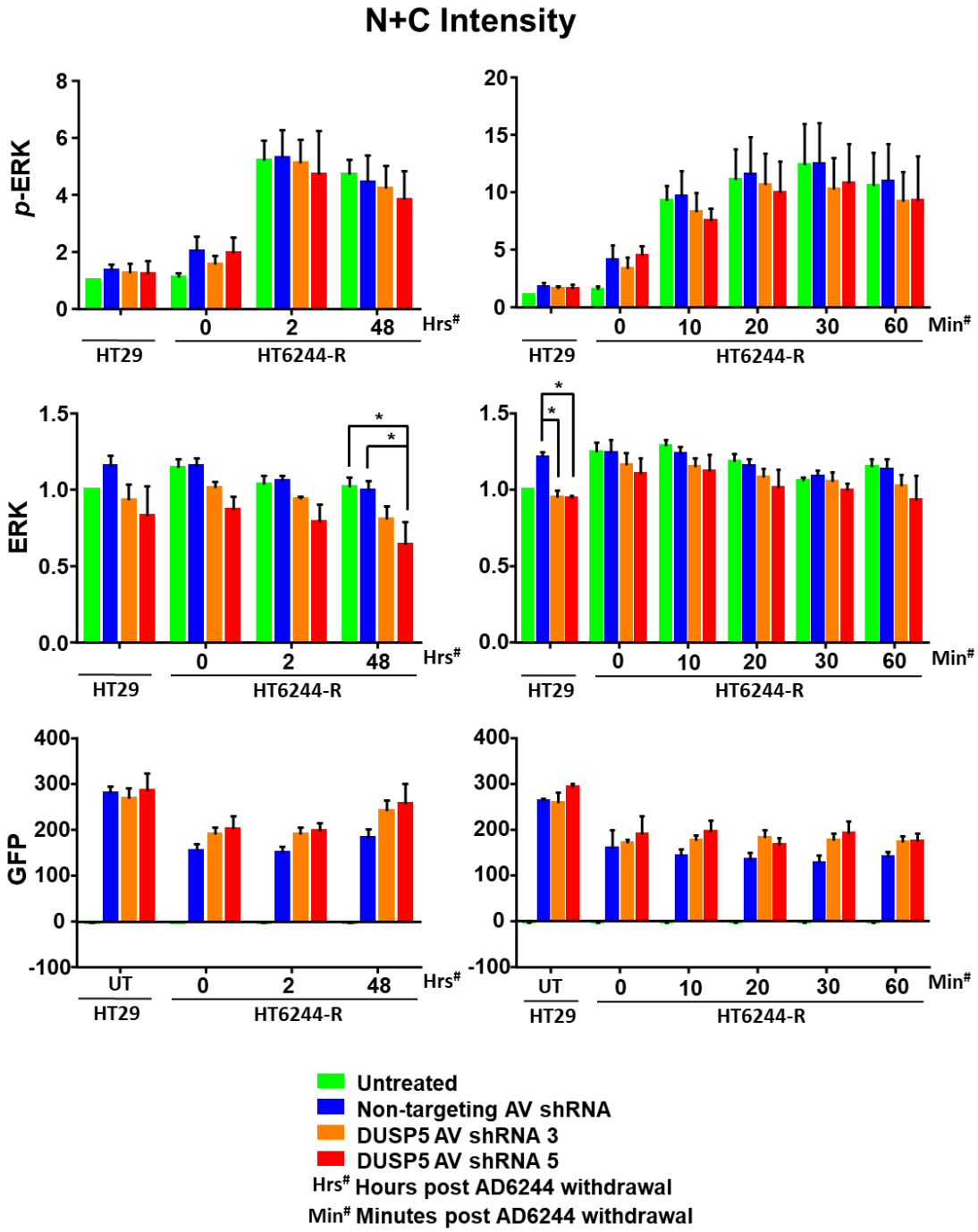

Figure 5.5, middle left). It is unclear why ERK levels seen in HT29 cells treated with non-targeting shRNA were not consistent with those in untreated HT29 samples. This discrepancy was not present in any other conditions, where these control samples generally showed similar results.

Analysis of the nuclear to cytoplasmic (N:C) ratio of *p*-ERK (N:C intensity

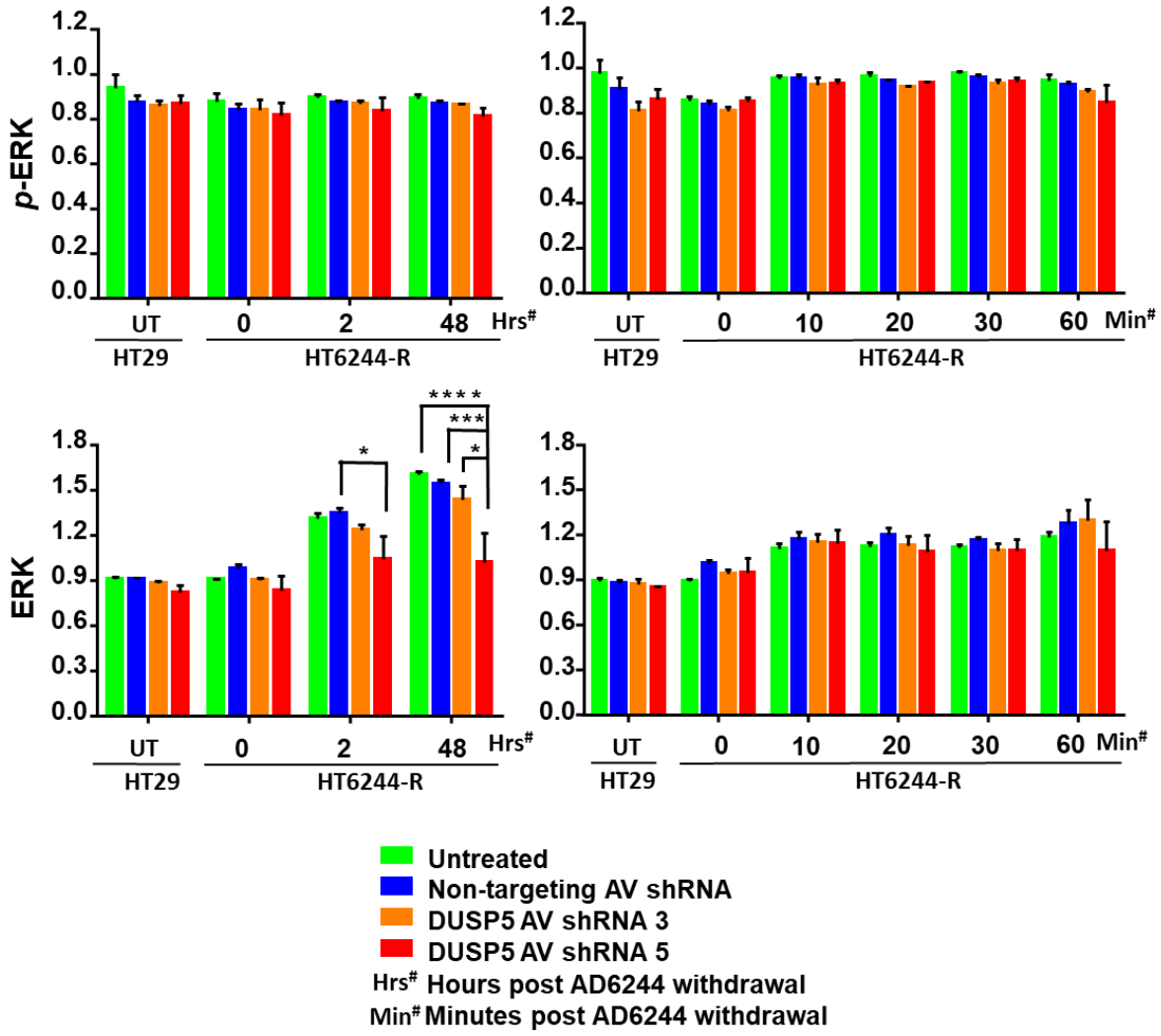

Figure 5.6**, top image panel) demonstrated a slight increase in the amount of *p*-ERK in the nucleus relative to the cytoplasm in H6244-R cells cultured in AZD6244-free conditions compared to H6244-R cells cultured in 1 μM AZD6244, between 10 and 60 minutes post-AZD6244 withdrawal. In all other conditions the N:C ratio of *p*-ERK appeared relatively consistent, falling between 0.8 and 1. This was similar to findings in H6244-R cells (Figure 4.7, Chapter 4). No noticable differences in this ratio between control HT29 and H6244-R cells and those**

treated with DUSP5-targeting shRNA adenovirus could be seen (

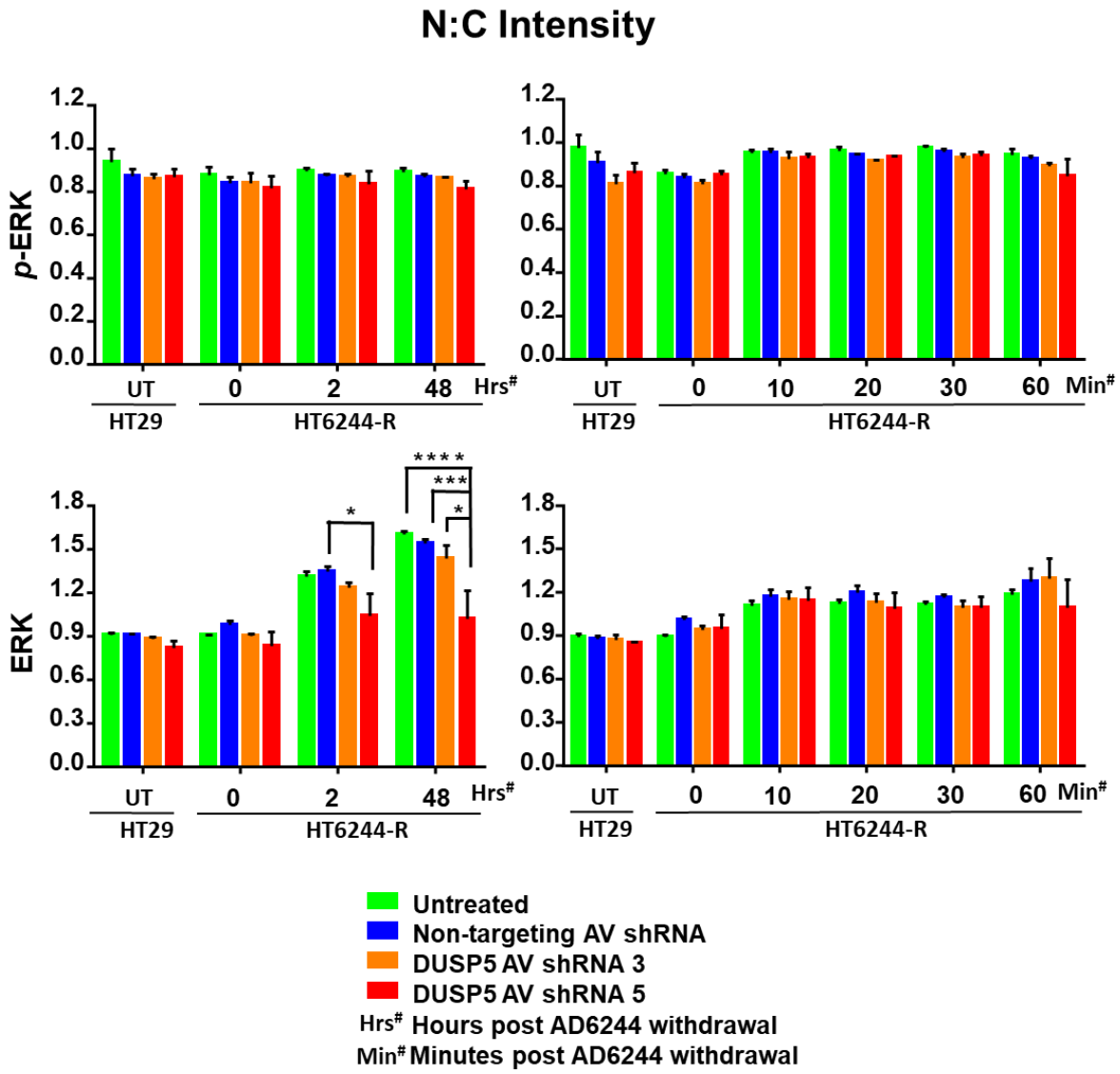

Figure **5**.**6**, top image panel).

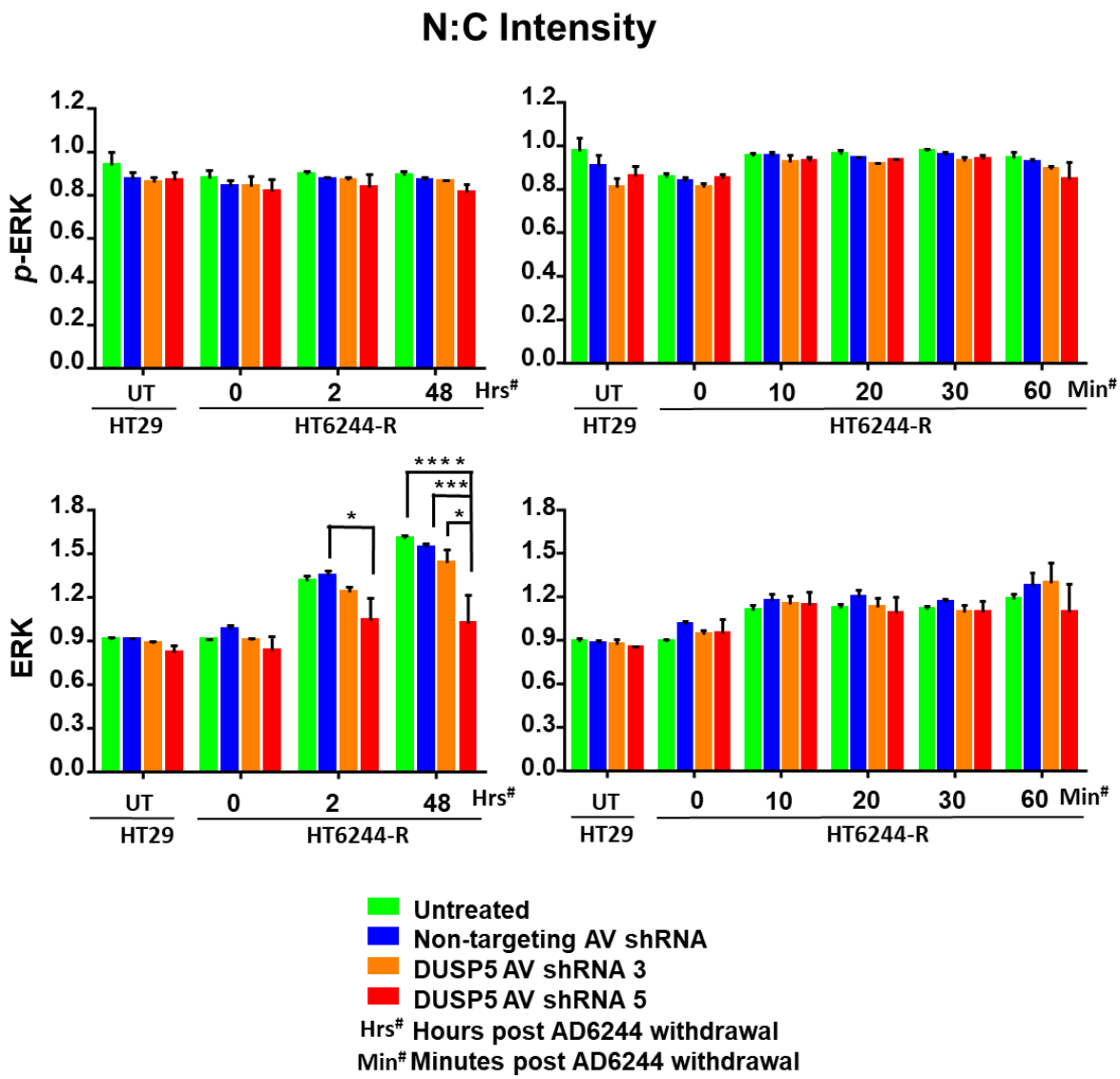

Figure 5.6 **Transient adenoviral knockdown of DUSP5 in HT6244-R cells leads to reduced nuclear accumulation of ERK.** HT29 and HT6244-R control cells were incubated alongside HT6244-R cells treated with VectorBuilder DUSP5-targeting shRNA adenovirus (AV) 3, 5 or non-targeting shRNA adenovirus hours 18 prior to AZD6244 treatment. Cells were maintained in indicated concentrations of AZD6244 for varying time periods prior to fixation and immunostaining. n=3 biological replicates, ± SEM. Statistical analysis performed using a One-way ANOVA and a post-hoc Tukey analysis, where (*) denotes a p-value less than 0.05, (**) denotes a p-value less than 0.01, (***) denotes a p-value less than 0.001 and (****) denotes a p-value less than 0.0001.

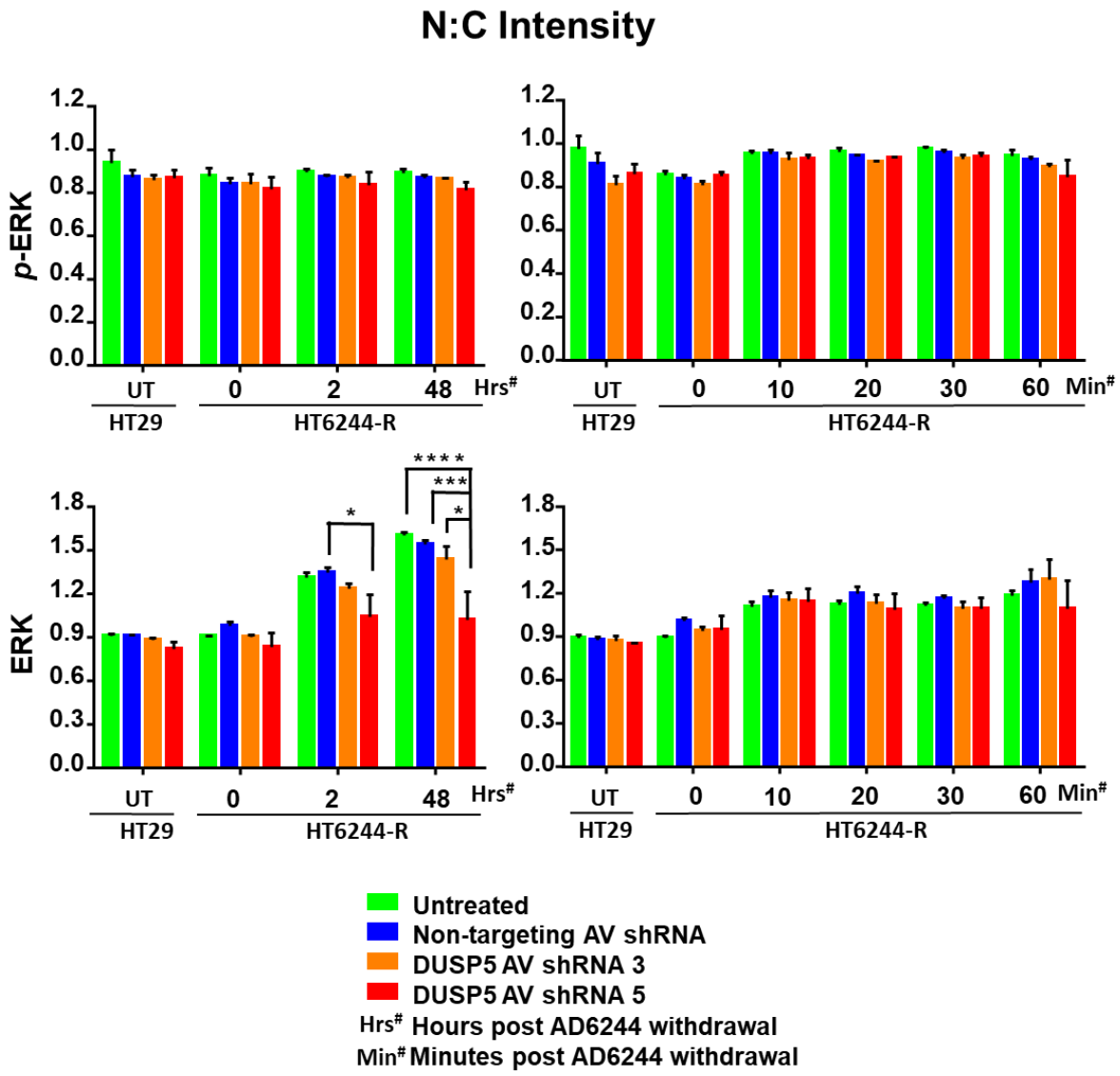

Figure 5.6 **(middle image panel) illustrates that the removal of AZD6244 from control HT6244-R cells was coincident with the nuclear accumulation of ERK. This was similar to findings for H6244-R cells (Figure 4.7, Chapter 4). Interestingly, the N:C ratio of ERK in HT6244-R cells treated with DUSP5-targeting shRNA 5 adenovirus was significantly lower than the N:C ratios of ERK in control HT6244-R cells, and HT6244-R cells treated with DUSP5-targeting**

shRNA 3 adenovirus after 48 hours of AZD6244 withdrawal (

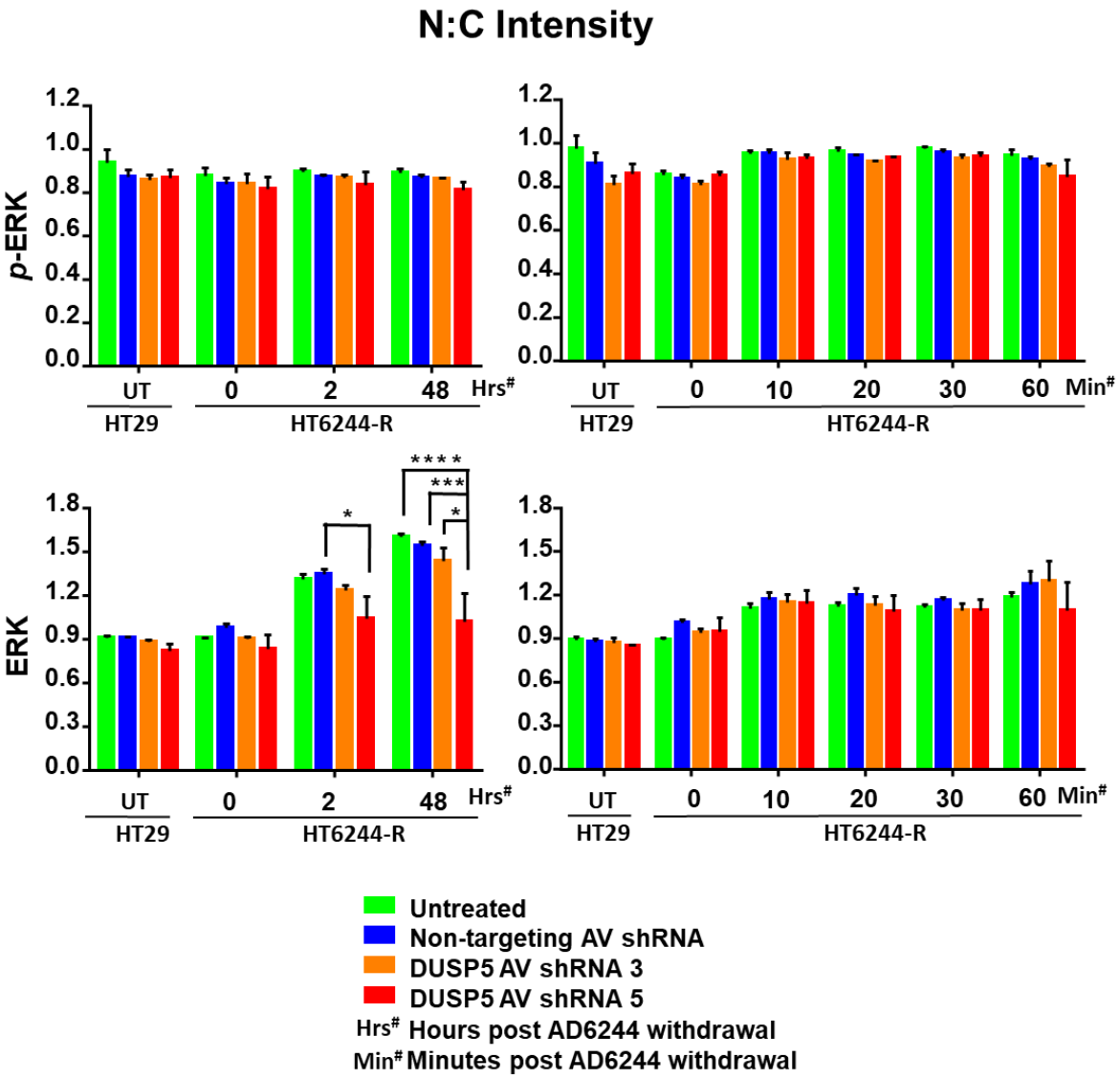

Figure **5**.**6**, middle left). This was indicative of reduced nuclear accumulation of ERK in these cells, similar to results seen in DUSP5 knockdown conditions in H6244-R cells (Figure 4.7, Chapter 4). However, in both H6244-R and HT6244-R cells, reduced nuclear acccumulation of ERK was seen in one but not both DUSP5 knockdown conditions.

While subtle changes in the spatiotemporal regulation of ERK were coincident with DUSP5 knockdown 48 hours after AZD6244 had been removed, no major changes in ERK activation or downstream ERK targets appeared to be linked to the reduction of DUSP5 protein in HT29 and HT6244-R cells. Inconsistencies seen in the effects on

the magnitude and cellular location of ERK between two DUSP5-targeting shRNA adenoviruses raised the question of whether these effects were in fact “on-target”.

In order to explore whether subtle differences in ERK levels and N:C ratios were consistently associated with DUSP5 knockdown compared to controls, and whether these effects may influence downstream cell fate in HT6244-R cells, we chose to establish a different method of DUSP5 knockdown. Ideally, we wanted a system that would allow for long-term DUSP5 repression in order to assess whether this would affect the fate of HT6244-R cells that had been cultured in the absence of AZD6244 for prolonged periods (up to 12 days). Work by Sale *et al*. (2019) demonstrated that major effects of AZD6244 deprivation in HT6244-R cells were only evident after 3 to 6 days of drug withdrawal, when these cells began to die. We reasoned that it was possible that the effects of DUSP5 knockdown may also only be evident after prolonged drug withdrawal. As HT29/HT6244-R cells are not easily transfected through lipid-based means, using CRISPR/Cas9 constructs to knockout DUSP5 in these cells would be challenging. Instead, we chose to establish stable lentiviral HT6244-R cell lines that were able to express DUSP5 shRNA upon induction.

5.3.2. Optimising DUSP5 knockdown in inducible shRNA lentiviral HT6244-R cell lines

HT6244-R cell lines that were able to express non-targeting shRNA or one of two DUSP5-targeting shRNAs were established as described in Chapter 2. During puromycin selection of these cell lines, an untransfected HT6244-R control culture was seeded alongside the lentiviral HT6244-R cell lines and selection was completed once all cells in this culture had died. After selection, experiments were set up to assess the response of the shRNA-expressing HT6244-R cell lines to doxycycline. Through these experiments we hoped to detect any off-target effects of doxycycline on cell growth and general cell health (as assessed by visual inspection) as well as on *p*-ERK activation and DUSP5 expression.

Stable HT6244-R non-targeting shRNA, DUSP5-targeting shRNA 1 and DUSP5-targeting shRNA 3 cell lines were exposed to increasing levels of doxycycline for 24 hours. Whole-cell lysates were then harvested and subjected to western blot analysis

to assess DUSP5 knockdown efficiency as well as any effects on *p*-ERK. Visual observation of cells exposed to up to 1 ug.mL^{-1} doxycycline did not reveal any obvious signs of cellular stress. Immunoblot results from these experiments revealed that even at 1 ug.mL^{-1} doxycycline, only a partial reduction in DUSP5 expression could be seen. Additionally, increasing concentrations of doxycycline did not appear to affect protein levels of *p*-ERK (Figure 5.7). Although cells present in each HT6244-R shRNA cell population were presumed to have incorporated lentiviral DNA due to their apparent puromycin resistance, it is possible that multiple copies of DUSP5-targeting shRNA may have been necessary to confer robust DUSP5 knockdown. In order to increase this likelihood, we made use of the GFP marker present in the inducible lentiviral construct and used flow cytometry to sort out a sub-population of cells in each cell line that had relatively high levels of GFP fluorescence. Each HT6244-R shRNA cell population was incubated with 1 ug.mL^{-1} doxycycline for 24 hours prior to cell sorting. Cells within a relative range of mid to high levels of GFP were selected and cultured for further experimentation.

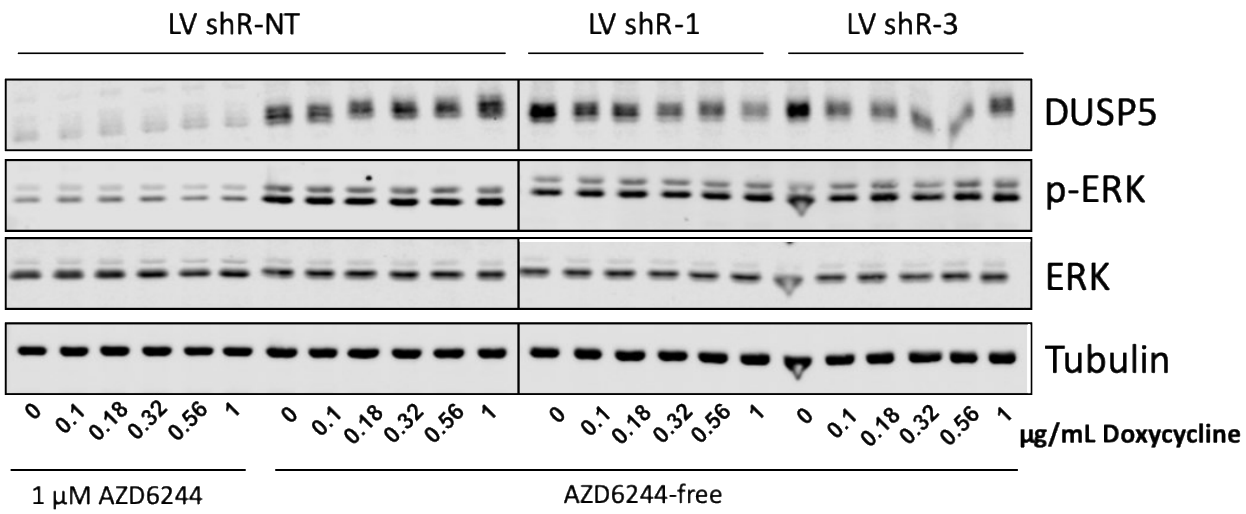

Figure 5.7 Assessing the effect of doxycycline dose escalation on p-ERK and DUSP5 protein levels. HT6244-R non-targeting shRNA, DUSP5-targeting shRNA 1 and DUSP5-targeting shRNA 3 cell lines were exposed to increasing levels of doxycycline for 24 hours. In "AZD6244-free" conditions, culture media was replaced with AZD6244-free media 2 hours prior to cell lysis. Cell lysates were fractioned by SDS-PAGE and western blotted with the indicated antibodies to assess relative protein levels. n = 1 biological repeat.

5.3.3. Stable integration and induction of doxycycline-inducible shRNA constructs in MEKi-resistant HT29 cells

Using mid to high GFP-expressing subpopulations of the original HT6244-R shRNA cell lines we investigated whether robust DUSP5 knockdown could be achieved using tolerable doses of doxycycline. We also investigated whether DUSP5 knockdown was coincident with any changes in *p*-ERK, ERK and downstream markers of ERK activation, $p21^{CIP1}$ and BIM. Figure 5.8 western blot images and quantification figures show improved DUSP5 knockdown, with 59% and 91% knockdown in HT6244-R shRNA 1 and 3 cell lines, respectively, 2 hours after AZD6244 removal. DUSP5 knockdown was increased 48 hours after drug withdrawal with 73% and 92% knockdown in HT6244-R shRNA 1 and 3 cell lines, respectively (Figure 5.8b). However, despite improved DUSP5 knockdown, no obvious changes in *p*-ERK, ERK, BIM and $p21^{CIP1}$ could be seen relative to controls within 48 hours of AZD6244 withdrawal (Figure 5.8 and Appendix Figure A7).

A

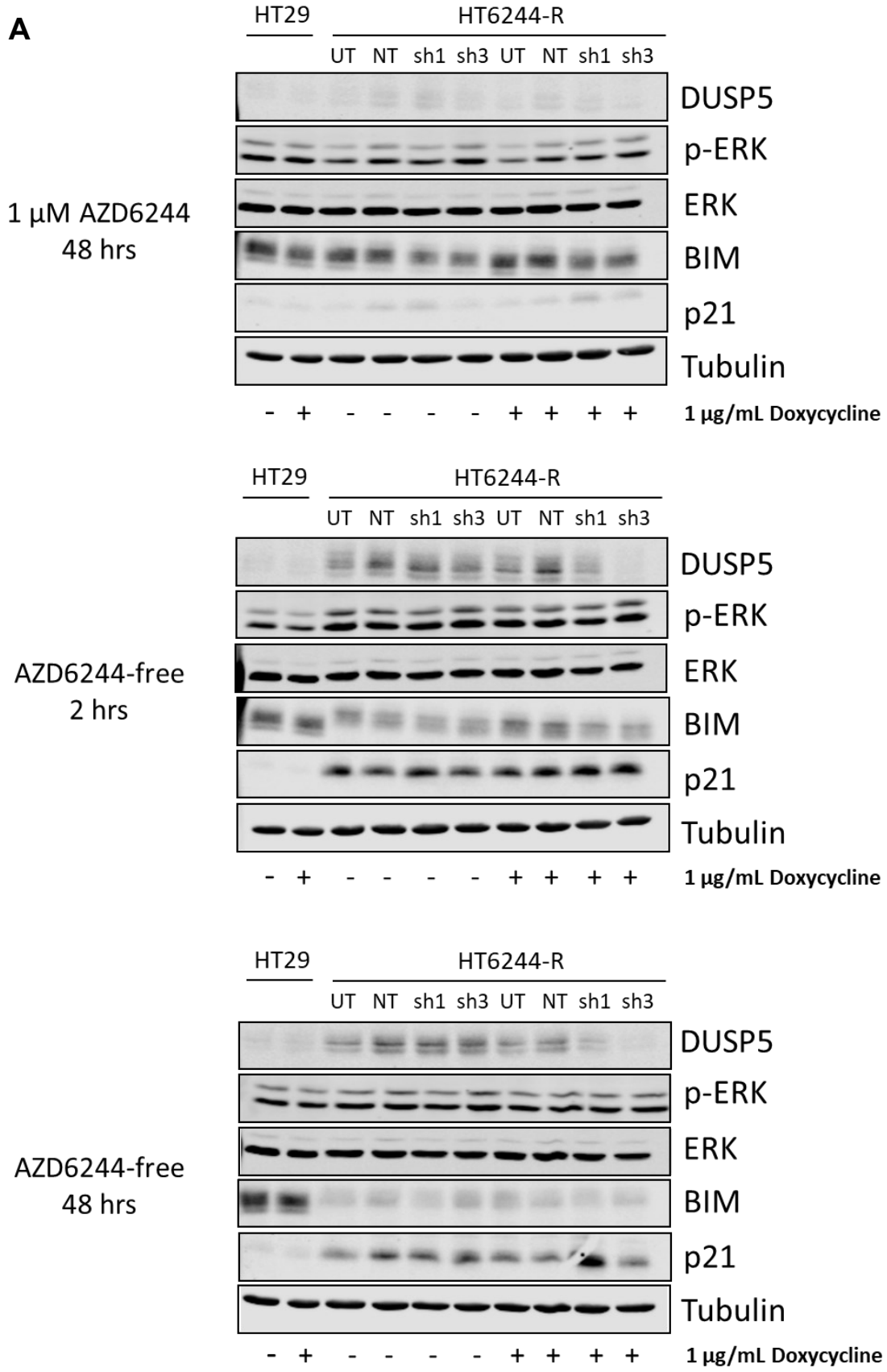
HT29
HT6244-R
UT NT sh1 sh3 UT NT sh1 sh3
DUSP5
p-ERK
ERK
BIM
p21
Tubulin
- + - - - - + + + +
1 µg/mL Doxycycline
1 µM AZD6244
48 hrs
AZD6244-free
2 hrs
AZD6244-free
48 hrs

B

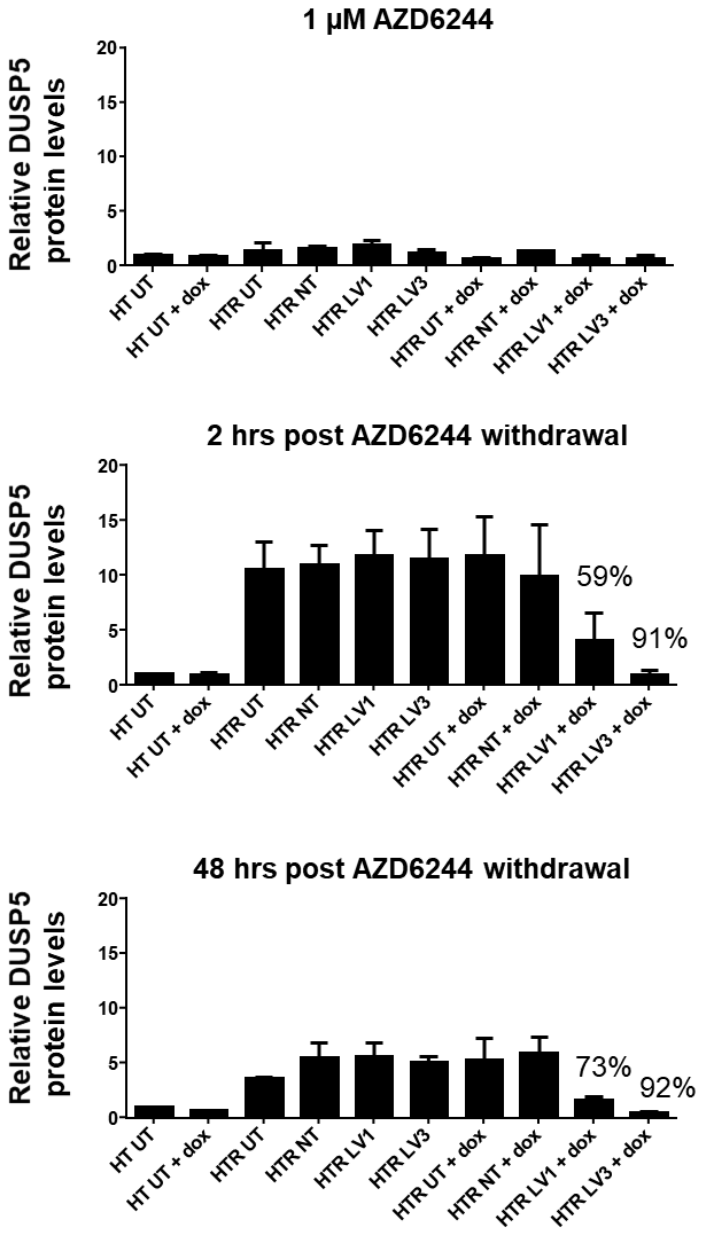

Figure 5.8 HT6244-R DUSP5-targeting shRNA 1 and 3 cell lines show markedly reduced DUSP5 levels upon doxycycline induction. HT6244-R shRNA cell lines were incubated with 1 μg.mL^{-1} doxycycline for 48 hours. Culture media was replaced with AZD6244-free media (containing doxycycline) 2 or 48 hours prior to cell lysis in appropriate conditions. Cells lysates were fractioned by SDS-PAGE and western blotted with the indicated antibodies to assess relative protein levels. A) Western blot images. Images are representative of results from 3 separate experiments. B) Quantification results. Relative intensities of protein bands were quantified using Liquor's Image Studio Lite software. Percentage DUSP5 knockdown relative to the non-targeting shRNA control shown. n=3 biological replicates, ± SEM.

Alongside western blot experiments, we performed experiments with similar conditions for high content microscopy analysis to investigate whether subtle changes in ERK protein levels and cellular location seen in adenoviral experiments were replicated in this model. Like results seen in previous H6244-R HCM experiments (

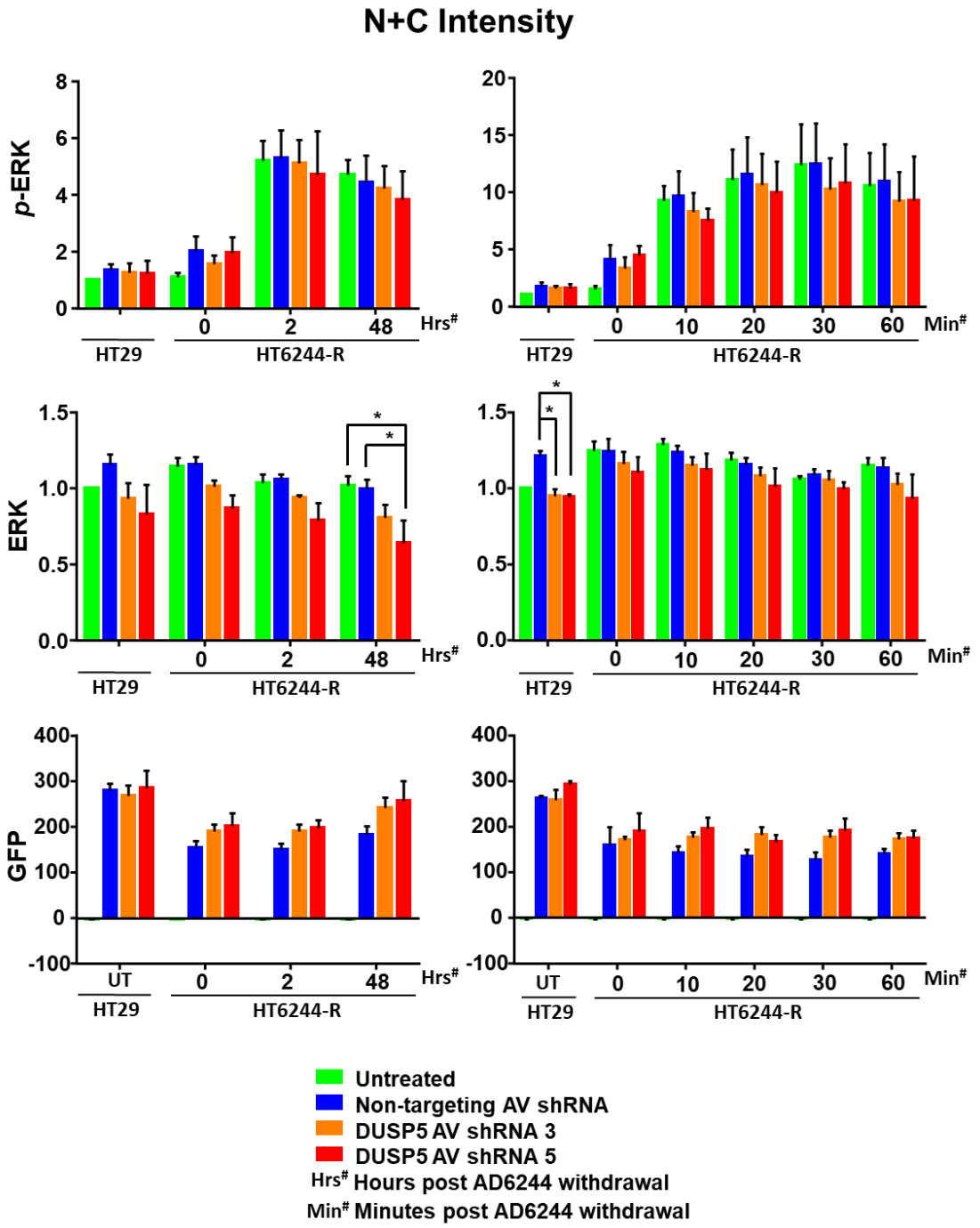

Figure 5.5 and

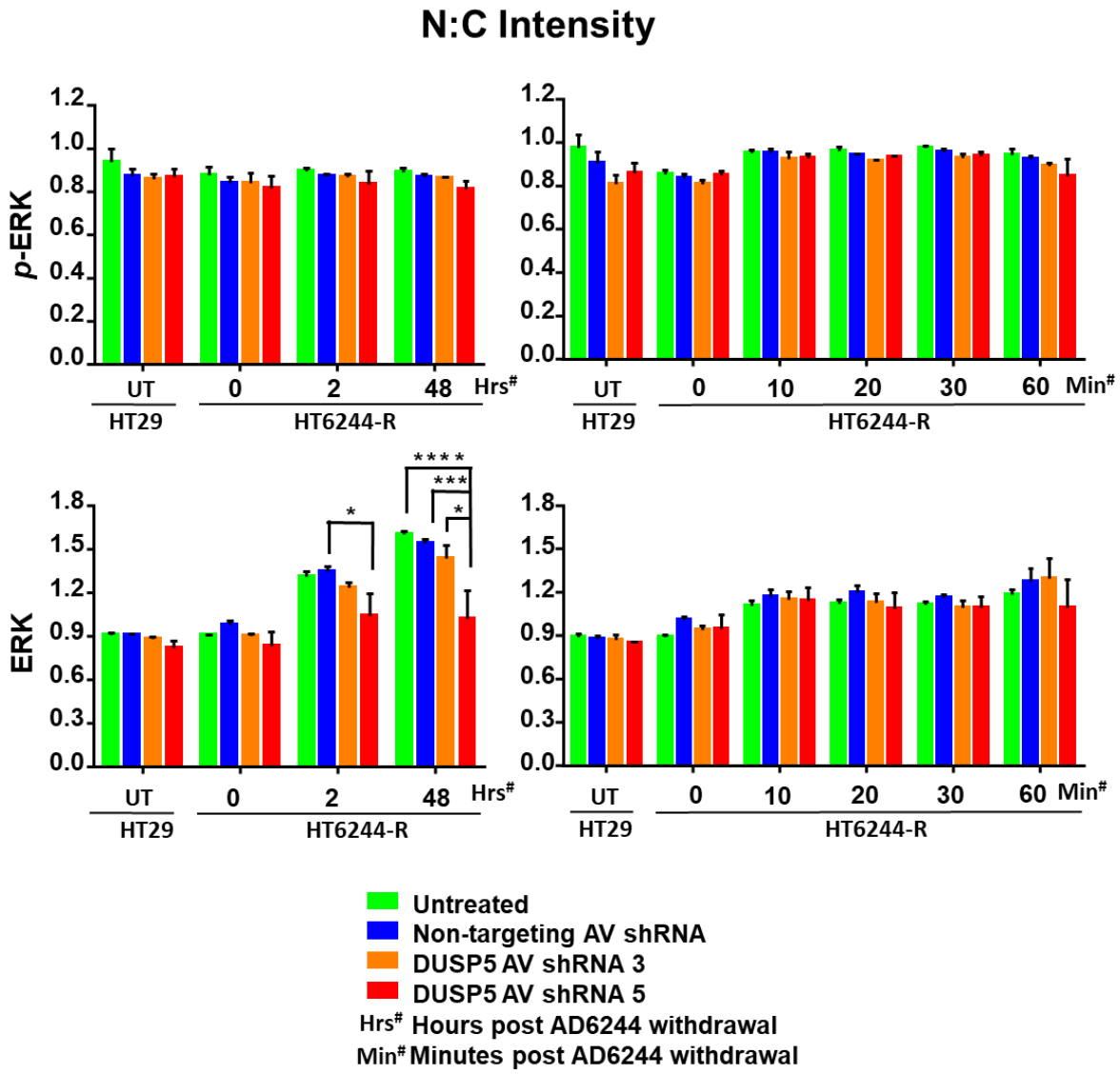

Figure **5**.**6**), control HT6244-R cells showed a similar spatiotemporal response to AZD6244 removal as H6244-R cells, albeit with higher levels of variability. Also similar to results in adenoviral DUSP5 knockdown experiments, DUSP5 knockdown induced by doxycycline addition did not appear to have any marked effect on *p*-ERK in a 48-hour time course experiment (Figure 5.9, top left). Additionally, while reduced ERK levels were coincident with one of two DUSP5-targeting shRNAs (shRNA 3) relative to controls (Figure 5.9, middle left), this trend was seen both in the presence and absence of doxycycline and was therefore unlikely a result of DUSP5 knockdown.

In shorter time course experiments, both *p*-ERK and ERK protein levels appeared slightly decreased relative to untreated and non-targeting shRNA control HT6244-R

cell lines in the absence of doxycycline (i.e. with normal DUSP5 expression) (Figure 5.9, top and middle right). However, in doxycycline-induced DUSP5 knockdown conditions *p*-ERK and ERK levels were increased relative to unstimulated conditions, but not to untreated and non-targeting shRNA HT6244-R control lines. This could indicate that in “normal” conditions, manipulation of these cells had somehow led to off-target effects on ERK and *p*-ERK levels resulting in slightly reduced basal levels of these proteins. These levels then became increased relative to basal levels upon DUSP5 knockdown. In saying that, the trends described here were not statistically significant and variability in this data effectively excluded the possibility of any clear or reliable data interpretations.

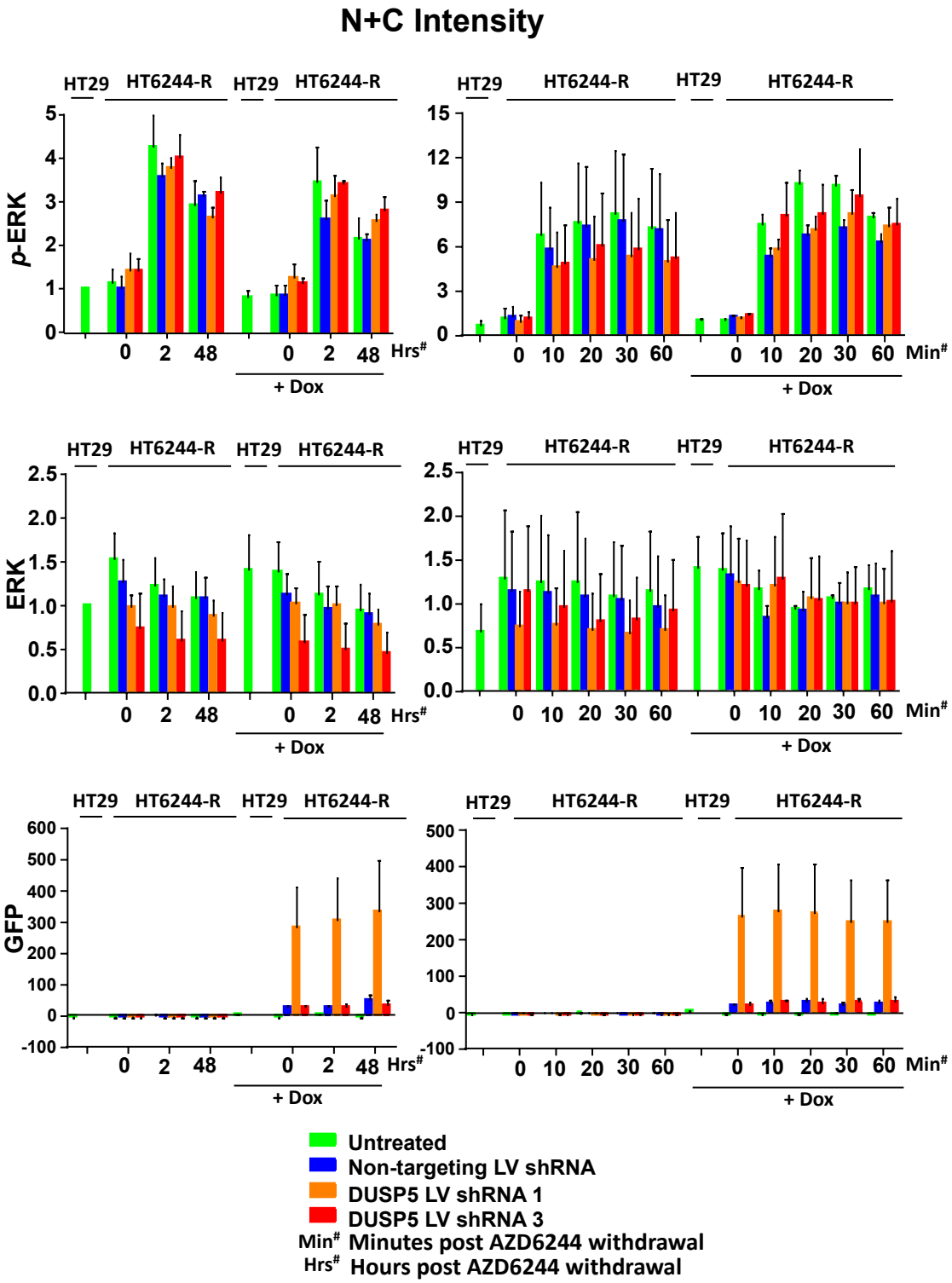

Figure 5.9 Transient knockdown of DUSP5 leads to increased levels of p-ERK and ERK in DUSP5-targeting shRNA cell lines. HT6244-R shRNA cell lines were incubated with 1 μg.mL^{-1} doxycycline for 48 hours. Cells were maintained in indicated concentrations of AZD6244 for varying time periods prior to fixation and immunostaining. n=3 biological replicates, ± SEM.

Finally, these data revealed marked differences in GFP expression between HT6244-R shRNA cell lines, with HT6244-R shRNA 1 showing approximately 100 times greater GFP expression than the non-targeting shRNA and shRNA 3 HT6244-R cell lines (Figure 5.9, bottom image panel). While this did not appear to result in any obvious off-target differences between these cell lines, it was indicative of large variability in the range of GFP expressed in cells chosen by cell sorting and should have been controlled for.

The N:C ratios of *p*-ERK and ERK in HT6244-R shRNA cell line experiments were similar to those seen in previous experiments with HT6244-R and H6244-R cells. The N:C ratio of *p*-ERK in HT6244-R cells increaseed slightly within 10 minutes of AZD6244 removal, but was relatively consistent across all other conditions (Figure 5.10, top image panel). The ratio of nuclear to cytoplasmic ERK markedly increaseed with AZD6244 removal, suggesting a shift of ERK from the cytoplasm to the nucleus (Figure 5.10, middle image panel). These trends were consistent across all HT6244-R shRNA lines and doxycycline-induced DUSP5 repression was not coincident with any noticeable changes in N:C ratios of either *p*-ERK or ERK relative to the controls.

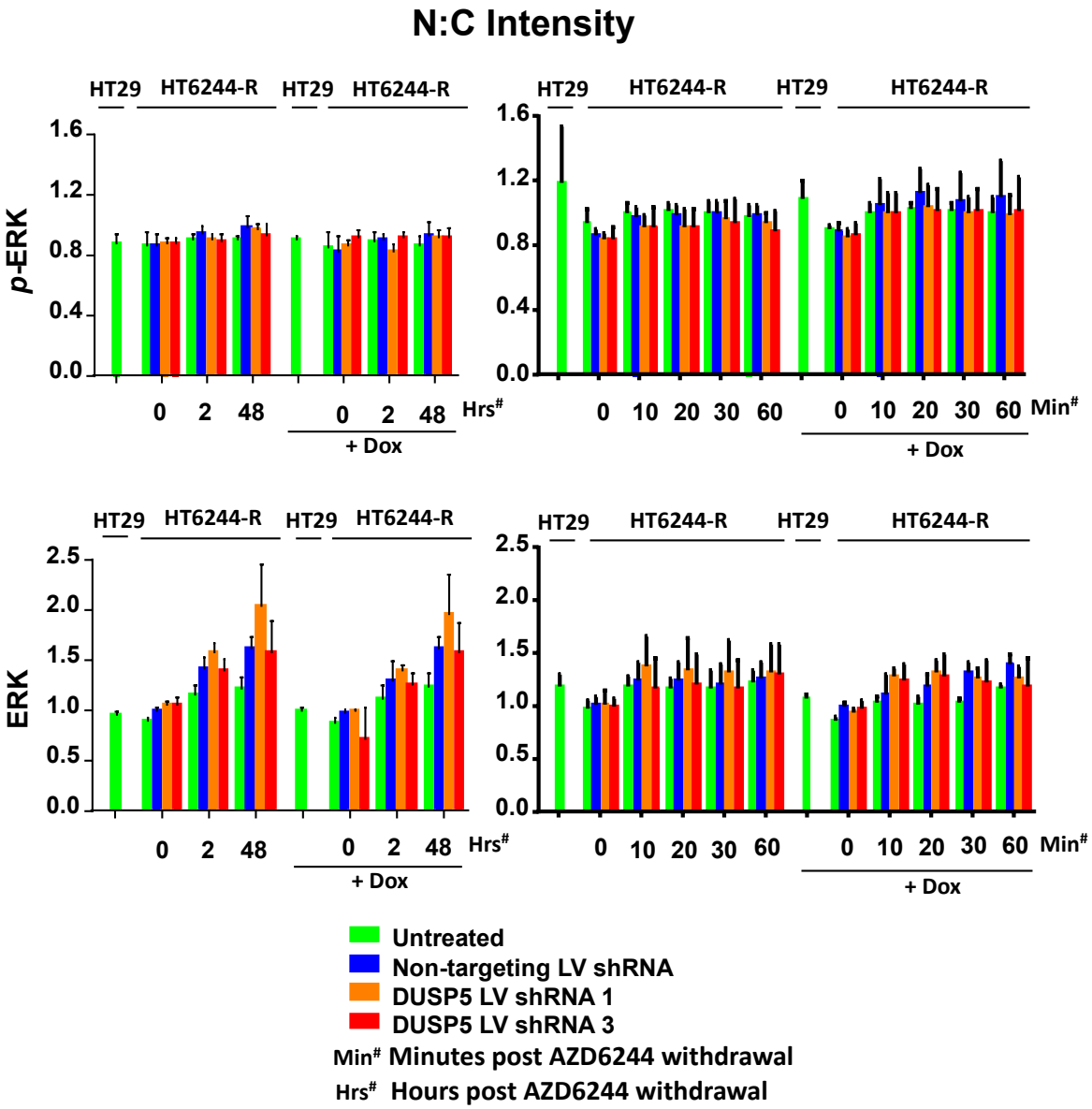

Figure 5.10 Transient knockdown of DUSP5 in HT6244-R cell lines does not affect N:C ratios of *p*-ERK and ERK in response to AZD6244. HT6244-R shRNA cell lines were incubated with 1 μg.mL^{-1} doxycycline for 48 hours. Cells were maintained in indicated concentrations of AZD6244 for varying time periods prior to fixation and immunostaining. n=3 biological replicates, ± SEM.

5.3.4. Sustained DUSP5 loss in MEKi-resistant HT29 cells is coincident with subtle changes in cellular responses to AZD6244 withdrawal

In parallel with experiments performed to assess the effects of DUSP5 knockdown on *p*-ERK and ERK in HT6244-R cells exposed to short-term AZD6244 withdrawal, we investigated whether DUSP5 repression would influence the consequences of long-term AZD6244 removal from these cells. Work by Sale *et al*. (2019) demonstrated that after approximately 6 days of drug withdrawal HT6244-R cells began to die (Figure 5.1). Cell death was associated with upregulation of the pro-apoptotic protein NOXA, activation of another pro-apoptotic protein BID, PARP cleavage and post-translational processing of LC3, indicating that these cells enter apoptosis and/or autophagy in response to AZD6244 withdrawal.

Figure 5.11 illustrates the results of a 12-day AZD6244 withdrawal experiment in HT6244-R shRNA cell lines, while Appendix figure A8 contains quantification of three biological repeats performed using Licor imaging and analysis. Cells were seeded at varying densities in order to achieve similar cell densities at the time of cell lysis for different incubation periods (3, 6, 9 or 12 days). HT29 cells and HT6244-R cells incubated with AZD6244 were included to control for off-target signalling effects that could result from this format of long-term experimental cell culture without passage. In addition to previous targets described, we chose to assess PARP cleavage as a predictive indicator of cell death, as well as NOXA, the pro-apoptotic BLC2 protein implicated in mediating cell death in AZD6244-deprived HT6244-R cells. Unfortunately, attempts to detect NOXA in any conditions were unsuccessful and so these immunoblots were not included.

As expected, in control conditions (without DUSP5 knockdown) 3 days of AZD6244 withdrawal led to heightened *p*-ERK and DUSP5 levels relative to parental HT29 and HT6244-R cells cultured in routine conditions (AZD6244-free and 1 μM AZD6244, respectively). Increased *p*-ERK seen in drug-withdrawal conditions was also coincident with increased $p21^{CIP1}$ expression and decreased BIM expression (Figure 5.11 and Appendix Figure A8). In DUSP5 knockdown conditions, there were no clear differences in *p*-ERK and $p21^{CIP1}$ levels compared to controls at after 3 days of drug withdrawal.

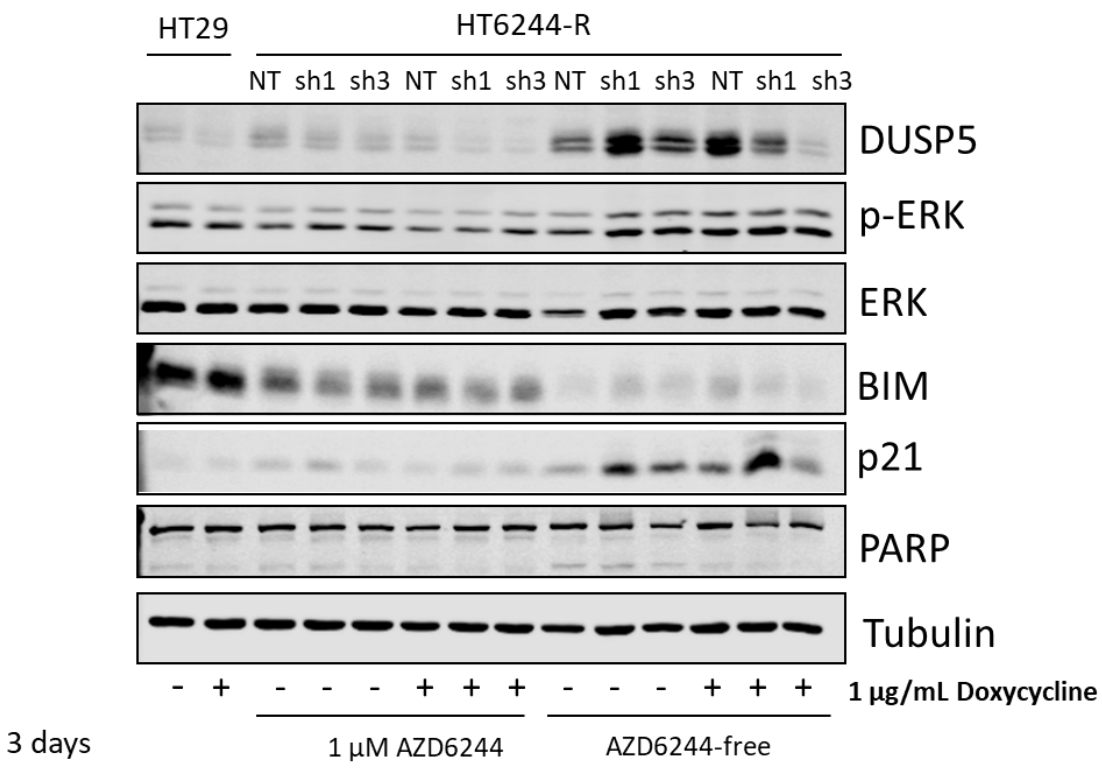
HT29
HT6244-R
NT sh1 sh3 NT sh1 sh3 NT sh1 sh3 NT sh1 sh3
DUSP5
p-ERK
ERK
BIM
p21
PARP
Tubulin
- + - - - + + + - - - + + +
1 µg/mL Doxycycline
1 µM AZD6244
AZD6244-free

3 days

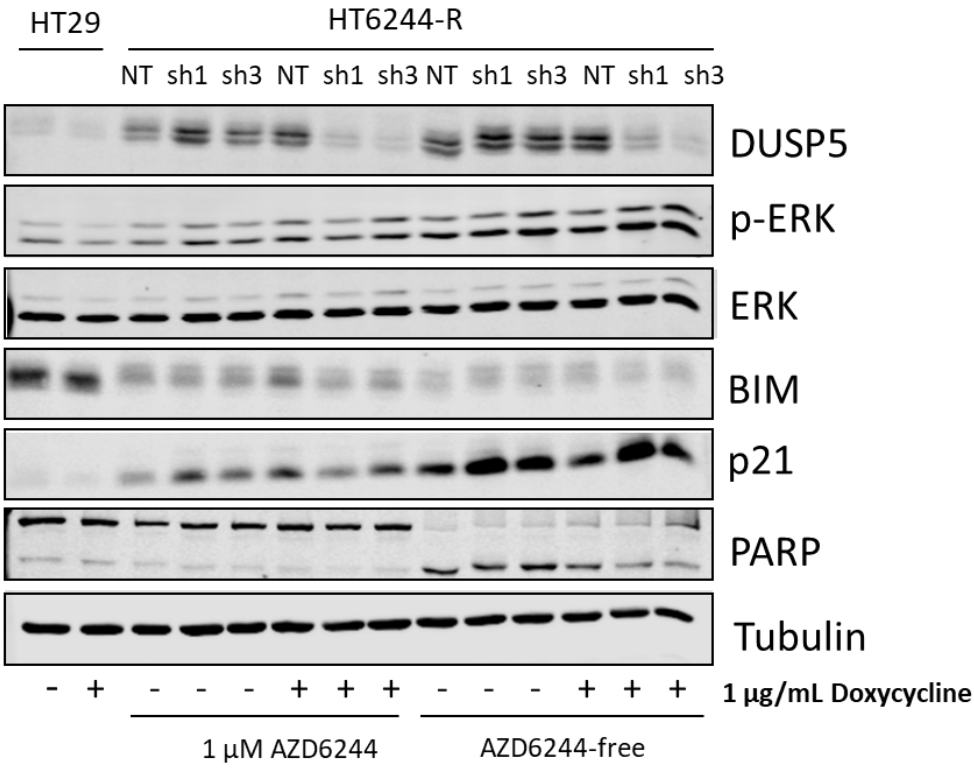
HT29
HT6244-R
NT sh1 sh3 NT sh1 sh3 NT sh1 sh3 NT sh1 sh3
DUSP5
p-ERK
ERK
BIM
p21
PARP
Tubulin
- + - - - + + + - - - + + +
1 µg/mL Doxycycline
1 µM AZD6244
AZD6244-free

6 days

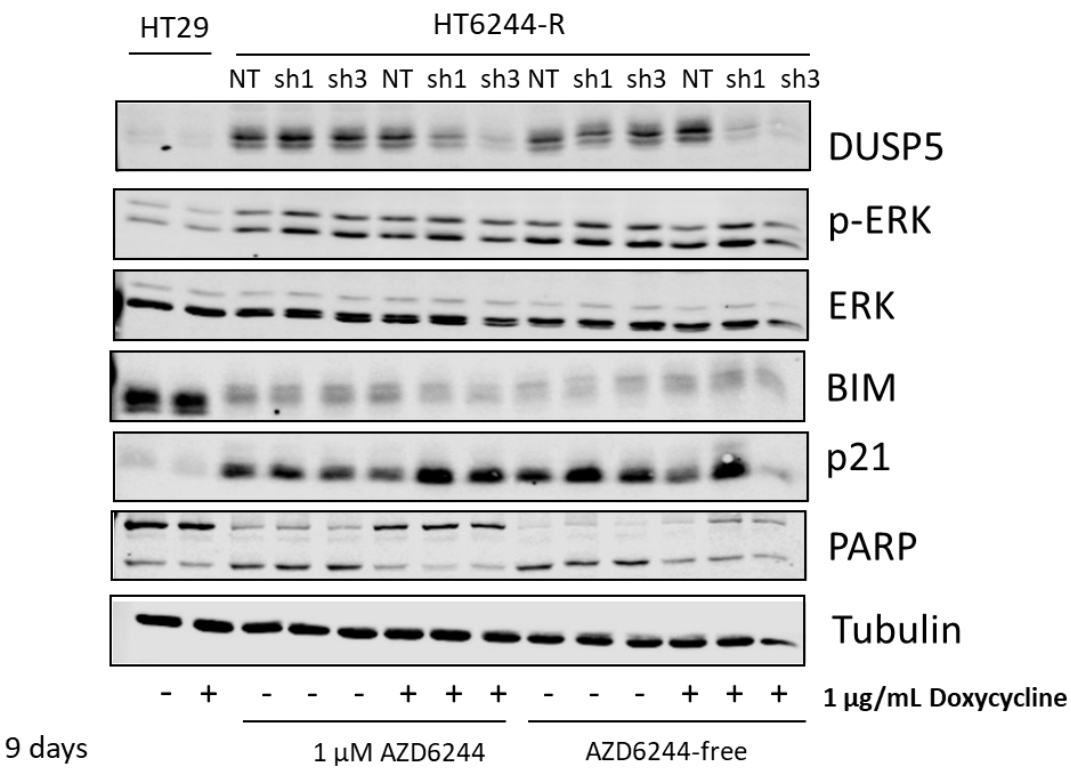
HT29
HT6244-R
NT sh1 sh3 NT sh1 sh3 NT sh1 sh3 NT sh1 sh3
DUSP5
p-ERK
ERK
BIM
p21
PARP
Tubulin
- + - - - + + + - - - + + +
1 µg/mL Doxycycline
9 days
1 µM AZD6244
AZD6244-free

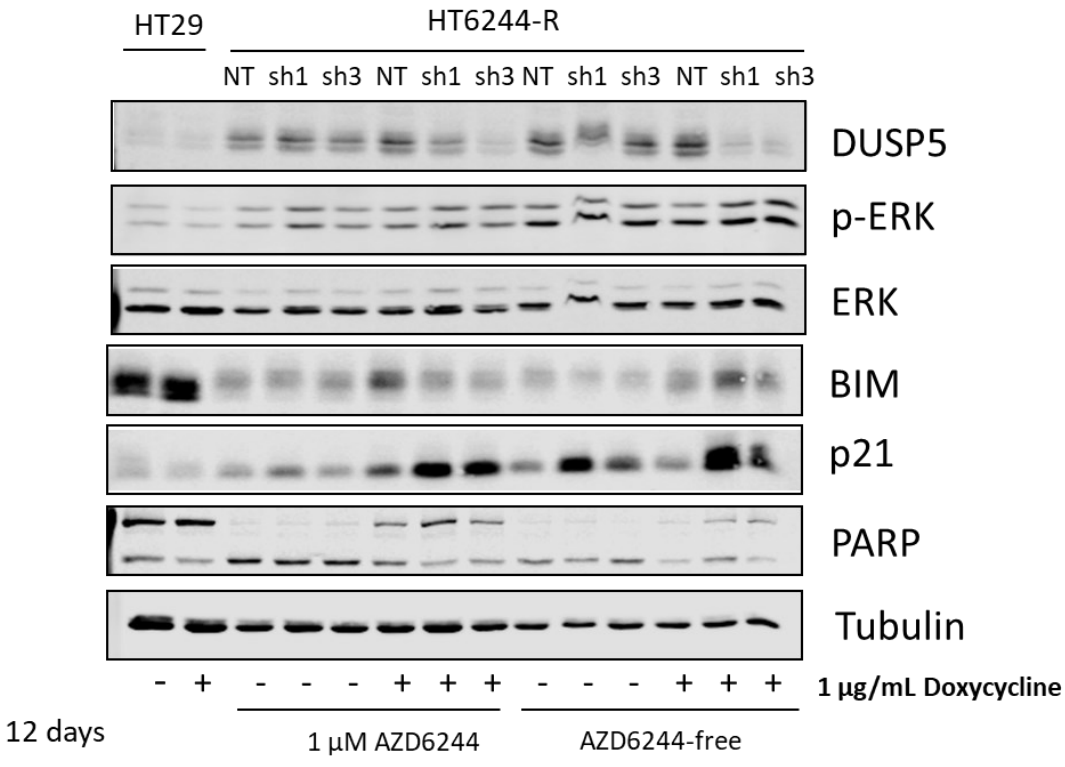
HT29
HT6244-R
NT sh1 sh3 NT sh1 sh3 NT sh1 sh3 NT sh1 sh3
DUSP5
p-ERK
ERK
BIM
p21
PARP
Tubulin
- + - - - + + + - - - + + +
1 µg/mL Doxycycline
12 days
1 µM AZD6244
AZD6244-free

Figure 5.11 Sustained DUSP5 knockdown in HT6244-R cell lines exposed to long-term AZD6244 withdrawal is coincident with subtle changes in *p*-ERK, $p21^{CIP1}$, BIM and PARP cleavage. HT29 and HT6244-R shRNA cell lines were incubated with or without 1 $\mu g.mL^{-1}$ doxycycline for 48 hours before culture media was replaced with AZD6244-free media or media containing 1 μm AZD6244 (with or without doxycycline). Cells were incubated for a further 3, 6, 9 or 12 days before cell lysis. Samples were fractioned by SDS-PAGE and western blotted with the indicated antibodies to assess relative protein levels. Images are representative of results from 3 separate experiments.

Unexpectedly, after 6 days of incubation, DUSP5 expression and slightly higher levels of *p*-ERK were apparent in control HT6244-R cells cultured in 1 μM AZD6244 (Figure 5.11 and Appendix Figure A8). While culture media was refreshed in all experimental conditions after 3 days of incubation, it was not changed after this time point. This was in an effort to retain any dead cells that may have accumulated in the culture suspension between 6 and 12 days of incubation. It is possible that during this time AZD6244 may have degraded, resulting in these cells showing signs of AZD6244 withdrawal. Interestingly in these conditions, where *p*-ERK levels are raised but not to the same extent as in intended AZD6244-free conditions in HT6244-R cells, a subtle difference in BIM levels was be seen between samples from the non-targeting shRNA HT6244-R line and those from DUSP5 knockdown lines shRNA 1 and 3. In the presence of doxycycline, levels of BIM protein appeared to be lower in DUSP5 knockdown lines compared to the non-targeting shRNA control line (Figure 5.11 and Appendix Figure A8). This trend was also apparent in HT6244-R cells incubated for 9 and 12 days with AZD6244 and doxycycline, as seen in Figure 5.11 and Appendix Figure A8. In the same conditions (1 μM AZD6244, 1 $\mu g.mL^{-1}$ doxycycline) after 12 days of incubation, a subtle increase in *p*-ERK levels in DUSP5 knockdown samples relative to non-targeting shRNA samples was seen. This was coincident with slightly increased $p21^{CIP1}$ levels and decreased PARP cleavage in DUSP5 knockdown conditions relative to the non-targeting shRNA control.

In conditions of 6 and 9 days of AZD6244 withdrawal, a relative increase in *p*-ERK in DUSP5 knockdown samples shRNA 1 and 3 compared to non-targeting shRNA samples was seen (Figure 5.11 and Appendix Figure A8). However, while *p*-ERK levels in the DUSP5 knockdown conditions were higher than the non-targeting shRNA control, they were not markedly different to no-doxycycline controls. Also coincident with AZD6244 withdrawal, was an increase in $p21^{CIP1}$ expression after 6 days of incubation (Appendix Figure A8). This was also seen in 9- and 12-day samples and was most apparent in the HT6244-R shRNA 1 cell line incubated with doxycycline.

Similar to results from experiments performed by Sale *et al*. (2019), evidence of PARP cleavage was seen across all AZD6244-withdrawal conditions from 6 days onwards. In Appendix Figure A8, signal quantification was performed on the 89 kDa cleaved product of PARP, therefore an increase in this measure should reflect increased PARP cleavage (Figure 5.11 and Appendix Figure A8). Unexpectedly, when PARP cleavage was increasingly evident in HT6244-R cells after 9 and 12 days of incubation (both in AZD6244 and AZD6244-free conditions), a striking correlation was seen between doxycycline administration and decreased PARP cleavage. This correlation indicated that doxycycline administration was somehow protecting cells from PARP cleavage (Figure 5.11 and Appendix Figure A8). After 12 days of drug withdrawal, a correlation could also be seen between doxycycline administration and increased BIM expression. An explanation for these off-target effects is unclear and confounds comparisons between doxycycline conditions and no-doxycycline controls. It also raises concerns as to other off-target effects of doxycycline in these findings. In light of this, interpretation of the effects of DUSP5 knockdown in these experiments may be restricted to comparisons between HT29, non-targeting shRNA and DUSP5-targeting shRNA 1 and 3 cell lines cultured in the presence of doxycycline, bearing in mind the as yet unknown effects of doxycycline alone.

In addition to these concerns, a comparison of these findings to those from similar experiments conducted by Sale *et al.* (2019) showed higher levels of PARP cleavage in control conditions (H6244-R cells cultured with AZD6244) in our results than was present in their results after 9 and 12 days of culture. While it is possible that AZD6244 had become degraded in our control conditions, this observation indicated that it was also possible that cellular stress and cell death was occurring both with and without

AZD6244 in our experiments. Based on observations made during experimental culture, this could have been caused by factors such as cell crowding and nutrient depletion. While we attempted to control for both of these potential issues, the innate tendency of HT29 and H6244-R cells to grow in large, tightly packed colonies (especially following low-density seeding) and restricted media refreshment could inevitably have contributed to increased cellular stress.

In conclusion, while some subtle changes in *p*-ERK, $p21^{CIP1}$ and BIM expression and PARP cleavage were coincident with DUSP5 knockdown in HT6244-R cells cultured in different AZD6244 conditions for prolonged periods, these changes were not substantial or consistent. Additionally, the confounding effects of doxycycline and other experimental variables precluded any reliable assessment of the signalling events that were observed in these results.

5.4. Discussion

Similar to studies in HCT116 and H6244-R cell lines, we have used high content imaging to assess spatial and temporal components of ERK hyperactivation in response to AZD6244 withdrawal in HT6244-R cells. Additionally, with DUSP5-targeting shRNA delivered through either adenoviral or inducible lentiviral constructs, we have evaluated the effects of transient or sustained DUSP5 loss in these conditions. In short-term (up to 48-hour) AZD6244-withdrawal and DUSP5 knockdown experiments, DUSP5 ablation did not appear to change whole-cell levels of *p*-ERK. While there was some evidence that DUSP5 loss was coincident with decreased accumulation of total ERK in the nucleus, these observations were not consistent between different DUSP5-targeting siRNAs. In longer term western blotting experiments, DUSP5 knockdown was coincident with subtle increases in *p*-ERK and $p21^{CIP1}$, reduced BIM expression and PARP cleavage in some conditions, however these observations were also inconsistent. In addition to this, issues with the experimental design and the presence of implicit off target effects and variables precluded the reliable interpretation of these results. While these findings don't exclude a potential role for DUSP5 in regulating oncogenic ERK signalling in this model, they could indicate that this role is limited, or perhaps redundant.

High content imaging and analysis revealed that the spatiotemporal aspects of ERK hyperactivation in HT6244-R cells in response to AZD6244 removal are much the same as in H6244-R cells. Enhancement of *p*-ERK is seen within 10 minutes of drug withdrawal, decreases slightly within 2 hours and then is maintained for the duration of the response measured (48 hours in short-term assays). Western blotting analyses confirm that similar to results in Sale *et al*. (2019), ERK hyperactivation is sustained long thereafter, for at least 12 days. Interestingly, the accumulation of both *p*-ERK and total ERK in the nucleus, events that were coincident with ERK activation, is not as pronounced as in H6244-R cells. While this could hold some biological relevance, it may just reflect how morphological differences in these cells can impact image-based quantification. Similar to observations in H6244-R cells, after 2 hours of ERK hyperactivation *p*-ERK becomes more evenly distributed within the cell once again, while total ERK remains more predominantly in the nucleus. These results are interesting and provide new insight into the spatiotemporal behaviour of hyperactive ERK in the context of upstream signalling amplification.

In short-term AZD6244-withdrawal experiments with H6244-R cells, no relative increases in whole-cell *p*-ERK levels were detected in DUSP5 knockdown conditions with either western blot analysis or high content microscopy. Additionally, high content imaging analysis did not reveal any effects of DUSP5 loss on the nuclear to cytoplasmic distribution of *p*-ERK. The latter observation was consistent with results from similar H6244-R experiments, however, most notably, DUSP5 knockdown did appear to substantially enhance whole-cell *p*-ERK levels in H6244-R cells. Additionally, when DUSP5 expression was disrupted in AZD6244-deprived H6244-R cells, a decrease in the accumulation of total ERK in the nucleus was seen. In HT6244-R cells cultured without AZD6244 and exposed to adenoviral DUSP5-targeting shRNA constructs there was some evidence of this phenotype in HCM and western blot results. This was accompanied by what appeared to be a decrease in total ERK levels in the presence of DUSP5-targeting shRNA. However, these observations were not consistent between two different DUSP5-targeting shRNA sequences used. Similar analyses performed with HT6244-R lentiviral shRNA cell lines produced results that were for the most part, consistent with those seen with adenoviral shRNA constructs, albeit with higher levels of deviation in repeated measures.

In conjunction with the assessment of relative *p*-ERK and ERK levels in HT6244-R cells cultured without AZD6244 for up to 48 hours, $p21^{CIP1}$ and BIM protein levels were monitored as they generally served as reliable indicators of increased ERK activity. In comparable experiments performed in Sale *et al.* (2019), ERK hyperactivation was concomitant with $p21^{CIP1}$ induction and BIM repression in these conditions. Like with *p*-ERK, no differences in $p21^{CIP1}$ and BIM expression were observed when DUSP5 levels were reduced with either adenoviral or lentiviral shRNA in 48-hour experiments.

In a final bid to expose a potential role for DUSP5 in regulating ERK hyperactivation in H6244-R cells, we used HT6244-R lentiviral shRNA cell lines to combine long-term AZD6244 withdrawal with prolonged DUSP5 knockdown. These experiments were based on western blot analyses performed by Sale *et al.* (2019) that characterised the cell death phenotype observed in HT6244-R cells cultured in the absence of AZD6244 for 6 or more days. In addition to DUSP5, *p*-ERK, ERK, $p21^{CIP1}$ and BIM levels we chose to evaluate levels of PARP cleavage as a general marker of cell death, and NOXA, the pro-apoptotic protein implicated in mediating cell death. We included

p21^{CIP1} and BIM in longer term experiments despite their seemingly indirect roles in the cell death phenotype previously characterised in similar experiments (Sale et al., 2019). We reasoned that potential changes in *p*-ERK levels may not only result in the enhancement or acceleration of cell death but could alter cell fate entirely. For example, the upregulation of ERKs' pro-survival BCL2 family targets and repression of pro-apoptotic targets such as BIM, combined with upregulation of the CDK inhibitor p21^{CIP1} could tip the balance of proliferative, anti-proliferative, pro-survival and pro-apoptotic effectors and drive cells into to early senescence rather than death.

Apart from inconsistencies in HT6244-R control conditions that served to monitor long term culture of HT6244-R cells in AZD6244 alongside AZD6244-free conditions, results seen in HCT116 and HT6244-R cells without DUSP5 ablation were generally similar to those seen in comparable experiments in Sale *et al*. (2019). However, subsequent analysis of doxycycline-induced DUSP5 knockdown conditions revealed a number of issues with the experimental set up, including off target effects of doxycycline administration in control conditions. Interestingly, PARP cleavage appeared reduced in all doxycycline conditions, indicating that these off-target effects were "protecting" cells from the cell death phenotype. Doxycycline has been shown to induce apoptosis caspase-mediated apoptosis in hela cells (Wu et al., 2006) and melanoma cells, where it was linked to JNK signalling (Shieh et al., 2010), however this generally occurred at concentrations above 10 μg.mL^{-1}. Interestingly, when administered at lower concentrations (1 μg.mL^{-1}) doxycycline enhanced cell survival in human pluripotent stem cells through the activation of the PI3K/AKT signalling pathway (Chang et al., 2014). It is therefore theoretically possible that in our cell model, doxycycline administration was able to offset pro-apoptotic signalling and reduce cell death.

While the caveats of our experimental format prevented us from making any conclusive interpretations based on this data, some interesting observations were noted when we restricted our analysis to results from doxycycline-treated samples only. While these observations were not all together consistent, some evidence of subtle differences in DUSP5 shRNA lines compared to NT shRNA line were seen. These included subtle increases in *p*-ERK and p21^{CIP1} expression, enhanced BIM repression and reduced PARP cleavage. In theory, if these observations were indeed consequences of DUSP5 loss they might suggest that the effects increased *p*-ERK

has on more immediate signalling effectors like $p21^{CIP1}$ and BIM could drive cells into senescence and circumvent the initiation of cell death. While this mechanism is theoretically possible, evidence of its likelihood cannot be drawn from this experimental data.

5.5. Limitations and future work

The limitations of the work completed to assess the influence of DUSP5 in the regulation of ERK in HT29 and HT6244-R cells have been discussed in some detail. While it is possible that these limitations precluded us from deriving any conclusive data from our experiments, it is also entirely possible that our difficulty in establishing substantial or consistent effects of DUSP5 loss in this cell model is due to its limited or redundant role in the signalling events we have investigated. Indeed, previous experiments that assessed the impact of MKP loss in HeLa cells revealed more substantial effects on ERK responses when DUSP/MKP proteins were knocked down in combinations (Caunt *et al.*, 2008). It is possible that in HT6244-R cells, the expression of other MKPs and or other negative feedback regulators of ERK could compensate for DUSP5 loss in response to AZD6244 withdrawal.

Early experiments revealed that both DUSP4 and DUSP6, in addition to DUSP5 were induced in HT6244-R cells cultured in the absence of AZD6244. It would be interesting to see how loss of one or both of these proteins alone, or in combination with DUSP5 would influence the spatiotemporal dynamics of ERK activation as well as downstream effects in HT6244-R cells. Additionally, high throughput RNA screening could be employed to provide information on the global response of ERK pathway related proteins to AZD6244 withdrawal in HT6244-R cells. This could confirm or contradict the importance of MKPs in this model or reveal other potential feedback regulators that act to restrain hyperactive ERK. In the context of HT6244-R cells, where ERK hyperactivation induced by drug-withdrawal leads to the death of previously drug-resistant cells, knowledge of signalling regulators that act to counteract this could be of clinical significance.

Chapter 6. Concluding Remarks

As dynamic negative regulators of ERK activity, MKPs may play important roles in ERK-driven cancers. This may be especially true in the context of drug-resistance, where cessation of drug administration or “drug holidays” can lead to sustained ERK hyperactivation in some cancer models. In these scenarios MKP expression may be enhanced and could function to restrain the anti-proliferative or pro-apoptotic effects of ERK hyperactivation.

This work has shown that in ERK-addicted, mutant BRAF- and KRAS-driven CRC lines and derivative cell lines that have evolved resistance to MEK inhibition, the expression profiles of prominent MKPs DUSP4, DUSP5 and DUSP6 are cell-line specific and temporally distinct. Despite this, removal of MEKi and the subsequent hyperactivation of ERK leads to robust induction of DUSP4, DUSP5 and DUSP6 in MEKi-resistant HCT116 (H6244-R) and HT29 (HT6244-R) cells and DUSP4 and DUSP6 in MEKi-resistant COLO205 (C6244-R) cells. Furthermore, experiments demonstrating the impact of DUSP5 loss in H6244-R cells suggest that DUSP5 expression is able to modulate the effects of ERK hyperactivation and thus, could influence cell fate in this $KRAS^{G13D}$ model. These effects appear to be mediated by enhanced ERK hyperactivation induced by DUSP5 ablation, however the specificity and extent of this modulation could more definitively validated through more detailed characterisation experiments coupled with DUSP5 rescue experiments.

In the $BRAF^{V600E}$-driven HT6244-R cell model where removal of MEK inhibition and ERK hyperactivation lead to cell death, the effects of DUSP5 loss were unclear. This may have been a result of confounding experimental influences, but it could also reflect a limited or redundant role of DUSP5 in these cells. It is possible that other MKPs such as DUSP4 can compensate for DUSP5 loss or may even constitute more relevant biological regulators in this context. The relative influence of DUSP4 and DUSP6 on AZD6244 administration and withdrawal in all three MEKi-resistant CRC models would be an interesting avenue to explore in future.

References

Adachi, M., Fukuda, M., Nishida, E., 2000. Nuclear export of MAP kinase (ERK) involves a MAP kinase kinase (MEK)-dependent active transport mechanism. J. Cell Biol. 148, 849–856. https://doi.org/10.1083/jcb.148.5.849

Aksamitiene, E., Kiyatkin, A., Kholodenko, B., 2012. Cross-talk between mitogenic Ras/MAPK and survival PI3K/Akt pathways: a fine balance. Biochem. Soc. Trans. 40, 139–146. https://doi.org/10.1016/j.seppur.2006.01.013.http

Alessi, D.R., Gomez, N., Moorhead, G., Lewis, T., Keyse, S.M., Cohen, P., 1995. Inactivation of p42 MAP kinase by protein phosphatase 2A and a protein tyrosine phosphatase, but not CL100, in various cell lines. Curr. Biol. 5, 283–295. https://doi.org/10.1016/S0960-9822(95)00059-5

Andreyev, H.J.N., Norman, A.R., Cunningham, D., Oates, J.R., Clarke, P.A., 1998. Kirsten ras mutations in patients with colorectal cancer: The multicenter "RASCAL" study. J. Natl. Cancer Inst. 90, 675–684. https://doi.org/10.1093/jnci/90.9.675

Arkell, R.S., Dickinson, R.J., Squires, M., Hayat, S., Keyse, S.M., Cook, S.J., 2008. DUSP6/MKP-3 inactivates ERK1/2 but fails to bind and inactivate ERK5. Cell. Signal. 20, 836–843. https://doi.org/10.1016/j.cellsig.2007.12.014

Arnold, M., Sierra, M.S., Laversanne, M., Soerjomataram, I., Jemal, A., Bray, F., 2017. Global patterns and trends in colorectal cancer incidence and mortality. Gut 66, 683–691. https://doi.org/10.1136/gutjnl-2015-310912

Ashwell, J.D., 2006. The many paths to p38 mitogen-activated protein kinase activation in the immune system. Nat. Rev. Immunol. 6, 532–540. https://doi.org/10.1038/nri1865

Balmanno, K., Chell, S.D., Gillings, A.S., Hayat, S., Cook, S.J., 2009. Intrinsic resistance to the MEK1/2 inhibitor AZD6244 (ARRY-142886) is associated with weak ERK1/2 signalling and/or strong PI3K signalling in colorectal cancer cell lines. Int. J. Cancer 125, 2332–2341. https://doi.org/10.1002/ijc.24604

Balmanno, K., Cook, S.J., 2009. Tumour cell survival signalling by the ERK1/2 pathway. Cell Death Differ. 16, 368–377. https://doi.org/10.1038/cdd.2008.148

Balmanno, K., Cook, S.J., 1999. Sustained MAP kinase activation is required for the expression of cyclin D1, p21Cip1 and a subset of AP-1 proteins in CCL39 cells. Oncogene 18, 3085–97. https://doi.org/10.1038/sj.onc.1202647

Banerji, U., Camidge, D.R., Verheul, H.M.W., Agarwal, R., Sarker, D., Kaye, S.B., Desar, I.M.E., Timmer-Bonte, J.N.H., Eckhardt, S.G., Lewis, K.D., Brown, K.H., Cantarini, M. V., Morris, C., George, S.M.A., Smith, P.D., Van Herpen, C.M.L., 2010. The first-in-human study of the hydrogen sulfate (hyd-sulfate) capsule of the MEK1/2 inhibitor AZD6244 (ARRY-142886): A phase I open-label multicenter trial in patients with advanced cancer. Clin. Cancer Res. 16, 1613–1623. https://doi.org/10.1158/1078-0432.CCR-09-2483

Bardwell, L., 2006. Mechanisms of MAPK signalling specificity. Biochem. Soc. Trans. 34, 837–841. https://doi.org/10.1042/BST0340837

Barr, R.K., Bogoyevitch, M.A., 2001. The c-Jun N-terminal protein kinase family of mitogen-activated protein kinases (JNK MAPKs). Int. J. Biochem. Cell Biol. 33, 1047–1063. https://doi.org/10.1016/S1357-2725(01)00093-0

Bennouna, J., Lang, I., Valladares-Ayerbes, M., Boer, K., Adenis, A., Escudero, P., Kim, T.Y., Pover, G.M., Morris, C.D., Douillard, J.Y., 2011. A Phase II, open-label, randomised study to assess the efficacy and safety of the MEK1/2 inhibitor AZD6244 (ARRY-142886) versus capecitabine monotherapy in patients with colorectal cancer who have failed one or two prior chemotherapeutic regimens. Invest. New Drugs 29, 1021–1028. https://doi.org/10.1007/s10637-010-9392-8

Bertin, S., Lozano-Ruiz, B., Bachiller, V., García-Martínez, I., Herdman, S., Zapater, P., Francés, R., Such, J., Lee, J., Raz, E., González-Navajas, J.M., 2015. Dual-specificity phosphatase 6 regulates CD4+ T-cell functions and restrains spontaneous colitis in IL-10-deficient mice. Mucosal Immunol. 8, 505–515. https://doi.org/10.1038/mi.2014.84

Bertoli, C., Skotheim, J.M., Bruin, R.A.M. De, 2015. Control of cell cycle transcription during G1 and S phases Cosetta. Nat. Rev. Mol. Cell Biol. 14, 518–528. https://doi.org/10.1038/nrm3629.Control

Bhalla, U.S., Ram, P.T., Iyengar, R., 2002. MAP kinase phosphatase as a locus of flexibility in a mitogen-activated protein kinase signaling network. Science (80-.). 297, 1018–1023. https://doi.org/10.1126/science.1068873

Bonni, A., Brunet, A., West, A.E., Datta, S.R., Takasu, M.A., Greenberg, M.E., 1999. Cell survival promoted by the Ras-MAPK signaling pathway by transcription-dependent and -independent mechanisms. Science (80-.). 286, 1358–1362. https://doi.org/10.1126/science.286.5443.1358

Bos. J. L.,1989. ras Oncogenes in human cancer: A review. Cancer Res. 49, 4682–4689.

Bouchard, C., Thieke, K., Maier, A., Saffrich, R., Hanley-Hyde, J., Ansorge, W., Reed, S., Sicinski, P., Bartek, J., Eilers, M., 1999. Direct induction of cyclin D2 by Myc contributes to cell cycle progression and sequestration of p27. EMBO J. 18, 5321–5333. https://doi.org/10.1093/emboj/18.19.5321

Boucher, M.J., Morisset, J., Vachon, P.H., Reed, J.C., Lain, J., Rivard, N., 2000. MEK/ERK signaling pathway regulates the expression of Bcl-2, Bcl-X(L), and Mcl-1 and promotes survival of human pancreatic cancer cells. J. Cell. Biochem. 79, 355–369. https://doi.org/10.1002/1097-4644(20001201)79:3<355::AID-JCB20>3.0.CO;2-0

Boulton, T.G., Nye, S.H., Robbins, D.J., Ip, N.Y., Radzlejewska, E., Morgenbesser, S.D., DePinho, R.A., Panayotatos, N., Cobb, M.H., Yancopoulos, G.D., 1991. ERKs: A family of protein-serine/threonine kinases that are activated and tyrosine phosphorylated in response to insulin and NGF. Cell 65, 663–675. https://doi.org/10.1016/0092-8674(91)90098-J

Brondello, J.M., Brunet, A., Pouysségur, J., McKenzie, F.R., 1997. The dual specificity mitogen-activated protein kinase phosphatase-1 and -2 are induced by the p42/p44(MAPK) cascade. J. Biol. Chem. 272, 1368–1376.

https://doi.org/10.1074/jbc.272.2.1368

Brondello, J.M., Pouysségur, J., McKenzie, F.R., 1999. Reduced MAP kinase phosphatase-1 degradation after p42/p44(MAPK)- dependent phosphorylation. Science (80-.). 286, 2514–2517. https://doi.org/10.1126/science.286.5449.2514

Brunet, A., Roux, D., Lenormand, P., Dowd, S., Keyse, S., Pouysségur, J., 1999. Nuclear translocation of p42/p44 mitogen-activated protein kinase is required for growth factor-induced gene expression and cell cycle entry. EMBO J. 18, 664–674. https://doi.org/10.1093/emboj/18.3.664

Buffet, C., Catelli, M.G., Hecale-Perlemoine, K., Bricaire, L., Garcia, C., Gallet-Dierick, A., Rodriguez, S., Cormier, F., Groussin, L., 2015. Dual specificity Phosphatase 5, a specific negative regulator of ERK signaling, is induced by serum response factor and Elk-1 transcription factor. PLoS One 10, 1–21. https://doi.org/10.1371/journal.pone.0145484

Buscà, R., Pouysségur, J., Lenormand, P., 2016. ERK1 and ERK2 map kinases: Specific roles or functional redundancy? Front. Cell Dev. Biol. 4, 1–23. https://doi.org/10.3389/fcell.2016.00053

Cagnol, S., Chambard, J.C., 2010. ERK and cell death: Mechanisms of ERK-induced cell death - Apoptosis, autophagy and senescence. FEBS J. 277, 2–21. https://doi.org/10.1111/j.1742-4658.2009.07366.x

Cagnol, S., Rivard, N., 2013. Oncogenic KRAS and BRAF activation of the MEK/ERK signaling pathway promotes expression of dual-specificity phosphatase 4 (DUSP4/MKP2) resulting in nuclear ERK1/2 inhibition. Oncogene 32, 564–576. https://doi.org/10.1038/onc.2012.88

Cai, C., Chen, J.Y., Han, Z.D., He, H.C., Chen, J.H., Chen, Y.R., Yang, S.B., Wu, Y.D., Zeng, Y.R., Zou, J., Liang, Y.X., Dai, Q.S., Jiang, F.N., Zhong, W. De, 2015. Down-regulation of dual-specificity phosphatase 5 predicts poor prognosis of patients with prostate cancer. Int. J. Clin. Exp. Med. 8, 4186–4194.

Camps, M., Chabert, C., Muda, M., Boschert, U., Gillieron, C., Arkinstall, S., 1998a. Induction of the mitogen-activated protein kinase phosphatase MKP3 by nerve growth factor in differentiating PC12. FEBS Lett. 425, 271–276. https://doi.org/10.1016/S0014-5793(98)00250-6

Camps, M., Nichols, A., Arkinstall, S., 2000. Dual specificity phosphatases: A gene family for control of MAP kinase function. FASEB J. 14, 6–16. https://doi.org/10.1096/fasebj.14.1.6

Camps, M., Nichols, A., Gillieron, C., Antonsson, B., Muda, M., Chabert, C., Boschert, U., Arkinstall, S., 1998b. Catalytic activation of the phosphatase MKP-3 by ERK2 mitogen-activated protein kinase. Science (80-.). 280, 1262–1265. https://doi.org/10.1126/science.280.5367.1262

Canagarajah, B.J., Khokhlatchev, A., Cobb, M.H., Goldsmith, E.J., 1997. Activation mechanism of the MAP kinase ERK2 by dual phosphorylation. Cell 90, 859–869. https://doi.org/10.1016/S0092-8674(00)80351-7

Cartlidge, R.A., Thomas, G.R., Cagnol, S., Jong, K.A., Molton, S.A., Finch, A.J., McMahon, M., 2008. Oncogenic BRAFV600E inhibits BIM expression to promote melanoma cell survival. Pigment Cell Melanoma Res. 21, 534–544. https://doi.org/10.1111/j.1755-148X.2008.00491.x

Carvajal, R.D., Piperno-Neumann, S., Kapiteijn, E., Chapman, P.B., Frank, S., Joshua, A.M., Piulats, J.M., Wolter, P., Cocquyt, V., Chmielowski, B., Evans, T.R.J., Gastaud, L., Linette, G., Berking, C., Schachter, J., Rodrigues, M.J., Shoushtari, A.N., Clemett, D., Ghiorghiu, D., Mariani, G., Spratt, S., Lovick, S., Barker, P., Kilgour, E., Lai, Z., Schwartz, G.K., Nathan, P., 2018. Selumetinib in combination with dacarbazine in patients with metastatic uveal melanoma: A Phase III, Multicenter, Randomized Trial (SUMIT). J. Clin. Oncol. 36, 1232–1239. https://doi.org/10.1200/JCO.2017.74.1090

Catalanotti, F., Reyes, G., Jesenberger, V., Galabova-Kovacs, G., De Matos Simoes, R., Carugo, O., Baccarini, M., 2009. A Mek1-Mek2 heterodimer determines the strength and duration of the Erk signal. Nat. Struct. Mol. Biol. 16, 294–303. https://doi.org/10.1038/nsmb.1564

Catalanotti, F., Solit, D.B., Pulitzer, M.P., Berger, M.F., Scott, S.N., Iyriboz, T., Lacouture, M.E., Panageas, K.S., Wolchok, J.D., Carvajal, R.D., Schwartz, G.K., Rosen, N., Chapman, P.B., 2013. Phase II trial of MEK inhibitor selumetinib (AZD6244, ARRY-142886) in patients with BRAFV600E/K-mutated melanoma. Clin. Cancer Res. 19, 2257–2264. https://doi.org/10.1158/1078-0432.CCR-12-3476

Caunt, C.J., Armstrong, S.P., Rivers, C.A., Norman, M.R., McArdle, C.A., 2008a. Spatiotemporal regulation of ERK2 by dual specificity phosphatases. J. Biol. Chem. 283, 26612–26623. https://doi.org/10.1074/jbc.M801500200

Caunt, C.J., Keyse, S.M., 2013. Dual-specificity MAP kinase phosphatases (MKPs): Shaping the outcome of MAP kinase signalling. FEBS J. 280, 489–504. https://doi.org/10.1111/j.1742-4658.2012.08716.x

Caunt, C.J., Rivers, C.A., Conway-Campbell, B.L., Norman, M.R., McArdle, C.A., 2008b. Epidermal growth factor receptor and protein kinase C signaling to ERK2: Spatiotemporal regulation of ERK2 by dual specificity phosphatases. J. Biol. Chem. 283, 6241–6252. https://doi.org/10.1074/jbc.M706624200

Caunt, C. J., Sale, M.J., Smith, P.D., Cook, S.J., 2015. MEK1 and MEK2 inhibitors and cancer therapy: The long and winding road. Nat. Rev. Cancer 15, 577–592. https://doi.org/10.1038/nrc4000

Chan, D.W., Liu, V.W.S., Tsao, G.S.W., Yao, K.M., Furukawa, T., Chan, K.K.L., Ngan, H.Y.S., 2008. Loss of MKP3 mediated by oxidative stress enhances tumorigenicity and chemoresistance of ovarian cancer cells. Carcinogenesis 29, 1742–1750. https://doi.org/10.1093/carcin/bgn167

Chang, L., Karin, M., 2001. Mammalian MAP kinase signalling cascades. Nature 410, 37–40. https://doi.org/10.1038/35065000

Chang, M.Y., Rhee, Y.H., Yi, S.H., Lee, S.J., Kim, R.K., Kim, H., Park, C.H., Lee, S.H., 2014. Doxycycline enhances survival and self-renewal of human pluripotent stem cells. Stem Cell Reports 3, 353–364.

https://doi.org/10.1016/j.stemcr.2014.06.013

Chapman, P.B., Hauschild, A., Robert, C., Haanen, J.B., Ascierto, P., Larkin, J., Dummer, R., Garbe, C., Testori, A., Maio, M., Hogg, D., Lorigan, P., Lebbe, C., Jouary, T., Schadendorf, D., Ribas, A., O'Day, S.J., Sosman, J.A., Kirkwood, J.M., Eggermont, A.M.M., Dreno, B., Nolop, K., Li, J., Nelson, B., Hou, J., Lee, R.J., Flaherty, K.T., McArthur, G.A., 2011. Improved survival with vemurafenib in melanoma with BRAF V600E mutation. N. Engl. J. Med. 364, 2507–2516. https://doi.org/10.1056/NEJMoa1103782

Chipuk, J.E., Moldoveanu, T., Llambi, F., Parsons, M.J., Green, D.R., 2010. The BCL-2 Family Reunion. Mol. Cell 37, 299–310. https://doi.org/10.1016/j.molcel.2010.01.025

Chuderland, D., Seger, R., 2005. Protein-protein interactions in the regulation of the extracellular signal-regulated kinase. Mol. Biotechnol. 29, 57–74. https://doi.org/10.1385/MB:29:1:57

Claassen, G.F., Hann, S.R., 2000. A role for transcriptional repression of p21CIP1 by c-Myc in overcoming transforming growth factor β-induced cell-cycle arrest. Proc. Natl. Acad. Sci. U. S. A. 97, 9498–9503. https://doi.org/10.1073/pnas.150006697

Cook, S.J., McCormick, F., 1993. Inhibition by cAMP of Ras-dependent activation of Raf. Science (80-.). 262, 1069–1072. https://doi.org/10.1126/science.7694367

Cook, S.J., Stuart, K., Gilley, R., Sale, M.J., 2017. Control of cell death and mitochondrial fission by ERK1/2 MAP kinase signalling. FEBS J. 284, 4177–4195. https://doi.org/10.1111/febs.14122

Corcoran, R.B., Atreya, C.E., Falchook, G.S., Kwak, E.L., Ryan, D.P., Bendell, J.C., Hamid, O., Messersmith, W.A., Daud, A., Kurzrock, R., Pierobon, M., Sun, P., Cunningham, E., Little, S., Orford, K., Motwani, M., Bai, Y., Patel, K., Venook, A.P., Kopetz, S., 2015. Combined BRAF and MEK inhibition with dabrafenib and trametinib in BRAF V600-Mutant colorectal cancer. J. Clin. Oncol. 33, 4023–4031. https://doi.org/10.1200/JCO.2015.63.2471

Corcoran, R.B., Ebi, H., Turke, A.B., Coffee, E.M., Nishino, M., Cogdill, A.P., Brown, R.D., Pelle, P. Della, Dias-Santagata, D., Hung, K.E., Flaherty, K.T., Piris, A., Wargo, J.A., Settleman, J., Mino-Kenudson, M., Engelman, J.A., 2012. EGFR-mediated reactivation of MAPK signaling contributes to insensitivity of BRAF-mutant colorectal cancers to RAF inhibition with vemurafenib. Cancer Discov. 2, 227–235. https://doi.org/10.1158/2159-8290.CD-11-0341

Dankort, D., Curley, D.P., Cartlidge, R.A., Nelson, B., Karnezis, A.N., Damsky, W.E., You, M.J., DePinho, R.A., McMahon, M., Bosenberg, M., 2009. BrafV 600E cooperates with Pten loss to induce metastatic melanoma. Nat. Genet. 41, 544–552. https://doi.org/10.1038/ng.356

Das Thakur, M., Salangsang, F., Landman, A.S., Sellers, W.R., Pryer, N.K., Levesque, M.P., Dummer, R., McMahon, M., Stuart, D.D., 2013. Modelling vemurafenib resistance in melanoma reveals a strategy to forestall drug resistance. Nature 494, 251–255. https://doi.org/10.1038/nature11814

Davies, B.R., Logie, A., McKay, J.S., Martin, P., Steele, S., Jenkins, R., Cockerill, M.,

Cartlidge, S., Smith, P.D., 2007. AZD6244 (ARRY-142886), a potent inhibitor of mitogen-activated protein kinase/extracellular signal-regulated kinase kinase 1/2 kinases: mechanism of action in vivo, pharmacokinetic/pharmacodynamic relationship, and potential for combination in preclinical. Mol. Cancer Ther. 6, 2209–2219. https://doi.org/10.1158/1535-7163.MCT-07-0231

Davies, H., Bignell, G.R., Cox, C., Stephens, P., Edkins, S., Clegg, S., Teague, J., Woffendin, H., Garnett, M.J., Bottomley, W., Davis, N., Dicks, E., Ewing, R., Floyd, Y., Gray, K., Hall, S., Hawes, R., Hughes, J., Kosmidou, V., Menzies, A., Mould, C., Parker, A., Stevens, C., Watt, S., Hooper, S., Wilson, R., Jayatilake, H., Gusterson, B. a, Cooper, C., Shipley, J., Hargrave, D., Pritchard-Jones, K., Maitland, N., Chenevix-Trench, G., Riggins, G.J., Bigner, D.D., Palmieri, G., Cossu, A., Flanagan, A., Nicholson, A., Ho, J.W.C., Leung, S.Y., Yuen, S.T., Weber, B.L., Seigler, H.F., Darrow, T.L., Paterson, H., Marais, R., Marshall, C.J., Wooster, R., Stratton, M.R., Futreal, P.A., 2002. Mutations of the BRAF gene in human cancer. Nature 417, 949–954. https://doi.org/10.1038/nature00766

Degl'Innocenti, D., Romeo, P., Tarantino, E., Sensi, M., Cassinelli, G., Catalano, V., Lanzi, C., Perrone, F., Pilotti, S., Seregni, E., Pierotti, M.A., Greco, A., Borrello, M.G., 2013. DUSP6/MKP3 is overexpressed in papillary and poorly differentiated thyroid carcinoma and contributes to neoplastic properties of thyroid cancer cells. Endocr. Relat. Cancer 20, 23–37. https://doi.org/10.1530/ERC-12-0078

Deschênes-Simard, X., Kottakis, F., Meloche, S., Ferbeyre, G., 2014. ERKs in cancer: Friends or foes? Cancer Res. 74, 412–419. https://doi.org/10.1158/0008-5472.CAN-13-2381

Dhillon, A.S., Hagan, S., Rath, O., Kolch, W., 2007. MAP kinase signalling pathways in cancer. Oncogene 26, 3279–90. https://doi.org/10.1038/sj.onc.1210421

Dhomen, N., Reis-Filho, J.S., da Rocha Dias, S., Hayward, R., Savage, K., Delmas, V., Larue, L., Pritchard, C., Marais, R., 2009. Oncogenic Braf Induces Melanocyte Senescence and Melanoma in Mice. Cancer Cell 15, 294–303. https://doi.org/10.1016/j.ccr.2009.02.022

Dijkers, P.F., Medema, R.H., Lammers, J.W.J., Koenderman, L., Coffer, P.J., 2000. Expression of the pro-apoptotic Bcl-2 family member Bim is regulated by the forkhead transcription factor FKHR-L1. Curr. Biol. 10, 1201–1204. https://doi.org/10.1016/S0960-9822(00)00728-4

Dobrowolski, S., Harter, M., Stacey, D.W., 1994. Cellular ras activity is required for passage through multiple points of the G0/G1 phase in BALB/c 3T3 cells. Mol. Cell. Biol. 14, 5441–5449. https://doi.org/10.1128/mcb.14.8.5441

Dombi, E., Baldwin, A., Marcus, L.J., Fisher, M.J., Weiss, B., Kim, A., Whitcomb, P., Martin, S., Aschbacher-Smith, L.E., Rizvi, T.A., Wu, J., Ershler, R., Wolters, P., Therrien, J., Glod, J., Belasco, J.B., Schorry, E., Brofferio, A., Starosta, A.J., Gillespie, A., Doyle, A.L., Ratner, N., Widemann, B.C., 2016. Activity of selumetinib in neurofibromatosis type 1-related plexiform neurofibromas. N. Engl. J. Med. 375, 2550–2560. https://doi.org/10.1056/NEJMoa1605943

Domina, A.M., Vrana, J.A., Gregory, M.A., Hann, S.R., Craig, R.W., 2004. MCL1 is

phosphorylated in the PEST region and stabilized upon ERK activation in viable cells, and at additional sites with cytotoxic okadaic acid or taxol. Oncogene 23, 5301–5315. https://doi.org/10.1038/sj.onc.1207692

Dougherty, M.K., Müller, J., Ritt, D.A., Zhou, M., Zhou, X.Z., Copeland, T.D., Conrads, T.P., Veenstra, T.D., Lu, K.P., Morrison, D.K., 2005. Regulation of Raf-1 by direct feedback phosphorylation. Mol. Cell 17, 215–224. https://doi.org/10.1016/j.molcel.2004.11.055

Dry, J.R., Pavey, S., Pratilas, C.A., Harbron, C., Runswick, S., Hodgson, D., Chresta, C., McCormack, R., Byrne, N., Cockerill, M., Graham, A., Beran, G., Cassidy, A., Haggerty, C., Brown, H., Ellison, G., Dering, J., Taylor, B.S., Stark, M., Bonazzi, V., Ravishankar, S., Packer, L., Xing, F., Solit, D.B., Finn, R.S., Rosen, N., Hayward, N.K., French, T., Smith, P.D., 2010. Transcriptional pathway signatures predict MEK addiction and response to selumetinib (AZD6244). Cancer Res. 70, 2264–2273. https://doi.org/10.1158/0008-5472.CAN-09-1577

Dumaz, N., Marais, R., 2003. Protein kinase A blocks Raf-1 activity by stimulating 14-3-3 binding and blocking Raf-1 interaction with Ras. J. Biol. Chem. 278, 29819–29823. https://doi.org/10.1074/jbc.C300182200

Ebisuya, M., Kondoh, K., Nishida, E., 2005. The duration, magnitude and compartmentalization of ERK MAP kinase activity: mechanisms for providing signaling specificity. J. Cell Sci. 118, 2997–3002. https://doi.org/10.1242/jcs.02505

Eblaghie, M.C., Lunn, J.S., Dickinson, R.J., Münsterberg, A.E., Sanz-Ezquerro, J.-J., Farrell, E.R., Mathers, J., Keyse, S.M., Storey, K., Tickle, C., 2003. Negative Feedback Regulation of FGF Signaling Levels by Pyst1/MKP3 in Chick Embryos. Curr. Biol. 13, 1009–1018. https://doi.org/10.1016/S0960-9822(03)00381-6

Eblen, S.T., Slack-Davis, J.K., Tarcsafalvi, A., Parsons, J.T., Weber, M.J., Catling, A.D., 2004. Mitogen-Activated Protein Kinase Feedback Phosphorylation Regulates MEK1 Complex Formation and Activation during Cellular Adhesion. Mol. Cell. Biol. 24, 2308–2317. https://doi.org/10.1128/mcb.24.6.2308-2317.2004

Ekerot, M., Stavridis, M.P., Delavaine, L., Mitchell, M.P., Staples, C., Owens, D.M., Keenan, I.D., Dickinson, R.J., Storey, K.G., Keyse, S.M., 2008. Negative-feedback regulation of FGF signalling by DUSP6/MKP-3 is driven by ERK1/2 and mediated by Ets factor binding to a conserved site within the DUSP6 / MKP - 3 gene promoter. Biochem. J. 412, 287–298. https://doi.org/10.1042/BJ20071512

Elgendy, M., Sheridan, C., Brumatti, G., Martin, S.J., 2011. Oncogenic Ras-Induced Expression of Noxa and Beclin-1 Promotes Autophagic Cell Death and Limits Clonogenic Survival. Mol. Cell 42, 23–35. https://doi.org/10.1016/j.molcel.2011.02.009

English, J., Pearson, G., Wilsbacher, J., Swantek, J., Karandikar, M., Xu, S., Cobb, M.H., 1999. New Insights into the Control of MAP Kinase Pathways. Exp. Cell Res. 253, 255–270. https://doi.org/10.1006/excr.1999.4687

Fang, J.Y., Richardson, B.C., 2005. The MAPK signalling pathways and colorectal cancer. Lancet Oncol. 6, 322–327. https://doi.org/10.1016/S1470-2045(05)70168-6

Farooq, A., Zhou, M.M., 2004. Structure and regulation of MAPK phosphatases. Cell. Signal. 16, 769–779. https://doi.org/10.1016/j.cellsig.2003.12.008

Feng, B., Jiao, P., Helou, Y., Li, Y., He, Q., Walters, M.S., Salomon, A., Xu, H., 2014. Mitogen-Activated protein kinase phosphatase 3 (mkp-3)- Deficient mice are resistant to diet-induced obesity. Diabetes 63, 2924–2934. https://doi.org/10.2337/db14-0066

Flaherty, K.T., Puzanov, I., Kim, K.B., Ribas, A., McArthur, G.A., Sosman, J.A., O'Dwyer, P.J., Lee, R.J., Grippo, J.F., Nolop, K., Chapman, P.B., 2010. Inhibition of Mutated, Activated BRAF in Metastatic Melanoma. N. Engl. J. Med. 363, 809–819. https://doi.org/10.1056/NEJMoa1002011

Freed, E., Symons, M., Macdonald, S.G., McCormick, F., Ruggieri, R., 1994. Binding of 14-3-3 proteins to the protein kinase Raf and effects on its activation. Science (80-.). 265, 1713–1716. https://doi.org/10.1126/science.8085158

Fukuda, H., Imamura, M., Tanaka, Y., Iwata, M., Hirose, H., Kaku, K., Maegawa, H., Watada, H., Tobe, K., Kashiwagi, A., Kawamori, R., Maeda, S., 2012. A Single Nucleotide Polymorphism within DUSP9 Is Associated with Susceptibility to Type 2 Diabetes in a Japanese Population. PLoS One 7, 6–12. https://doi.org/10.1371/journal.pone.0046263

Fukuda, M., Gotoh, I., Gotoh, Y., Nishida, E., 1996. Cytoplasmic Localization of Mitogen-activated Protein Kinase Kinase Directed by Its NH 2 -terminal , Leucine-rich Short Amino Acid Sequence , Which Acts as a Nuclear Export Signal *. J. Biol. Chem. 271, 20024–20028.

Fukuda, M., Gotoh, Y., Nishida, E., 1997. Interaction of MAP kinase with MAP kinase kinase: Its possible role in the control of nucleocytoplasmic transport of MAP kinase. EMBO J. 16, 1901–1908. https://doi.org/10.1093/emboj/16.8.1901

Furukawa, T., Fujisaki, R., Yoshida, Y., Kanai, N., Sunamura, M., Abe, T., Takeda, K., Matsuno, S., Horii, A., 2005. Distinct progression pathways involving the dysfunction of DUSP6/MKP-3 in pancreatic intraepithelial neoplasia and intraductal papillary-mucinous neoplasms of the pancreas. Mod. Pathol. 18, 1034–42. https://doi.org/10.1038/modpathol.3800383

Furukawa, T., Sunamura, M., Motoi, F., Matsuno, S., Horii, A., 2003. Potential tumor suppressive pathway involving DUSP6/MKP-3 in pancreatic cancer. Am. J. Pathol. 162, 1807–15. https://doi.org/10.1016/S0002-9440(10)64315-5

Good, M.C., Zalatan, J.G., Lim, W.A., 2011. Scaffold Proteins: Hubs for Controlling the Flow of Cellular Information. Science (80-.). 332, 680–686. https://doi.org/10.1126/science.1198701

Gotoh, Y., Nishida, E., Yamashita, T., Hoshi, M., Kawakami, M., Sakai, H., 1990. Microtubule-associated-protein (MAP) kinase activated by nerve growth factor and epidermal growth factor in PC12 cells. Identity with the mitogen-activated MAP kinase of fibroblastic cells. Eur. J. Biochem. 193, 661–669. https://doi.org/10.1111/j.1432-1033.1990.tb19384.x

Graves, L.M., Guy, H.I., Kozlowski, P., Huang, M., Lazarowski, E., Pope, R.M., Collins, M.A., Dahlstrand, E.N., Earp, H.S., Evans, D.R., 2000. Regulation of carbamoyl phosphate synthetase by MAP kinase. Nature 403, 328–332. https://doi.org/10.1038/35002111

Groom, L.A., Sneddon, A.A., Alessi, D.R., Dowd, S., Keyse, S.M., 1996. Differential regulation of the MAP, SAP and RK/p38 kinases by Pyst1, a novel cytosolic dual-specificity phosphatase. EMBO J. 15, 3621–3632. https://doi.org/10.1002/j.1460-2075.1996.tb00731.x

Haigis, K.M., Kendall, K.R., Wang, Y., Cheung, A., Haigis, M.C., Glickman, J.N., Niwa-Kawakita, M., Sweet-Cordero, A., Sebolt-Leopold, J., Shannon, K.M., Settleman, J., Giovannini, M., Jacks, T., 2008. Differential effects of oncogenic K-Ras and N-Ras on proliferation, differentiation and tumor progression in the colon. Nat. Genet. 40, 600–608. https://doi.org/10.1038/ng.115

Hanahan, D., Weinberg, R.A., 2011. Hallmarks of cancer: The next generation. Cell 144, 646–674. https://doi.org/10.1016/j.cell.2011.02.013

Hatzivassiliou, G., Haling, J.R., Chen, H., Song, K., Price, S., Heald, R., Hewitt, J.F.M., Zak, M., Peck, A., Orr, C., Merchant, M., Hoeflich, K.P., Chan, J., Luoh, S.-M., Anderson, D.J., Ludlam, M.J.C., Wiesmann, C., Ultsch, M., Friedman, L.S., Malek, S., Belvin, M., 2013. Mechanism of MEK inhibition determines efficacy in mutant KRAS- versus BRAF-driven cancers. Nature 501, 232–236. https://doi.org/10.1038/nature12441

Hatzivassiliou, G., Song, K., Yen, I., Brandhuber, B.J., Anderson, D.J., Alvarado, R., Ludlam, M.J., Stokoe, D., Gloor, S.L., Vigers, G., Morales, T., Aliagas, I., Liu, B., Sideris, S., Hoeflich, K.P., Jaiswal, B.S., Seshagiri, S., Koeppen, H., Belvin, M., Friedman, L.S., Malek, S., 2010. RAF inhibitors prime wild-type RAF to activate the MAPK pathway and enhance growth. Nature 464, 431–435. https://doi.org/10.1038/nature08833

Hauschild, A., Grob, J.-J., Demidov, L. V, Jouary, T., Gutzmer, R., Millward, M., Rutkowski, P., Blank, C.U., Miller, W.H., Kaempgen, E., Martín-Algarra, S., Karaszewska, B., Mauch, C., Chiarion-Sileni, V., Martin, A.-M., Swann, S., Haney, P., Mirakhur, B., Guckert, M.E., Goodman, V., Chapman, P.B., 2012. Dabrafenib in BRAF-mutated metastatic melanoma: a multicentre, open-label, phase 3 randomised controlled trial. Lancet 380, 358–365. https://doi.org/10.1016/S0140-6736(12)60868-X

Heidorn, S.J., Milagre, C., Whittaker, S., Nourry, A., Niculescu-Duvas, I., Dhomen, N., Hussain, J., Reis-Filho, J.S., Springer, C.J., Pritchard, C., Marais, R., 2010. Kinase-Dead BRAF and Oncogenic RAS Cooperate to Drive Tumor Progression through CRAF. Cell 140, 209–221. https://doi.org/10.1016/j.cell.2009.12.040

Hermeking, H., Rago, C., Schuhmacher, M., Li, Q., Barrett, J.F., Obaya, A.J., O'Connell, B.C., Mateyak, M.K., Tam, W., Kohlhuber, F., Dang, C. V., Sedivy, J.M., Eick, D., Vogelstein, B., Kinzler, K.W., 2000. Identification of CDK4 as a target of c-MYC. Proc. Natl. Acad. Sci. U. S. A. 97, 2229–2234. https://doi.org/10.1073/pnas.050586197

Hochholdinger, F., Baier, G., Nogalo, A., Bauer, B., Grunicke, H.H., Überall, F.,

1999. Novel Membrane-Targeted ERK1 and ERK2 Chimeras Which Act as Dominant Negative, Isotype-Specific Mitogen-Activated Protein Kinase Inhibitors of Ras-Raf-Mediated Transcriptional Activation of c- fos in NIH 3T3 Cells . Mol. Cell. Biol. 19, 8052–8065. https://doi.org/10.1128/mcb.19.12.8052

Holderfield, M., Deuker, M.M., McCormick, F., McMahon, M., 2014. Targeting RAF kinases for cancer therapy: BRAF-mutated melanoma and beyond. Nat. Rev. Cancer 14, 455–67. https://doi.org/10.1038/nrc3760

Holderfield, M., Merritt, H., Chan, J., Wallroth, M., Tandeske, L., Zhai, H., Tellew, J., Hardy, S., Hekmat-Nejad, M., Stuart, D., McCormick, F., Nagel, T., 2013. RAF Inhibitors Activate the MAPK Pathway by Relieving Inhibitory Autophosphorylation. Cancer Cell 23, 594–602. https://doi.org/10.1016/j.ccr.2013.03.033

Holohan, C., Van Schaeybroeck, S., Longley, D.B., Johnston, P.G., 2013. Cancer drug resistance: an evolving paradigm. Nat. Rev. Cancer 13, 714–726. https://doi.org/10.1038/nrc3599

Hrustanovic, G., Olivas, V., Pazarentzos, E., Tulpule, A., Asthana, S., Blakely, C.M., Okimoto, R.A., Lin, L., Neel, D.S., Sabnis, A., Flanagan, J., Chan, E., Varella-Garcia, M., Aisner, D.L., Vaishnavi, A., Ou, S.-H.I., Collisson, E.A., Ichihara, E., Mack, P.C., Lovly, C.M., Karachaliou, N., Rosell, R., Riess, J.W., Doebele, R.C., Bivona, T.G., 2015. RAS-MAPK dependence underlies a rational polytherapy strategy in EML4-ALK-positive lung cancer. Nat. Med. 21, 1038–47. https://doi.org/10.1038/nm.3930

Hsu, S.F., Lee, Y. Bin, Lee, Y.C., Chung, A.L., Apaya, M.K., Shyur, L.F., Cheng, C.F., Ho, F.M., Meng, T.C., 2018. Dual specificity phosphatase DUSP6 promotes endothelial inflammation through inducible expression of ICAM-1. FEBS J. 285, 1593–1610. https://doi.org/10.1111/febs.14425

Huang, C.-Y., Tan, T.-H., 2012. DUSPs, to MAP kinases and beyond. Cell Biosci. 2, 24. https://doi.org/10.1186/2045-3701-2-24

Huse, M., Kuriyan, J., 2002. The conformational plasticity of protein kinases. Cell 109, 275–282. https://doi.org/10.1016/S0092-8674(02)00741-9

Ichikawa, K., Kubota, Y., Nakamura, T., Weng, J.S., Tomida, T., Saito, H., Takekawa, M., 2015. MCRIP1, an ERK Substrate, Mediates ERK-Induced Gene Silencing during Epithelial-Mesenchymal Transition by Regulating the Co-Repressor CtBP. Mol. Cell 58, 35–46. https://doi.org/10.1016/j.molcel.2015.01.023

Jacobs, D., Glossip, D., Xing, H., Muslin, A.J., Kornfeld, K., 1999. Multiple docking sites on substrate proteins form a modular system that mediates recognition by ERK MAP kinase. Genes Dev. 13, 163–175. https://doi.org/10.1101/gad.13.2.163

Jänne, P.A., Van Den Heuvel, M.M., Barlesi, F., Cobo, M., Mazieres, J., Crinò, L., Orlov, S., Blackhall, F., Wolf, J., Garrido, P., Poltoratskiy, A., Mariani, G., Ghiorghiu, D., Kilgour, E., Smith, P., Kohlmann, A., Carlile, D.J., Lawrence, D., Bowen, K., Vansteenkiste, J., 2017. Selumetinib plus docetaxel compared with docetaxel alone and progression-free survival in patients with KRAS-mutant

advanced non-small cell lung cancer: The SELECT-1 randomized clinical trial. JAMA - J. Am. Med. Assoc. 317, 1844–1853. https://doi.org/10.1001/jama.2017.3438

Jeanneteau, F., Deinhardt, K., Miyoshi, G., Bennett, A.M., Chao, M. V, 2010. The MAP kinase phosphatase MKP-1 regulates BDNF-induced axon branching. Nat. Neurosci. 13, 1373–1379. https://doi.org/10.1038/nn.2655

Jeong, D.G., Yoon, T.S., Kim, J.H., Shim, M.Y., Jung, S.K., Son, J.H., Ryu, S.E., Kim, S.J., 2006. Crystal Structure of the Catalytic Domain of Human MAP Kinase Phosphatase 5: Structural Insight into Constitutively Active Phosphatase. J. Mol. Biol. 360, 946–955. https://doi.org/10.1016/j.jmb.2006.05.059

Jin, J., Pawson, T., 2012. Modular evolution of phosphorylation-based signalling systems. Philos. Trans. R. Soc. B Biol. Sci. 367, 2540–2555. https://doi.org/10.1098/rstb.2012.0106

Jin, Z., El-Deiry, W.S., 2005. Overview of cell death signaling pathways. Cancer Biol. Ther. 4, 147–171. https://doi.org/10.4161/cbt.4.2.1508

Johnson, L.N., Lewis, R.J., 2001. Structural basis for control by phosphorylation. Chem. Rev. 101, 2209–2242. https://doi.org/10.1021/cr000225s

Johnson, L.N., Noble, M.E.M., Owen, D.J., 1996. Active and inactive protein kinases: Structural basis for regulation. Cell 85, 149–158. https://doi.org/10.1016/S0092-8674(00)81092-2

Joseph, E.W., Pratilas, C.A., Poulikakos, P.I., Tadi, M., Wang, W., Taylor, B.S., Halilovic, E., Persaud, Y., Xing, F., Viale, A., Tsai, J., Chapman, P.B., Bollag, G., Solit, D.B., Rosen, N., 2010. The RAF inhibitor PLX4032 inhibits ERK signaling and tumor cell proliferation in a V600E BRAF-selective manner. Proc Natl Acad Sci U S A 107, 14903–14908. https://doi.org/10.1073/pnas.1008990107

Karlsson, M., Mandl, M., Keyse, S.M., 2006. Spatio-temporal regulation of mitogen-activated protein kinase (MAPK) signalling by protein phosphatases. Biochem Soc Trans 34, 842–845. https://doi.org/BST0340842 [pii]\n10.1042/BST0340842

Karlsson, M., Mathers, J., Dickinson, R.J., Mandl, M., Keyse, S.M., 2004. Both nuclear-cytoplasmic shuttling of the dual specificity phosphatase MKP-3 and its ability to anchor MAP kinase in the cytoplasm are mediated by a conserved nuclear export signal. J. Biol. Chem. 279, 41882–41891. https://doi.org/10.1074/jbc.M406720200

Karnoub, A.E., Weinberg, R.A., 2008. Ras oncogenes: split personalities. Nat. Rev. Mol. Cell Biol. 9, 517–31. https://doi.org/10.1038/nrm2438

Katagiri, C., Masuda, K., Urano, T., Yamashita, K., Araki, Y., Kikuchi, K., Shima, H., 2005. Phosphorylation of Ser-446 determines stability of MKP-7. J. Biol. Chem. 280, 14716–14722. https://doi.org/10.1074/jbc.M500200200

Kennedy, N.J., Davis, R.J., 2003. Role of JNK in tumor development. Cell Cycle 2, 199–201.

Kidger, A.M., Keyse, S.M., 2016. The regulation of oncogenic Ras/ERK signalling by dual-specificity mitogen activated protein kinase phosphatases (MKPs). Semin. Cell Dev. Biol. 50, 125–132. https://doi.org/10.1016/j.semcdb.2016.01.009

Kidger, A.M., Rushworth, L.K., Stellzig, J., Davidson, J., Bryant, C.J., Bayley, C., Caddye, E., Rogers, T., Keyse, S.M., Caunt, C.J., 2017. Dual-specificity phosphatase 5 controls the localized inhibition, propagation, and transforming potential of ERK signaling. Proc. Natl. Acad. Sci. 114, E317–E326. https://doi.org/10.1073/pnas.1614684114

Kidger, A.M., Sipthorp, J., Cook, S.J., 2018. ERK1/2 inhibitors: New weapons to inhibit the RAS-regulated RAF-MEK1/2-ERK1/2 pathway. Pharmacol. Ther. 187, 45–60. https://doi.org/10.1016/j.pharmthera.2018.02.007

Kondoh, K., Nishida, E., 2007. Regulation of MAP kinases by MAP kinase phosphatases. Biochim. Biophys. Acta - Mol. Cell Res. 1773, 1227–1237. https://doi.org/10.1016/j.bbamcr.2006.12.002

Krishna, M., Narang, H., 2008. The complexity of mitogen-activated protein kinases (MAPKs) made simple. Cell. Mol. Life Sci. 65, 3525–3544. https://doi.org/10.1007/s00018-008-8170-7

Kucharska, A., Rushworth, L.K., Staples, C., Morrice, N. a., Keyse, S.M., 2009a. Regulation of the inducible nuclear dual-specificity phosphatase DUSP5 by ERK MAPK. Cell. Signal. 21, 1794–1805. https://doi.org/10.1016/j.cellsig.2009.07.015

Kyriakis, J.M., Avruch, J., 2001. Mammalian mitogen-activated protein kinase signal transduction pathways activated by stress and inflammation. Physiol. Rev. 81, 807–869. https://doi.org/10.1152/physrev.2001.81.2.807

Lai, A.Z., Cory, S., Zhao, H., Gigoux, M., Monast, A., Guiot, M.-C., Huang, S., Tofigh, A., Thompson, C., Naujokas, M., Marcus, V. a., Bertos, N., Sehat, B., Perera, R.M., Bell, E.S., Page, B.D.G., Gunning, P.T., Ferri, L.E., Hallett, M., Park, M., 2014a. Dynamic Reprogramming of Signaling Upon Met Inhibition Reveals a Mechanism of Drug Resistance in Gastric Cancer. Sci. Signal. 7, ra38–ra38. https://doi.org/10.1126/scisignal.2004839

Lake, D., Corrêa, S.A.L., Müller, J., 2016. Negative feedback regulation of the ERK1/2 MAPK pathway. Cell. Mol. Life Sci. 73, 4397–4413. https://doi.org/10.1007/s00018-016-2297-8

Lampaki, S., Lazaridis, G., Zarogoulidis, K., Kioumis, I., Papaiwannou, A., Tsirgogianni, K., Karavergou, A., Tsiouda, T., Karavasilis, V., Yarmus, L., Darwiche, K., Freitag, L., Sakkas, A., Kantzeli, A., Baka, S., Hohenforst-Schmidt, W., Zarogoulidis, P., 2015. Defining the role of tyrosine kinase inhibitors in early stage non-small cell lung cancer. J. Cancer 6, 568–574. https://doi.org/10.7150/jca.11893

Lavoie, H., Therrien, M., 2015. Regulation of RAF protein kinases in ERK signalling. Nat. Rev. Mol. Cell Biol. 16, 281–298. https://doi.org/10.1038/nrm3979

Lefloch, R., Pouyssegur, J., Lenormand, P., 2008. Single and Combined Silencing of ERK1 and ERK2 Reveals Their Positive Contribution to Growth Signaling

Depending on Their Expression Levels. Mol. Cell. Biol. 28, 511–527. https://doi.org/10.1128/mcb.00800-07

Lehr, S., Kotzka, J., Avci, H., Sickmann, A., Meyer, H.E., Herkner, A., Muller-Wieland, D., 2004. Identification of major ERK-related phosphorylation sites in Gab1. Biochemistry 43, 12133–12140. https://doi.org/10.1021/bi049753e

Lemmon, M.A., Schlessinger, J., 2010. Cell signaling by receptor tyrosine kinases. Cell 141, 1117–1134. https://doi.org/10.1016/j.cell.2010.06.011

Ley, R., Balmanno, K., Hadfield, K., Weston, C., Cook, S.J., 2003. Activation of the ERK1/2 signaling pathway promotes phosphorylation and proteasome-dependent degradation of the BH3-only protein, Bim. J. Biol. Chem. 278, 18811–18816. https://doi.org/10.1074/jbc.M301010200

Li, C., Scott, D.A., Hatch, E., Tian, X., Mansour, S.L., 2007. Dusp6 (Mkp3) is a negative feedback regulator of FgF-stimulated ERK signaling during mouse development. Development 134, 167–176. https://doi.org/10.1242/dev.02701

Lin, Y.W., Chuang, S.M., Yang, J.L., 2003. ERK1/2 achieves sustained activation by stimulating MAPK phosphatase-1 degradation via the ubiquitin-proteasome pathway. J. Biol. Chem. 278, 21534–21541. https://doi.org/10.1074/jbc.M301854200

Lito, P., Saborowski, A., Yue, J., Solomon, M., Joseph, E., Gadal, S., Saborowski, M., Kastenhuber, E., Fellmann, C., Ohara, K., Morikami, K., Miura, T., Lukacs, C., Ishii, N., Lowe, S., Rosen, N., 2014. Disruption of CRAF-mediated MEK activation is required for effective MEK inhibition in KRAS mutant tumors. Cancer Cell 25, 697–710. https://doi.org/10.1016/j.ccr.2014.03.011

Little, A S, Balmanno, K., Sale, M.J., Newman, S., Dry, J.R., Hampson, M., Edwards, P.A., Smith, P.D., Cook, S.J., 2011. Amplification of the driving oncogene, KRAS or BRAF, underpins acquired resistance to MEK1/2 inhibitors in colorectal cancer cells. Sci Signal 4, ra17. https://doi.org/10.1126/scisignal.2001752

Liu, Y.L., Lai, F., Wilmott, J.S., Yan, X.G., Liu, X.Y., Luan, Q., Guo, S.T., Jiang, C.C., Tseng, H.Y., Scolyer, R.A., Jin, L., Zhang, X.D., 2014. Noxa upregulation by oncogenic activation of MEK/ERK through CREB promotes autophagy in human melanoma cells. Oncotarget 5, 11237–11251.

Loew, R., Heinz, N., Hampf, M., Bujard, H., Gossen, M., 2010. Improved Tet-responsive promoters with minimized background expression. BMC Biotechnol. 10, 1–13. https://doi.org/10.1186/1472-6750-10-81

Lu, Z., Xu, S., 2006. ERK1/2 MAP kinases in cell survival and apoptosis. IUBMB Life 58, 621–631. https://doi.org/10.1080/15216540600957438

Maloney, L., Kane, K., Eckhardt, S.G., Simmons, H., Adjei, A.A., Wilson, D., Poch, G., Leong, S., Morris, C., Molina, J.R., Gore, L., Chow, L., Gordon, G., Franklin, W., Litwiler, K., Marlow, A., Haney, J., Cohen, R.B., Brown, S., Hanson, L.J., 2008. Phase I Pharmacokinetic and Pharmacodynamic Study of the Oral, Small-Molecule Mitogen-Activated Protein Kinase Kinase 1/2 Inhibitor

AZD6244 (ARRY-142886) in Patients With Advanced Cancers. J. Clin. Oncol. 26, 2139–2146. https://doi.org/10.1200/jco.2007.14.4956

Mandl, M., Slack, D.N., Keyse, S.M., 2005. Specific Inactivation and Nuclear Anchoring of Extracellular Signal-Regulated Kinase 2 by the Inducible Dual-Specificity Protein Phosphatase DUSP5. Mol. Cell. Biol. 25, 1830–1845. https://doi.org/10.1128/MCB.25.5.1830-1845.2005

Marchetti, S., Gimond, C., Touboul, T., Roux, D., Pagès, G., 2005. Extracellular signal-regulated kinases phosphorylate mitogen-activated protein kinase phosphatase 3 / DUSP6 at serines 159 and 197 , two sites critical for its proteasomal degradation. Mol Cell Biol 25, 854–864. https://doi.org/10.1128/MCB.25.2.854

Marshall, C.., 1995. Specificity of receptor tyrosine kinase signaling: Transient versus sustained extracellular signal-regulated kinase activation. Cell 80, 179–185. https://doi.org/10.1016/0092-8674(95)90401-8

Matsubayashi, Y., Fukuda, M., Nishida, E., 2001. Evidence for Existence of a Nuclear Pore Complex-mediated, Cytosol-independent Pathway of Nuclear Translocation of ERK MAP Kinase in Permeabilized Cells. J. Biol. Chem. 276, 41755–41760. https://doi.org/10.1074/jbc.M106012200

McKay, M.M., Morrison, D.K., 2007. Integrating signals from RTKs to ERK/MAPK. Oncogene 26, 3113–21. https://doi.org/10.1038/sj.onc.1210394

Meharena, H.S., Chang, P., Keshwani, M.M., Oruganty, K., Nene, A.K., Kannan, N., Taylor, S.S., Kornev, A.P., 2013. Deciphering the Structural Basis of Eukaryotic Protein Kinase Regulation. PLoS Biol. 11. https://doi.org/10.1371/journal.pbio.1001680

Meloche, S., Pouysségur, J., 2007. The ERK1/2 mitogen-activated protein kinase pathway as a master regulator of the G1- to S-phase transition. Oncogene 26, 3227–39. https://doi.org/10.1038/sj.onc.1210414

Mendoza, M.C., Er, E.E., Blenis, J., 2011. The Ras-ERK and PI3K-mTOR pathways: cross-talk and compensation. Trends Biochem. Sci. 36, 320–328. https://doi.org/10.1016/j.tibs.2011.03.006

Messina, S., Frati, L., Leonetti, C., Zuchegna, C., Di Zazzo, E., Calogero, A., Porcellini, A., 2011. Dual-specificity phosphatase DUSP6 has tumor-promoting properties in human glioblastomas. Oncogene 30, 3813–20. https://doi.org/10.1038/onc.2011.99

Mitin, N., Rossman, K.L., Der, C.J., 2005. Signaling interplay in ras superfamily function. Curr. Biol. 15, 563–574. https://doi.org/10.1016/j.cub.2005.07.010

Montero-Conde, C., Ruiz-Llorente, S., Dominguez, J.M., Knauf, J.A., Viale, A., Sherman, E.J., Ryder, M., Ghossein, R.A., Rosen, N., Fagin, J.A., 2013. Relief of feedback inhibition of HER3 transcription by RAF and MEK inhibitors attenuates their antitumor effects in BRAF-mutant thyroid carcinomas. Cancer Discov. 3, 520–33. https://doi.org/10.1158/2159-8290.CD-12-0531

Morrison, D.K., Davis, R.J., 2003. Regulation of MAP kinase signaling modules by

scaffold proteins in mammals. Annu. Rev. Cell Dev. Biol. 19, 91–118. https://doi.org/10.1146/annurev.cellbio.19.111401.091942

Muda, M., Theodosiou, A., Rodrigues, N., Boschert, U., Camps, M., Gillieron, C., Davies, K., Ashworth, A., Arkinstall, S., 1996. The Dual Specificity Phosphatases M3/6 and MKP-3 Are Highly Selective for Inactivation of Distinct Mitogen-activated Protein Kinases. J. Biol. Chem. 271, 27205–27208. https://doi.org/10.1074/jbc.271.44.27205

Murphy, L.O., Blenis, J., 2006. MAPK signal specificity: the right place at the right time. Trends Biochem. Sci. 31, 268–275. https://doi.org/10.1016/j.jsg.2005.10.009

Murphy, L.O., Smith, S., Chen, R.H., Fingar, D.C., Blenis, J., 2002. Molecular, interpretation of ERK signal duration by immediate early gene products. Nat. Cell Biol. 4, 556–564. https://doi.org/10.1038/ncb822

Nguyen, A., Burack, W.R., Stock, J.L., Kortum, R., Chaika, O. V., Afkarian, M., Muller, W.J., Murphy, K.M., Morrison, D.K., Lewis, R.E., McNeish, J., Shaw, A.S., 2002. Kinase Suppressor of Ras (KSR) Is a Scaffold Which Facilitates Mitogen-Activated Protein Kinase Activation In Vivo. Mol. Cell. Biol. 22, 3035–3045. https://doi.org/10.1128/mcb.22.9.3035-3045.2002

Nguyen, T.T., Scimeca, J.C., Filloux, C., Peraldi, P., Carpentier, J.L., Van Obberghen, E., 1993. Co-regulation of the mitogen-activated protein kinase, extracellular signal-regulated kinase 1, and the 90-kDa ribosomal S6 kinase in PC12 cells. Distinct effects of the neurotrophic factor, nerve growth factor, and the mitogenic factor, epidermal growth . J. Biol. Chem. 268, 9803–9810.

Nichols, A., Camps, M., Gillieron, C., Chabert, C., Brunet, A., Wilsbacher, J., Cobb, M., Pouyssegur, J., Shaw, J.P., Arkinstall, S., 2000. Substrate recognition domains within extracellular signal-regulated kinase mediate binding and catalytic activation of mitogen-activated protein kinase phosphatase-3. J. Biol. Chem. 275, 24613–24621. https://doi.org/10.1074/jbc.M001515200

Nunes-Xavier, C.E., Tárrega, C., Cejudo-Marín, R., Frijhoff, J., Sandin, Å., Östman, A., Pulido, R., 2010. Differential up-regulation of MAP kinase phosphatases MKP3/DUSP6 and DUSP5 by Ets2 and c-Jun converge in the control of the growth arrest versus proliferation response of MCF-7 breast cancer cells to phorbol ester. J. Biol. Chem. 285, 26417–26430. https://doi.org/10.1074/jbc.M110.121830

Okudela, K., Yazawa, T., Woo, T., Sakaeda, M., Ishii, J., Mitsui, H., Shimoyamada, H., Sato, H., Tajiri, M., Ogawa, N., Masuda, M., Takahashi, T., Sugimura, H., Kitamura, H., 2009. Down-regulation of DUSP6 expression in lung cancer: its mechanism and potential role in carcinogenesis. Am. J. Pathol. 175, 867–881. https://doi.org/10.2353/ajpath.2009.080489

Olson, J.M., Hallahan, A.R., 2004. p38 MAP kinase: A convergence point in cancer therapy. Trends Mol. Med. 10, 125–129. https://doi.org/10.1016/j.molmed.2004.01.007

Orton, R.J., Sturm, O.E., Vyshemirsky, V., Calder, M., Gilbert, D.R., Kolch, W., 2005. Computational modelling of the receptor-tyrosine-kinase-activated MAPK

pathway. Biochem. J. 392, 249–261. https://doi.org/10.1042/BJ20050908

Owens, D.M., Keyse, S.M., 2007. Differential regulation of MAP kinase signalling by dual-specificity protein phosphatases. Oncogene 26, 3203–3213. https://doi.org/10.1038/sj.onc.1210412

Packer, L.M., East, P., Reis-Filho, J.S., Marais, R., 2009. Identification of direct transcriptional targets of V600EBRAF/ MEK signalling in melanoma. Pigment Cell Melanoma Res. 22, 785–798. https://doi.org/10.1111/j.1755-148X.2009.00618.x

Pearson, G., Robinson, F., Beers Gibson, T., Xu, B.E., Karandikar, M., Berman, K., Cobb, M.H., 2001. Mitogen-activated protein (MAP) kinase pathways: regulation and physiological functions. Endocr. Rev. 22, 153–183. https://doi.org/10.1210/edrv.22.2.0428

Perlson, E., Michaelevski, I., Kowalsman, N., Ben-Yaakov, K., Shaked, M., Seger, R., Eisenstein, M., Fainzilber, M., 2006. Vimentin Binding to Phosphorylated Erk Sterically Hinders Enzymatic Dephosphorylation of the Kinase. J. Mol. Biol. 364, 938–944. https://doi.org/10.1016/j.jmb.2006.09.056

Phuchareon, J., McCormick, F., Eisele, D.W., Tetsu, O., 2015. EGFR inhibition evokes innate drug resistance in lung cancer cells by preventing Akt activity and thus inactivating Ets-1 function. Proc. Natl. Acad. Sci. U. S. A. 112, E3855-63. https://doi.org/10.1073/pnas.1510733112

Picco, G., Russo, M., Bardelli, A., Valtorta, E., Linnebacher, M., Di Nicolantonio, F., Cancelliere, C., Martinoglio, B., Lamba, S., Siena, S., Sartore-Bianchi, A., Cordero, F., Corti, G., Veronese, S., Buscarino, M., Mottolese, M., Beccuti, M., Isella, C., Medico, E., 2015. The molecular landscape of colorectal cancer cell lines unveils clinically actionable kinase targets. Nat. Commun. 6, 1–10. https://doi.org/10.1038/ncomms8002

Pop, C., Salvesen, G.S., 2009. Human caspases: Activation, specificity, and regulation. J. Biol. Chem. 284, 21777–21781. https://doi.org/10.1074/jbc.R800084200

Pouyssegur, J., Volmat, V., Lenormand, P., 2002. Fidelity and spatio-temporal control in MAP kinase (ERKs) signalling. Biochem Pharmacol 64, 755–763. https://doi.org/10.1016/S0006-2952(02)01135-8

Pratilas, C.A., Taylor, B.S., Ye, Q., Viale, A., Sander, C., Solit, D.B., Rosen, N., 2009. (V600E)BRAF is associated with disabled feedback inhibition of RAF-MEK signaling and elevated transcriptional output of the pathway. Proc Natl Acad Sci U S A 106, 4519–4524. https://doi.org/10.1073/pnas.0900780106

Pulido, R., Zúñiga, Á., Ullrich, A., 1998. PTP-SL and STEP protein tyrosine phosphatases regulate the activation of the extracellular signal-regulated kinases ERK1 and ERK2 by association through a kinase interaction motif. EMBO J. 17, 7337–7350. https://doi.org/10.1093/emboj/17.24.7337

Ramos, J. W, 2008. The regulation of extracellular signal-regulated kinase (ERK) in mammalian cells. Int. J. Biochem. Cell Biol. 40, 2707–2719. https://doi.org/10.1016/j.biocel.2008.04.009

Ranganathan, A., Yazicioglu, M.N., Cobb, M.H., 2006. The nuclear localization of ERK2 occurs by mechanisms both independent of and dependent on energy. J. Biol. Chem. 281, 15645–15652. https://doi.org/10.1074/jbc.M513866200

Reszka, A.A., Bulinski, J.C., Krebs, E.G., Fischer, E.H., 1997. Mitogen-activated protein kinase/extracellular signal-regulated kinase 2 regulates cytoskeletal organization and chemotaxis via catalytic and microtubule-specific interactions. Mol. Biol. Cell 8, 1219–1232. https://doi.org/10.1091/mbc.8.7.1219

Robinson, M.J., Stippec, S. a, Goldsmith, E., White, M. a, Cobb, M.H., 1998. A constitutively active and nuclear form of the MAP kinase ERK2 is sufficient for neurite outgrowth and cell transformation. Curr. Biol. 8, 1141–1150. https://doi.org/10.1016/S0960-9822(07)00485-X

Rosenbaum, D.M., Rasmussen, S.G.F., Kobilka, B.K., 2009. The structure and function of G-protein-coupled receptors. Nature 459, 356–363. https://doi.org/10.1038/nature08144

Roskoski, R., 2012. MEK1/2 dual-specificity protein kinases: Structure and regulation. Biochem. Biophys. Res. Commun. 417, 5–10. https://doi.org/10.1016/j.bbrc.2011.11.145

Rousseau, D., Kaspar, R., Rosenwald, I., Gehrke, L., Sonenberg, N., 1996. Translation initiation of ornithine decarboxylase and nucleocytoplasmic transport of cyclin D1 mRNA are increased in cells overexpressing eukaryotic initiation factor 4E. Proc. Natl. Acad. Sci. U. S. A. 93, 1065–1070. https://doi.org/10.1073/pnas.93.3.1065

Rushworth, L.K., Hindley, A.D., Neill, E.O., Kolch, W., 2006. Regulation and Role of Raf-1 / B-Raf Heterodimerization. Mol Cell Biol 26, 2262–2272. https://doi.org/10.1128/MCB.26.6.2262

Rushworth, L. K, Kidger, A.M., Delavaine, L., Stewart, G., van Schelven, S., Davidson, J., Bryant, C.J., Caddye, E., East, P., Caunt, C.J., Keyse, S.M., 2014. Dual-specificity phosphatase 5 regulates nuclear ERK activity and suppresses skin cancer by inhibiting mutant Harvey-Ras (HRasQ61L)-driven SerpinB2 expression. Proc. Natl. Acad. Sci. U. S. A. 111, 18267–72. https://doi.org/10.1073/pnas.1420159112

Russo, A., Franchina, T., Ricciardi, G.R.R., Picone, A., Ferraro, G., Zanghì, M., Toscano, G., Giordano, A., Adamo, V., 2015. A decade of EGFR inhibition in EGFR-mutated non small cell lung cancer (NSCLC): Old successes and future perspectives. Oncotarget 6, 26814–25. https://doi.org/10.18632/oncotarget.4254

Sale, M.J., Balmanno, K., Saxena, J., Ozono, E., Wojdyla, K., McIntyre, R.E., Gilley, R., Woroniuk, A., Howarth, K.D., Hughes, G., Dry, J.R., Arends, M.J., Caro, P., Oxley, D., Ashton, S., Adams, D.J., Saez-Rodriguez, J., Smith, P.D., Cook, S.J., 2019. MEK1/2 inhibitor withdrawal reverses acquired resistance driven by BRAFV600E amplification whereas KRASG13D amplification promotes EMT-chemoresistance. Nat. Commun. 10, 2030. https://doi.org/10.1038/s41467-019-09438-w

Sale, M.J., Cook, S.J., 2014. Intrinsic and acquired resistance to MEK1/2 inhibitors in

cancer. Biochem. Soc. Trans. 42, 776–83. https://doi.org/10.1042/BST20140129

Sale, M.J., Cook, S.J., 2013. That which does not kill me makes me stronger; Combining ERK1/2 pathway inhibitors and BH3 mimetics to kill tumour cells and prevent acquired resistance. Br. J. Pharmacol. 169, 1708–1722. https://doi.org/10.1111/bph.12220

Sale, M.J., Cook, S.J., 2012. The BH3 mimetic ABT-263 synergizes with the MEK1/2 inhibitor selumetinib/AZD6244 to promote BIM-dependent tumour cell death and inhibit acquired resistance. Biochem. J. 450, 285–294. https://doi.org/10.1042/bj20121212

Samatar, A. a., Poulikakos, P.I., 2014. Targeting RAS–ERK signalling in cancer: promises and challenges. Nat. Rev. Drug Discov. 13, 928–942. https://doi.org/10.1038/nrd4281

Scheid, M.P., Schubert, K.M., Duronio, V., 1999. Regulation of bad phosphorylation and association with Bcl-x(L) by the MAPK/Erk kinase. J. Biol. Chem. 274, 31108–31113. https://doi.org/10.1074/jbc.274.43.31108

Seternes, O.M., Kidger, A.M., Keyse, S.M., 2019. Dual-specificity MAP kinase phosphatases in health and disease. Biochim. Biophys. Acta - Mol. Cell Res. 1866, 124–143. https://doi.org/10.1016/j.bbamcr.2018.09.002

Sewing, A., Wiseman, B., Lloyd, A.C., Land, H., 1997. High-intensity Raf signal causes cell cycle arrest mediated by p21Cip1. Mol. Cell. Biol. 17, 5588–97.

Shao, Y., Aplin, A.E., 2012. ERK2 phosphorylation of serine 77 regulates Bmf pro-apoptotic activity. Cell Death Dis. 3, 1–10. https://doi.org/10.1038/cddis.2011.137

She, Q.B., Wei-Ya, M., Zhong, S., Dong, Z., 2002. Activation of JNK1, RSK2, and MSK1 is involved in serine 112 phosphorylation of Bad by ultraviolet B radiation. J. Biol. Chem. 277, 24039–24048. https://doi.org/10.1074/jbc.M109907200

Sheridan, C., Brumatti, G., Elgendy, M., Brunet, M., Martin, S.J., 2010. An ERK-dependent pathway to Noxa expression regulates apoptosis by platinum-based chemotherapeutic drugs. Oncogene 29, 6428–6441. https://doi.org/10.1038/onc.2010.380

Shieh, J.M., Huang, T.F., Hung, C.F., Chou, K.H., Tsai, Y.J., Wu, W. Bin, 2010. Activation of c-Jun N-terminal kinase is essential for mitochondrial membrane potential change and apoptosis induced by doxycycline in melanoma cells. Br. J. Pharmacol. 160, 1171–1184. https://doi.org/10.1111/j.1476-5381.2010.00746.x

Shin, S., Dimitri, C.A., Yoon, S.O., Dowdle, W., Blenis, J., 2010. ERK2 but Not ERK1 Induces Epithelial-to-Mesenchymal Transformation via DEF Motif-Dependent Signaling Events. Mol. Cell 38, 114–127. https://doi.org/10.1016/j.molcel.2010.02.020

Shin, S.H., Park, S.Y., Kang, G.H., 2013. Down-regulation of dual-specificity phosphatase 5 in gastric cancer by promoter CpG island hypermethylation and

its potential role in carcinogenesis. Am. J. Pathol. 182, 1275–1285. https://doi.org/10.1016/j.ajpath.2013.01.004

Shojaee, S., Caeser, R., Buchner, M., Park, E., Swaminathan, S., Hurtz, C., Geng, H., Chan, L.N., Klemm, L., Hofmann, W.K., Qiu, Y.H., Zhang, N., Coombes, K.R., Paietta, E., Molkentin, J., Koeffler, H.P., Willman, C.L., Hunger, S.P., Melnick, A., Kornblau, S.M., Müschen, M., 2015. Erk Negative Feedback Control Enables Pre-B Cell Transformation and Represents a Therapeutic Target in Acute Lymphoblastic Leukemia. Cancer Cell 28, 114–128. https://doi.org/10.1016/j.ccell.2015.05.008

Slack, D.N., Seternes, O.M., Gabrielsen, M., Keyse, S.M., 2001. Distinct Binding Determinants for ERK2/p38α and JNK MAP Kinases Mediate Catalytic Activation and Substrate Selectivity of MAP Kinase Phosphatase-1. J. Biol. Chem. 276, 16491–16500. https://doi.org/10.1074/jbc.M010966200

Smith, P.D., Cartlidge, S., Logie, A., Davies, B.R., Cockerill, M., Jenkins, R., Steele, S., Martin, P., McKay, J.S., 2007. AZD6244 (ARRY-142886), a potent inhibitor of mitogen-activated protein kinase/extracellular signal-regulated kinase kinase 1/2 kinases: mechanism of action in vivo, pharmacokinetic/pharmacodynamic relationship, and potential for combination in preclinical. Mol. Cancer Ther. 6, 2209–2219. https://doi.org/10.1158/1535-7163.mct-07-0231

Soda, M., Choi, Y.L., Enomoto, M., Takada, S., Yamashita, Y., Ishikawa, S., Fujiwara, S., Watanabe, H., Kurashina, K., Hatanaka, H., Bando, M., Ohno, S., Ishikawa, Y., Aburatani, H., Niki, T., Sohara, Y., Sugiyama, Y., Mano, H., 2007. Identification of the transforming EML4-ALK fusion gene in non-small-cell lung cancer. Nature 448, 561–566. https://doi.org/10.1038/nature05945

Soloaga, A., Thomson, S., Wiggin, G.R., Rampersaud, N., Dyson, M.H., Hazzalin, C.A., Mahadevan, L.C., Arthur, J.S.C., 2003. MSK2 and MSK1 mediate the mitogen- and stress-induced phosphorylation of histone H3 and HMG-14. EMBO J. 22, 2788–2797. https://doi.org/10.1093/emboj/cdg273

Song, Y., Gale, C.-M., Cappuzzo, F., Engelman, J.A., Mok, T., Johnson, B.E., Cantley, L.C., Park, J.O., Holmes, A.J., Janne, P.A., Zejnullahu, K., Zhao, X., Mitsudomi, T., Lee, C., Christensen, J., Kosaka, T., Hyland, C., Lindeman, N., Rogers, A.M., 2007. MET Amplification Leads to Gefitinib Resistance in Lung Cancer by Activating ERBB3 Signaling. Science (80-.). 316, 1039–1043. https://doi.org/10.1126/science.1141478

Staples, C.J., Owens, D.M., Maier, J. V., Cato, A.C.B., Keyse, S.M., 2010. Cross-talk between the p38α and JNK MAPK pathways mediated by MAP kinase phosphatase-1 determines cellular sensitivity to UV radiation. J. Biol. Chem. 285, 25928–25940. https://doi.org/10.1074/jbc.M110.117911

Stefanovsky, V., Langlois, F., Gagnon-Kugler, T., Rothblum, L.I., Moss, T., 2006. Growth factor signaling regulates elongation of RNA polymerase I transcription in mammals via UBF phosphorylation and r-chromatin remodeling. Mol. Cell 21, 629–639. https://doi.org/10.1016/j.molcel.2006.01.023

Tanoue, T., Adachi, M., Moriguchi, T., Nishida, E., 2000. A conserved docking motif in MAP kinases common to substrates, activators and regulators. Nat. Cell Biol. 2, 110–116. https://doi.org/10.1038/35000065

Tanoue, T., Maeda, R., Adachi, M., Nishida, E., 2001. Identification of a docking groove on ERK and p38 MAP kinases that regulates the specificity of docking interactions. EMBO J. 20, 466–479. https://doi.org/10.1093/emboj/20.3.466

Tanoue, T., Moriguchi, T., Nishida, E., 1999. Molecular cloning and characterization of a novel dual specificity phosphatase, MKP-5. J. Biol. Chem. 274, 19949–19956. https://doi.org/10.1074/jbc.274.28.19949

Tanoue, T., Yamamoto, T., Nishida, E., 2002. Modular structure of a docking surface on MAPK phosphatases. J. Biol. Chem. 277, 22942–22949. https://doi.org/10.1074/jbc.M202096200

Tebbutt, N.C., Tögel, L., Mariadason, J.M., Dhillon, A.S., Chatterton, Z., Arango, D., Chüeh, A.C., Murone, C., Chionh, F., Al-Obaidi, S., Wu, R., Luk, I., Sieber, O.M., Dávalos-Salas, M., Williams, D., Nightingale, R., Buchanan, D.D., 2018. DUSP5 is methylated in CIMP-high colorectal cancer but is not a major regulator of intestinal cell proliferation and tumorigenesis. Sci. Rep. 8, 1–11. https://doi.org/10.1038/s41598-018-20176-9

Tetsu, O., McCormick, F., 2003. Proliferation of cancer cells despite CDK2 inhibition. Cancer Cell 3, 233–245. https://doi.org/10.1016/S1535-6108(03)00053-9

Theodosiou, A., Ashworth, A., 2002. Protein family review MAP kinase phosphatases Gene organization and evolutionary history. Genome Biol. 1–10. https://doi.org/https://doi.org/10.1186/gb-2002-3-7-reviews3009

Thiery, J.P., Acloque, H., Huang, R.Y.J., Nieto, M.A., 2009. Epithelial-Mesenchymal Transitions in Development and Disease. Cell 139, 871–890. https://doi.org/10.1016/j.cell.2009.11.007

Torii, S., Kusakabe, M., Yamamoto, T., Maekawa, M., Nishida, E., 2004. Sef is a spatial regulator for Ras/MAP kinase signaling. Dev. Cell 7, 33–44. https://doi.org/10.1016/j.devcel.2004.05.019

Torii, S., Yamamoto, T., Tsuchiya, Y., Nishida, E., 2006. ERK MAP kinase in G1 cell cycle progression and cancer. Cancer Sci. 97, 697–702. https://doi.org/10.1111/j.1349-7006.2006.00244.x

Townsend, K.J., Zhou, P., Qian, L., Bieszczad, C.K., Lowrey, C.H., Yen, A., Craig, R.W., 1999. Regulation of MCL1 through a serum response factor/elk-1-mediated mechanism links expression of a viability-promoting member of the BCL2 family to the induction of hematopoietic cell differentiation. J. Biol. Chem. 274, 1801–1813. https://doi.org/10.1074/jbc.274.3.1801

VanBrocklin, M.W., Verhaegen, M., Soengas, M.S., Holmen, S.L., 2009. Mitogen-activated protein kinase inhibition induces translocation of bmf to promote apoptosis in melanoma. Cancer Res. 69, 1985–1994. https://doi.org/10.1158/0008-5472.CAN-08-3934

Vartanian, S., Bentley, C., Brauer, M.J., Li, L., Shirasawa, S., Sasazuki, T., Kim, J.S., Haverty, P., Stawiski, E., Modrusan, Z., Waldman, T., Stokoe, D., 2013. Identification of mutant K-Ras-dependent phenotypes using a panel of isogenic cell lines. J. Biol. Chem. 288, 2403–2413. https://doi.org/10.1074/jbc.M112.394130

Villanueva, J., Infante, J.R., Krepler, C., Reyes-Uribe, P., Samanta, M., Chen, H.-Y., Li, B., Swoboda, R.K., Wilson, M., Vultur, A., Fukunaba-Kalabis, M., Wubbenhorst, B., Chen, T.Y., Liu, Q., Sproesser, K., DeMarini, D.J., Gilmer, T.M., Martin, A.-M., Marmorstein, R., Schultz, D.C., Speicher, D.W., Karakousis, G.C., Xu, W., Amaravadi, R.K., Xu, X., Schuchter, L.M., Herlyn, M., Nathanson, K.L., 2013. Concurrent MEK2 Mutation and BRAF Amplification Confer Resistance to BRAF and MEK Inhibitors in Melanoma. Cell Rep. 4, 1090–1099. https://doi.org/10.1016/j.celrep.2013.08.023

Volmat, V., Camps, M., Arkinstall, S., Pouysségur, J., Lenormand, P., 2001. The nucleus, a site for signal termination by sequestration and inactivation of p42/p44 MAP kinases. J. Cell Sci. 114, 3433–3443.

von Kriegsheim, A., Baiocchi, D., Birtwistle, M., Sumpton, D., Bienvenut, W., Morrice, N., Yamada, K., Lamond, A., Kalna, G., Orton, R., Gilbert, D., Kolch, W., Kriegsheim, A. Von, Baiocchi, D., Birtwistle, M., Sumpton, D., Bienvenut, W., Morrice, N., Yamada, K., Lamond, A., Kalna, G., Orton, R., Gilbert, D., Kolch, W., von Kriegsheim, A., Baiocchi, D., Birtwistle, M., Sumpton, D., Bienvenut, W., Morrice, N., Yamada, K., Lamond, A., Kalna, G., Orton, R., Gilbert, D., Kolch, W., 2009. Cell fate decisions are specified by the dynamic ERK interactome. Nat. Cell Biol. 11, 1458–1464. https://doi.org/10.1038/ncb1994

Waha, Anke, Felsberg, J., Hartmann, W., Von Dem Knesebeck, A., Mikeska, T., Joos, S., Wolter, M., Koch, A., Yan, P.S., Endl, E., Wiestler, O.D., Reifenberger, G., Pietsch, T., Waha, Andreas, 2010. Epigenetic downregulation of mitogen-activated protein kinase phosphatase MKP-2 relieves its growth suppressive activity in glioma cells. Cancer Res. 70, 1689–1699. https://doi.org/10.1158/0008-5472.CAN-09-3218

Wan, P.T.C., Garnett, M.J., Roe, S.M., Lee, S., Niculescu-Duvaz, D., Good, V.M., Project, C.G., Jones, C.M., Marshall, C.J., Springer, C.J., Barford, D., Marais, R., 2004. Mechanism of activation of the RAF-ERK signaling pathway by oncogenic mutations of B-RAF. Cell 116, 855–867. https://doi.org/10.1016/S0092-8674(04)00215-6

Waskiewicz, A.J., Johnson, J.C., Penn, B., Mahalingam, M., Kimball, S.R., Cooper, J.A., 1999. Phosphorylation of the Cap-Binding Protein Eukaryotic Translation Initiation Factor 4E by Protein Kinase Mnk1 In Vivo. Mol. Cell. Biol. 19, 1871–1880. https://doi.org/10.1128/mcb.19.3.1871

Whitehurst, A.W., Wilsbacher, J.L., You, Y., Luby-Phelps, K., Moore, M.S., Cobb, M.H., 2002. ERK2 enters the nucleus by a carrier-independent mechanism. Proc. Natl. Acad. Sci. U. S. A. 99, 7496–7501. https://doi.org/10.1073/pnas.112495999

Wickenden, J.A., Jin, H., Johnson, M., Gillings, A.S., Newson, C., Austin, M., Chell, S.D., Balmanno, K., Pritchard, C.A., Cook, S.J., 2008. Colorectal cancer cells with the BRAF(V600E) mutation are addicted to the ERK1/2 pathway for growth factor-independent survival and repression of BIM. Oncogene 27, 7150–7161. https://doi.org/10.1038/onc.2008.335

Woods, D., Parry, D., Cherwinski, H., Bosch, E., Lees, E., McMahon, M., 1997a. Raf-induced proliferation or cell cycle arrest is determined by the level of Raf

activity with arrest mediated by p21Cip1. Mol. Cell. Biol. 17, 5598–5611.

Wu, J., Liu, T., Xie, J., Xin, F., Guo, L., 2006. Mitochondria and calpains mediate caspase-dependent apoptosis induced by doxycycline in HeLa cells. Cell. Mol. Life Sci. 63, 949–957. https://doi.org/10.1007/s00018-005-5565-6

Wu, J.J., Zhang, L., Bennett, A.M., 2005. The Noncatalytic Amino Terminus of Mitogen-Activated Protein Kinase Phosphatase 1 Directs Nuclear Targeting and Serum Response Element Transcriptional Regulation. Mol. Cell. Biol. 25, 4792–4803. https://doi.org/10.1128/mcb.25.11.4792-4803.2005

Wu, Z., Xiao, G., Xu, H., Wu, Z., Jiao, P., Huang, X., Feng, B., Feng, Y., Yang, S., 2010. gluconeogenesis through dephosphorylation of forkhead box O1 in mice Find the latest version : MAPK phosphatase – 3 promotes hepatic gluconeogenesis through dephosphorylation of forkhead box O1 in mice. Mol. Cell. Endocrinol. 120, 3901–3911. https://doi.org/10.1172/JCI43250.inducing

Yamamoto, T., Ebisuya, M., Ashida, F., Okamoto, K., Yonehara, S., Nishida, E., 2006. Continuous ERK Activation Downregulates Antiproliferative Genes throughout G1 Phase to Allow Cell-Cycle Progression. Curr. Biol. 16, 1171–1182. https://doi.org/10.1016/j.cub.2006.04.044

Yang, J.Y., Zong, C.S., Xia, W., Yamaguchi, H., Ding, Q., Xie, X., Lang, J.Y., Lai, C.C., Chang, C.J., Huang, W.C., Huang, H., Kuo, H.P., Lee, D.F., Li, L.Y., Lien, H.C., Cheng, X., Chang, K.J., Hsiao, C.D., Tsai, F.J., Tsai, C.H., Sahin, A.A., Muller, W.J., Mills, G.B., Yu, D., Hortobagyi, G.N., Hung, M.C., 2008. ERK promotes tumorigenesis by inhibiting FOXO3a via MDM2-mediated degradation. Nat. Cell Biol. 10, 138–148. https://doi.org/10.1038/ncb1676

Ye, P., Xiang, M., Liao, H., Liu, J., Luo, H., Wang, Y., Huang, L., Chen, M., Xia, J., 2019. Dual-Specificity Phosphatase 9 Protects Against Nonalcoholic Fatty Liver Disease in Mice Through ASK1 Suppression. Hepatology 69, 76–93. https://doi.org/10.1002/hep.30198

Yeh, T.C., Marsh, V., Bernat, B.A., Ballard, J., Colwell, H., Evans, R.J., Parry, J., Smith, D., Brandhuber, B.J., Gross, S., Marlow, A., Hurley, B., Lyssikatos, J., Lee, P.A., Winkler, J.D., Koch, K., Wallace, E., 2007. Biological characterization of ARRY-142886 (AZD6244), a potent, highly selective mitogen-activated protein kinase kinase 1/2 inhibitor. Clin. Cancer Res. 13, 1576–1583. https://doi.org/10.1158/1078-0432.CCR-06-1150

Yoon, S., Seger, R., 2006. The extracellular signal-regulated kinase: Multiple substrates regulate diverse cellular functions. Growth Factors 24, 21–44. https://doi.org/10.1080/02699050500284218

Yun, J., Rago, C., Cheong, I., Pagliarini, R., Angenendt, P., Rajagopalan, H., Schmidt, K., Willson, J.K. V, Markowitz, S., Zhou, S., Diaz, L. a, Velculescu, V.E., Lengauer, C., Kinzler, K.W., Vogelstein, B., Papadopoulos, N., 2009. Glucose deprivation contributes to the development of KRAS pathway mutations in tumor cells. Science 325, 1555–9. https://doi.org/10.1126/science.1174229

Zhang, Y., Blattman, J.N., Kennedy, N.J., Duong, J., Hguyen, T., Wang, Y., Davis, R.J., Greenberg, P.D., Flavell, R.A., Dong, C., 2004. Regulation of innate and

adaptive immune responses by MAP kinase phosphatase 5. Nature 430, 793–797. https://doi.org/10.1038/nature02764

Zhang, Y., Nallaparaju, K.C., Liu, X., Jiao, H., Reynolds, J.M., Wang, Z.-X., Dong, C., 2015. MAPK Phosphatase 7 Regulates T Cell Differentiation via Inhibiting ERK-Mediated IL-2 Expression. J. Immunol. 194, 3088–3095. https://doi.org/10.4049/jimmunol.1402638

Zhang, Z., Kobayashi, S., Borczuk, A.C., Leidner, R.S., LaFramboise, T., Levine, A.D., Halmos, B., 2010. Dual specificity phosphatase 6 (DUSP6) is an ETS-regulated negative feedback mediator of oncogenic ERK signaling in lung cancer cells. Carcinogenesis 31, 577–586. https://doi.org/10.1093/carcin/bgq020

Zheng, C.F., Guan, K.L., 1994. Activation of MEK family kinases requires phosphorylation of two conserved Ser/Thr residues. EMBO J. 13, 1123–1131. https://doi.org/10.1002/j.1460-2075.1994.tb06361.x

Zheng, X., Carstens, J.L., Kim, J., Scheible, M., Kaye, J., Sugimoto, H., Wu, C., Lebleu, V.S., Kalluri, R., Biology, C., 2015. EMT Program is Dispensable for Metastasis but Induces Chemoresistance in Pancreatic Cancer. Nature 527, 525–530. https://doi.org/10.1038/nature16064.EMT

Zhou, B., Zhang, Z.Y., 1999. Mechanism of mitogen-activated protein kinase phosphatase-3 activation by ERK2. J. Biol. Chem. 274, 35526–35534. https://doi.org/10.1074/jbc.274.50.35526

Zhou, X., Vink, M., Klaver, B., Berkhout, B., Das, A.T., 2006. Optimization of the Tet-On system for regulated gene expression through viral evolution. Gene Ther. 13, 1382–1390. https://doi.org/10.1038/sj.gt.3302780

Zimmermann, S., Moelling, K., 1999. Phosphorylation and regulation of Raf by Akt (protein kinase B). Science (80-.). 286, 1741–1744. https://doi.org/10.1126/science.286.5445.1741

Appendix

Map of pGSH1-GFP: 5318 bps, Circular DNA

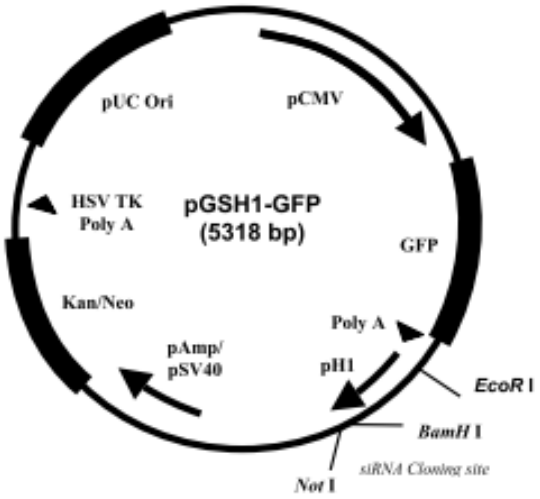

Vector Elements

Element	Start-End	Description
pCMV	59-808	human CMV promoter sequence
GFP	843-1500	Green Fluorescent Protein gene sequence
Poly A	1572-1801	Transcription stop and polyadenylation sequence
pH1 promoter	1808-1900	H1 RNA Polymerase III promoter
pAmp/pSV40	2689-3030	Ampicillin and SV40 promoters (in tandem)
Kan/Neo	3152-3942	Kanamycin and Neomycin resistance gene sequence
HSV TK Poly A	4182-4200	HSV Thymidine Kinase polyadenylation signal sequence.
pUC Ori	4531-5174	pUC origin of replication sequence.

MCS sequence of linearized pGSH1-GFP (spanning nucleotides 1931-2016)

Figure A1 pGSH1-GFP shRNA expression vector (Genlantis). shRNA oligonucleotides digested with NotI and BamHI are ligated into the pGSH1-GFP vector downstream of an H1 promoter.

A

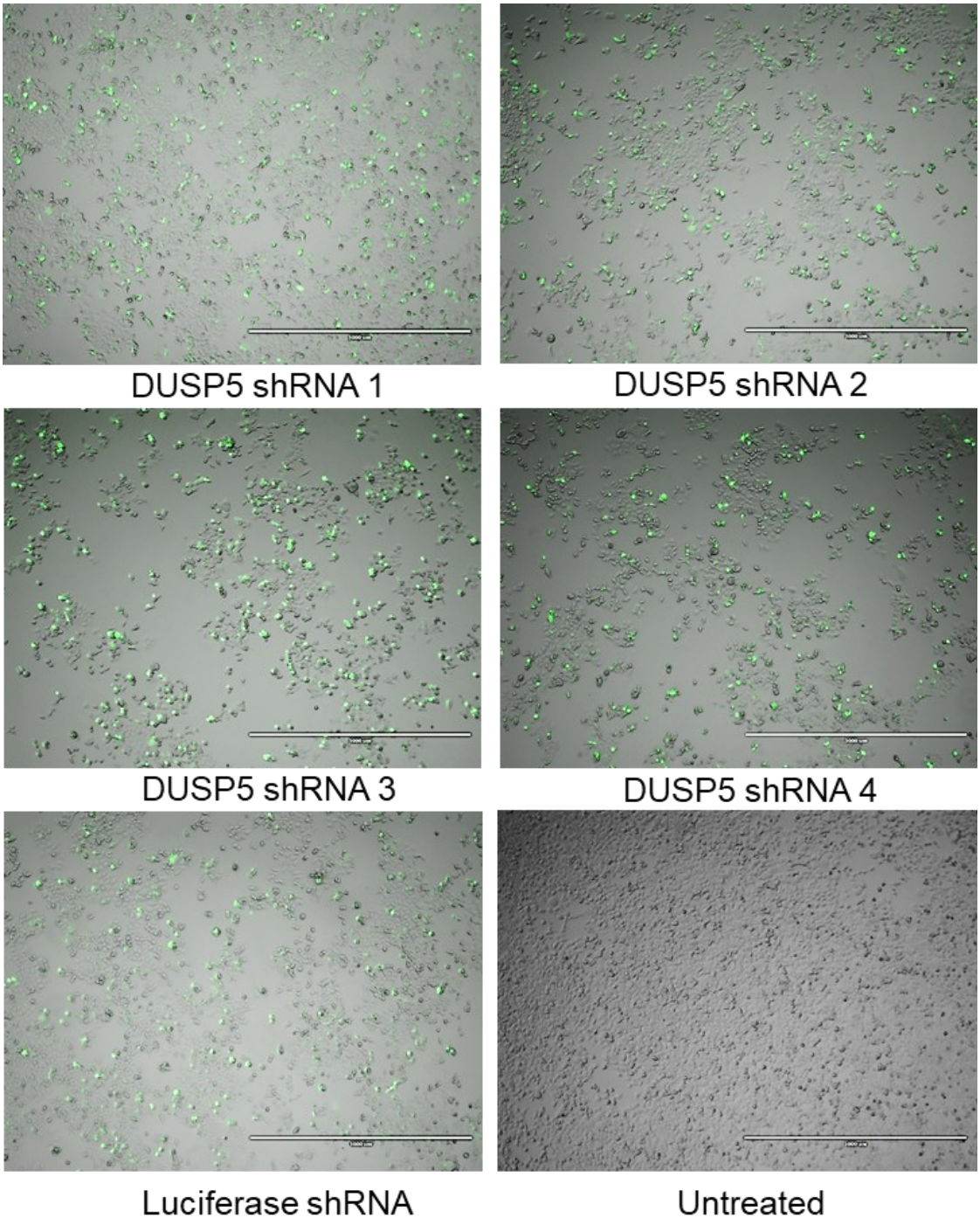

Figure A2. A) pGSH1-GFP shRNA constructs were transfected into HCT116 cells with high efficiency. HCT116 cells were transfected with shRNA constructs using Lipofectamine LTX Plus and imaged by an EVOS microscope 48 hours after transfection. Each image is a composite of a single view taken in two different light channels, visible light and GFP.

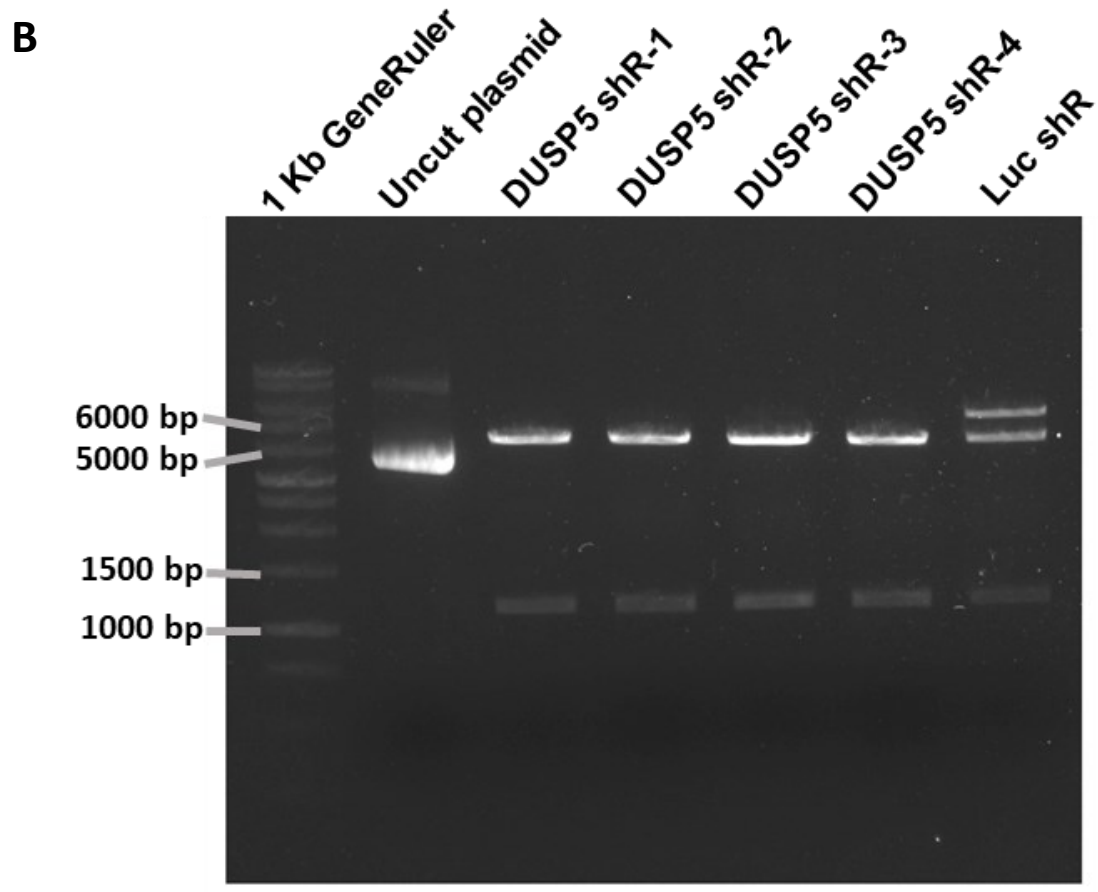

Figure A2 continued. B) Analytical digests for the generation of pGSH1-GFP shRNA constructs. Samples were incubated with *XhoI* and *HindIII* enzymes for 3 hours at 37 °C. Sample digests were analysed through gel electrophoresis.

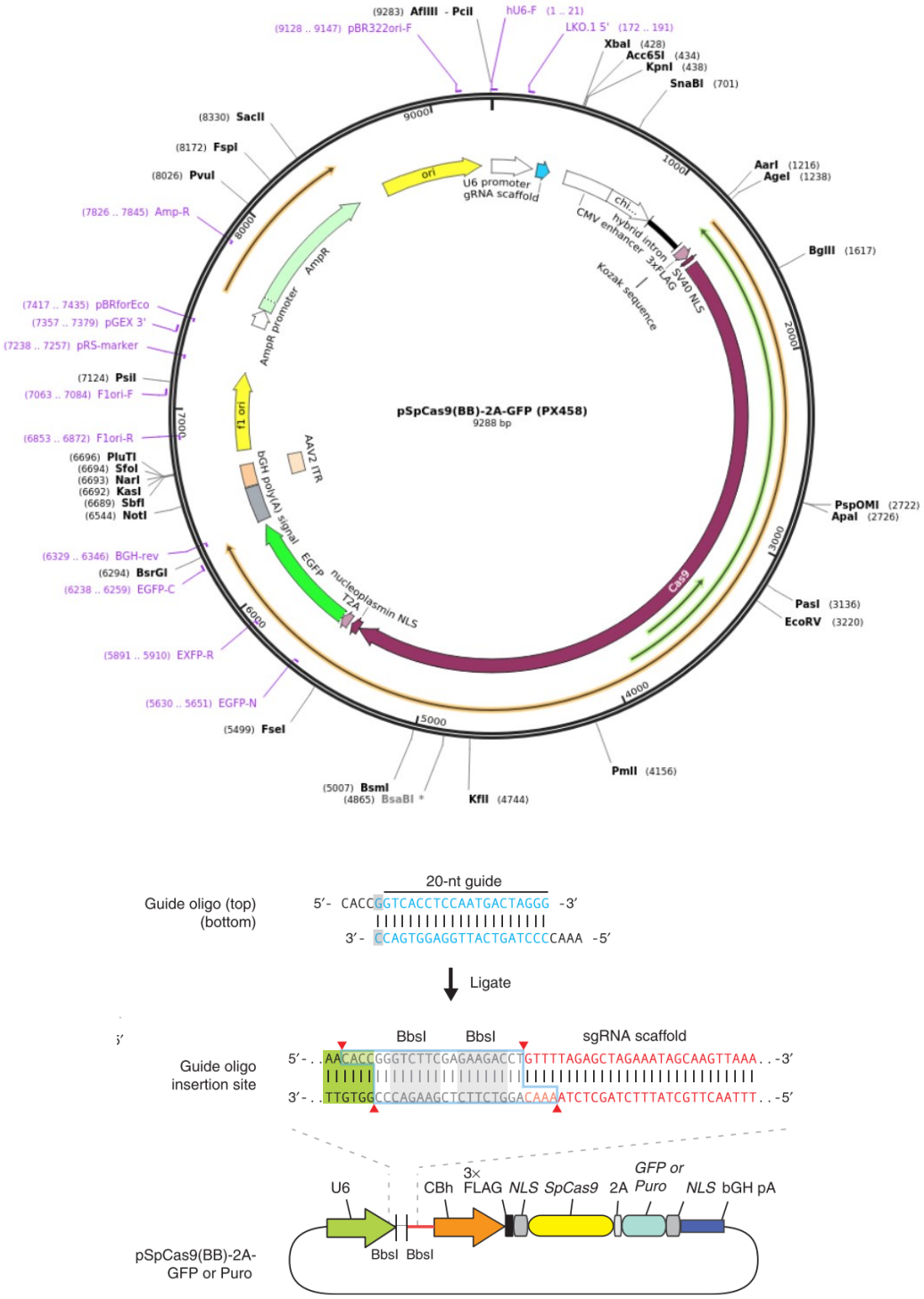

Figure A3 pSpCas9(BB)-2A-GFP CRISPR/Cas9 genome-editing vector. Guide oligonucleotide DNA is cloned into the pSpCas9(BB)-2A-GFP vector through a *BbsI* digestion and a T7 ligase reaction. sgRNA expression is driven by the upstream U6 promoter, while the Cas9 nuclease is controlled by a CMV enhancer element.

A

Vector Summary

Vector ID:	VB160415-1039avr
Vector Name:	pAV[shRNA]-EGFP-U6>Scramble_shRNA
Vector Type:	Adenovirus shRNA knockdown vector
Vector Size:	34997 bp
Viral Genome Size:	32915 bp
shRNA:	Scramble_shRNA
Target Sequence:	CCTAAGGTTAAGTCGCCCTCG
Marker:	EGFP

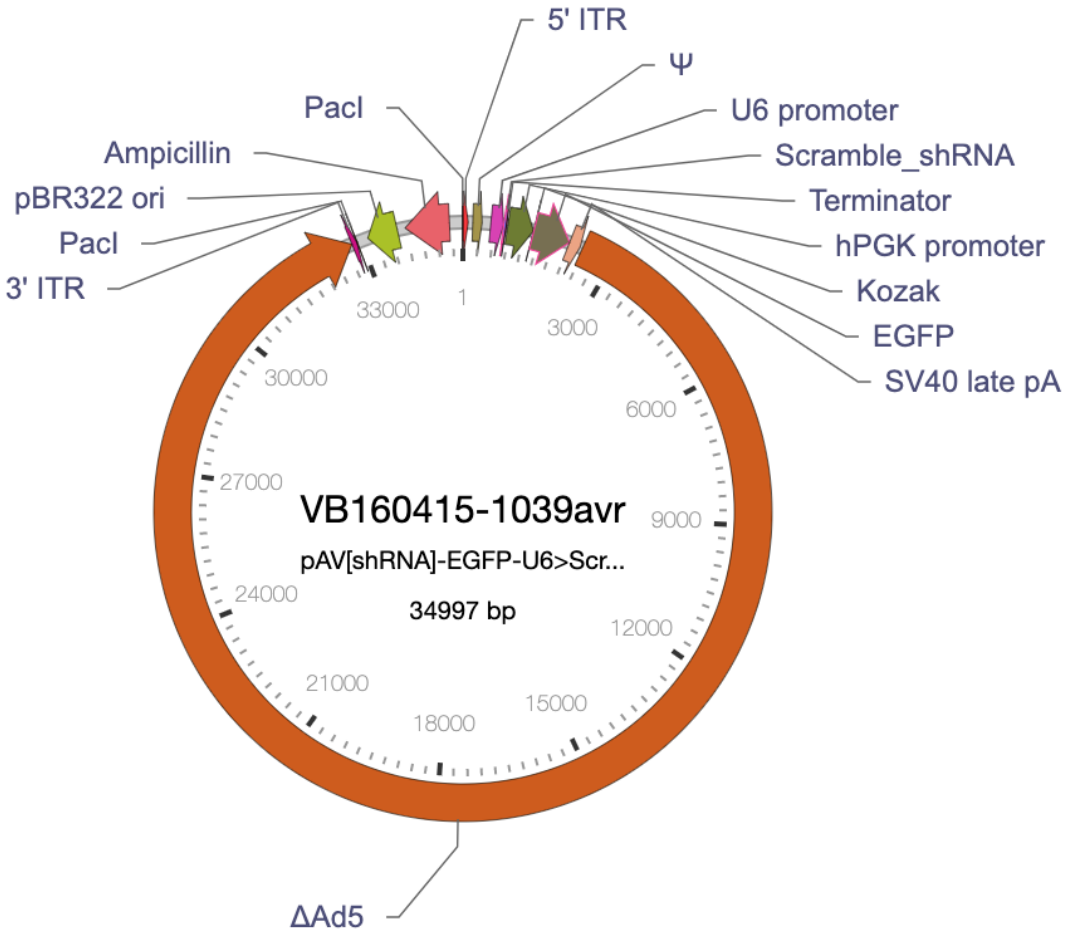

B

Vector Summary

Vector ID	VB160928-1062fkd
Vector Name (official)	pAV[shRNA]-EGFP-U6>hDUSP5[shRNA#3]
Date Created (Pacific Time)	2016-09-28
Size	34997 bp
Vector Type	Adenovirus shRNA knockdown vector
Inserted shRNA	hDUSP5[shRNA#3]
Target Sequence	CCTGTCCTTCTGTGTGCTTAT
Inserted Marker	EGFP
Copy Number	High
Bacterial Resistance	Ampicillin
Cloning Host	Stbl3

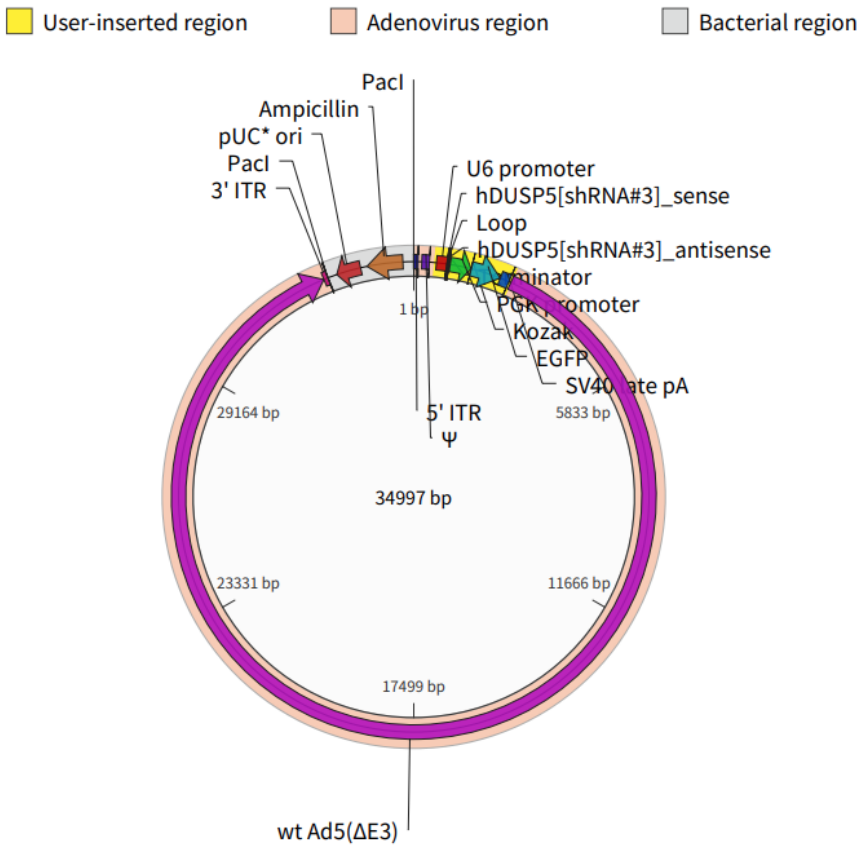

C

Vector Summary

Vector ID	VB160928-1063ghp
Vector Name (official)	pAV[shRNA]-EGFP-U6>hDUSP5[shRNA#5]
Date Created (Pacific Time)	2016-09-28
Size	34997 bp
Vector Type	Adenovirus shRNA knockdown vector
Inserted shRNA	hDUSP5[shRNA#5]
Target Sequence	GAGACTTTCTACTCGGAATAT
Inserted Marker	EGFP
Copy Number	High
Bacterial Resistance	Ampicillin
Cloning Host	Stbl3

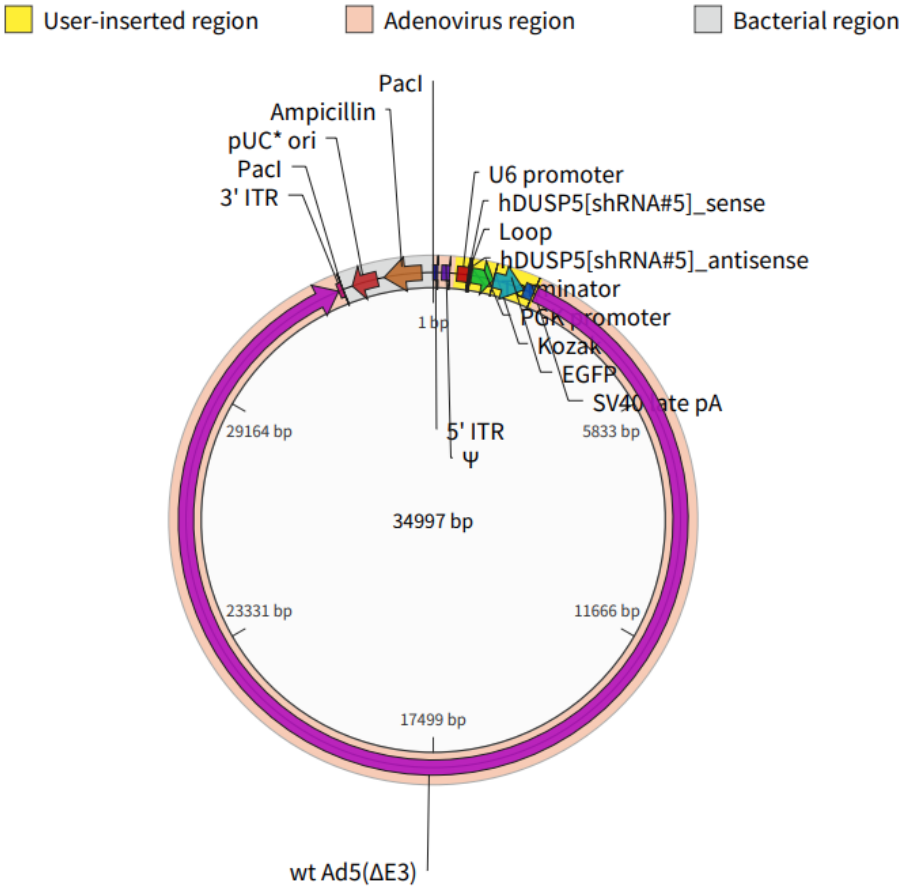

Figure A4 pAV-EGFP-U6-shRNA vectors. VectorBuilder adenoviral shRNA vectors. All shRNA sequences are controlled by a U6 promoter while the EGFP reporter gene is downstream of a PGK promoter sequence. A) Non-targeting scrambled shRNA adenovirus vector. B) DUSP5-targeting shRNA 3 adenovirus vector. C) DUSP5-targeting shRNA 5 adenovirus vector.

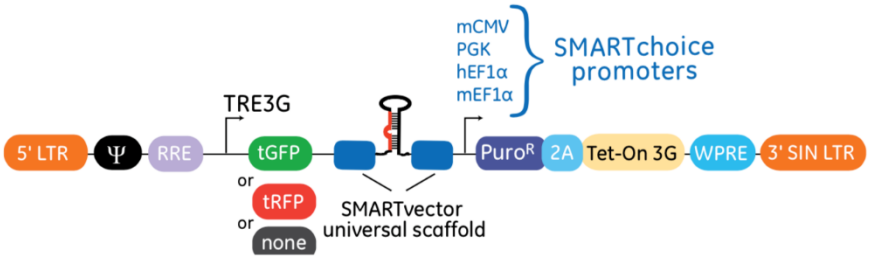

Figure 1. Elements of the SMARTvector Inducible Lentiviral shRNA vector.

Vector Element	Utility
5' LTR	5' Long Terminal Repeat is necessary for lentiviral particle production and integration of the construct into the host cell genome
Ψ	Psi packaging sequence allows lentiviral genome packaging using lentiviral packaging systems
RRE	Rev Response Element enhances titer by increasing packaging efficiency of full-length lentiviral genomes
TRE3G	Inducible promoter with Tetracycline Response Elements which is activated by the Tet-On 3G protein in the presence of doxycycline
tGFP or tRFP	TurboGFP or TurboRFP reporter for visual tracking of transduction and expression upon doxycycline induction
SMARTvector universal scaffold	Optimized proprietary scaffold based on native primary microRNA in which gene-targeting sequence is embedded
Puro^R	Puromycin resistance gene permits antibiotic selection of transduced cells
2A	Self-cleaving peptide that enables the expression of both Puro^R and Tet-On 3G transactivator from a single RNA pol II promoter
Tet-On 3G	Encodes the doxycycline-regulated transactivator protein, which binds to TRE3G only in the presence of doxycycline
WPRE	Woodchuck Hepatitis Post-transcriptional Regulatory Element enhances transgene expression in target cells
3' SIN LTR	3' Self-inactivating Long Terminal Repeat for generation of replication-incompetent lentiviral particles

Figure A5 Dharmacon™ SMARTvector™ Inducible Lentiviral shRNA vector components. This inducible lentivirus vector controls shRNA expression through the Tet-On 3G bipartite induction system. The system is comprised of the TRE3G inducible RNA polymerase II promoter and the Tet-On 3G transactivator protein.

Table A1 Set of 3 SMARTvector Inducible Human DUSP5 mCMV-TurboGFP shRNA glycerol set (Dharmacon).

Reference code	shRNA sequence	Target region
V3SH11252-227015515	5'-TTCAACTGGGCCACCCTGG-3'	ORF
V3SH11252-228300931	5'-ACGGTGATCAGCTTATGCC-3'	UTR
V3SH11252-229023400	5'-AGCGAGGTGAGGACGACAC-3'	ORF

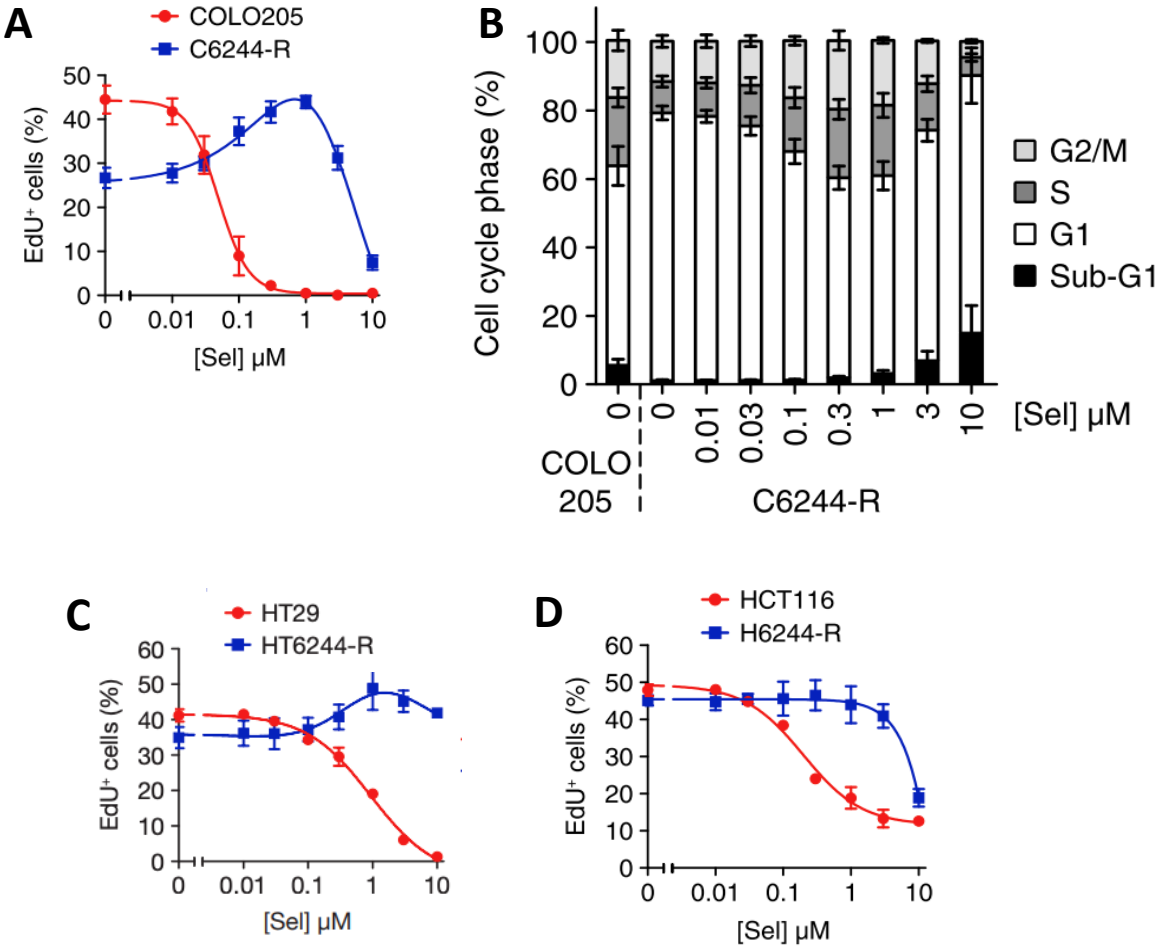

Figure A6 Assessment of cell proliferation in response to AZD6244 dosing with EdU-labelling and flow cytometry in parental and AZD6244-resistant colorectal cancer cell lines COLO205, HT29 and HCT116. Cells were treated as indicated with AZD6244 (Sel) for 72 hours. A,C,D) Percent EdU-positive (EdU+) cells was determined by high-content image analysis. Results are normalized to parental controls. B) Cell cycle distribution data was determined through DNA staining and flow cytometry. This figure was adapted from Sale et al. (2019) with permission from Nature communications.

Table A2 HCM data statistics for Figure 4.5

	Cell line	Measure	AZD6244 (μM)	Samples with statistically different mean values	p-value
A	H6244-R	*p*-ERK levels	0	Untreated vs. DUSP5 siRNA-03 Non-targeting siRNA vs. DUSP5 siRNA-03	0.00452817 0.00611164
B	H6244-R	*p*-ERK levels	0.001	Untreated vs. DUSP5 siRNA-03 Non-targeting siRNA vs. DUSP5 siRNA-03	0.000908593 0.00151157
C	H6244-R	*p*-ERK levels	0.01	Untreated vs. DUSP5 siRNA-03 Non-targeting siRNA vs. DUSP5 siRNA-03	0.0194521 0.0046851
D	H6244-R	*p*-ERK levels	0.1	Untreated vs. DUSP5 siRNA-03 Non-targeting siRNA vs. DUSP5 siRNA-03	0.00682528 0.00138319
E	H6244-R	*p*-ERK levels	1	Untreated vs. DUSP5 siRNA-03 Non-targeting siRNA vs. DUSP5 siRNA-03	0.0253414 0.0166136
F	H6244-R	*p*-ERK levels	10	Untreated vs. DUSP5 siRNA-03 Non-targeting siRNA vs. DUSP5 siRNA-03	0.01124 0.000361403
G	HCT116	% S-phase	0.001	Non-targeting siRNA vs. DUSP5 siRNA-03	0.0246425
H	HCT116	% S-phase	0.01	Non-targeting siRNA vs. DUSP5 siRNA-03	0.0146271
I	HCT116	% S-phase	0.1	Non-targeting siRNA vs. DUSP5 siRNA-03	0.0114953
J	HCT116	% S-phase	1	Untreated vs. DUSP5 siRNA-03 Non-targeting siRNA vs. DUSP5 siRNA-01 Non-targeting siRNA vs. DUSP5 siRNA-03	0.00352202 0.00612226 0.00177258
K	HCT116	% S-phase	10	Non-targeting siRNA vs. DUSP5 siRNA-03	0.00653337
L	H6244-R	% S-phase	0	Untreated vs. DUSP5 siRNA-03	0.00819301

Table A3 HCM data statistics for Figure 4.6

p-ERK N+C intensity 2-hour time course

Table Analyzed	pERK 2 hrs N+C Int				
Two-way ANOVA	Ordinary				
Alpha	0.05				
Source of Variation	% of total variation	P value	P value summary	Significant?	
Interaction	6.475	0.0268	*	Yes	
Row Factor	55.5	< 0.0001	****	Yes	
Column Factor	27.86	< 0.0001	****	Yes	
ANOVA table	SS	DF	MS	F (DFn, DFd)	P value
Interaction	65.86	18	3.659	F (18, 56) = 1.981	P = 0.0268
Row Factor	564.5	6	94.08	F (6, 56) = 50.95	P < 0.0001
Column Factor	283.4	3	94.47	F (3, 56) = 51.16	P < 0.0001
Residual	103.4	56	1.847		
Number of missing values	0				
Within each row, compare columns (simple effects within rows)					
Number of families	7				
Number of comparisons per family	6				
Alpha	0.05				
Tukey's multiple comparisons test	Mean Diff.	95% CI of diff.	Significant?	Summary	
HCT116					
Untreated vs. Non-targeting siRNA	-0.3454	-3.283 to 2.593	No	ns	
Untreated vs. DUSP5 siRNA 1	0.02086	-2.917 to 2.959	No	ns	
Untreated vs. DUSP5 siRNA 3	-0.476	-3.414 to 2.462	No	ns	
Non-targeting siRNA vs. DUSP5 siRNA 1	0.3662	-2.572 to 3.304	No	ns	
Non-targeting siRNA vs. DUSP5 siRNA 3	-0.1306	-3.069 to 2.807	No	ns	
DUSP5 siRNA 1 vs. DUSP5 siRNA 3	-0.4969	-3.435 to 2.441	No	ns	
HCR 0					
Untreated vs. Non-targeting siRNA	-0.611	-3.549 to 2.327	No	ns	
Untreated vs. DUSP5 siRNA 1	-1.712	-4.650 to 1.225	No	ns	
Untreated vs. DUSP5 siRNA 3	-5.902	-8.840 to -2.964	Yes	****	
Non-targeting siRNA vs. DUSP5 siRNA 1	-1.102	-4.039 to 1.836	No	ns	
Non-targeting siRNA vs. DUSP5 siRNA 3	-5.291	-8.229 to -2.353	Yes	****	
DUSP5 siRNA 1 vs. DUSP5 siRNA 3	-4.19	-7.128 to -1.252	Yes	**	
HCR 10					
Untreated vs. Non-targeting siRNA	0.2891	-2.649 to 3.227	No	ns	
Untreated vs. DUSP5 siRNA 1	-1.603	-4.541 to 1.335	No	ns	
Untreated vs. DUSP5 siRNA 3	-4.141	-7.079 to -1.203	Yes	**	
Non-targeting siRNA vs. DUSP5 siRNA 1	-1.892	-4.830 to 1.046	No	ns	
Non-targeting siRNA vs. DUSP5 siRNA 3	-4.43	-7.368 to -1.492	Yes	**	
DUSP5 siRNA 1 vs. DUSP5 siRNA 3	-2.538	-5.476 to 0.4003	No	ns	

HCR 20					
Untreated vs. Non-targeting siRNA	0.8445	-2.093 to 3.782	No	ns	
Untreated vs. DUSP5 siRNA 1	-0.7253	-3.663 to 2.213	No	ns	
Untreated vs. DUSP5 siRNA 3	-4.861	-7.799 to -1.924	Yes	***	
Non-targeting siRNA vs. DUSP5 siRNA 1	-1.57	-4.508 to 1.368	No	ns	
Non-targeting siRNA vs. DUSP5 siRNA 3	-5.706	-8.644 to -2.768	Yes	****	
DUSP5 siRNA 1 vs. DUSP5 siRNA 3	-4.136	-7.074 to -1.198	Yes	**	
HCR 30					
Untreated vs. Non-targeting siRNA	0.5821	-2.356 to 3.520	No	ns	
Untreated vs. DUSP5 siRNA 1	-3.308	-6.246 to -0.3703	Yes	*	
Untreated vs. DUSP5 siRNA 3	-5.726	-8.664 to -2.789	Yes	****	
Non-targeting siRNA vs. DUSP5 siRNA 1	-3.89	-6.828 to -0.9525	Yes	**	
Non-targeting siRNA vs. DUSP5 siRNA 3	-6.309	-9.247 to -3.371	Yes	****	
DUSP5 siRNA 1 vs. DUSP5 siRNA 3	-2.418	-5.356 to 0.5197	No	ns	
HCR 60					
Untreated vs. Non-targeting siRNA	0.7172	-2.221 to 3.655	No	ns	
Untreated vs. DUSP5 siRNA 1	-2.194	-5.132 to 0.7442	No	ns	
Untreated vs. DUSP5 siRNA 3	-4.043	-6.981 to -1.106	Yes	**	
Non-targeting siRNA vs. DUSP5 siRNA 1	-2.911	-5.849 to 0.02703	No	ns	
Non-targeting siRNA vs. DUSP5 siRNA 3	-4.761	-7.699 to -1.823	Yes	***	
DUSP5 siRNA 1 vs. DUSP5 siRNA 3	-1.85	-4.788 to 1.088	No	ns	
HCR 120					
Untreated vs. Non-targeting siRNA	-0.1702	-3.108 to 2.768	No	ns	
Untreated vs. DUSP5 siRNA 1	-4.288	-7.226 to -1.350	Yes	**	
Untreated vs. DUSP5 siRNA 3	-5.373	-8.311 to -2.435	Yes	****	
Non-targeting siRNA vs. DUSP5 siRNA 1	-4.118	-7.056 to -1.180	Yes	**	
Non-targeting siRNA vs. DUSP5 siRNA 3	-5.202	-8.140 to -2.264	Yes	***	
DUSP5 siRNA 1 vs. DUSP5 siRNA 3	-1.084	-4.022 to 1.854	No	ns	

ERK N+C intensity 2-hour time course

Table Analyzed	ERK 2 hrs N+C Int				
Two-way ANOVA	Ordinary				
Alpha	0.05				
Source of Variation	% of total variation	P value	P value summary	Significant?	
Interaction	3.319	0.9995	ns	No	
Row Factor	16.47	0.0069	**	Yes	
Column Factor	34.31	< 0.0001	****	Yes	
ANOVA table	SS	DF	MS	F (DFn, DFd)	P value
Interaction	0.2985	18	0.01658	F (18, 56) = 0.2250	P = 0.9995
Row Factor	1.481	6	0.2468	F (6, 56) = 3.349	P = 0.0069
Column Factor	3.085	3	1.028	F (3, 56) = 13.95	P < 0.0001
Residual	4.127	56	0.0737		
Number of missing values	0				
Within each row, compare columns (simple effects within rows)					
Number of families	7				
Number of comparisons per family	6				
Alpha	0.05				
Tukey's multiple comparisons test	Mean Diff.	95% CI of diff.	Significant?	Summary	
HCT116					
Untreated vs. Non-targeting siRNA	-0.2209	-0.8078 to 0.3661	No	ns	
Untreated vs. DUSP5 siRNA 1	-0.4993	-1.086 to 0.08769	No	ns	
Untreated vs. DUSP5 siRNA 3	-0.406	-0.9929 to 0.1810	No	ns	
Non-targeting siRNA vs. DUSP5 siRNA 1	-0.2784	-0.8653 to 0.3086	No	ns	
Non-targeting siRNA vs. DUSP5 siRNA 3	-0.1851	-0.7720 to 0.4019	No	ns	
DUSP5 siRNA 1 vs. DUSP5 siRNA 3	0.0933	-0.4936 to 0.6803	No	ns	
HCR 0					
Untreated vs. Non-targeting siRNA	-0.03744	-0.6244 to 0.5495	No	ns	
Untreated vs. DUSP5 siRNA 1	-0.3858	-0.9727 to 0.2012	No	ns	
Untreated vs. DUSP5 siRNA 3	-0.4666	-1.054 to 0.1204	No	ns	
Non-targeting siRNA vs. DUSP5 siRNA 1	-0.3483	-0.9353 to 0.2386	No	ns	
Non-targeting siRNA vs. DUSP5 siRNA 3	-0.4291	-1.016 to 0.1578	No	ns	
DUSP5 siRNA 1 vs. DUSP5 siRNA 3	-0.08079	-0.6677 to 0.5062	No	ns	
HCR 10					
Untreated vs. Non-targeting siRNA	-0.01177	-0.5987 to 0.5752	No	ns	
Untreated vs. DUSP5 siRNA 1	-0.3463	-0.9332 to 0.2407	No	ns	
Untreated vs. DUSP5 siRNA 3	-0.4398	-1.027 to 0.1472	No	ns	
Non-targeting siRNA vs. DUSP5 siRNA 1	-0.3345	-0.9215 to 0.2524	No	ns	
Non-targeting siRNA vs. DUSP5 siRNA 3	-0.428	-1.015 to 0.1590	No	ns	
DUSP5 siRNA 1 vs. DUSP5 siRNA 3	-0.09349	-0.6804 to 0.4935	No	ns	

HCR 20					
Untreated vs. Non-targeting siRNA	0.02547	-0.5615 to 0.6124	No	ns	
Untreated vs. DUSP5 siRNA 1	-0.2499	-0.8368 to 0.3371	No	ns	
Untreated vs. DUSP5 siRNA 3	-0.5396	-1.127 to 0.04740	No	ns	
Non-targeting siRNA vs. DUSP5 siRNA 1	-0.2753	-0.8623 to 0.3116	No	ns	
Non-targeting siRNA vs. DUSP5 siRNA 3	-0.565	-1.152 to 0.02193	No	ns	
DUSP5 siRNA 1 vs. DUSP5 siRNA 3	-0.2897	-0.8766 to 0.2973	No	ns	
HCR 30					
Untreated vs. Non-targeting siRNA	0.06418	-0.5228 to 0.6511	No	ns	
Untreated vs. DUSP5 siRNA 1	-0.3759	-0.9628 to 0.2111	No	ns	
Untreated vs. DUSP5 siRNA 3	-0.5415	-1.128 to 0.04547	No	ns	
Non-targeting siRNA vs. DUSP5 siRNA 1	-0.4401	-1.027 to 0.1469	No	ns	
Non-targeting siRNA vs. DUSP5 siRNA 3	-0.6057	-1.193 to -0.01871	Yes	*	
DUSP5 siRNA 1 vs. DUSP5 siRNA 3	-0.1656	-0.7526 to 0.4213	No	ns	
HCR 60					
Untreated vs. Non-targeting siRNA	0.04254	-0.5444 to 0.6295	No	ns	
Untreated vs. DUSP5 siRNA 1	-0.2233	-0.8102 to 0.3637	No	ns	
Untreated vs. DUSP5 siRNA 3	-0.3823	-0.9693 to 0.2046	No	ns	
Non-targeting siRNA vs. DUSP5 siRNA 1	-0.2658	-0.8528 to 0.3211	No	ns	
Non-targeting siRNA vs. DUSP5 siRNA 3	-0.4248	-1.012 to 0.1621	No	ns	
DUSP5 siRNA 1 vs. DUSP5 siRNA 3	-0.159	-0.7460 to 0.4279	No	ns	
HCR 120					
Untreated vs. Non-targeting siRNA	0.02142	-0.5655 to 0.6084	No	ns	
Untreated vs. DUSP5 siRNA 1	-0.2213	-0.8083 to 0.3656	No	ns	
Untreated vs. DUSP5 siRNA 3	-0.2922	-0.8791 to 0.2948	No	ns	
Non-targeting siRNA vs. DUSP5 siRNA 1	-0.2428	-0.8297 to 0.3442	No	ns	
Non-targeting siRNA vs. DUSP5 siRNA 3	-0.3136	-0.9005 to 0.2734	No	ns	
DUSP5 siRNA 1 vs. DUSP5 siRNA 3	-0.07083	-0.6578 to 0.5161	No	ns	

p-ERK N+C intensity 48-hour time course

Table Analyzed	pERK 48 hrs N+C Int				
Two-way ANOVA	Ordinary				
Alpha	0.05				
Source of Variation	% of total variation	P value	P value summary	Significant?	
Interaction	6.565	0.408	ns	No	
Row Factor	42.03	< 0.0001	****	Yes	
Column Factor	29.66	< 0.0001	****	Yes	
ANOVA table	SS	DF	MS	F (DFn, DFd)	P value
Interaction	29.36	9	3.262	F (9, 32) = 1.074	P = 0.4080
Row Factor	187.9	3	62.65	F (3, 32) = 20.62	P < 0.0001
Column Factor	132.6	3	44.2	F (3, 32) = 14.55	P < 0.0001
Residual	97.22	32	3.038		
Number of missing values	0				
Within each row, compare columns (simple effects within rows)					
Number of families	4				
Number of comparisons per family	6				
Alpha	0.05				
Tukey's multiple comparisons test	Mean Diff.	95% CI of diff.	Significant?	Summary	
HCT116					
Untreated vs. Non-targeting siRNA	-0.1522	-4.008 to 3.704	No	ns	
Untreated vs. DUSP5 siRNA 1	-0.1924	-4.048 to 3.663	No	ns	
Untreated vs. DUSP5 siRNA 3	-1.259	-5.115 to 2.597	No	ns	
Non-targeting siRNA vs. DUSP5 siRNA 1	-0.04026	-3.896 to 3.816	No	ns	
Non-targeting siRNA vs. DUSP5 siRNA 3	-1.107	-4.963 to 2.749	No	ns	
DUSP5 siRNA 1 vs. DUSP5 siRNA 3	-1.067	-4.922 to 2.789	No	ns	
HCR 0					
Untreated vs. Non-targeting siRNA	-0.4184	-4.274 to 3.437	No	ns	
Untreated vs. DUSP5 siRNA 1	-1.402	-5.258 to 2.453	No	ns	
Untreated vs. DUSP5 siRNA 3	-4.253	-8.109 to -0.3972	Yes	*	
Non-targeting siRNA vs. DUSP5 siRNA 1	-0.984	-4.840 to 2.872	No	ns	
Non-targeting siRNA vs. DUSP5 siRNA 3	-3.835	-7.690 to 0.02129	No	ns	
DUSP5 siRNA 1 vs. DUSP5 siRNA 3	-2.851	-6.706 to 1.005	No	ns	
HCR 4					
Untreated vs. Non-targeting siRNA	-0.3978	-4.254 to 3.458	No	ns	
Untreated vs. DUSP5 siRNA 1	-3.571	-7.427 to 0.2849	No	ns	
Untreated vs. DUSP5 siRNA 3	-5.78	-9.635 to -1.924	Yes	**	
Non-targeting siRNA vs. DUSP5 siRNA 1	-3.173	-7.029 to 0.6827	No	ns	
Non-targeting siRNA vs. DUSP5 siRNA 3	-5.382	-9.238 to -1.526	Yes	**	
DUSP5 siRNA 1 vs. DUSP5 siRNA 3	-2.209	-6.064 to 1.647	No	ns	
HCR 48					
Untreated vs. Non-targeting siRNA	-0.6592	-4.515 to 3.197	No	ns	
Untreated vs. DUSP5 siRNA 1	-2.258	-6.114 to 1.598	No	ns	
Untreated vs. DUSP5 siRNA 3	-5.695	-9.550 to -1.839	Yes	**	
Non-targeting siRNA vs. DUSP5 siRNA 1	-1.599	-5.455 to 2.257	No	ns	
Non-targeting siRNA vs. DUSP5 siRNA 3	-5.035	-8.891 to -1.180	Yes	**	
DUSP5 siRNA 1 vs. DUSP5 siRNA 3	-3.436	-7.292 to 0.4194	No	ns	

ERK N+C intensity 48-hour time course

Table Analyzed	ERK 48 hrs N+C Int				
Two-way ANOVA	Ordinary				
Alpha	0.05				
Source of Variation	% of total variation	P value	P value summary	Significant?	
Interaction	3.78	0.715	ns	No	
Row Factor	25.65	< 0.0001	****	Yes	
Column Factor	51.01	< 0.0001	****	Yes	
ANOVA table	SS	DF	MS	F (DFn, DFd)	P value
Interaction	0.1295	9	0.01439	F (9, 32) = 0.6871	P = 0.7150
Row Factor	0.8791	3	0.293	F (3, 32) = 13.99	P < 0.0001
Column Factor	1.748	3	0.5827	F (3, 32) = 27.82	P < 0.0001
Residual	0.6704	32	0.02095		
Number of missing values	0				
Within each row, compare columns (simple effects within rows)					
Number of families	4				
Number of comparisons per family	6				
Alpha	0.05				
Tukey's multiple comparisons test	Mean Diff.	95% CI of diff.	Significant?	Summary	
HCT116					
Untreated vs. Non-targeting siRNA	0.02466	-0.2955 to 0.3448	No	ns	
Untreated vs. DUSP5 siRNA 1	-0.3293	-0.6495 to -0.009159	Yes	*	
Untreated vs. DUSP5 siRNA 3	-0.5407	-0.8608 to -0.2205	Yes	***	
Non-targeting siRNA vs. DUSP5 siRNA 1	-0.354	-0.6742 to -0.03382	Yes	*	
Non-targeting siRNA vs. DUSP5 siRNA 3	-0.5653	-0.8855 to -0.2451	Yes	***	
DUSP5 siRNA 1 vs. DUSP5 siRNA 3	-0.2113	-0.5315 to 0.1089	No	ns	
HCR 0					
Untreated vs. Non-targeting siRNA	0.03691	-0.2833 to 0.3571	No	ns	
Untreated vs. DUSP5 siRNA 1	-0.3579	-0.6781 to -0.03771	Yes	*	
Untreated vs. DUSP5 siRNA 3	-0.4902	-0.8104 to -0.1700	Yes	**	
Non-targeting siRNA vs. DUSP5 siRNA 1	-0.3948	-0.7150 to -0.07462	Yes	*	
Non-targeting siRNA vs. DUSP5 siRNA 3	-0.5271	-0.8473 to -0.2070	Yes	***	
DUSP5 siRNA 1 vs. DUSP5 siRNA 3	-0.1323	-0.4525 to 0.1878	No	ns	
HCR 4					
Untreated vs. Non-targeting siRNA	-0.04612	-0.3663 to 0.2741	No	ns	
Untreated vs. DUSP5 siRNA 1	-0.3593	-0.6795 to -0.03910	Yes	*	
Untreated vs. DUSP5 siRNA 3	-0.3527	-0.6729 to -0.03249	Yes	*	
Non-targeting siRNA vs. DUSP5 siRNA 1	-0.3132	-0.6333 to 0.007021	No	ns	
Non-targeting siRNA vs. DUSP5 siRNA 3	-0.3066	-0.6267 to 0.01363	No	ns	
DUSP5 siRNA 1 vs. DUSP5 siRNA 3	0.006612	-0.3136 to 0.3268	No	ns	
HCR 48					
Untreated vs. Non-targeting siRNA	0.07042	-0.2498 to 0.3906	No	ns	
Untreated vs. DUSP5 siRNA 1	-0.2708	-0.5909 to 0.04943	No	ns	
Untreated vs. DUSP5 siRNA 3	-0.2345	-0.5547 to 0.08565	No	ns	
Non-targeting siRNA vs. DUSP5 siRNA 1	-0.3412	-0.6614 to -0.02100	Yes	*	
Non-targeting siRNA vs. DUSP5 siRNA 3	-0.305	-0.6251 to 0.01523	No	ns	
DUSP5 siRNA 1 vs. DUSP5 siRNA 3	0.03623	-0.2840 to 0.3564	No	ns	

Table A4 HCM data statistics for Figure 4.7

p-ERK N:C intensity 2-hour time course

Table Analyzed	pERK 2 hrs N:C Int BGC				
Two-way ANOVA	Ordinary				
Alpha	0.05				
Source of Variation	% of total variation	P value	P value summary	Significant?	
Interaction	32.67	0.0246	*	Yes	
Row Factor	13.86	0.0295	*	Yes	
Column Factor	2.813	0.3836	ns	No	
ANOVA table	SS	DF	MS	F (DFn, DFd)	P value
Interaction	1.739	18	0.09659	F (18, 56) = 2.007	P = 0.0246
Row Factor	0.7374	6	0.1229	F (6, 56) = 2.553	P = 0.0295
Column Factor	0.1497	3	0.04989	F (3, 56) = 1.036	P = 0.3836
Residual	2.695	56	0.04813		
Number of missing values	0				
Within each row, compare columns (simple effects within rows)					
Number of families	7				
Number of comparisons per family	6				
Alpha	0.05				
Tukey's multiple comparisons test	Mean Diff.	95% CI of diff.	Significant?	Summary	
HCT116					
Untreated vs. Non-targeting siRNA	0.07261	-0.4017 to 0.5469	No	ns	
Untreated vs. DUSP5 siRNA 1	-0.6374	-1.112 to -0.1631	Yes	**	
Untreated vs. DUSP5 siRNA 3	-0.6229	-1.097 to -0.1486	Yes	**	
Non-targeting siRNA vs. DUSP5 siRNA 1	-0.71	-1.184 to -0.2357	Yes	**	
Non-targeting siRNA vs. DUSP5 siRNA 3	-0.6955	-1.170 to -0.2212	Yes	**	
DUSP5 siRNA 1 vs. DUSP5 siRNA 3	0.01449	-0.4598 to 0.4888	No	ns	
HCR 0					
Untreated vs. Non-targeting siRNA	0.03489	-0.4394 to 0.5092	No	ns	
Untreated vs. DUSP5 siRNA 1	-0.05551	-0.5298 to 0.4188	No	ns	
Untreated vs. DUSP5 siRNA 3	-0.03669	-0.5110 to 0.4376	No	ns	
Non-targeting siRNA vs. DUSP5 siRNA 1	-0.0904	-0.5647 to 0.3839	No	ns	
Non-targeting siRNA vs. DUSP5 siRNA 3	-0.07158	-0.5459 to 0.4027	No	ns	
DUSP5 siRNA 1 vs. DUSP5 siRNA 3	0.01882	-0.4555 to 0.4931	No	ns	
HCR 10					
Untreated vs. Non-targeting siRNA	0.0421	-0.4322 to 0.5164	No	ns	
Untreated vs. DUSP5 siRNA 1	0.07489	-0.3994 to 0.5492	No	ns	
Untreated vs. DUSP5 siRNA 3	0.191	-0.2833 to 0.6653	No	ns	
Non-targeting siRNA vs. DUSP5 siRNA 1	0.03279	-0.4415 to 0.5071	No	ns	
Non-targeting siRNA vs. DUSP5 siRNA 3	0.1489	-0.3254 to 0.6232	No	ns	
DUSP5 siRNA 1 vs. DUSP5 siRNA 3	0.1161	-0.3582 to 0.5904	No	ns	

HCR 20					
Untreated vs. Non-targeting siRNA	0.08433	-0.3900 to 0.5586	No	ns	
Untreated vs. DUSP5 siRNA 1	0.1109	-0.3634 to 0.5852	No	ns	
Untreated vs. DUSP5 siRNA 3	0.3464	-0.1279 to 0.8208	No	ns	
Non-targeting siRNA vs. DUSP5 siRNA 1	0.02658	-0.4477 to 0.5009	No	ns	
Non-targeting siRNA vs. DUSP5 siRNA 3	0.2621	-0.2122 to 0.7364	No	ns	
DUSP5 siRNA 1 vs. DUSP5 siRNA 3	0.2355	-0.2388 to 0.7098	No	ns	
HCR 30					
Untreated vs. Non-targeting siRNA	0.09839	-0.3759 to 0.5727	No	ns	
Untreated vs. DUSP5 siRNA 1	0.1249	-0.3494 to 0.5992	No	ns	
Untreated vs. DUSP5 siRNA 3	0.3018	-0.1725 to 0.7761	No	ns	
Non-targeting siRNA vs. DUSP5 siRNA 1	0.02654	-0.4478 to 0.5009	No	ns	
Non-targeting siRNA vs. DUSP5 siRNA 3	0.2034	-0.2709 to 0.6777	No	ns	
DUSP5 siRNA 1 vs. DUSP5 siRNA 3	0.1769	-0.2975 to 0.6512	No	ns	
HCR 60					
Untreated vs. Non-targeting siRNA	-0.005541	-0.4799 to 0.4688	No	ns	
Untreated vs. DUSP5 siRNA 1	0.0384	-0.4359 to 0.5127	No	ns	
Untreated vs. DUSP5 siRNA 3	0.2367	-0.2377 to 0.7110	No	ns	
Non-targeting siRNA vs. DUSP5 siRNA 1	0.04395	-0.4304 to 0.5183	No	ns	
Non-targeting siRNA vs. DUSP5 siRNA 3	0.2422	-0.2321 to 0.7165	No	ns	
DUSP5 siRNA 1 vs. DUSP5 siRNA 3	0.1983	-0.2761 to 0.6726	No	ns	
HCR 120					
Untreated vs. Non-targeting siRNA	-0.03393	-0.5082 to 0.4404	No	ns	
Untreated vs. DUSP5 siRNA 1	-0.06655	-0.5409 to 0.4078	No	ns	
Untreated vs. DUSP5 siRNA 3	-0.09087	-0.5652 to 0.3835	No	ns	
Non-targeting siRNA vs. DUSP5 siRNA 1	-0.03262	-0.5069 to 0.4417	No	ns	
Non-targeting siRNA vs. DUSP5 siRNA 3	-0.05694	-0.5313 to 0.4174	No	ns	
DUSP5 siRNA 1 vs. DUSP5 siRNA 3	-0.02432	-0.4986 to 0.4500	No	ns	

ERK N:C intensity 2-hour time course

Table Analyzed	ERK 2 hrs N:C Int BGC				
Two-way ANOVA	Ordinary				
Alpha	0.05				
Source of Variation	% of total variation	P value	P value summary	Significant?	
Interaction	12.07	0.0051	**	Yes	
Row Factor	54.5	< 0.0001	****	Yes	
Column Factor	18.26	< 0.0001	****	Yes	
ANOVA table	SS	DF	MS	F (DFn, DFd)	P value
Interaction	1.124	18	0.06244	F (18, 56) = 2.476	P = 0.0051
Row Factor	5.074	6	0.8456	F (6, 56) = 33.53	P < 0.0001
Column Factor	1.7	3	0.5667	F (3, 56) = 22.47	P < 0.0001
Residual	1.412	56	0.02522		
Number of missing values	0				
Within each row, compare columns (simple effects within rows)					
Number of families	7				
Number of comparisons per family	6				
Alpha	0.05				
Tukey's multiple comparisons test	Mean Diff.	95% CI of diff.	Significant?	Summary	
HCT116					
Untreated vs. Non-targeting siRNA	0.07158	-0.2718 to 0.4149	No	ns	
Untreated vs. DUSP5 siRNA 1	-0.005478	-0.3488 to 0.3379	No	ns	
Untreated vs. DUSP5 siRNA 3	-0.04692	-0.3903 to 0.2964	No	ns	
Non-targeting siRNA vs. DUSP5 siRNA 1	-0.07706	-0.4204 to 0.2663	No	ns	
Non-targeting siRNA vs. DUSP5 siRNA 3	-0.1185	-0.4618 to 0.2248	No	ns	
DUSP5 siRNA 1 vs. DUSP5 siRNA 3	-0.04144	-0.3848 to 0.3019	No	ns	
HCR 0					
Untreated vs. Non-targeting siRNA	0.02394	-0.3194 to 0.3673	No	ns	
Untreated vs. DUSP5 siRNA 1	-0.01347	-0.3568 to 0.3299	No	ns	
Untreated vs. DUSP5 siRNA 3	0.02498	-0.3184 to 0.3683	No	ns	
Non-targeting siRNA vs. DUSP5 siRNA 1	-0.03741	-0.3807 to 0.3059	No	ns	
Non-targeting siRNA vs. DUSP5 siRNA 3	0.00104	-0.3423 to 0.3444	No	ns	
DUSP5 siRNA 1 vs. DUSP5 siRNA 3	0.03845	-0.3049 to 0.3818	No	ns	
HCR 10					
Untreated vs. Non-targeting siRNA	0.06009	-0.2832 to 0.4034	No	ns	
Untreated vs. DUSP5 siRNA 1	0.1137	-0.2296 to 0.4571	No	ns	
Untreated vs. DUSP5 siRNA 3	0.4934	0.1500 to 0.8367	Yes	**	
Non-targeting siRNA vs. DUSP5 siRNA 1	0.05363	-0.2897 to 0.3970	No	ns	
Non-targeting siRNA vs. DUSP5 siRNA 3	0.4333	0.08995 to 0.7766	Yes	**	
DUSP5 siRNA 1 vs. DUSP5 siRNA 3	0.3797	0.03632 to 0.7230	Yes	*	

HCR 20					
Untreated vs. Non-targeting siRNA	0.01761	-0.3257 to 0.3609	No	ns	
Untreated vs. DUSP5 siRNA 1	0.09831	-0.2450 to 0.4416	No	ns	
Untreated vs. DUSP5 siRNA 3	0.4141	0.07081 to 0.7575	Yes	*	
Non-targeting siRNA vs. DUSP5 siRNA 1	0.0807	-0.2626 to 0.4240	No	ns	
Non-targeting siRNA vs. DUSP5 siRNA 3	0.3965	0.05320 to 0.7399	Yes	*	
DUSP5 siRNA 1 vs. DUSP5 siRNA 3	0.3158	-0.02750 to 0.6592	No	ns	
HCR 30					
Untreated vs. Non-targeting siRNA	-0.05112	-0.3945 to 0.2922	No	ns	
Untreated vs. DUSP5 siRNA 1	0.113	-0.2304 to 0.4563	No	ns	
Untreated vs. DUSP5 siRNA 3	0.3983	0.05496 to 0.7416	Yes	*	
Non-targeting siRNA vs. DUSP5 siRNA 1	0.1641	-0.1792 to 0.5074	No	ns	
Non-targeting siRNA vs. DUSP5 siRNA 3	0.4494	0.1061 to 0.7928	Yes	**	
DUSP5 siRNA 1 vs. DUSP5 siRNA 3	0.2853	-0.05802 to 0.6287	No	ns	
HCR 60					
Untreated vs. Non-targeting siRNA	-0.05088	-0.3942 to 0.2925	No	ns	
Untreated vs. DUSP5 siRNA 1	0.1288	-0.2146 to 0.4721	No	ns	
Untreated vs. DUSP5 siRNA 3	0.4556	0.1123 to 0.7989	Yes	**	
Non-targeting siRNA vs. DUSP5 siRNA 1	0.1797	-0.1637 to 0.5230	No	ns	
Non-targeting siRNA vs. DUSP5 siRNA 3	0.5065	0.1631 to 0.8498	Yes	**	
DUSP5 siRNA 1 vs. DUSP5 siRNA 3	0.3268	-0.01652 to 0.6701	No	ns	
HCR 120					
Untreated vs. Non-targeting siRNA	0.05202	-0.2913 to 0.3954	No	ns	
Untreated vs. DUSP5 siRNA 1	0.4934	0.1501 to 0.8368	Yes	**	
Untreated vs. DUSP5 siRNA 3	0.7584	0.4151 to 1.102	Yes	****	
Non-targeting siRNA vs. DUSP5 siRNA 1	0.4414	0.09808 to 0.7847	Yes	**	
Non-targeting siRNA vs. DUSP5 siRNA 3	0.7064	0.3631 to 1.050	Yes	****	
DUSP5 siRNA 1 vs. DUSP5 siRNA 3	0.265	-0.07833 to 0.6083	No	ns	

p-ERK N:C intensity 48-hour time course

Table Analyzed	pERK 48 hrs N:C Int BGC				
Two-way ANOVA	Ordinary				
Alpha	0.05				
Source of Variation	% of total variation	P value	P value summary	Significant?	
Interaction	32.98	0.0212	*	Yes	
Row Factor	5.572	0.2812	ns	No	
Column Factor	16.82	0.0155	*	Yes	
ANOVA table	SS	DF	MS	F (DFn, DFd)	P value
Interaction	0.4591	9	0.05101	F (9, 32) = 2.628	P = 0.0212
Row Factor	0.07756	3	0.02585	F (3, 32) = 1.332	P = 0.2812
Column Factor	0.2341	3	0.07804	F (3, 32) = 4.021	P = 0.0155
Residual	0.6211	32	0.01941		
Number of missing values	0				
Within each row, compare columns (simple effects within rows)					
Number of families	4				
Number of comparisons per family	6				
Alpha	0.05				
Tukey's multiple comparisons test	Mean Diff.	95% CI of diff.	Significant?	Summary	
HCT116					
Untreated vs. Non-targeting siRNA	0.01054	-0.2977 to 0.3187	No	ns	
Untreated vs. DUSP5 siRNA 1	-0.4022	-0.7104 to -0.09397	Yes	**	
Untreated vs. DUSP5 siRNA 3	-0.4929	-0.8011 to -0.1847	Yes	***	
Non-targeting siRNA vs. DUSP5 siRNA 1	-0.4127	-0.7209 to -0.1045	Yes	**	
Non-targeting siRNA vs. DUSP5 siRNA 3	-0.5035	-0.8117 to -0.1953	Yes	***	
DUSP5 siRNA 1 vs. DUSP5 siRNA 3	-0.09076	-0.3990 to 0.2174	No	ns	
HCR 0					
Untreated vs. Non-targeting siRNA	0.09868	-0.2095 to 0.4069	No	ns	
Untreated vs. DUSP5 siRNA 1	0.0005614	-0.3076 to 0.3088	No	ns	
Untreated vs. DUSP5 siRNA 3	0.04511	-0.2631 to 0.3533	No	ns	
Non-targeting siRNA vs. DUSP5 siRNA 1	-0.09812	-0.4063 to 0.2101	No	ns	
Non-targeting siRNA vs. DUSP5 siRNA 3	-0.05357	-0.3618 to 0.2546	No	ns	
DUSP5 siRNA 1 vs. DUSP5 siRNA 3	0.04455	-0.2636 to 0.3527	No	ns	
HCR 4					
Untreated vs. Non-targeting siRNA	0.04393	-0.2643 to 0.3521	No	ns	
Untreated vs. DUSP5 siRNA 1	-0.05285	-0.3610 to 0.2553	No	ns	
Untreated vs. DUSP5 siRNA 3	-0.07495	-0.3831 to 0.2332	No	ns	
Non-targeting siRNA vs. DUSP5 siRNA 1	-0.09678	-0.4050 to 0.2114	No	ns	
Non-targeting siRNA vs. DUSP5 siRNA 3	-0.1189	-0.4271 to 0.1893	No	ns	
DUSP5 siRNA 1 vs. DUSP5 siRNA 3	-0.0221	-0.3303 to 0.2861	No	ns	
HCR 48					
Untreated vs. Non-targeting siRNA	0.09721	-0.2110 to 0.4054	No	ns	
Untreated vs. DUSP5 siRNA 1	0.06545	-0.2428 to 0.3736	No	ns	
Untreated vs. DUSP5 siRNA 3	0.1032	-0.2050 to 0.4114	No	ns	
Non-targeting siRNA vs. DUSP5 siRNA 1	-0.03176	-0.3400 to 0.2764	No	ns	
Non-targeting siRNA vs. DUSP5 siRNA 3	0.005962	-0.3022 to 0.3142	No	ns	
DUSP5 siRNA 1 vs. DUSP5 siRNA 3	0.03773	-0.2705 to 0.3459	No	ns	

ERK N:C intensity 48-hour time course

Table Analyzed	ERK 48 hrs N:C Int BGC				
Two-way ANOVA	Ordinary				
Alpha	0.05				
Source of Variation	% of total variation	P value	P value summary	Significant?	
Interaction	13.7	0.0008	***	Yes	
Row Factor	64.86	< 0.0001	****	Yes	
Column Factor	10.44	< 0.0001	****	Yes	
ANOVA table	SS	DF	MS	F (DFn, DFd)	P value
Interaction	1.179	9	0.131	F (9, 32) = 4.430	P = 0.0008
Row Factor	5.581	3	1.86	F (3, 32) = 62.91	P < 0.0001
Column Factor	0.8981	3	0.2994	F (3, 32) = 10.12	P < 0.0001
Residual	0.9463	32	0.02957		
Number of missing values	0				
Within each row, compare columns (simple effects within rows)					
Number of families	4				
Number of comparisons per family	6				
Alpha	0.05				
Tukey's multiple comparisons test	Mean Diff.	95% CI of diff.	Significant?	Summary	
HCT116					
Untreated vs. Non-targeting siRNA	-0.02312	-0.4035 to 0.3573	No	ns	
Untreated vs. DUSP5 siRNA 1	-0.05064	-0.4311 to 0.3298	No	ns	
Untreated vs. DUSP5 siRNA 3	-0.09948	-0.4799 to 0.2809	No	ns	
Non-targeting siRNA vs. DUSP5 siRNA 1	-0.02752	-0.4079 to 0.3529	No	ns	
Non-targeting siRNA vs. DUSP5 siRNA 3	-0.07636	-0.4568 to 0.3041	No	ns	
DUSP5 siRNA 1 vs. DUSP5 siRNA 3	-0.04884	-0.4293 to 0.3316	No	ns	
HCR 0					
Untreated vs. Non-targeting siRNA	-0.01222	-0.3926 to 0.3682	No	ns	
Untreated vs. DUSP5 siRNA 1	-0.05584	-0.4363 to 0.3246	No	ns	
Untreated vs. DUSP5 siRNA 3	0.013	-0.3674 to 0.3934	No	ns	
Non-targeting siRNA vs. DUSP5 siRNA 1	-0.04362	-0.4240 to 0.3368	No	ns	
Non-targeting siRNA vs. DUSP5 siRNA 3	0.02522	-0.3552 to 0.4056	No	ns	
DUSP5 siRNA 1 vs. DUSP5 siRNA 3	0.06884	-0.3116 to 0.4493	No	ns	
HCR 4					
Untreated vs. Non-targeting siRNA	0.1257	-0.2547 to 0.5061	No	ns	
Untreated vs. DUSP5 siRNA 1	0.3843	0.003905 to 0.7648	Yes	*	
Untreated vs. DUSP5 siRNA 3	0.798	0.4176 to 1.178	Yes	****	
Non-targeting siRNA vs. DUSP5 siRNA 1	0.2586	-0.1218 to 0.6391	No	ns	
Non-targeting siRNA vs. DUSP5 siRNA 3	0.6723	0.2919 to 1.053	Yes	***	
DUSP5 siRNA 1 vs. DUSP5 siRNA 3	0.4137	0.03325 to 0.7941	Yes	*	
HCR 48					
Untreated vs. Non-targeting siRNA	-0.1341	-0.5145 to 0.2464	No	ns	
Untreated vs. DUSP5 siRNA 1	0.2043	-0.1761 to 0.5847	No	ns	
Untreated vs. DUSP5 siRNA 3	0.6049	0.2245 to 0.9853	Yes	***	
Non-targeting siRNA vs. DUSP5 siRNA 1	0.3383	-0.04208 to 0.7188	No	ns	
Non-targeting siRNA vs. DUSP5 siRNA 3	0.739	0.3585 to 1.119	Yes	****	
DUSP5 siRNA 1 vs. DUSP5 siRNA 3	0.4006	0.02019 to 0.7810	Yes	*	

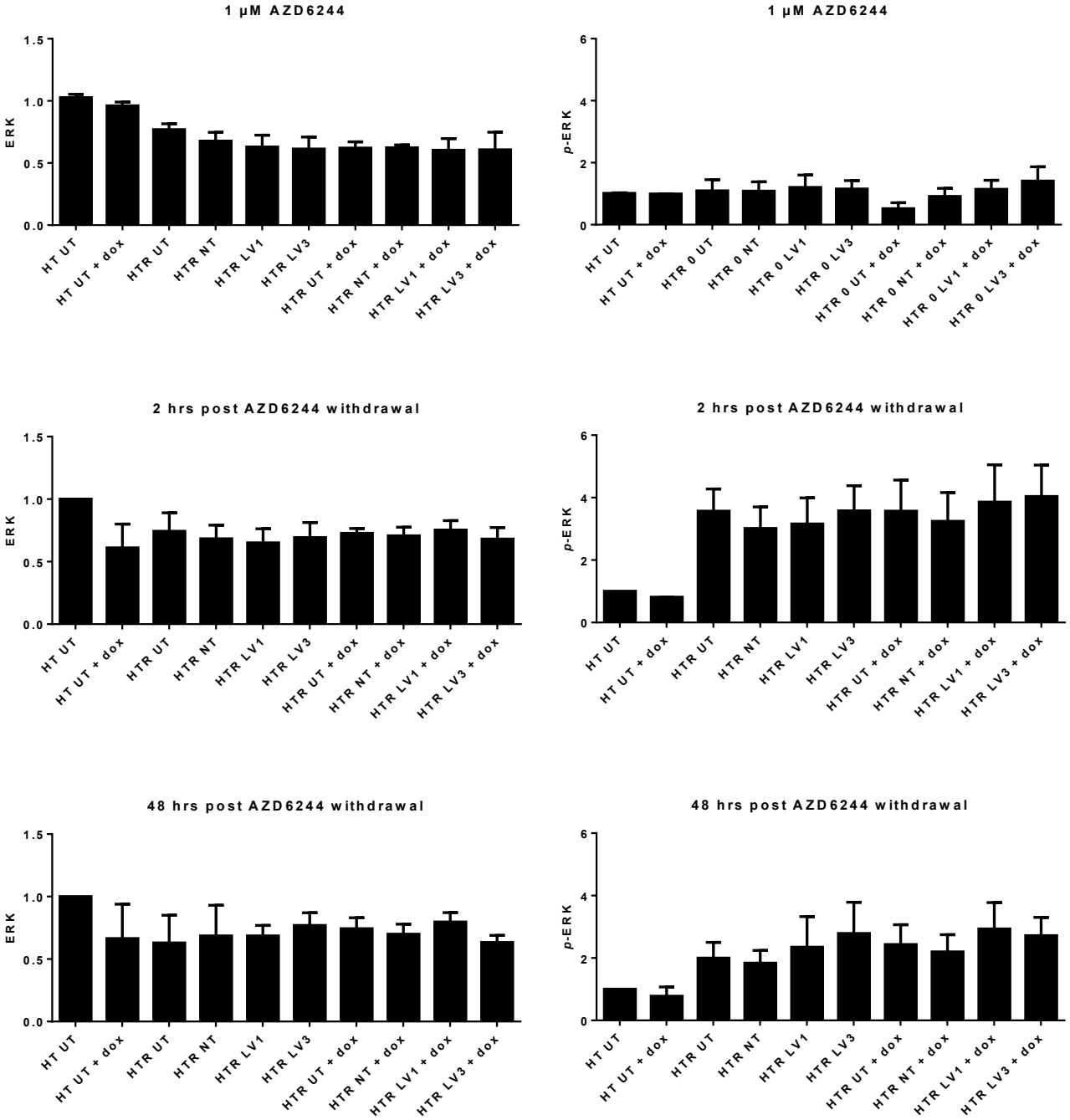

Figure A7 western blot quantification data for figure 5.7. HT6244-R shRNA cell lines were incubated with 1 μg.mL^{-1} doxycycline for 48 hours. Culture media was replaced with AZD6244-free media (containing doxycycline) 2 or 48 hours prior to cell lysis in appropriate conditions. Cells lysates were fractioned by SDS-PAGE and western blotted with the indicated antibodies to assess relative protein levels. Relative intensities of protein bands were quantified using Liquor's Image Studio Lite software. n=3 biological replicates, ± SEM.

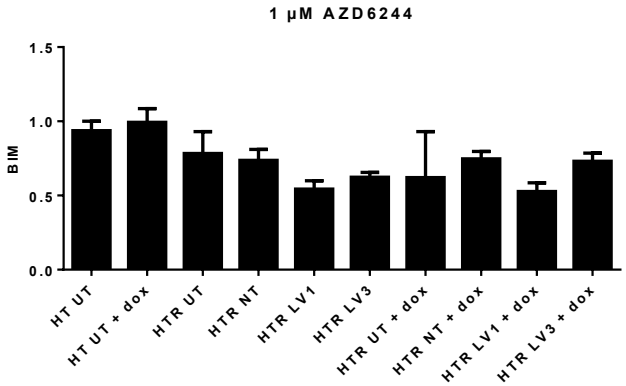

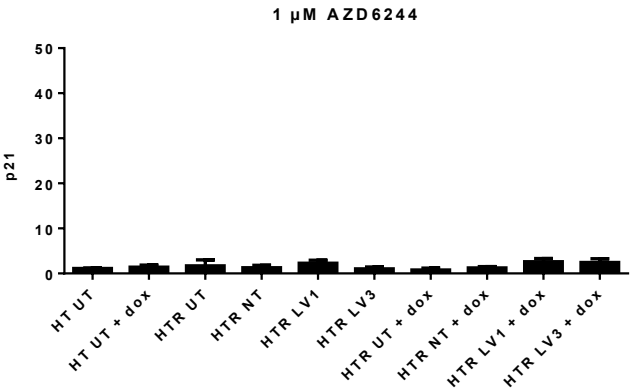

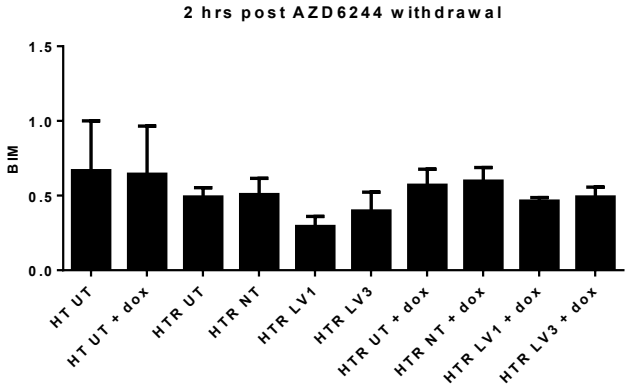

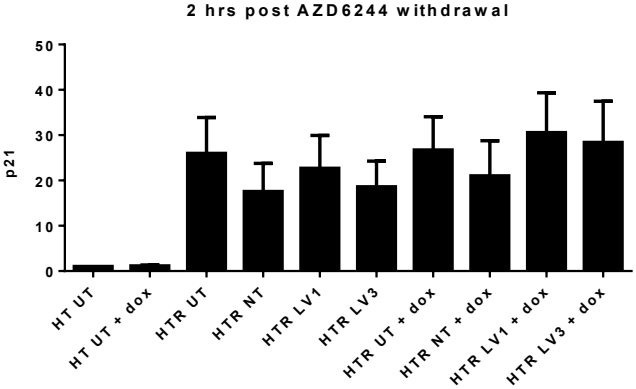

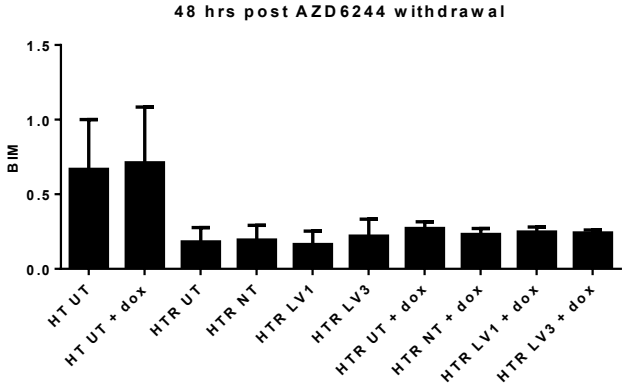

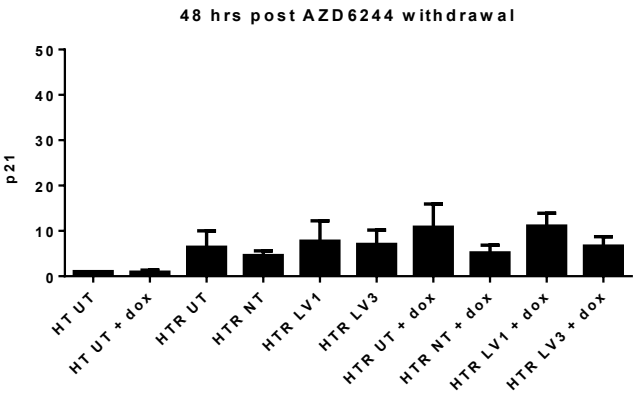

Figure A7 western blot quantification data for figure 5.7 continued.

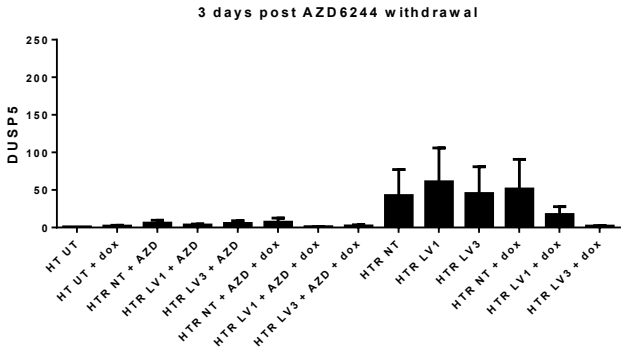

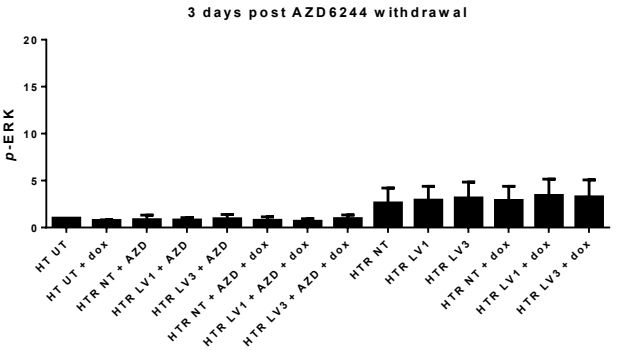

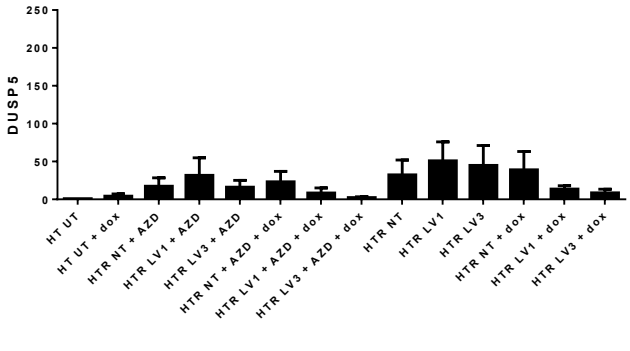

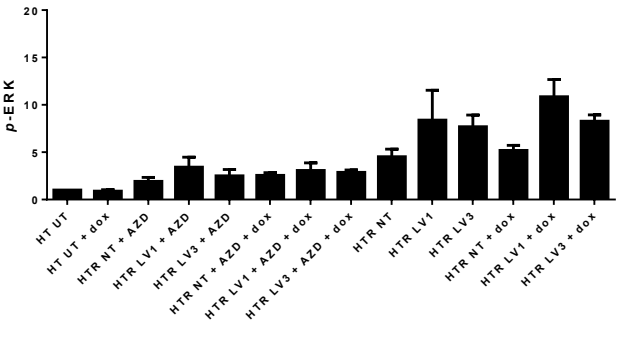

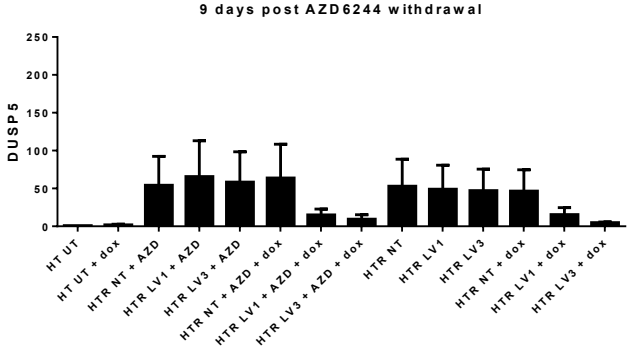

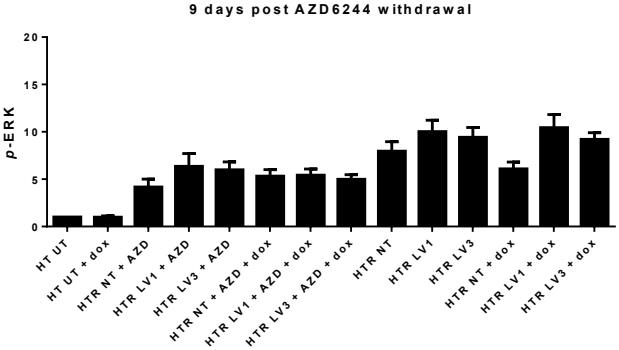

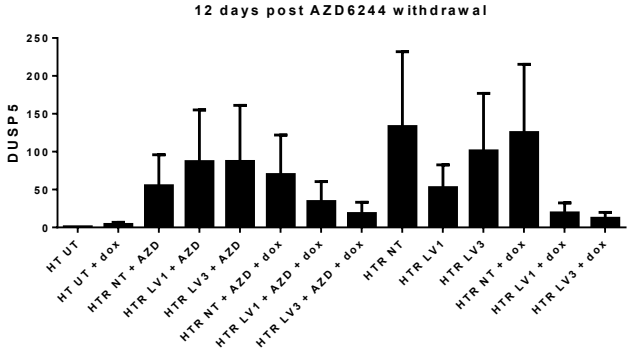

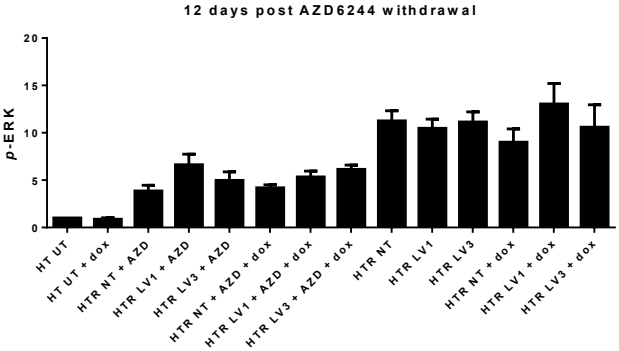

Figure A8 western blot quantification data for figure 5.10.

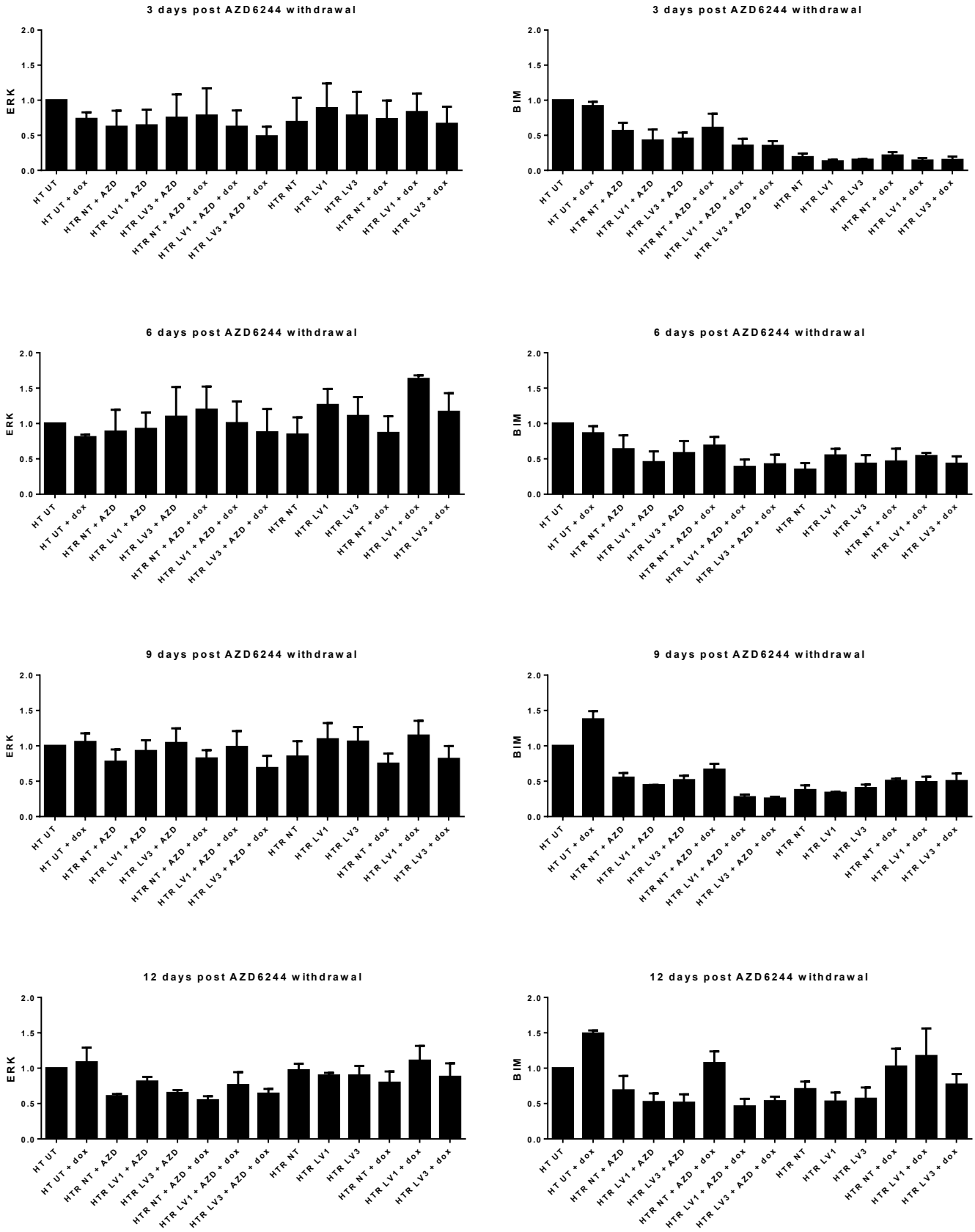

Figure A8 western blot quantification data for figure 5.10 continued

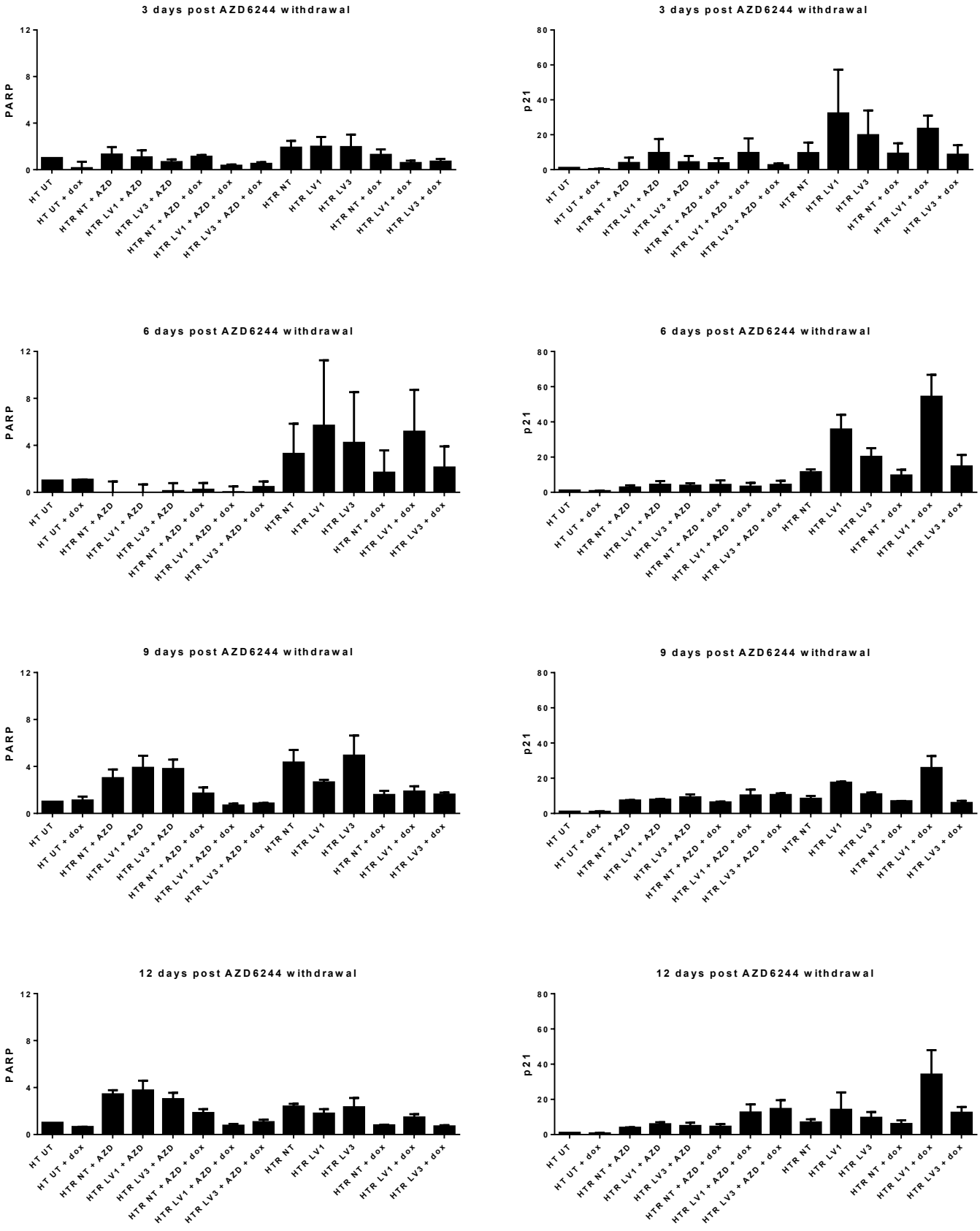

Figure A8 western blot quantification data for figure 5.10 continued

Figure A8 western blot quantification data for figure 5.10. Sustained DUSP5 knockdown in HT6244-R cell lines exposed to long-term AZD6244 withdrawal is coincident with subtle changes in *p*-ERK, $p21^{CIP1}$, BIM and PARP cleavage. HT29 and HT6244-R shRNA cell lines were incubated with or without 1 $\mu g.mL^{-1}$ doxycycline for 48 hours before culture media was replaced with AZD6244-free media or media containing 1 μm AZD6244 (with or without doxycycline). Cells were incubated for a further 3, 6, 9 or 12 days before cell lysis. Samples were fractioned by SDS-PAGE and western blotted with the indicated antibodies to assess relative protein levels. Relative intensities of protein bands were quantified using Liquor's Image Studio Lite software. n=3 biological replicates, ± SEM.